Repositioning study of flubendazole for treating lung cancer and meningoencephalitis using an oral lipid nanosystem

by

Megumi Nishitani Yukuyama

A thesis submitted in partial fulfillment of the requirements for the degree of

Doctor of Philosophy

Faculty of Pharmacy and Pharmaceutical Sciences

University of Alberta

ABSTRACT

Nanoemulsions have wide application, presenting several properties such as the solubilization of poorly soluble drugs in water, promoting the increase of their bioavailability, allowing greater stability of the formulation and, due to its property as a carrier, promoting their modified release. Nanoemulsion development and optimization can be rationally performed using a suitable design of experiment (DoE). Among the processes for obtaining nanoemulsions, D-phase emulsification method (DPE) is considered advantageous because it allows the development of nanoemulsions without requiring the use of specific equipment, strict adjustment of the hydrophilic-lipophilic balance of the system, high temperatures, surfactant concentrations, or solvents. Through the combination of DPE and DoE, nanoemulsions with a mean particle size of less than 100 nm and a high concentration of the oil phase (60.0% w/w) were obtained using oil approved for oral use and which offered greater drug solubility for flubendazole (FLZ). FLZ belongs to class II of the biopharmaceutical classification system, and is a microtubule targeting agent (MTA) and candidate for drug repositioning for several diseases. In vivo trials have been performed for treating cryptococcal meningitis and malignant wounds in lung cancer: results of murine model have shown efficacy of approximately 30% in reducing fungal burden in brain and 100% of prevention in malignant wound emergence. The nontoxicity of this nanoemulsion was demonstrated in a test using an invertebrate model of *Galleria mellonella*. For the in vitro evaluation of the oral efficacy of this nanoemulsion, a pilot dissolution method specific to the nanoemulsion was developed, through the optimization of the biphasic method combined with the modified cylinder method. Results of drug release profile showed agreement between the results obtained in this dissolution test and the results obtained in vivo, indicating the superiority of the

developed nanoemulsion compared to the drug in suspension or control, and possible mechanisms for the respective results were discussed. Additionally, review articles were published describing several mechanisms of action of MTA in lung cancer, and targeting nanostructured systems to the lymphatic system in cancer treatments. Thus, the present work indicates the potential of the nanoemulsion containing FLZ as a new drug or adjuvant drug for treating cryptococcal meningitis and lung cancer.

RESUMO

As nanoemulsões possuem aplicação abrangente, apresentando diversas propriedades como a solubilização de fármacos pouco solúveis em água, promovendo o aumento da sua biodisponibilidade, permitindo maior estabilidade da formulação e, em função de sua propriedade como carreador, promove a liberação modificada desses. O desenvolvimento das nanoemulsões e sua otimização podem ser planejados de forma racional empregando desenho de experimento (DoE) adequado. Entre os processos de obtenção, a emulsificação empregando fase D (EFD) é considerada vantajosa por possibilitar o desenvolvimento de nanoemulsões sem o uso de equipamentos específicos, nem ajuste rigoroso de equilíbrio hidrófilo-lipófilo do sistema, de elevadas temperaturas e de concentrações de tensoativos, e nem de solventes. Por meio da combinação de EFD e DoE, foram obtidas nanoemulsões com diâmetro hidrodinâmico médio inferior a 100 nm e elevada concentração de fase oleosa (60,0% m/m), utilizando lipídios líquidos aprovados para uso oral e que ofereceram maior solubilidade ao fármaco flubendazol (FLZ). O FLZ pertence a classe II do sistema de classificação biofarmacêutica, e é um agente de direcionamento de microtúbulos (acrônimo de microtubule targeting agentes, MTA) e candidato a reposicionamento de fármacos para diversas doenças. Ensaios *in vivo* foram realizados para o tratamento de meningite criptocócica e feridas malignas em câncer de pulmão: os resultados do modelo murino mostraram eficácia de aproximadamente 30% na redução da carga fúngica no cérebro e 100% de prevenção no surgimento de feridas malignas. A não toxicidade dessa nanoemulsão foi demonstrada em ensaio empregando modelo invertebrado de *Galleria mellonella*. Para a avaliação in vitro da eficácia oral dessa nanoemulsão, foi desenvolvido um método piloto de dissolução específico para nanoemulsão, por meio da otimização de método bifásico combinado ao método de cilindro modificado. Resultados de perfil de liberação de fármaco demonstraram

concordância do resultado obtido nesse teste de dissolução com os resultados obtidos *in vivo*, indicando a superioridade da nanoemulsão desenvolvida em comparação ao fármaco em suspensão ou controle, e possíveis mecanismos para respectivos resultados foram discutidos. Adicionalmente, foram publicados artigos de revisão descrevendo diversos mecanismos de ação de MTA em câncer de pulmão, e direcionamento de sistemas nanoestruturados ao sistema linfático nos tratamentos de câncer. Dessa forma, o presente trabalho indica o potencial da nanoemulsão contendo FLZ como novo medicamento ou medicamento adjuvante para tratamento de meningite criptocócica e câncer de pulmão.

PREFACE

This thesis is an original work completed by Megumi Nishitani Yukuyama under the supervision of Prof. Dr. Raimar Löbenberg at the University of Alberta, the supervision of Prof. Dr. Nádia Bou-Chacra and co-supervision of Prof. Gabriel de Araujo at the University of São Paulo.

Chapter 2 "Rational design of oral flubendazole-loaded nanoemulsion for brain delivery in cryptococcosis" is a research manuscript published in *Colloids and Surface A, Physicochemical and Engineering Aspects*, 2021. DOI number: 10.1016/j.colsurfa.2021.127631, by Megumi Nishitani Yukuyama, Kelly Ishida, Gabriel Lima Barros de Araujo, Cristina de Castro Spadari, Aline de Souza, Raimar Löbenberg, Mirla Anali Bazan Henostroza, Beatriz Rabelo Folchini, Camilla Midori Peroni, Maria Christina Camasmie Peters, Isabela Fernandes de Oliveira, Mariana Yasue Saito Miyagi, and Nadia Araci Bou-Chacra.

Chapter 3 "Unveiling microtubule dynamics in lung cancer: recent findings and prospects for drug delivery treatment" is a review manuscript under review in *Journal of Drug Delivery Science and Technology*, 2022, under manuscript number JDDST-D-22-02961, by Megumi Nishitani Yukuyama, Aline de Souza, Mirla Anali Bazán Henostroza, Gabriel Lima Barros de Araujo, Raimar Löbenberg, Rafael de Oliveira Faria, Gabriel Batista de Souza, Lara Mendes Ferreira Guimaraes, Claudiana Lameu, Beatriz Rabelo Folchini, Camilla Midori Peron, Isabela Fernandes Oliveira, Mariana Yasue Saito Miyagi, and Nádia Araci Bou-Chacra.

Chapter 4 "Malignant wound – The influence of oil components in flubendazole-loaded nanoemulsions in A549 lung cancer xenograft-bearing mice" is a research manuscript published in *Journal of Drug Delivery Science and Technology*, 2022. DOI number: 10.1016/j.jddst.2022.103963, by Megumi Nishitani Yukuyama, Lara Mendes Ferreira Guimaraes, Rafael Scheliga Segovia, Claudiana Lameu, Gabriel Lima Barros de Araujo, Raimar Löbenberg, Aline de Souza, Mirla Anali Baz´an Henostroza, Beatriz Rabelo Folchini, Camilla Midori Peroni,

Mariana Yasue Saito Miyagi, Isabela Fernandes Oliveira, Jose Fernando Rinaldi Alvarenga, Jarlei Fiamoncini, and Nadia Araci Bou-Chacra.

Chapter 5 "Cancer treatment in the lymphatic system: A prospective targeting employing nanostructured systems" is a review manuscript published in *International Journal of Pharmaceutics,* 2020, DOI number 10.1016/j.ijpharm.2020.119697, by Megumi Nishitani Yukuyama, Gabriel Lima Barros de Araujo, Aline de Souza, Raimar Löbenberg, Eduardo José Barbosa, Mirla Anali Bazán Henostroza, Nataly Paredes da Rocha, Isabela Fernandes de Oliveira, Beatriz Rabelo Folchini, Camilla Midori Peroni, Jessica Fagionato Masiero, and Nádia Araci Bou-Chacra.

Chapter 6 "Biphasic dissolution combined with modified cylinder method—a new promising method for dissolution test in drug-loaded nanoemulsions" is a research manuscript published in *International Journal of Pharmaceutics,* 2023, under DOI number 10.1016/j.ijpharm.2022.122554, by Megumi Nishitani Yukuyama, Jieyu Zuo, Chulhun Park, Malaz Yousef, Mirla Anali Bazán Henostroza, Gabriel Lima Barros de Araujo, Nádia Araci Bou-Chacra and Raimar Löbenberg.

Appendix 1 "Nanomaterials for haircare applications" in the book *Nanocosmetics, Fundamentals, Applications and Toxicity*, is a book chapter published by Elsevier, 2020, under DOI number 10.1016/B978-0-12-822286-7.00010-3, by Megumi Nishitani Yukuyama, Gabriel Lima Barros De Araujo, and Nadia Araci Bou-Chacra.

Appendix 2 "Nanoemulsions containing plant oils: How do they influence hair treatment?" is a research manuscript published in *International Journal of Cosmetic Science*, 2021, under DOI number 10.1111/ics.12667, by Fernanda Leika Tamashiro, Megumi Nishitani Yukuyama (equivalent author), Maria Valéria Robles Velasco, GLB De Araújo, and Nadia Araci Bou-Chacra. I contributed equally in this manuscript.

Appendix 3 "BR1020210138050 and BR1020210138017" are abstracts of patents approved in Brazil based on the results of developments carried out in this study.

Appendix 4 "Revisiting Flubendazole Through Nanocrystal Technology: Statistical Design, Characterization and Its Potential Inhibitory Effect on Xenografted Lung Tumor Progression in Mice" is a research manuscript published in *Journal of Cluster Science*, 2022, under DOI number 10.1007/s10876-022-02220-x, by Debora de Souza Gonçalves, Megumi Nishitani Yukuyama (equivalent author), Mariana Yasue Saito Miyagi, Tamara Juliane Vieira Silva, Claudiana Lameu, Nadia Araci Bou-Chacra, and Gabriel Lima Barros de Araujo. I contributed equally in this manuscript.

ACKNOWLEDGEMENTS

Table of Contents

Contents

List of tables

List of figures

List of abbreviation

AA	Alopecia areata
AIDS	Acquired immunodeficiency syndrome
AGA	Androgenic alopecia
Alg	Alginate
ALK	Anaplastic lymphoma kinase
AM	Alveolar macrophage
AmB	Amphotericin B
ANOVA	Analysis of variance
AOAO	Apical-out airway organoid
APCs	Antigen-presenting cells
Au-NP	Gold nanoparticle
BBB	Blood-brain barriers
BBR	Berberine
BCS	Biopharmaceutical Classification System
BCSFB	Blood-cerebrospinal fluid barrier
BD	Biphasic dissolution method
b i d	Bis in die, twice (two times) a day
BR	Blank, drug-free
BRAF	v-Raf murine sarcoma viral oncogene homolog B1
Cas	Contrast agents
CANE	Carvacrol nanoemulsion
CCT3	Chaperonin-containing T-complex protein-1 subunit 3
CDDP	*cis*-Diamminedichloroplatinum (II)
CHP	Cholesteryl pullulan
CIA	Chemotherapy-induced alopecia
Cin-CNCs	Cinnamate-functionalized cellulose nanocrystals

CM	Cryptococcal meningitis
CMC	Critical micelle concentration
CM NE	Drug-free nanoemulsion containing Capmul MCM and Maisine CC® as oil phase
CMF NE	FLZ-loaded nanoemulsion containing Capmul MCM and Maisine CC® as oil phase
CMS	Dendritic core-multi shell particles
CNS	Central nervous system
CNTs	Carbon nanotubes
CP	Choroid plexus
CpG DNA	Covalently linked oligonucleotide agonist
CRC	Human colorectal cancer
CS	Cigarette smokers
CSF	Cerebrospinal fluid
CS-NPs	Chitosan nanoparticles
CSO-SA	Chitosan oligomer-stearic acid
CTLA-4	Cytotoxic T lymphocyte antigen 4
C-1305	Acridanone derivative 5-dimethylaminopropylamino-8-hydroxytriazoloacridinone
(d)	Desirability of compound
DCs	Dendritic cells
DF	Degrees of freedom
DHI	Dioxyindole
DHT	Dihydrotestosterone
DIF	Diferuloylmethane
dLN	Draining lymph node
DLS	Dynamic Light Scattering
DM1-NO	Nitrosylated maytansinoid DM1
DoE	Design of experiment
DOX	Doxorubicin

DPC	Dermal papilla cells
DPE	D-phase emulsification process
D phase	Isotropic surfactant phase
dPG-NG	pH-responsive-dendritic-polyglycerol-nanogel
DR	Drug repositioning
DTX	Docetaxel
5DSA	Spin-labeled 5-doxyl stearic acid
EC	Electronic cigarette
EGFR	Epidermal growth factor receptor
EPR	Enhanced permeability and retention
FDA	Food and Drug Administration
FGFR	Fibroblast growth factor receptor
FITC	Fluorescein isothiocyanate
FLU	Flubendazole
FLZ	Flubendazole
FS	Flubendazole in suspension
F value	Value on the F distribution
G2/M	G2 segment and mitosis prophase of cells
GD	Gestational day
GEM	Gemcitabine
GI	Gastrointestinal
GNP	Gold nanoparticle
GRAS	Generally recognized as safe
HCD	Hydroxypropyl-β-cyclodextrin
HE	Eosin-hematoxylin
HEVs	High endothelial venules
hFTN	Human ferritin heavy chain
HLB	Hydrophilic-lipophilic balance

HM	Hybrid micelle
HP-β-CD	2-hydroxypropyl-β-cyclodextrin
HPH	High pressure homogenization
HSP	Heat shock proteins
ICG	Indocyanine green
IFN -γ	Interferon gamma
IVIVC	In vitro-in vivo correlation
KRAS	Kirsten rat sarcoma virus
L-Amb	Liposome of combination of amphotericin with flucytosine
LCP	Lipid calcium phosphate
LEC	Lymphatic endothelial cells
LNs	Lymph nodes
LUAD	Lung adenocarcinoma
MAF M, MF	Flubendazole-loaded nanoemulsion with Maisine CC®
MBZ	Mebendazole
MC	Modified cylinder dissolution method
MCP-1	Monocyte chemoattractant protein-1
MDA	Microtubule-destabilizing agents
MDR	Multidrug resistance
MET	Mesenchymal to epithelial transition
MFS	Miltefosine
MIC	Minimum inhibitory concentration
MIP-1	Macrophage inflammatory protein-1
MITF	Microphthalmia transcription factor
MMA	Methyl methacrylate
Mmb 1p	Microtubule-mitochondria binding protein
MPMBs	Multifunctional polymer microbubbles
MPS	Mean particle size

MRI	Magnetic resonance imaging
MS (adj)	Adjusted sequential mean square
MSA	Microtubule-stabilizing agent
MTA	Microtubule targeting agent
MW	Malignant wound
MWCNTs	Multi-walled carbon nanotubes
NE	Nanoemulsion
NEK2	Never-in-mitosis-related kinase 2
NF-kB	Nuclear factor kappa B
NIMA	Never-in-mitosis
NIR	Near-infrared
NLCs	Nanostructured lipid carriers
NME	New molecular entities
NOAEL	No-observed-adverse-effect level
NP	Nanoparticle
NS	Nonsmokers
NSCLC	Non-small cell lung cancer
O/D	Oil-in-surfactant
OFI	*Opuntia ficus indica L. inermis*
OVA	Ovalbumin
O/W	Oil-in-water
PAuNRs	Polymeric gold nanorods
PBPK	Physiologically based pharmacokinetic
PBS	Phosphate-buffered saline
PCL	Poly(ε-caprolactone)
PDI, PI	Polydispersity index
PEG	Polyethylene glycol
PEG-PE	Diblock copolymers, poly-(ethylene glycol) phosphoethanolamine

P-gp	P-glycoprotein
PIC	Phase inversion composition
PIT	Phase inversion temperature
PLA	Poly-lactic acid
PLGA	Poly(lactic-co-glycolic acid)
PLGA-b-PEG	Poly(lactide-co-glycolic)-*block*-poly(ethylene glycol)
POD	Podophyllotoxin
POSS	Polyhedral Oligo Silsequioxanes
PSA	Polyethylenimine-stearic acid conjugate
PTT	Photothermal therapy
PTX	Paclitaxel
PUFA	Polyunsaturated fatty acids
P-value	Lack-of-fit adjustment
R^2	Multiple correlation coefficient
R^2 (aj)	Adjusted multiple correlation coefficient
R^2 (pred)	Predicted correlation coefficient
RGD-CuS-Cy5.5	Fluorescent copper sulfide (CuS) nanoparticle
SAC	Metaphase-spindle-assembly-checkpoint
SCLC	Small cell lung cancer
SCS	Subcapsular sinus
SEM	Scanning electron microscope
SLN	Solid lipid nanoparticle
SLNDs	Sentinel lymph nodes
SMCs	Smooth muscle cells
SPC-160002	5-(N-methylmaleimid-3-yl)-chromone
SQ	2-methoxy-5((3,4,5-trimethosyphenyl) seleninyl) phenol
SS (adj).	Sequential sums of squares
SVNPs	Synthetic vaccine based on poly(γ-glutamic acid)
TACC3	Transforming acidic coiled-coil-containing protein 3

TAM	Tumor-associated macrophages
TDLN	Tumor-draining lymph node
TEM	Transmission electron microscope
Tim-3	T-cell immunoglobulin domain and mucin domain-3
TLRs	Toll-like receptors
TNBC	Triple-negative breast cancer
TND	Tropical neglected disease
TNF- α	tumor necrosis factor α
TP	Testosterone
TRITC	Tetramethylrhodamine
TSA	Tumor-specific antigen
Tyrp 1	Tyrosinase-related protein 1
US	Ultrasound
VCR	Vincristine
VDAC	Voltage-dependent anion channels
VEGF	Vascular endothelial growth factor
WHO	World Health Organisation
W/O	water-in-oil
w/w	weight/weight
ZP	Zeta potential
5-α R	5-α reductase

CHAPTER 1 GENERAL INTRODUCTION

1.1.   DRUG REPOSITIONING

Currently, identifying and validating new molecular entities (NME) for the discovery of new drugs involve high risk due to the extensive development time (from 10 to 17 years) (MORGAN et al., 2011) and the high cost (approximately US $1.3 billion) (DIMASI; GRABOWSKI; HANSEN, 2016). Despite the efforts involved and the increase in investment in recent decades, studies indicate that there was no significant increase in the NME approval rate between 1976 and 2013 (SHIM; LIU, 2014). In the United States, about 1 in every 1,000 drugs, in the development phase, enter clinical studies in humans after preclinical testing. However, 9 out of 10 potential candidates are rejected in these human trials (ARROWSMITH, 2011).

A study report of failures in phase II of NME, carried out between 2011 and 2012, revealed problems related to the efficacy (56%) and safety (28%) of these drug candidates. When classified by therapeutic area, these failures occur, more frequently in the areas of oncology and central nervous system disorders, totaling 44% of failures, being 30% and 14%, respectively (ARROWSMITH; MILLER, 2013). Faced with the high cost and inefficiency in discovering new drugs (JAHCHAN et al., 2013), there is an urgent need for alternative approaches that allow the rational use of the existing therapeutic arsenal (SHIM; LIU, 2014).

Drug repositioning (DR) is defined as the identification of new indications or new use for existing drugs (JAHCHAN et al., 2013), with established and proven human safety (LOTFI SHAHREZA et al., 2018). DR allows for benefitting from the known pharmacokinetic and pharmacodynamic properties, as well as information about tolerability and established adverse effects of a given drug, allowing for reducing (SHIM; LIU, 2014) the drug development from 10-17 years to 3-12 years (LOTFI SHAHREZA et al., 2018) and advancing clinical trials for new indications (NYGREN et al., 2013). Recent studies indicate DR in treatments for cancer, orphan diseases and infections caused by resistant microorganisms (JAHCHAN et al., 2013; LOTFI SHAHREZA et al., 2018). There are approximately 4,000 drugs approved worldwide for use in humans, thus making DR an attractive strategy for developing future drugs (SHIM; LIU, 2014).

The difference between the terms drug repositioning and repurposing is describes as: *'Drug repositioning can be defined more precisely as the process of exploring new indications for an already approved drug while drug repurposing includes overall re-development approaches*

grounded in the identical chemical structure of the active drug moiety as in the original product' (Roy, S. et al, 2021).

Moreover, DR is of increasing interest from governments, nongovernmental agencies and academic researchers (LOTFI SHAHREZA et al., 2018), accounting for approximately 30% of new drugs approved by the Food and Drug Administration (FDA), in recent years (JIN; WONG, 2014). An example of success refers to sildenafil (Viagra, Pfizer), with an initial indication for hypertension. Additionally, the drugs Itraconazole (antifungal), Nelfinavir (antiretroviral) and Disulfiram (treatment of alcoholism), are in phases II and III of clinical research, as alternatives for treating cancer (SHIM; LIU, 2014). Such examples show the growing interest of companies in the search of new drugs to launch using the DR strategy (YOSHIDA, 2017).

In treating cancer, despite the high number of drugs developed during recent decades (JAHCHAN et al., 2013), their demand continues to grow due to factors such as resistance to these drugs (LOTFI SHAHREZA et al., 2018). On the other hand, resources allocated for the development drugs to combat neglected diseases have remained stagnant since 2009, as a result of the reluctance of pharmaceutical companies to invest in nonprofit ventures (COHEN; STURGEON; COHEN, 2014). Recent studies carried out with the drug flubendazole (FLZ) - an agent that blocks cell division and induces apoptosis - highlighted the potential activity of this drug in several pathogenic condition, including cancer (HOU et al., 2015; KRÁLOVÁ et al., 2013) and neglected diseases such as cryptococcal meningitis (O'NEILL et al., 2015). Such repositioning would enable new opportunities to respond to these demands, overcoming the limitations of the conventional process of developing new drugs.

1.2. FLUBENDAZOLE AND ITS REPOSITIONING PERSPECTIVE

1.2.1. *Flubendazole and its description*

FLZ is an anthelmintic belonging to the benzimidazole family. Developed in 1970 and marketed by Janssen Pharmaceutical (LONGO et al., 2013), this drug is effective against a broad spectrum of gastrointestinal nematodes in humans and some animal species (CEBALLOS et al., 2014). FLZ has a molar mass equivalent to 313.29 g/mol, low solubility in water (0.0334 mg/mL),

pKa 3.6 and 9.6 and logP 3.00 (VIALPANDO et al., 2016), belonging to class II of the Biopharmaceutics Classification System (CEBALLOS et al., 2014).

In human, this drug is currently marketed as Fluvermal® for oral administration. The indications and dosages are 100 mg as a single dose for enterobiasis, or 100 mg bid for 3 days for treatment of ascariasis, hookworm infection and trichuriasis.

Studies of FLZ metabolism in human liver describe that reduced FLZ is the only metabolite formed, not the hydrolyzed one (STUCHLÍKOVÁ et al., 2018) , and the enzyme carbonyl reductases showed greater activity in cytosol than microsomes in pheasant, pig and human liver (KUBÍČEK et al., 2019; NOBILIS et al., 2007) . Furthermore, it is suggested that NADPH is the preferred coenzyme for this reduction process in human liver. FLZ is a pro-chiral substrate and FLZ carbony reduction proved to be strictly stereospecific in human liver (KUBÍČEK et al., 2019). Preferential formation of approximately 93-97% of (+)-reduced FLZ has been recorded compared to 3-7% of (-)-enatiomer in pigs and pheasants (NOBILIS et al., 2007) , and approximately 75% in ovine blood plasma (NOBILIS et al., 2008) (**Figure 1.1**). Interesting studies have indicated the low intrinsic hepatic clearance of FLZ and its low risk of metabolism-based interaction with other drugs in the human liver (KUBÍČEK et al., 2019; STUCHLÍKOVÁ et al., 2018) . Additionally, FLZ showed a significant difference between cells: it entered in greater amount and it was less reduced in metastatic cells than in non-metastatic or non-cancerous cells, indicating this drug as an interesting candidate for anti-cancer therapy (STUCHLÍKOVÁ et al., 2018) .
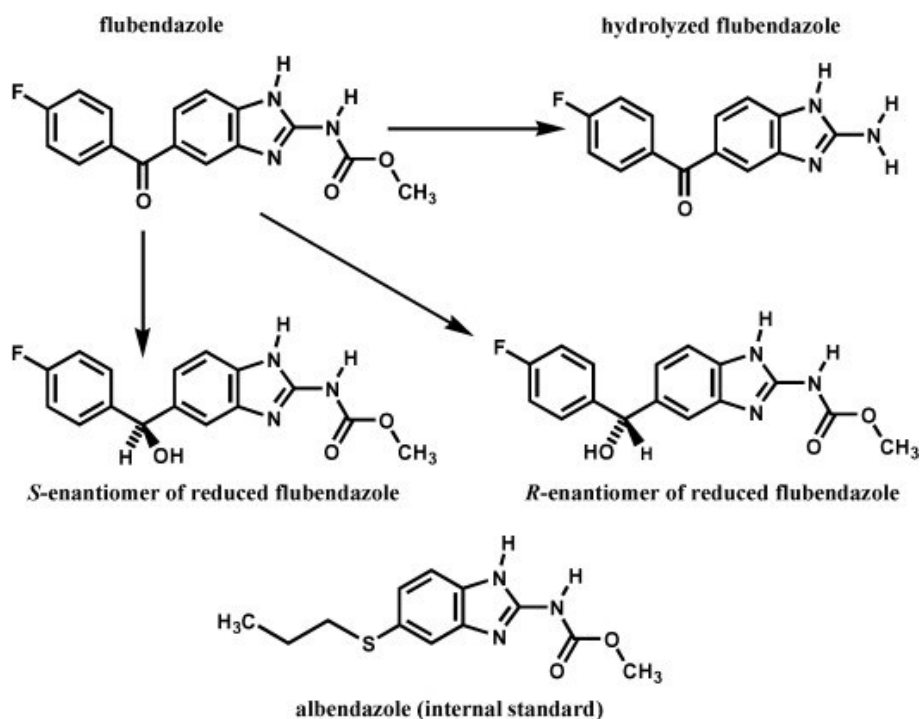
Figure 1.1: Molecular structure of flubendazole and its metabolites

Source: (NOBILIS et al., 2008)

The pharmacokinetic parameters of FLZ and other benzimidazole drugs are shown in **Table 1.1**, their structures in **Figure1.2** and the physic-chemical properties of flubendazole are described in **Chapter 6**.

Table 1.1: Pharmacokinetic parameters for benzimidazole drugs and their metabolites in plasma.

Compound	$C_{(max)}$	$t_{(max)}$ (h)	$AUC_{(0-72\,h)}$	$t_{(1/2)}$ (h)	Metabolite	Administration	Reference
FLZ	40 pmol/ ml	10	830 pmol h /ml	55	FLZH; (+)FLZR	single oral administration of FLZ in	(Nobilis et al., 2008)

						young ram (30 mg/kg)	
FLZH	56 pmol/ ml	10	1267 pmol h /ml	23	---	single oral administration of FLZ in young ram (30 mg/kg)	(Nobilis et al., 2008)
(+)FLZR	327 pmol/ ml	10	6287 pmol h /ml	17	---	single oral administration of FLZ in young ram (30 mg/kg)	(Nobilis et al., 2008)
MBZ	92.0 ± 2.03 µg/ml	8.0 ± 0.0	2946 ± 80.80 mg/L*h	212.1 ± 52.81	MBZ-NH2, MBZ-OH	i.m. administration of MBZ at 20 mg/Kg to Japanese puffer fish (n=5)	(Men et al., 2022)
MBZ-NH$_2$	23.2 ± 2.56 µg/ml	10.0 ± 0.0	384.0 ± 82.50 mg/L*h	212.1 ± 52.81	---	i.m. administration of MBZ at 20 mg/Kg to Japanese puffer fish (n=5)	(Men et al., 2022)
MBZ-OH	16.8 ± 0.7 µg/ml	10.0 ± 0.0	635.5 ± 19.76 mg/L*h	87.3 ± 25.3	---	i.m. administration of MBZ at 20 mg/Kg to Japanese puffer fish (n=5)	(Men et al., 2022)

ALB	Not detectable	Not detectable	Not reported	Not reported	ALB sulphoxide	oral dose in man of ALB 400 mg ($\sim$ 6–8 mg/kg)	(Dayan, 2003)
ALB sulphoxide	0.20 – 0.25 µg/ml	2 - 3	2.00 ± 2.77 µg h/ml	8 - 12	---	oral dose in human of ALB 400 mg ($\sim$ 6–8 mg/kg)	(Dayan, 2003; Marrinefl et al., 1986)
OFZ	6,770 ± 2,200 ng/ml	1.99 (1.35-7.92)	109,000 ± 44,900 h.ng/ml	11.0 ± 5.2	OFZS; FBZ	oral dose in human of OFZ (60 mg/kg)	(An et al., 2019)

FLZ: flubendazole; **FLZH:** hydrolyzed flubendazole; **(+)FLZR:** (+)-reduced flubendazole; **MBZ:** mebendazole; **MBZ-NH₂:** 2-amino-5(6)-benzoylbenzimidazole; **MBZ-OH:** 5-hydroxymebendazole; **ALB:** albendazole; **OFZ:** oxfendazole; **OFZS:** oxfendazole sulphone; **FBZ:** Fenbendazole.

Albendazole

Mebendazole

Fenbendazole
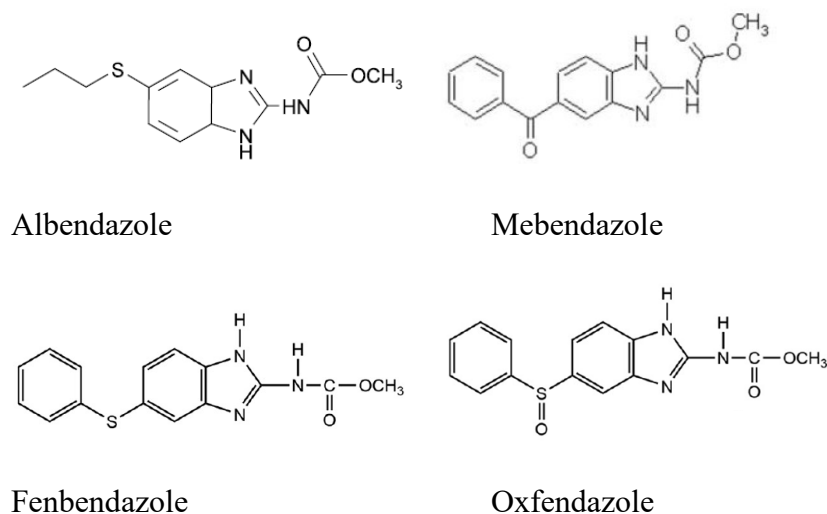
Oxfendazole

Figure 1.2: Molecular structure of albendazole, mebendazole, fenbendazole and oxfendazole

Source: (An et al., 2019; Dayan, 2003)

Concerning the toxicity, FLZ showed modifications in lymphoid, haematological and gastrointestinal systems upon increased exposure and repeated dosing in rats and dogs, and in liver in dogs. But these effects were partially reversible (LACHAU-DURAND et al, 2019).

FLZ acts by inhibiting the polymerization of the protein tubulin, a component of the microtubule cytoskeleton that performs critical cellular functions throughout the cell cycle (PARKER et al., 2017). The chromosomal nondisjunction caused by this inhibition during cell mitosis disrupts the tubulo-microtubule balance of cells, causing interruption of nutrient transport and, consequently, cell death (MACKENZIE; GEARY, 2011). Additionally, glycogen depletion and the low generation of ATP necessary for parasite survival, caused by irreversible blockage of exogenous glucose uptake, result in its death and gradual elimination from the intestine (ISLAN et al., 2017).

However, the low water solubility of FLZ limits its use in systemic use formulations (VIGH et al., 2017). Different strategies to solve these limitations have been proposed, such as FLZ in association with hydroxypropyl-β-cyclodextrin (HCD) (CEBALLOS et al., 2014), with HCD and polyvinylpyrrolidone (VIGH et al., 2017), in addition to the association with maleic acid (DE ARAUJO et al., 2018) . These studies demonstrated a significant increase in the bioavailability of drugs in nanostructured systems compared to FLZ in aqueous suspension.

1.2.2. *Cryptococcal meningitis*

Cryptococcal meningitis (CM) is an opportunistic infection caused generally in people with acquired immunodeficiency syndrome (AIDS). This disease causes approximately 180,000 deaths annually regardless of widespread access to antiretroviral therapy, with the highest incidence in sub-Saharan Africa. Seventy percent of deaths are reached in these countries, due to insufficient antiretroviral treatment or treatment adherence problems (LAWRENCE; BOYER-CHAMMARD; JARVIS, 2019; SPADARI et al., 2020). Nevertheless, the growing number of HIV-negative patients concerns authorities in other countries, where the incidence of CM in patients with other

types of immunosuppression, such as the naturally occurring one, or even those who are supposedly immunocompetent, has been growing. For example, in the United States of America, in hospitalizations for CM, 25% of deaths are caused by non-HIV-related CM, and represent approximately 30% of all CM-related deaths (WILLIAMSON et al., 2016).

CM is a subacute meningoencephalitis, generally caused by inhalation of yeasts or spores of Cryptococcus *spp.* These organisms can be inhaled from the environment (i.e., soil, trees and pigeon feces, recognized as carriers), kept in a dormant stage in the alveoli of the lung, and can proliferate and develop as cryptococcal pneumonia or pulmonary cryptococcoma. Cryptococcus can disseminate to several organs. But as a result of its neurotropism, it frequently progresses to cryptococcal meningitis, cerebral cryptococcoma, or cryptococcal meningoencephalitis in more advanced and critical stages (CHEN; MEYER; SORRELL, 2014; HULL; HEITMAN, 2002) (**Figure 1.2**). This preference of cryptococcus for the central nervous system (CNS) is related to its specific virulence factors, such as specific urease and metalloproteinases that ease penetration through the blood-brain barrier (BBB). In addition, there are neuroimmunomodulation promoting enzymes and mechanisms that support survival in a poor-nutrient environment, such as in the brain (COELHO; BOCCA; CASADEVALL, 2014). *Cryptococcus spp* have a dense polysaccharide capsule, which protects them against parasitic amoeba in the environment, and in humans, for survival against attacks by alveolar macrophages at the primary site of infection. Within their species, *Cryptococcus neoformans* and *Cryptococcus gattii* are the two main causes of human infections (KRONSTAD et al., 2011; ZARAGOZA et al., 2009). Among them, *C. neoformans* is the main causative agent of cryptococcal disease, especially in people with HIV. However, *C. gattii* has attracted attention due to its growing outbreaks in recent years in several countries with temperate climates, including northern Europe (CHOWDHARY et al., 2012) and states in the US (HARRIS et al., 2013). In addition, *C. gattii* predominantly affects immunocompetent individuals, for reasons that are still unclear (HARRIS et al., 2011; NGAMSKULRUNGROJ et al., 2012; SPEED; DUNT, 1995).
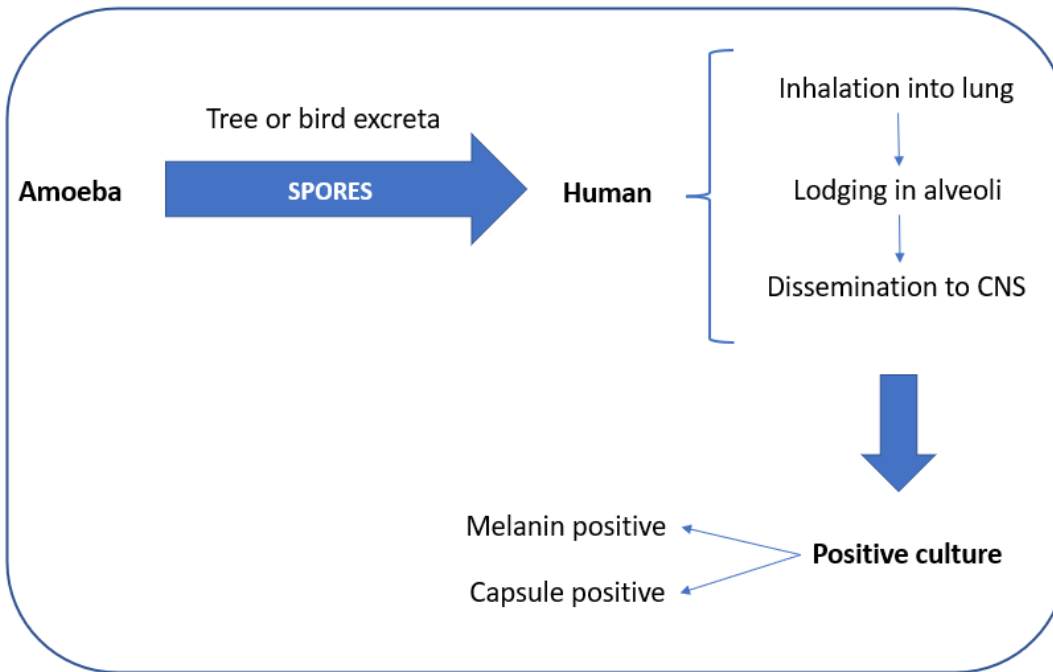
Figure 1.3: Infectious cycle of *C. neoformans* - inhalation of basidiospores from the environment by humans; spread to the central nervous system (CNS); test in culture medium

Source: adaptation of HULL; HEITMAN, 2002

Patients with CM generally present symptoms like fever, headache, nausea, vomiting, visual symptoms, altered mental status, and eventually coma, with no difference in clinical manifestations between different pathogenic strains (FISHER et al., 2012). Currently, the standard diagnosis of CM is a positive culture of cerebrospinal fluid. However, new studies for detecting CrAg, the polysaccharide of the cryptococcal capsule, released in the cerebrospinal fluid and in the patient's blood, have emerged as potential diagnoses (LAWRENCE; BOYER-CHAMMARD; JARVIS, 2019). For treatment, they usually involve the use of intravenous amphotericin B, associated with fluconazole or flucytosine. However, problems related to toxicity and high cost of administration have been one of the challenges faced. In high-income countries, a liposome of combination of amphotericin (L-Amb) with flucytosine is being tested in a phase III study. L-Amb has the advantage of allowing short-term treatment, due to the potential use of high dosage due to reduced toxicity and effective penetration into brain tissue (LESTNER et al., 2017). Treatment with

amphotericin B (AmB) is expensive and requires hospital administration, while treatment with flucytosine requires careful blood monitoring. As a result, in underprivileged populations, treatment of cryptococcal meningitis is performed with fluconazole, which is only partially effective. According to the 2016 Global Neglected Disease Incentives Report (G-Finder), meningoencephalitis is considered one of the most neglected diseases worldwide (CHAPMAN et al., 2017). Although AIDS-related, cryptococcal meningitis meets the WHO definition of a tropical neglected disease (TND); this disease: (1) extremely affects populations in poverty and causing substantial morbidity and mortality, (2) mainly affects populations living in subtropical and tropical areas, (3) is immediately amendable to widespread control, elimination or eradication, and (4) is overlooked by researchers (MOLLOY et al., 2017).

In recent years, nanostructured systems represent a promising alternative due to the possible improvement in drug transport and penetration in the central nervous system, overcoming the blood-brain barrier (BBB) (WOHLFART; GELPERINA; KREUTER, 2012). Studies employing AmB-poly(lactic acid)-b-poly(ethylene glycol) (AMB-PLA-b-PEG) nanoparticles have demonstrated an increased concentration of AmB in the brain and significantly reduced fungal burden in the brain and toxicity of Amb. This study was performed in a mouse model of cryptococcosis and compared with AmB deoxycholate (REN et al., 2009). Another study involving nanoparticles of alginate (Alg) loaded with miltefosine (MFS) was performed as an antifungal alternative. MFS is an alkylphosphocholine analogue, synthesized and evaluated in the 1980s for antineoplastic activity and indicated as a potential antifungal agent. Antifungal activity using larval models of *Galleria mellonella* infected with *C. neoformans* and *C. gattii* demonstrated that the MFS-Alg nanoparticle prolonged the survival of larvae infected by these fungi, with reduced toxic effect (SPADARI et al., 2020).

Recent research carried out by Nixon and collaborators, using FLZ as an efficient agent against *C. neoformans*, showed potent in vitro activity with a minimum inhibitory concentration (MIC) of 0.125 mg/L. Oral in vivo testing in mice comparing this FLZ nanodispersion with hicle-treated controls showed a 2-log reduction in fungal burden (NIXON et al., 2018). These findings demonstrate the relevance of developing new drugs using FLZ for the effective treatment of meningoencephalitis.

1.2.3. Lung cancer

Lung cancer is one of the main sources of death caused by tumors worldwide. Although the occurrence of lung cancer has been decreasing annually due to changes in behavior (for example, smoking cessation) and advances in detection techniques and treatments for this disease (AMERICAN CANCER SOCIETY, 2013), there is still a need for more effective drugs for its treatment.

For treating lung cancer, the following alternatives currently exist: surgery for early-stage patients, radiotherapy, chemotherapy (sometimes in combination with another drug), combination with immunotherapy or adjuvant therapies. The most commonly applied chemotherapy drugs are carboplatin, cisplatin, docetaxel, paclitaxel and gemcitabine, which have limited therapeutic efficacy and serious side effects (CHOUDHURY et al., 2019; THAKUR, 2019).

In addition, cancer treatments face challenges due to multidrug resistance (MDR) due to the overexpression of multidrug transporters, such as P-glycoprotein (P-gp), which is encoded by the ABC transporter family gene (ATP – binding cassette). This transporter is capable of expelling several anticancer drugs from the interior of the cell, including vinblastine, colchicine, and paclitaxel. Furthermore, MDR related to changes in the course of apoptosis may increase the expression of anti-apoptotic genes, including nuclear factor kappa B (NF-kB) and Bcl-2 (WONG, 2020).

More in-depth description about lung cancer is found in **Chapter 3** of this thesis.

FLZ has demonstrated potential antiproliferative activity in several cancer cells, such as hepatocellular, leukemic, ovarian, myeloma, melanoma, breast, lymphoma, and neuroblastoma (HOU et al., 2015; KRÁLOVÁ et al., 2013; MICHAELIS et al., 2015). These include cells resistant to vinblastine, a conventional microtubule depolymerizing agent. The effect of FLZ in these resistant cells, by overexpression of P-gp to vinblastine (SPAGNUOLO et al., 2010), is explained by the possible binding site, which is distinct from the binding sites of vinblastine and vincristine (KRÁLOVÁ et al., 2013).

Lin and et al. (2019) demonstrated effective antitumor activity of FLZ in three human colorectal cancer (CRC) cell lines and in an in vivo nude mouse model. The results showed the

inhibition of the transcription of the STAT3 target genes and the upregulation of the main genes regulated by autophagy, when FLZ was used, which indicated this drug as a distinct therapeutic alternative in the neoadjuvant chemotherapy of CRC (LIN et al., 2019). Another study employing FLZ for treating triple-negative breast cancer (TNBC) demonstrated induction of cell death, sub-G1 accumulation, annexin V externalization, PARP cleavage, and caspase-3 and -7 activation in TNBC cells (OH et al., 2018).

Moreover, in vitro tests of FLZ conjugated with 2-hydroxypropyl-β-cyclodextrin demonstrated improved antiproliferative activity of this complex against A 549 cells (MINDA et al., 2021), and cell viability, Beclin-1 and P62 expression were analyzed and showed significant efficacy of FLZ when compared to control groups (HOVEIZI; FAKHARZADEH JAHROMI, 2020). However, it is lacking in vivo assays to compare FLZ in nanostructured systems with other preparations in lung cancer xenografted models.

1.2.4. Lymphatic filariasis

Onchocerciasis and lymphatic filariasis are neglected diseases caused by filarial nematodes – Wuchereria bancrofti, Brugia malayi, and Brugia timori –, the former being responsible for 90% of cases of lymphatic filariasis. The World Health Organization (WHO) aims to eliminate onchocerciasis and eradicate lymphatic filariasis by 2020 (O'NEILL et al., 2015) .

Lymphatic filariasis is transmitted by different types of mosquitoes such as Culex, Anopheles and Aedes. The adult parasites lodge in the lymphatic vessels of the human host and can survive for approximately 6 to 8 years, producing millions of immature larvae called microfilariae. The circulation of these parasites impairs the normal function of the lymphatic system and kidney, affecting the patient's immune system. Acute symptoms involve local inflammation of the skin, lymph nodes, and lymph vessels; subsequently, they result in chronic lymphedema or elephantiasis.

More than 51 million people were infected with lymphatic filariasis by the year 2018, and about a 36 million people remain with this chronic disease manifestation. Approximately 860 million people in 47 countries are still under threat. The spread of this infection can be limited by

using preventive chemotherapy, administered annually, for at least 5 years (WORLD HEALTH ORGANIZATION, 2022) .

The drugs used for mass administration, in populations at risk, are essentially microfilaricidal agents (O'NEILL et al., 2015) such as albendazole, ivermectin and diethylcarbamazine citrate. However, these drugs have some potentially serious adverse effects on the eyes and skin (CEBALLOS et al., 2014; LONGO et al., 2013), in addition to the possibility of severe manifestations in the central nervous system (coma and death) in coinfected patients. Additionally, adult parasites that survive microfilaricides reproduce for several years (VIGH et al., 2017) – and the manifestation of elephantiasis is caused by these adult parasites.

Study in an early 1980s indicated the superior efficacy of FLZ compared to diethylcarbamazine against onchocerciasis in clinical study with 12 months follow-up. Although FLZ showed limitations due to inflammation at the injection site, it's safety was higher than diethylcarbamazine. In view of the above, the use of drugs with potentially greater efficacy, such as FLZ, due to its proven high macrofilaricidal activity, is of fundamental importance (O'NEILL et al., 2015) .

1.2.5. *Lymphatic system and lipid nanosystems*

Advances in studies related to lymphangiogenesis reveal the growing interest in the importance of the lymphatic system in the involvement of several diseases. The lymphatic system plays an important role in drug distribution, in triggering adaptive immunity, as well as in the dissemination of cancer cells in the final stage of the disease (YOSHIMATSU et al., 2016).

One of the relevant activities of the lymphatic system is its role as an efficient means of transporting lipids to the blood system and tissues. Lipids administered orally enter in the intestinal lumen and are internalized by cells of the small intestine, the enterocytes. Subsequently, they are associated with chylomicrons, the lipoproteins of enterocytes, considered as the most efficient form of secretion for the lymphatic circulation (DIXON, 2010) . Highly liposoluble drugs can be generally transported through the intestinal lymphatic system, avoiding blood circulation and consequent first-pass hepatic metabolism (YÁÑEZ et al., 2011) . After being directed to the

lymphatic capillaries, these drugs are transported to the lymph nodes, which act as reservoirs of these drugs, and, finally, are conducted to the systemic circulation (CAI et al., 2011; RYAN et al., 2014) . In this context, the lymphatic absorption of drugs through the intestine plays an essential role in increasing the bioavailability of different drugs (CAI et al., 2011; RYAN et al, 2014).

However, FLZ faces a barrier to targeting the lymphatic system by oral administration, due to its low solubility in water. Its incorporation in modified release systems, such as lipid nanosystems, has the benefits of increasing its bioavailability, reducing its toxicity, increasing its stability and directing it to the lymphatic system (PEREIRA et al., 2015; RYAN et al., 2014) . Examples of lipid nanosystems are nanoemulsions, nanostructured lipid carriers and solid lipid nanoparticles. Different studies, carried out based on the development of lipid nanosystems, show the importance of directing drugs to the lymphatic system. Sun et al. (D. SUN et al., 2014) optimized the lymphatic transport of acetylpuerarin in the treatment of brain injury, using nanoemulsion stabilized with D-α-tocopheryl polyethylene glycol 1000 succinate (TPGS). Another nanoemulsion study was carried out by Gao et al. (GAO et al., 2011) , using candesartan cilexetil, an antihypertensive prodrug. In association with Tween 80, soybean oil and Solutol® HS-15, researchers observed a significant improvement in its bioavailability via the lymphatic system. The solid lipid nanoparticle composed of nimodipine (antihypertensive drug), palmitic acid, Polaxamer 188 and soy lecithin, also demonstrated the increase of drug transport in the intestinal lymphatic (CHALIKWAR et al., 2012). In this sense, the rational selection of the components of the lipid phase and surfactant in the development of these systems will allow the encapsulation of the drug, promoting the possible targeting of the drug to the lymphatic system by oral administration (YÁÑEZ et al., 2011) .

Furthermore, recent advances in the cerebral lymphatic drainage system highlight the influence of several factors that may impact the progress of brain disease. Despite the more irregular lymphatic drainage system compared to other peripheral tissues and organs, such as the lack of conventional lymphatic vessels, it is crucial to maintain brain homeostasis. The cerebral lymphatic drainage system comprises the perivascular pathway, the olfactory/cervical lymphatic and meningeal drainage route, and the glymphatic system. These drainage systems are essential for clearing the interstitial fluid with its constituent molecules and waste, and also for immune responses and surveillance of the brain. Sun et al (2018) summarize several factors such as aging,

genetic factors, different lymphatic drainage pathways and relationships between their dysfunction and prognosis of several neurological diseases (B. L. SUN et al., 2018) .

1.3. NANOEMULSIONS AND D PHASE EMULSIFICATION PROCESS (DPE)

In order to increase the intratumoral accumulation of anticancer drugs, the application of nanostructured systems, mainly nanoemulsion, has been highlighted in recent years. Nanoemulsions have an extensive range of applications in pharmaceuticals, food and cosmetics, being considered a potential alternative delivery system. A rational development of nanoemulsion can offer improvement in the bioavailability of drugs that are poorly soluble in water, prevent drug degradation, P-gp efflux and decrease hepatic elimination (CHOUDHURY et al., 2019). Nanoemulsions are generally composed of biocompatible components, such as those generally recognized as safe (GRAS). They have an increased capacity for packaging hydrophobic drugs and modified release of these drugs, providing greater safety and efficacy (WONG, 2020). The versatility in nanoemulsion development allows the creation of different characteristics, such as variable size, surface charge, composition, possibility of attaching to, for example, tumor-specific ligands, or P-gp inhibitors (CHOUDHURY et al., 2019). Additionally, the estimated value of the nanoemulsion market is USD 14,760.4 million by 2026, with a compound annual growth rate expansion of 8.9% from 2018 to 2026 (WONG, 2020).

Nanoemulsions are colloidal systems composed of a lipid, aqueous, and surfactant phase. They can be classified as oil in water (O/W) or water in oil (W/O), having an internal liquid lipid phase and an external aqueous phase, or vice versa, respectively (SUN et al., 2015). Unlike other lipid nanosystems, such as nanostructured lipid carriers and solid lipid nanoparticles, nanoemulsions make use only of the liquid-lipid phase in their core. This characteristic gives nanoemulsions the solubilization of a large content of drugs that have low solubility in water (GANTA et al., 2014a), increasing their bioavailability, greater stability and property as a carrier (PARVEEN et al., 2011). Thus, the potential of nanoemulsions encompasses their application as a reservoir and being a multifunctional platform for several drug delivery systems (GANTA et al., 2014b). According to the type of surfactant selected, associated or conjugated polymers, nanoemulsions can be nonionic,

cationic, or anionic. They are kinetically stable systems, but thermodynamically unstable, unlike microemulsions considered thermodynamically stable (LALLEMAND et al., 2012).

In addition to the versatility of applicable components, there are different types of processes used to prepare nanoemulsions, basically classified as high and low energy processes. The former, related to the mechanical process, includes microfluidization, high pressure homogenization (HPH), and ultrasound methods. The high energy process mechanism consists of the generation of nanoscale particles through mechanical rupture of the internal phase by intensive disruptive forces involving cavitation, collision and compression (AKHAVAN et al., 2018; SOLANS et al., 2005; TRUJILLO-CAYADO et al., 2018). The latter, related to the physical-chemical method, involves phase inversion composition (PIC), phase inversion temperature (PIT), spontaneous emulsification and D-phase emulsification (DPE) methods. These involve spontaneous alteration of the interfacial curvature of the lipid and aqueous phase, using specific conditions that depend on the hydrophilic-lipophilic balance (HLB) of the system (IZQUIERDO et al., 2004). In recent decades, high-energy processes are the most used in studies of lipid nanosystems due to the advantage of not being dependent on the HLB of the components during the formation of nanosystems. However, high cost of investment in equipment and the limitation to compounds sensitive to shear and high temperatures, aroused interest in the use of low energy processes. Low-energy processes do not require specific and expensive equipment. Thus, they can save energy in large-scale production requiring less extreme temperature. But the rigorous adjustment of the HLB involves a significant investment of time and the use of a considerable amount of surfactants. Within this perspective, the DPE process has unique properties, allowing the development of nanoemulsions that do not require strict adjustment of HLB, nor high temperatures or concentration of surfactants compared to conventional phase inversion processes (PIT and PIC). Furthermore, DPE allows the formation of a nanoemulsion loading a high concentration of the internal oil phase, with no use of solvents, which are generally limitations in the spontaneous emulsification process (YUKUYAMA et al., 2016).

The DPE process was developed by Sagitani and collaborators in 1983, but so far, few studies have been published using this process. The DPE process requires the presence of a fourth element in the composition, the polyol, unlike conventional low-energy processes in which only the aqueous, oil and surfactant phase is used (SAGITANI, 1986). The presence of liquid crystal,

usually during the conventional phase inversion process, promotes the reduction of the interfacial tension between the oil and aqueous phases, to enable the conversion of emulsions in nanometric scales during the phase transition. However, the liquid crystal structure in most cases is rigid and does not allow dispersing and retaining a high amount of oil phase (SAGITANI, 1988). According to Endoo and Sagitani, the introduction of polyol in the initial phase of the EFD process allows the conversion of the rigid liquid crystal phase into the isotropic surfactant phase (D phase), which is more flexible. With the subsequent addition of the oil phase, the isotropic phase converts into the oil phase in surfactant (O/D), making the structure gradually viscous and translucent with the progressive increase in the oil phase. This O/D structure is presented as an internal oil phase surrounded by an isotropic continuous surfactant phase, which significantly reduces the interfacial tension between the phases. With the gradual addition of remaining water, this surface tension changes, enabling the rapid conversion of the O/D phase into O/W (ENDOO; SAGITANI, 1991) (**Figure 1.3**).
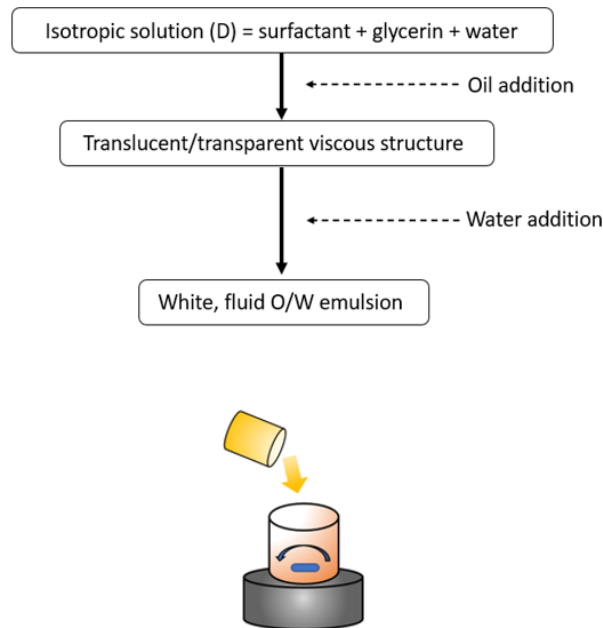
Figure 1.2: Schematic illustration of D-Phase emulsification method
O/W: oil-in-water
Source: Own authorship

It is considered challenging to obtain nanoemulsions from more polar oils than apolar oils, such as vegetable oils, when low energy processes are used. In a previous study using the DPE process, it was possible to obtain a nanoemulsion mean particle size (MPS) of approximately 30 nm, with 40.0% (w/w) of olive oil and only 2.0% (w/w) of hydrophilic surfactant (YUKUYAMA et al., 2018). Thus, the DPE process allows obtaining nanoemulsions with wide range types of oils, low surfactant concentration, using a single surfactant, without the need for specific equipment.

1.4. RATIONALE AND PREVIOUS STUDIES

Several studies contributed to developing nanoemulsions in lung cancer treatment, specifically with A549 - the human lung adenocarcinoma cell. Lee and team developed a tanshinone nanoemulsion for inhibiting A549 lung cancer cells. Tanshinone is a natural compound found in Salvia miltiorrhiza, and this nanoemulsion showed effective inhibition of A549 proliferation, penetration into the cytoplasm by endocytosis, upregulation of p21, p53 and p-JNK, and downregulation of CDK2, cyclin D1 and cyclin expression E1 in a dose-dependent manner. In addition, cell cycle impediment in the G0/G1 phase and alteration of the A549 cell microcompartment were observed. This 14.2 nm nanoemulsion was composed of Tween 80, ethanol, Capryol 90 and deionized water (LEE; LIANG; CHEN, 2016). Diferuloylmethane (DIF) is another plant-derived component with diverse pharmacological effects, including antitumor effects. It is derived from turmeric, with poor oral bioavailability and unable to reach target cells. A functional nanoemulsion hybrid lipid nanocarrier composed of diferuloylmethane (DNHLNs) was developed, using a thin film sonication dispersion method. DNHLNs increased by 1.43 to 3.23 times and 3.10 to 7.76 times, the absorption constants and permeabilities, respectively, and increased the relative bioavailability by 855% when compared to free DIF. Furthermore, DNHLNs showed higher inhibitory effects on A 549 cell viability than free DIF (SUN et al., 2016). Another multifunctional nanoemulsion was developed by trapping DNA and oppositely charged polysaccharide (CHIT)-based chitosan in the core of the nanoemulsion, loaded by indocyanine IR0780 and stabilized by gemini-type surfactants. This IR-780-charged nanocarrier covered by (DNA / CHIT) 4 bilayers had a particle size of 120 nm and a zeta potential (ZP) of +43 mV. The

in vitro test demonstrated a high internalization capacity of this nanocarrier in the A549 cell line (BAZYLIŃSKA; SACZKO, 2016). In another study, carvacrol, a monoterpenoid flavonoid from the thyme plant, was packed into a nanoemulsion by the ultrasound method. Carvacrol nanoemulsion (CANE), with a particle size of 99.1 nm and ZP of -29.89 mV, provided effective induction of apoptosis in doxorubicin-resistant A549 cells, cellular senescence and cell cycle arrest, and inhibition of autophagy (KHAN et al., 2018a). The same group developed an optimized CANE varying the proportions of carvacrol and polysorbate 80, and produced nanoemulsions from 105.5 to 169.8 nm with negative surface charge. Optimized CANE induced the production of reactive oxygen species, leading to the activation of key apoptosis regulators (p-JNK, Bax, Bcl2, cytochrome C release, caspase cascade activation). Furthermore, in vivo mouse model testing has emphasized its potential antitumor effect (KHAN et al., 2018b).

Regarding meningoencephalitis, as mentioned earlier, Nixon et al. (2018) evaluated the nanodispersion of the solid amorphous drug flubendazole in a murine model of cryptococcal meningitis. The nanodispersion showed oral bioavailability and delayed the cerebral fungal load, but the need for improvements in the formulation to inhibit this fungal load was highlighted (NIXON et al., 2018).

Despite several works published on nanoemulsions, so far, no development of nanoemulsions containing FLZ for lung cancer and meningoencephalitis treatment by oral administration has been found. Treatment of comorbidities using oral administration offers several advantages, such as ease of administration, no need for specifically trained personnel, low cost of treatment, and greater patient compliance. However, there are no effective methods for evaluating the in vitro efficacy of nanoemulsions containing drugs for oral use. Thus, there is also a need of developing a specific dissolution method to provide, for example, the selection of components and preparations containing FLZ during the development process, as well as the evaluation of the effectiveness of the final formulation.

1.5. HYPOTHESIS

1) FLZ, a drug previously evaluated for the treatment of meningoencephalitis caused by cryptococcosis, can be used as repositioning drug in the treatment of lung cancer.

2) Loading FLZ - a class II drug in CBS - in a nanoemulsion will overcome its bioavailability limitation.

3) The use of the D-Phase Emulsification method will allow to increase the loading capacity of the drug in the nanoemusion by increasing the oil concentration, decreasing the risk of toxicity by avoiding the use of high concentration of surfactant and also decreasing its mean particle size, without the use of a specific equipment.

4) The loading of FLZ in a nanoemulsion will allow to increase the effectiveness of the treatment in cryptococcosis with a safer drug concentration, compared to the previous result obtained by Nixon et al (2018).

5) The development of a new specific dissolution method for drug loaded in a nanoemulsion will allow to improve the correlation of its results with the in vivo test obtained for lung cancer and cryptococcosis, and provide a possible mechanistic insight of this dissolution profile.

1.6. OBJECTIVE

1.6.1. Overall objective

The present study aimed at the development and physical-chemical characterization of an oral FLZ-loaded nanoemulsion, and its in vivo anticancer and antifungal activities were evaluated. In addition, a specific dissolution method was developed for this FLZ-loaded nanoemulsion using a combination of a biphasic method with a modified cylinder method, with the aim of comparing different preparations using the drug FLZ.

1.6.2. Specific objective

(1) Development and optimization of stable FLZ-loaded nanoemulsion through the DPE process and statistic design

(2) Physical-chemical characterization of the nanoemulsions obtained

(3) Comparative study of FLZ-loaded nanoemulsion with different oils

(4) Evaluation of in vivo and in vitro efficacies of FLZ-loaded nanoemulsion against cryptococcal meningoencephalitis

(5) Evaluation of in vivo efficacy of FLZ-loaded nanoemulsion in the A549 xenographic model

(6) Development of a pilot dissolution method for FLZ-loaded nanoemulsion, through a combination of biphasic and modified cylinder methods, and comparative study with different preparations containing FLZ

1.7. REFERENCES

Akhavan, S., Assadpour, E., Katouzian, I., Jafari, S.M., 2018. Lipid nano scale cargos for the protection and delivery of food bioactive ingredients and nutraceuticals. Trends Food Sci Technol. https://doi.org/10.1016/j.tifs.2018.02.001

American Cancer Society, 2013. About Lung Cancer [WWW Document]. URL https://www.cancer.org/cancer/lung-cancer/about/what-is.html (accessed 11.6.22).

An, G., Murry, D.J., Gajurel, K., Bach, T., Deye, G., Stebounova, L. V., Codd, E.E., Horton, J., Gonzalez, A.E., Garcia, H.H., Ince, D., Hodgson-Zingman, D., Nomicos, E.Y.H., Conrad, T., Kennedy, J., Jones, W., Gilman, R.H., Winokur, P., 2019. Pharmacokinetics, safety, and tolerability of oxfendazole in healthy volunteers: A randomized, placebo-controlled first-inhuman single-dose escalation study. Antimicrob Agents Chemother 63. https://doi.org/10.1128/AAC.02255-18

Arrowsmith, J., 2011. Trial watch: Phase III and submission failures: 2007-2010. Nat Rev Drug Discov. https://doi.org/10.1038/nrd3375

Arrowsmith, J., Miller, P., 2013. Trial Watch: Phase II and Phase III attrition rates 2011-2012. Nat Rev Drug Discov. https://doi.org/10.1038/nrd4090

Bazylińska, U., Saczko, J., 2016. Nanoemulsion-templated polylelectrolyte multifunctional nanocapsules for DNA entrapment and bioimaging. Colloids Surf B Biointerfaces 137, 191–202. https://doi.org/10.1016/j.colsurfb.2015.07.056

Cai, S., Yang, Q., Bagby, T.R., Forrest, M.L., 2011. Lymphatic drug delivery using engineered liposomes and solid lipid nanoparticles. Adv Drug Deliv Rev. https://doi.org/10.1016/j.addr.2011.05.017

Ceballos, L., Mackenzie, C., Geary, T., Alvarez, L., Lanusse, C., 2014. Exploring the Potential of Flubendazole in Filariasis Control: Evaluation of the Systemic Exposure for Different Pharmaceutical Preparations. PLoS Negl Trop Dis 8. https://doi.org/10.1371/journal.pntd.0002838

Chalikwar, S.S., Belgamwar, V.S., Talele, V.R., Surana, S.J., Patil, M.U., 2012. Formulation and evaluation of Nimodipine-loaded solid lipid nanoparticles delivered via lymphatic transport system. Colloids Surf B Biointerfaces 97, 109–116. https://doi.org/10.1016/j.colsurfb.2012.04.027

Chapman, N., Abela-Oversteegen, L., Doubell, A., Chowdhary, V., Gurjav, U., Ong, M., 2017. NEGLECTED DISEASE RESEARCH AND DEVELOPMENT: A PIVOTAL MOMENT FOR GLOBAL HEALTH.

Chen, S.C.A., Meyer, W., Sorrell, T.C., 2014. Cryptococcus gattii infections. Clin Microbiol Rev 27, 980–1024. https://doi.org/10.1128/CMR.00126-13

Choudhury, H., Pandey, M., Gorain, B., Chatterjee, B., Madheswaran, T., Md, S., Mak, K.-K., Tambuwala, M., Chourasia, M.K., Kesharwani, P., 2019. Nanoemulsions as Effective Carriers for the Treatment of Lung Cancer, in: Nanotechnology-Based Targeted Drug Delivery Systems for Lung Cancer. Elsevier, pp. 217–247. https://doi.org/10.1016/b978-0-12-815720-6.00009-5

Chowdhary, A., Randhawa, H., Boekhout, T., Hagen, F., Klaassen, C., Meis, J., 2012. Temperate climate niche for Cryptococcus gattii in Northern Europe. Emerg Infect Dis. https://doi.org/10.3201/eid1801.111190

Coelho, C., Bocca, A.L., Casadevall, A., 2014. The Tools for Virulence of Cryptococcus neoformans, in: Advances in Applied Microbiology. Academic Press Inc., pp. 1–41. https://doi.org/10.1016/B978-0-12-800261-2.00001-3

Cohen, J.P., Sturgeon, G., Cohen, A., 2014. Measuring progress in neglected disease drug development. Clin Ther 36, 1037–1042. https://doi.org/10.1016/j.clinthera.2014.05.004

Dayan, A.D., 2003. Albendazole, mebendazole and praziquantel. Review of non-clinical toxicity and pharmacokinetics, in: Acta Tropica. Elsevier, pp. 141–159. https://doi.org/10.1016/S0001-706X(03)00031-7

De Araujo, G.L.B., Ferreira, F.F., Bernardes, C.E.S., Sato, J.A.P., Gil, O.M., De Faria, D.L.A., Loebenberg, R., Byrn, S.R., Ghisleni, D.D.M., Bou-Chacra, N.A., Pinto, T.J.A., Antonio, S.G., Ferraz, H.G., Zemlyanov, D., Gonçalves, D.S., Minas Da Piedade, M.E., 2018. A New Thermodynamically Favored Flubendazole/Maleic Acid Binary Crystal Form: Structure, Energetics, and in Silico PBPK Model-Based Investigation. Cryst Growth Des 18, 2377–2386. https://doi.org/10.1021/acs.cgd.7b01807

DiMasi, J.A., Grabowski, H.G., Hansen, R.W., 2016. Innovation in the pharmaceutical industry: New estimates of R&D costs. J Health Econ 47, 20–33. https://doi.org/10.1016/j.jhealeco.2016.01.012

Dixon, J.B., 2010. Lymphatic lipid transport: Sewer or subway? Trends in Endocrinology and Metabolism. https://doi.org/10.1016/j.tem.2010.04.003

ENDOO, M., Sagitani, H., 1991. Preparation of Triglyceride O/W Emulsions by D Phase Emulsification. Japan Oil Chemists' Society 40, 133–139. https://doi.org/10.5650/jos1956.40.133

Evans, T.C., Gavrilovich, E., Mihai, R.C., Isbasescu, I., Thelen, D., Martin, J.A., Slane, S.S., 2014. (12) Patent Application Publication (10) Pub . No .: US 2006/0222585 A1 Figure 1.

Fisher, M.C., Henk, D.A., Briggs, C.J., Brownstein, J.S., Madoff, L.C., McCraw, S.L., Gurr, S.J., 2012. Emerging fungal threats to animal, plant and ecosystem health. Nature. https://doi.org/10.1038/nature10947

Ganta, S., Singh, A., Patel, N.R., Cacaccio, J., Rawal, Y.H., Davis, B.J., Amiji, M.M., Coleman, T.P., 2014a. Development of egfr-targeted nanoemulsion for imaging and novel platinum therapy of ovarian cancer. Pharm Res 31, 2490–2502. https://doi.org/10.1007/s11095-014-1345-z

Ganta, S., Talekar, M., Singh, A., Coleman, T.P., Amiji, M.M., 2014b. Nanoemulsions in translational research - Opportunities and challenges in targeted cancer therapy. AAPS PharmSciTech. https://doi.org/10.1208/s12249-014-0088-9

Gao, F., Zhang, Z., Bu, H., Huang, Y., Gao, Z., Shen, J., Zhao, C., Li, Y., 2011. Nanoemulsion improves the oral absorption of candesartan cilexetil in rats: Performance and mechanism. Journal of Controlled Release 149, 168–174. https://doi.org/10.1016/j.jconrel.2010.10.013

Harris, J.R., Lockhart, S.R., Debess, E., Marsden-Haug, N., Goldoft, M., Wohrle, R., Lee, S., Smelser, C., Park, B., Chiller, T., 2011. Cryptococcus gattii in the united states: Clinical aspects of infection

with an emerging pathogen. Clinical Infectious Diseases 53, 1188–1195. https://doi.org/10.1093/cid/cir723

Harris, J.R., Lockhart, S.R., Sondermeyer, G., Vugia, D.J., Crist, M.B., D'Angelo, M.T., Sellers, B., Franco-Paredes, C., Makvandi, M., Smelser, C., Greene, J., Stanek, D., Signs, K., Nett, R.J., Chiller, T., Park, B.J., 2013. Cryptococcus gattii infections in multiple states outside the US Pacific Northwest. Emerg Infect Dis 19, 1620–1626. https://doi.org/10.3201/eid1910.130441

Hou, Z.-J., Luo, X., Zhang, W., Peng, F., Cui, B., Wu, S.-J., Zheng, F.-M., Xu, J., Xu, L.-Z., Long, Z.-J., Wang, X.-T., Li, G.-H., Wan, X.-Y., Yang, Y.-L., Liu, Q., 2015. Flubendazole, FDA-approved anthelmintic, targets breast cancer stem-like cells. Oncotarget 6, 6326–6340. https://doi.org/10.18632/oncotarget.3436

Hoveizi, E., Fakharzadeh Jahromi, F., 2020. Cytotoxic Effects of Flubendazole in Human Lung Cancer Cell Line A549. Jentashapir Journal of Cellular and Molecular Biology 11. https://doi.org/10.5812/jjcmb.108923

Hull, C.M., Heitman, J., 2002. Genetics of Cryptococcus neoformans. Annu Rev Genet. https://doi.org/10.1146/annurev.genet.36.052402.152652

Islan, G.A., Durán, M., Cacicedo, M.L., Nakazato, G., Kobayashi, R.K.T., Martinez, D.S.T., Castro, G.R., Durán, N., 2017. Nanopharmaceuticals as a solution to neglected diseases: Is it possible? Acta Trop. https://doi.org/10.1016/j.actatropica.2017.02.019

Izquierdo, P., Esquena, J., Tadros, T.F., Dederen, J.C., Feng, J., Garcia-Celma, M.J., Azemar, N., Solans, C., 2004. Phase behavior and nano-emulsion formation by the phase inversion temperature method. Langmuir 20, 6594–6598. https://doi.org/10.1021/la049566h

Jahchan, N.S., Dudley, J.T., Mazur, P.K., Flores, N., Yang, D., Palmerton, A., Zmoos, A.F., Vaka, D., Tran, K.Q.T., Zhou, M., Krasinska, K., Riess, J.W., Neal, J.W., Khatri, P., Park, K.S., Butte, A.J., Sage, J., 2013. A drug repositioning approach identifies tricyclic antidepressants as inhibitors of small cell lung cancer and other neuroendocrine tumors. Cancer Discov 3, 1364–1377. https://doi.org/10.1158/2159-8290.CD-13-0183

Jin, G., Wong, S.T.C., 2014. Toward better drug repositioning: Prioritizing and integrating existing methods into efficient pipelines. Drug Discov Today. https://doi.org/10.1016/j.drudis.2013.11.005

Khan, I., Bahuguna, A., Bhardwaj, M., Pal Khaket, T., Kang, S.C., 2018a. Carvacrol nanoemulsion evokes cell cycle arrest, apoptosis induction and autophagy inhibition in doxorubicin resistant-A549 cell line. Artif Cells Nanomed Biotechnol 46, 664–675. https://doi.org/10.1080/21691401.2018.1434187

Khan, I., Bahuguna, A., Kumar, P., Bajpai, V.K., Kang, S.C., 2018b. In vitro and in vivo antitumor potential of carvacrol nanoemulsion against human lung adenocarcinoma A549 cells via mitochondrial mediated apoptosis. Sci Rep 8. https://doi.org/10.1038/s41598-017-18644-9

Králová, V., Hanušová, V., Staňková, P., Knoppová, K., Čáňová, K., Skálová, L., 2013. Antiproliferative effect of benzimidazole anthelmintics albendazole, ricobendazole, and flubendazole in intestinal cancer cell lines. Anticancer Drugs 24, 911–919. https://doi.org/10.1097/CAD.0b013e3283648c69

Kronstad, J.W., Attarian, R., Cadieux, B., Choi, J., D'Souza, C.A., Griffiths, E.J., Geddes, J.M.H., Hu, G., Jung, W.H., Kretschmer, M., Saikia, S., Wang, J., 2011. Expanding fungal pathogenesis: Cryptococcus breaks out of the opportunistic box. Nat Rev Microbiol 9, 193–203. https://doi.org/10.1038/nrmicro2522

Kubíček, V., Skálová, L., Skarka, A., Králová, V., Holubová, J., Štěpánková, J., Šubrt, Z., Szotáková, B., 2019. Carbonyl reduction of flubendazole in the human liver: Strict stereospecificity, sex difference, low risk of drug interactions. Front Pharmacol 10. https://doi.org/10.3389/fphar.2019.00600

Lachau-Durand, S., Lammens, L., van der Leede, B.J., van Gompel, J., Bailey, G., Engelen, M., Lampo, A., 2019. Preclinical toxicity and pharmacokinetics of a new orally bioavailable flubendazole formulation and the impact for clinical trials and risk/benefit to patients. PLoS Neglected Tropical Diseases. 13. https://doi.org/10.1371/journal.pntd.0007026.

Lallemand, F., Daull, P., Benita, S., Buggage, R., Garrigue, J.-S., 2012. Successfully Improving Ocular Drug Delivery Using the Cationic Nanoemulsion, Novasorb. J Drug Deliv 2012, 1–16. https://doi.org/10.1155/2012/604204

Lawrence, D.S., Boyer-Chammard, T., Jarvis, J.N., 2019. Emerging concepts in HIV-associated cryptococcal meningitis. Curr Opin Infect Dis. https://doi.org/10.1097/QCO.0000000000000514

Lee, W.D., Liang, Y.J., Chen, B.H., 2016. Effects of tanshinone nanoemulsion and extract on inhibition of lung cancer cells A549. Nanotechnology 27. https://doi.org/10.1088/0957-4484/27/49/495101

Lestner, J., Mcentee, L., Johnson, A., Livermore, J., Whalley, S., Schwartz, J., Perfect, J.R., Harrison, T., Hope, W., 2017. Experimental Models of Short Courses of Liposomal Amphotericin B for Induction Therapy for Cryptococcal Meningitis. https://doi.org/10.1128/AAC

Lin, S., Yang, L., Yao, Y., Xu, L., Xiang, Y., Zhao, H., Wang, L., Zuo, Z., Huang, X., Zhao, C., 2019. Flubendazole demonstrates valid antitumor effects by inhibiting STAT3 and activating autophagy. Journal of Experimental and Clinical Cancer Research 38. https://doi.org/10.1186/s13046-019-1303-z

Longo, M., Zanoncelli, S., Colombo, P.A., Harhay, M.O., Scandale, I., Mackenzie, C., Geary, T., Madrill, N., Mazué, G., 2013. Effects of the benzimidazole anthelmintic drug flubendazole on rat embryos in vitro. Reproductive Toxicology 36, 78–87. https://doi.org/10.1016/j.reprotox.2012.12.004

Lotfi Shahreza, M., Ghadiri, N., Mousavi, S.R., Varshosaz, J., Green, J.R., 2018. A review of network-based approaches to drug repositioning. Brief Bioinform. https://doi.org/10.1093/bib/bbx017

Mackenzie, C.D., Geary, T.G., 2011. Flubendazole: A candidate macrofilaricide for lymphatic filariasis and onchocerciasis field programs. Expert Rev Anti Infect Ther. https://doi.org/10.1586/eri.11.30

Marrinefl, S.E., Morris, D.L., Dickson, B., Bogan, J.A., 1986. Pharmacokinetics of Albendazole in Man. Eur J Clin Pharmacol 30, 705–708.

Men, L., Zhang, Y., Li, K., Li, Z., Li, C., Zhang, X., Gong, X., Fang, L., 2022. Metabolism and pharmacokinetics of mebendazole in Japanese pufferfish (Takifugu rubripes). Food Additives and Contaminants - Part A 39, 912–924. https://doi.org/10.1080/19440049.2022.2052974

Michaelis, M., Agha, B., Rothweiler, F., Löschmann, N., Voges, Y., Mittelbronn, M., Starzetz, T., Harter, P.N., Abhari, B.A., Fulda, S., Westermann, F., Riecken, K., Spek, S., Langer, K., Wiese, M., Dirks, W.G., Zehner, R., Cinatl, Jaroslav, Wass, M.N., Cinatl, Jindrich, 2015. Identification of flubendazole as potential anti-neuroblastoma compound in a large cell line screen. Sci Rep 5. https://doi.org/10.1038/srep08202

Minda, D., Mioc, A., Banciu, C., Soica, C., Racoviceanu, R., Mioc, M., Macasoi, I., Avram, S., Voicu, A., Motoc, A., Trandafirescu, C., 2021. Cyclodextrin dispersion of mebendazole and flubendazole improves in vitro antiproliferative activity. Processes 9. https://doi.org/10.3390/pr9122185

Molloy, S.F., Chiller, T., Greene, G.S., Burry, J., Govender, N.P., Kanyama, C., Mfinanga, S., Lesikari, S., Mapoure, Y.N., Kouanfack, C., Sini, V., Temfack, E., Boulware, D.R., Dromer, F., Denning, D.W., Day, J., Stone, N.R.H., Bicanic, T., Jarvis, J.N., Lortholary, O., Harrison, T.S., Jaffar, S., Loyse, A., 2017. Cryptococcal meningitis: A neglected NTD? PLoS Negl Trop Dis 11. https://doi.org/10.1371/journal.pntd.0005575

Morgan, S., Grootendorst, P., Lexchin, J., Cunningham, C., Greyson, D., 2011. The cost of drug development: A systematic review. Health Policy (New York). https://doi.org/10.1016/j.healthpol.2010.12.002

Ngamskulrungroj, P., Chang, Y., Sionov, E., Kwon-Chunga, K.J., 2012. The primary target organ of cryptococcus gattii is different from that of cryptococcus neoformans in a murine model. mBio 3. https://doi.org/10.1128/mBio.00103-12

Nixon, G.L., McEntee, L., Johnson, A., Farrington, N., Whalley, S., Livermore, J., Natal, C., Washbourn, G., Bibby, J., Berry, N., Lestner, J., Truong, M., Owen, A., Lalloo, D., Charles, I., Hope, W., 2018. Repurposing and reformulation of the antiparasitic agent flubendazole for treatment of cryptococcal meningoencephalitis, a neglected fungal disease. Antimicrob Agents Chemother 62. https://doi.org/10.1128/AAC.01909-17

Nobilis, M., Jira, T., Lísa, M., Holčapek, M., Szotáková, B., Lamka, J., Skálová, L., 2007. Achiral and chiral high-performance liquid chromatographic determination of flubendazole and its metabolites in biomatrices using UV photodiode-array and mass spectrometric detection. J Chromatogr A 1149, 112–120. https://doi.org/10.1016/j.chroma.2007.01.013

Nobilis, M., Vybíralová, Z., Křížová, V., Kubíček, V., Soukupová, M., Lamka, J., Szotáková, B., Skálová, L., 2008. Sensitive chiral high-performance liquid chromatographic determination of anthelmintic flubendazole and its phase I metabolites in blood plasma using UV photodiode-array and fluorescence detection. Application to pharmacokinetic studies in sheep. J Chromatogr B Analyt Technol Biomed Life Sci 876, 89–96. https://doi.org/10.1016/j.jchromb.2008.10.032

Nygren, P., Fryknäs, M., Ågerup, B., Larsson, R., 2013. Repositioning of the anthelmintic drug mebendazole for the treatment for colon cancer. J Cancer Res Clin Oncol 139, 2133–2140. https://doi.org/10.1007/s00432-013-1539-5

Oh, E., Kim, Y.J., An, H., Sung, D., Cho, T.M., Farrand, L., Jang, S., Seo, J.H., Kim, J.Y., 2018. Flubendazole elicits anti-metastatic effects in triple-negative breast cancer via STAT3 inhibition. Int J Cancer 143, 1978–1993. https://doi.org/10.1002/ijc.31585

O'Neill, M., Geary, J.F., Agnew, D.W., Mackenzie, C.D., Geary, T.G., 2015. Invitro flubendazole-induced damage to vital tissues in adult females of the filarial nematode Brugia malayi. Int J Parasitol Drugs Drug Resist 5, 135–140. https://doi.org/10.1016/j.ijpddr.2015.06.002

Parker, A.L., Teo, W.S., McCarroll, J.A., Kavallaris, M., 2017. An emerging role for tubulin isotypes in modulating cancer biology and chemotherapy resistance. Int J Mol Sci. https://doi.org/10.3390/ijms18071434

Parveen, R., Baboota, S., Ali, J., Ahuja, A., Vasudev, S.S., Ahmad, S., 2011. Oil based nanocarrier for improved oral delivery of silymarin: In vitro and in vivo studies. Int J Pharm 413, 245–253. https://doi.org/10.1016/j.ijpharm.2011.04.041

Pereira, E.R., Jones, D., Jung, K., Padera, T.P., 2015. The lymph node microenvironment and its role in the progression of metastatic cancer. Semin Cell Dev Biol. https://doi.org/10.1016/j.semcdb.2015.01.008

Ren, T., Xu, N., Cao, C., Yuan, W., Yu, X., Chen, J., Ren, J., 2009. Preparation and therapeutic efficacy of polysorbate-80-coated amphotericin B/PLA-b-PEG nanoparticles. J Biomater Sci Polym Ed 20, 1369–1380. https://doi.org/10.1163/092050609X12457418779185

Roy S, Dhaneshwar S, Bhasin B. Drug Repurposing: An Emerging Tool for Drug Reuse, Recycling and Discovery. Curr Drug Res Rev. 2021;13(2):101-119. doi: 10.2174/2589977513666210211163711. PMID: 33573567.

Ryan, G.M., Kaminskas, L.M., Porter, C.J.H., 2014. Nano-chemotherapeutics: Maximising lymphatic drug exposure to improve the treatment of lymph-metastatic cancers. Journal of Controlled Release 193, 241–256. https://doi.org/10.1016/j.jconrel.2014.04.051

Sagitani, H., 1988. Formation of o/w emulsions by surfactant phase emulsification and the solution behavior of nonionic surfactant system in the emulsification process. J Dispers Sci Technol 9, 115–129. https://doi.org/10.1080/01932698808943980

Sagitani, H., 1986. Formation of Fine Emulsions by Surface Chemical Methods Focusing on the Mechanism of the Inversion Emulsification Method and the Surfactant (D) Phase Emulsification Method. Journal of Japan Oil Chemists' Society 35, 198–202. https://doi.org/10.5650/jos1956.35.198

Shim, J.S., Liu, J.O., 2014. Recent advances in drug repositioning for the discovery of new anticancer drugs. Int J Biol Sci. https://doi.org/10.7150/ijbs.9224

Solans, C., Izquierdo, P., Nolla, J., Azemar, N., Garcia-Celma, M.J., 2005. Nano-emulsions. Curr Opin Colloid Interface Sci. https://doi.org/10.1016/j.cocis.2005.06.004

Spadari, C. de C., Wirth, F., Lopes, L.B., Ishida, K., 2020. New approaches for cryptococcosis treatment. Microorganisms. https://doi.org/10.3390/microorganisms8040613

Spagnuolo, P.A., Hu, J., Hurren, R., Wang, X., Gronda, M., Sukhai, M.A., di Meo, A., Boss, J., Ashali, I., Zavareh, R.B., Fine, N., Simpson, C.D., Sharmeen, S., Rottapel, R., Schimmer, A.D., 2010. The antihelmintic flubendazole inhibits microtubule function through a mechanism distinct from Vinca alkaloids and displays preclinical activity in leukemia and myeloma. Blood 115, 4824–4833. https://doi.org/10.1182/blood-2009-09-243055

Speed, B., Dunt, D., 1995. Clinical and Host Differences Between Infections with the Two Varieties of Cryptococcus neoformans.

Stuchlíková, L., Králová, V., Lněničková, K., Zárybnický, T., Matoušková, P., Hanušová, V., Ambrož, M., Šubrt, Z., Skálová, L., 2018. The metabolism of flubendazole in human liver and cancer cell lines. Drug Test Anal 10, 1139–1146. https://doi.org/10.1002/dta.2369

Sun, B.L., Wang, L. hua, Yang, T., Sun, J. yi, Mao, L. lei, Yang, M. feng, Yuan, H., Colvin, R.A., Yang, X. yi, 2018. Lymphatic drainage system of the brain: A novel target for intervention of neurological diseases. Prog Neurobiol. https://doi.org/10.1016/j.pneurobio.2017.08.007

Sun, D., Wei, X., Xue, X., Fang, Z., Ren, M., Lou, H., Zhang, X., 2014. Enhanced oral absorption and therapeutic effect of acetylpuerarin based on D-α-tocopheryl polyethylene glycol 1000 succinate nanoemulsions. Int J Nanomedicine 9, 3413–3423. https://doi.org/10.2147/IJN.S63777

Sun, L., Wan, K., Hu, X., Zhang, Y., Yan, Z., Feng, J., Zhang, J., 2016. Functional nanoemulsion-hybrid lipid nanocarriers enhance the bioavailability and anti-cancer activity of lipophilic diferuloylmethane. Nanotechnology 27. https://doi.org/10.1088/0957-4484/27/8/085102

Sun, Y., Xia, Z., Zheng, J., Qiu, P., Zhang, L., McClements, D.J., Xiao, H., 2015. Nanoemulsion-based delivery systems for nutraceuticals: Influence of carrier oil type on bioavailability of pterostilbene. J Funct Foods 13, 61–70. https://doi.org/10.1016/j.jff.2014.12.030

Thakur, C., 2019. An Overview, Current Challenges of Drug Resistance, and Targeting Metastasis Associated With Lung Cancer, in: Nanotechnology-Based Targeted Drug Delivery Systems for Lung Cancer. Elsevier, pp. 21–38. https://doi.org/10.1016/b978-0-12-815720-6.00002-2

Trujillo-Cayado, L.A., Santos, J., Ramírez, P., Alfaro, M.C., Muñoz, J., 2018. Strategy for the development and characterization of environmental friendly emulsions by microfluidization technique. J Clean Prod 178, 723–730. https://doi.org/10.1016/j.jclepro.2018.01.028

Vialpando, M., Smulders, S., Bone, S., Jager, C., Vodak, D., van Speybroeck, M., Verheyen, L., Backx, K., Boeykens, P., Brewster, M.E., Ceulemans, J., Novoa de Armas, H., van Geel, K., Kesselaers, E., Hillewaert, V., Lachau-Durand, S., Meurs, G., Psathas, P., van Hove, B., Verreck, G., Voets, M., Weuts, I., Mackie, C., 2016. Evaluation of Three Amorphous Drug Delivery Technologies to Improve the Oral Absorption of Flubendazole. J Pharm Sci 105, 2782–2793. https://doi.org/10.1016/j.xphs.2016.03.003

Vigh, T., Démuth, B., Balogh, A., Galata, D.L., Van Assche, I., Mackie, C., Vialpando, M., Van Hove, B., Psathas, P., Borbás, E., Pataki, H., Boeykens, P., Marosi, G., Verreck, G., Nagy, Z.K., 2017. Oral bioavailability enhancement of flubendazole by developing nanofibrous solid dosage forms. Drug Dev Ind Pharm 43, 1126–1133. https://doi.org/10.1080/03639045.2017.1298121

Williamson, P.R., Jarvis, J.N., Panackal, A.A., Fisher, M.C., Molloy, S.F., Loyse, A., Harrison, T.S., 2016. Cryptococcal meningitis: Epidemiology, immunology, diagnosis and therapy. Nat Rev Neurol. https://doi.org/10.1038/nrneurol.2016.167

Wohlfart, S., Gelperina, S., Kreuter, J., 2012. Transport of drugs across the blood-brain barrier by nanoparticles. Journal of Controlled Release. https://doi.org/10.1016/j.jconrel.2011.08.017

Wong, T.W., 2020. Choice of nanocarrier for pulmonary delivery of cancer therapeutics. Expert Opin Drug Deliv. https://doi.org/10.1080/17425247.2020.1702021

World Health Organization, 2022. Lymphatic filariasis.

Yáñez, J.A., Wang, S.W.J., Knemeyer, I.W., Wirth, M.A., Alton, K.B., 2011. Intestinal lymphatic transport for drug delivery. Adv Drug Deliv Rev. https://doi.org/10.1016/j.addr.2011.05.019

Yoshida, G.J., 2017. Therapeutic strategies of drug repositioning targeting autophagy to induce cancer cell death: From pathophysiology to treatment. J Hematol Oncol. https://doi.org/10.1186/s13045-017-0436-9

Yoshimatsu, Y., Miyazaki, H., Watabe, T., 2016. Roles of signaling and transcriptional networks in pathological lymphangiogenesis. Adv Drug Deliv Rev. https://doi.org/10.1016/j.addr.2016.01.020

Yukuyama, M.N., Ghisleni, D.D.M., Pinto, T.J.A., Bou-Chacra, N.A., 2016. Nanoemulsion: Process selection and application in cosmetics - A review. Int J Cosmet Sci. https://doi.org/10.1111/ics.12260

Yukuyama, M.N., Oseliero, P.L.F., Kato, E.T.M., Lobënberg, R., de Oliveira, C.L.P., de Araujo, G.L.B., Bou-Chacra, N.A., 2018. High internal vegetable oil nanoemulsion: D-phase emulsification as a unique low energy process. Colloids Surf A Physicochem Eng Asp 554, 296–305. https://doi.org/10.1016/j.colsurfa.2018.06.023

Zaragoza, O., Rodrigues, M.L., de Jesus, M., Frases, S., Dadachova, E., Casadevall, A., 2009. Chapter 4 The Capsule of the Fungal Pathogen Cryptococcus neoformans. Adv Appl Microbiol. https://doi.org/10.1016/S0065-2164(09)01204-0

CHAPTER 2 – RATIONAL DESIGN OF ORAL FLUBENDAZOLE-LOADED NANOEMULSION FOR BRAIN DELIVERY IN CRYPTOCOCCOSIS

I am the first author and was responsible for conceptualization, methodology, investigation, writing - original draft

2.1. INTRODUCTION

Cryptococcal meningitis (CM) is an opportunistic infection occurring predominantly in patients with acquired immunodeficiency syndrome. It is a subacute meningoencephalitis, usually caused by inhaling yeasts or spores of *Cryptococcus* spp. present in the environment. After inhalation and a latent period in the alveoli of the lung, these organisms can proliferate and manifest as cryptococcal pneumonia or pulmonary cryptococcoma [1]. Cryptococci can spread to other organs, but due to their neurotropism, they often evolve to cerebral cryptococcoma, cryptococcal meningitis, or cryptococcal meningoencephalitis in more advanced and critical stages [2,3]. Despite widespread access to antiretroviral therapy, this disease causes approximately 180,000 deaths annually, with a higher incidence in sub-Saharan Africa. Mortality reaches 70% in these countries due to poor antiretroviral treatment or problems with treatment adherence [4,5]. However, the increasing number of HIV-negative patients has been a concern to authorities in other countries, where the incidence of CM has been growing in patients with other forms of immunosuppression such as natural or even apparently immunocompetent patients [6].

The predilection of cryptococci for the central nervous system has been associated with its specific virulence factors such as metalloproteinases and specific urease that facilitate penetration through the blood-brain barrier, enzymes that cause neuroimmunomodulation, in addition to mechanisms that facilitate survival in a nutrient-poor environment, such as in the brain [7]. *Cryptococcus* spp. has a thick polysaccharide capsule that surrounds the fungal cell impairing the host's immune response. The capsule avoids phagocytosis, but when this immunological event occurs, the yeast is able to survive, replicate and travel to the brain using macrophages as a Trojan horse. Moreover, the production of enzymes and melanin as well as biofilm formation contributed to the virulence and also favor resistance to antimicrobial agents and defense mechanisms of the host [8]. Symptoms associated with CM include headache, altered mental status, fever, nausea, vomiting, visual symptoms, and eventually, coma [9].

The currently available drugs for cryptococcosis therapy include amphotericin B administered intravenously, associated with 5-fluorocytosine and fluconazole even with poor outcomes and relapses. However, the high cost, problems concerning toxicity, and the increasing resistance of

these drugs highlights the increasing need for new strategies and alternatives for treating CM [5,10].

Flubendazole (FLZ) is an FDA-approved anthelmintic. In recent years, it has been reported to present antifungal activity against cryptococcosis [11]. However, FLZ belongs to class II in the Biopharmaceutical Classification System (BCS), which consists of drugs of high permeability but low aqueous solubility [12]. Almost 40% of new chemical entities present solubility problems in water, which negatively affects the bioavailability of these administered drugs [13]. Thus, incorporating those lipophilic drugs in a solubilized state in nanoemulsion is a promising approach to deliver them to the target site.

Nanoemulsion is an oil-in-water (O/W) or water-in-oil (W/O) structure composed of oil, water, and surfactant phases. Their mean particle size can range from 1 to 100 nm, or up to 1,000 nm since they present physicochemical or functional properties related to their dimension [14]. O/W nanoemulsion provides enhanced drug solubility, improved permeability, increased drug stability against premature hydrolytic, oxidative, or enzymatic degradation, and sustained drug release, which can reduce administered drug concentration and consequently its side effects [15,16].

The drugs currently available for treating cryptococcosis are administered intravenously, requiring trained professionals, which compromises patient compliance, leading to treatment abandonment and risk of increased drug resistance. In studies carried out with the use of flubendazole as an alternative, toxicity problems [17] and administration problems developed, such as injection site reactions [18]. Thus, there is an evident need for treatment with easy administration such as oral, low risk of toxicity, and affordable production cost, especially with regard to low-income countries. Under oral administration, the higher surface area of nanosized droplets increases the rate of drug diffusion into the outer phase of gastrointestinal (GI) fluid [19].

For this purpose, the D-Phase Emulsification (DPE) process was selected to enable preparing the O/W nanoemulsion by low-energy method, without the need for a specific tool, high pressure, or cavitation force as in the high-energy methods. Furthermore, this unique low-energy process does not require a strict adjustment of the hydrophilic-lipophilic-balance (HLB) of the system, nor high amounts of surfactant, which are challenging for conventional low-energy ones (i.e., phase inversion temperature – PIT or phase inversion composition – PIC methods) [20–22]. The combination of the DPE process with design of experiment (statistical design, DoE) opens the

possibility of developing an optimized O/W nanoemulsion with low particle size and high oil/surfactant ratio. This enables, in addition to the stability and safety related to the low concentration of surfactant and nonuse of solvent, the loading of a high concentration of the drug in a solubilized state in the oil in an O/W nanoemulsion. To the best of our knowledge, no study has been reported with an FLZ-loaded nanoemulsion for brain delivery administered by oral route to date.

Using a unique low-energy process, the DPE method, and a statistical design, the present work aims to show a process to design a FLZ-loaded combined with the rational selection of the components. This enables us to offer a new treatment alternative with multiple benefits for improving GI crossing, increasing antifungal efficacy in the brain, and minimizing systemic side effects.

2.2. MATERIAL

Flubendazole (FLZ) was obtained from the Company Changzhou Yabang—QH Pharmachem CO., LTD (Jiangsu, China). Maisine CC® (glyceryl monolinoleate) and Labrafac™ lipophile WL 1349® (Medium-chain triglycerides) were kindly donated by Gattefossée (Sao Paulo, Brazil); Miglyol® 812 N® (Medium-chain triglycerides) was a gift from IOI Oleo GmbH (Hamburg, Germany), and Captex 8000® (Glycerol Tricaprilat), Captex 300 EP / NF® (Glyceryl tricaprilate / Tricaprato) and Captex 355 EP / NF / JPE® (Glycerol Tricaprilate / Caprate) were kindly provided by ABITEC Corp. (Columbus, OH, US). Tween 80 and glycerin were purchased from Sigma-Aldrich (Brazil), Soluplus® was kindly donated from BASF (Brazil), and Milli-Q® ultrapure water was used.

2.3. METHODS

2.3.1. Preparation and optimization of nanoemulsions containing flubendazole

The development of the FLZ-loaded nanoemulsion using the DPE process was carried out first by selecting the lipid phase, followed by preparation and optimization using statistical design. The

selection of lipids aims to use a lipid that has already been approved for oral and pharmaceutical use, and which presents greater drug solubilization efficiency, preserving the stability of the final nanoemulsion.

The nanoemulsion was prepared by the DPE process according to the adaptation of the procedure described by Yukuyama et al. (2018) [23]: the isotropic mixture composed of surfactants, glycerin, and initial water was homogenized under magnetic stirring of 300 rpm at 25.0 ± 0.5 °C. The oil phase was added dropwise to this isotropic phase, and after completing the oil addition, the mixture was stirred for 20 minutes at the same condition. Subsequently, the remaining water was added dropwise to this mixture at 25.0 ± 0.5 °C and 300 rpm to form the final nanoemulsion (**Figure 2.1**).
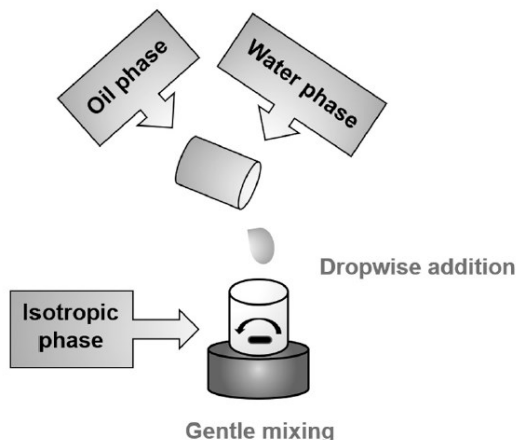
Figure 2.1: Preparation of flubendazole-loading nanoemulsion by D-Phase Emulsification process
Source: Own authorship

2.3.1.1. Selecting the lipid phase for preparing flubendazole-loaded nanoemulsion

The selection criteria for the lipid phase were as follows: liquid lipids (oils) with medium- to long-chains (C_{12} to C_{18}), commercially approved for oral administration and for pharmaceutical use. The oils were selected and subjected to a drug solubility test. FLZ and oils were added to a beaker, heated, and kept at a constant temperature between 90 to 95 °C under stirring, at 400 rpm, using a magnetic bar. The selected oils and FLZ are stable at this temperature range. An additional amount of oil was gradually incorporated until the drug was completely solubilized. After cooling,

the drug solubilization state in each oil was monitored by visual assessment for two weeks at temperature of 4.0 ± 0.5 °C and 25.0 ± 0.5 °C to detect possible drug precipitation.

2.3.1.2.   D-emulsification process (EFD) and design of experiment (DoE) for nanoemulsion preparation

A statistical approach (DoE) was used for preparations, according to the procedure described by Yukuyama et al. (2018) [23]. The independent variable was the composition parameter: the concentrations of oil phase, glycerin, and initial water. The dependent variable or response was the mean particle size (MPS). The matrices of experiments were generated using Minitab software version 18 (State College, PA, US).

2.3.1.3.   Optimization of flubendazole-loaded nanoemulsion

The Minitab 18 statistical software response optimizer tool was used to optimize the response by the desirability composite function method. The aim was to identify the highest oil phase concentration and the lowest mean particle size (MPS) of FLZ-loaded nanoemulsion. The desirability of compound (d) ranges from zero to one. One represents the lowest MPS, and zero, the largest.

2.3.2. Characterization of flubendazole-loaded nanoemulsion

2.3.2.1.   Determination of mean particle size (MPS) and polydispersity index (PDI)

The MPS and PDI of nanoemulsions were evaluated using the dynamic light scattering (DLS) method. The preparations were diluted in the appropriate ratio with Milli-Q® ultrapure water, and the results correspond to the means of three determinations, using a 90° angle. The measurements were performed with Zetasizer Nano ZS90 equipment (Malvern Instruments, Malvern, UK).

The Z average size (or mean) measured by this instrument is the intensity weighted mean hydrodynamic size mean ('harmonic intensity averaged particle diameter') of the ensemble collection of particles measured by DLS.

A value of the hydrodynamic diameter can be calculated from measurements of the diffusion coefficient by means of the Stokes–Einstein equation:

$$D_h = \frac{k_B T}{3\pi\eta D_t}$$

where

D_h = diffusion coefficient

D_t = hydrodynamic diameter

k_B = Boltzmann constant

T = temperature

η = medium viscosity

2.3.2.2.   Flubendazole entrapment efficiency

The entrapment efficiency was assessed by centrifuging the FLZ-loaded nanoemulsion with an ultrafilter (Amicon®Ultra 50 kDa - 0.5 mL) in the Centrifuge 5424-11, Eppendorf® equipment at 5000 rpm, 25 °C for 10 minutes. The FLZ in the nanoemulsion was extracted using double distilled water with an appropriate dilution. The supernatant sample (free FLZ) was analyzed by Evolution 201 spectrophotometer at 310 nm (Thermo Fisher Scientific Inc., Waltham, MA, USA).

The entrapment efficiency (EE%) was calculated by the following **Eq. (2.1)**:

$$EE\ \% = \frac{\text{weight of total FLZ– weight of FLZ in the supernatant}}{\text{weight of total FLZ}} \times 100 \qquad \textbf{(Equation 2.1)}$$

2.3.2.3.   Stability of flubendazole-loaded nanoemulsion

The nanoemulsions were stored in a borosilicate glass bottle for three months at 25 ± 0.5 °C. MPS and PDI analyses and visual inspection of the systems were carried out immediately after their preparation and at 30-day intervals.

2.3.3.   *In vitro and in vivo evaluation of anti-cryptococcal activity of flubendazole-loaded nanoemulsion*

Cryptococcus neoformans H99 (ATCC 208821) and *Cryptococcus gattii* (ATCC 56990) were used in this study. The isolates were stored in brain and heart infusion broth with 20% glycerol at -80 °C. For use in experiments, the isolates were recovered in Sabouraud dextrose medium, and the yeasts were subcultured twice in Sabouraud dextrose agar for 48 to 72 h at 35 ºC.

2.3.3.1.   In vitro antifungal activity

The minimum inhibitory concentration (MIC) of crude-free flubendazole (FLZ) and flubendazole-loaded nanoemulsion (MAF M) were determined by the broth microdilution method [24]. FLZ and the standard antifungal amphotericin B (AMB) were dissolved in DMSO. FLZ, AMB and nanoemulsions were serially diluted (1:2) in RPMI 1640 medium buffered with 0.16 M of 3-morpholinopropane-1-sulfonic acid (both from Sigma-Aldrich, St. Louis, MO, USA) in 96-well flat-bottomed microplates. A 100-µL aliquot of the fungal suspension was added to the wells obtaining a final fungal concentration of 0.5 to 2.5 x 10^3 CFU/mL, and the concentrations of 0.12 to 64 µg/mL for AMB or crude-free FLZ and 0.1 to 75 µg/mL for FLZ in nanoemulsion. In parallel, FLZ-free nanoemulsion (MAF M BR) was diluted under the same conditions to assess the possible interference of the formulation's constituents in the antifungal activity. The microplates were incubated for 48 to72 h at 35 ºC, and the MIC was determined by observing the fungi under an inverted optical microscope, and it was defined as the lowest concentration that inhibited 90% of fungal growth compared to the growth of untreated cells.

2.3.3.2. Toxicity in an invertebrate model of *Galleria mellonella*

The toxicity of FLZ, at a dose of 5 mg/kg, in nanoemulsions (MAF M) and FLZ-free MAF (MAF M BR) were evaluated by injecting 10 µL into the last pro-leg of the *G. mellonella* larvae (2.0 cm to 2.5 cm in length) with the aid of Hamilton syringes [25]. Larvae that received only PBS were included in the trial as a control group for the vehicle and the mechanical injury caused by the needle (n = 20 larvae/group). The larvae were incubated at 37 ºC and survival was monitored every 24 h for up to 5 days to construct the survival curve. In parallel, the surviving larvae were evaluated for their movement, cocoon formation, and melanization, and the morbidity curve was constructed following the grade model in which the larvae health index is calculated as the sum of the evaluated criteria [26].

2.3.3.3. Antifungal efficacy of flubendazole-loaded nanoemulsion in a murine model of systemic cryptococcosis

Male mice of BALB/c strain, aged 6 to 8 weeks and with an average weight of 25 g, were kept in pathogen-free conditions with water and food *ad libitum* in the Animal Experimentation vivarium of the Department of Microbiology (ICB/USP). All experimental protocols were previously approved by the Ethics Committee for Animal Use of the Institute of Biomedical Sciences (CEUA-ICB / USP, nº. Reg 68/2014) and followed the National Institutes of Health guide for the care and use of Laboratory animals (NIH Publications No. 8023, revised 1978).

C. neoformans H99 yeasts were cultivated twice in Sabouraud dextrose broth for 48 to 72 h at 35 °C. The fungal suspension was adjusted to 1×10^7 CFU/mL of PBS for infection of 100 µL of the inoculum (1×10^6 CFU) into the tail vein of the mice. After 1 hour of infection, the animals (4 - 5 per group) were orally treated by gavage method with 200 µL b.i.d. for five days with FLZ 0.8 mg/kg in aqueous suspension (FLZ S) or FLZ-loaded nanoemulsion (MAF M). The infected and untreated animals (NT group) received water(vehicle) as a control of the fungal infection.

On the seventh day after infection, the animals were euthanized. The organs (lung and brain) were excised, weighed, macerated in PBS, and plated on Sabouraud dextrose agar with 50 µg/mL chloramphenicol, incubated at 35 °C for 72 h. The number of colonies was counted to calculate

colony-forming units per gram of tissue (CFU/g) and, subsequently, the results expressed in Log CFU/g. A fraction of each tissue was separated during the removal of the organs, fixed in 10% formaldehyde in PBS, sectioned, and stained with eosin-hematoxylin (HE) for histopathological analysis.

2.4. RESULTS

2.4.1. *Preparation, optimization and physicochemical characterization of flubendazole-loaded nanoemulsions*

2.4.1.1. Selecting the lipid phase for developing a flubendazole-loaded nanoemulsion

According to the literature survey, the following oils, all commercialized for oral pharmaceutical administration with different chemical structures, were selected and subjected to the drug's solubility test. The results of the solubility test are shown in **Table 2.1.**

Table 2.1: Flubendazole solubility in liquid lipids.

Samples	Flubendazole[a] (mg)	Lipid[a] (g)	Solubilization (0 day)
Maisine CC®	5.06	15.01	Yes[b]
Labrafac Lip. WC1349®	5.25	24.86	Yes
Miglyol 812®	5.32	33.32	Yes
Captex 8000®	5.78	34.39	No
Captex 300®	5.05	38.66	No
Captex 355®	5.65	42.56	No

[a] total amount of drug / lipid used in the solubility test;

[b] no presence of precipitate during 14 days visual analysis

Maisine CC® showed superior FLZ solubilization compared to other lipids. Different from the triglycerides, the monoglyceride containing Maisine CC® may present higher polarity. The FLZ,

despite its low water solubility, has a particular polarity that may have contributed to the higher solubility of the oil compared to other triglycerides.

There was no precipitation of drug at 4.0 and 25.0 ± 0.5 °C after 14-day stability test with Maisine CC®, indicating the solubilized state of the drug in this oil.

According to this solubility result, the following FLZ concentration was used in the subsequent tests, as oil phase: 5.0 mg of FLZ in 15 g of Maisine CC®.

2.4.1.2. D-Phase Emulsification (DPE) process - Design of Experiment (DoE)

Design of experiment (DoE) allows evaluating multiple interactions between independent variables in experiments, unlike the conventional method one-factor-at-a-time [27]. The Box-Behnken response surface tool was used in this study. It indicates the main effects and interactions of the evaluated factors, with the advantage of reducing the number of experiments compared to other response surface methods, such as the central composite design. The method of obtaining the nanoemulsions and their optimization must be planned rationally, using the appropriate design of experiments. Thus, the study will allow for understanding of the process and preparation variables that influence the product's quality characteristics, highlighting their respective advantages and disadvantages.

The influence of independent variables: concentration of oil phase, glycerin, and initial water on MPS characteristics was evaluated. The test matrix (**Table 2.2**) shows the concentrations used for the variables: oil phase, glycerin, and initial water. The matrix and the analysis of the results were performed using Minitab 18 software, with Box-Behnken response surface tool with three central points.

The surfactants were used in the fixed concentrations of 2.0% (w/w) of Tween 80 and 3.0% (w/w) of the Soluplus®: H_2O mixture (1: 2). It corresponds to the total of 3.0% (w/w) surfactant phase. The remaining water was q.s. 100.0% (w/w).

According to the results shown in **Table 2.2**, the MPS of the prepared nanoemulsions varied from 35.88 to 1000 nm and PDI at the minimum value of 0.399.

Table 2.2: Box-Behnken experimental matrix for developing flubendazole-loaded nanoemulsion

Order	Oil phase (% w/w)	Glycerin (%w/w)	Initial water (%w/w)	MPS (nm)	PDI
1	50.0	3.0	2.0	35.88 ± 1.52	0.421 ± 0.024
2	60.0	5.0	1.0	58.09 ± 4.41	0.507 ± 0.041
3	60.0	4.0	0.0	49.65 ± 4.31	0.399 ± 0.107
4	40.0	5.0	1.0	1000	
5	40.0	4.0	0.0	1000	
6	50.0	4.0	1.0	45.10 ± 2.52	0.451 ± 0.021
7	40.0	3.0	1.0	1000	
8	60.0	4.0	2.0	50.10 ± 4.22	0.486 ± 0.035
9	50.0	4.0	1.0	38.48 ± 1.25	0.452 ± 0.002
10	50.0	3.0	0.0	45.60 ± 3.56	0.501 ± 0.012
11	50.0	5.0	2.0	32.81 ± 1.26	0.436 ± 0.014
12	60.0	3.0	1.0	35.21 ± 0.98	0.475 ± 0.012
13	50.0	4.0	1.0	42.76 ± 1.36	0.527 ± 0.102
14	40.0	4.0	2.0	1000	
15	50.0	5.0	0.0	44.82 ± 1.46	0.440 ± 0.046

MPS: mean particle size and **PDI:** polydispersity index

The analysis of variance (ANOVA) of the resulting quadratic polynomial models for the MPS of the FLZ-loaded nanoemulsion is shown in **Table 2.3**. The significant independent variable was the lipid concentration ($P = 0.000$). The lack of adjustment was not significant ($P = 0.267$), indicating minimal pure errors and the good adequacy of the proposed quadratic polynomial model.

Table 2.3: Analysis of variance for different models fitted-response to evaluate the mean particle size (MPS) of flubendazole-loaded nanoemulsion with the following variables: lipid, glycerin and initial water concentration (all % w/w)

Source	DF	SS (adj.)	MS (adj.)	F-value	P-value
Model	7	2684061	383437	13899.91	0.000
Linear	3	1811710	603903	21891.99	0.000
Oil (% w/w)	1	1811609	1811609	65672.29	**0.000**
Glycerin (%w/w)	1	45	45	1.64	0.241
Initial water (%w/w)	1	57	57	2.05	0.195
Square	1	872218	872218	31618.61	0.000
Oil (%w/w)* Oil (%w/w)	1	872218	872218	31618.61	**0.000**
Interaction	3	132	44	1.60	0.274
Oil (%w/w)* Glycerin (%w/w)	1	131	131	4.74	0.066
Oil (%w/w)* Initial water (%w/w)	1	0	0	0.00	0.967
Glycerin (%w/w))* Initial water (%w/w)	1	1	1	0.05	0.834
Error	7	193	28		
Lack of fit	5	171	34	3.03	**0.267**
Pure error	2	23	11	*	*
Total	14	2684254			

R^2 = 99.99 %; **R^2(aj)** = 99.99; **R^2(pred)** = 99.95%

DF: degrees of freedom; **SS (adj).:** sequential sums of squares; **MS (adj):** adjusted sequential mean square; **F value:** value on the F distribution; **P-value:** lack-of-fit adjustment; **R^2:** multiple correlation coefficient; **R^2 (aj):** adjusted multiple correlation coefficient; **R^2 (pred):** predicted correlation coefficient.

The quadratic regression model demonstrated the coefficient of determination (R^2) for the MPS of 99.99%, indicating that this response value can be attributed to the identified independent variables. The adjusted determination coefficient (R^2 aj) was 99.99%, revealing an excellent

statistical model. The predicted determination coefficient of the adjusted model (R^2 prev) was 99.95%, indicating how well the model predicts responses to new observations (**Table 2.3**).

The quadratic model for MPS of FLZ-loaded nanoemulsion was generated, as shown in the regression equation, in noncoded factor units (**Equation 2.2**):

MPS (nm) = 14609.8 - 533.24 Oil - 25.6 Glycerin - 0.9 Initial Water + 4.83 Oil * Oil + 0.57Oil * Glycerin + 0.01Oil * Initial Water - 0.57 Glycerin * Initial Water (all % w/w)   (**Equation 2.2**)

According to the residual plots shown in **Figure 2.2**, the points show linear behavior in the normal probability plot, and the histogram showed a normal residual distribution. They are in a homoscedastic linear model with normally distributed errors. The graph of residuals versus the adjusted value indicated the noncorrelation between the model of residues and the adjusted values. The residuals versus the order of the data showed random behavior around the residual zero line, indicating that the error terms are independent, with no serial correlation.
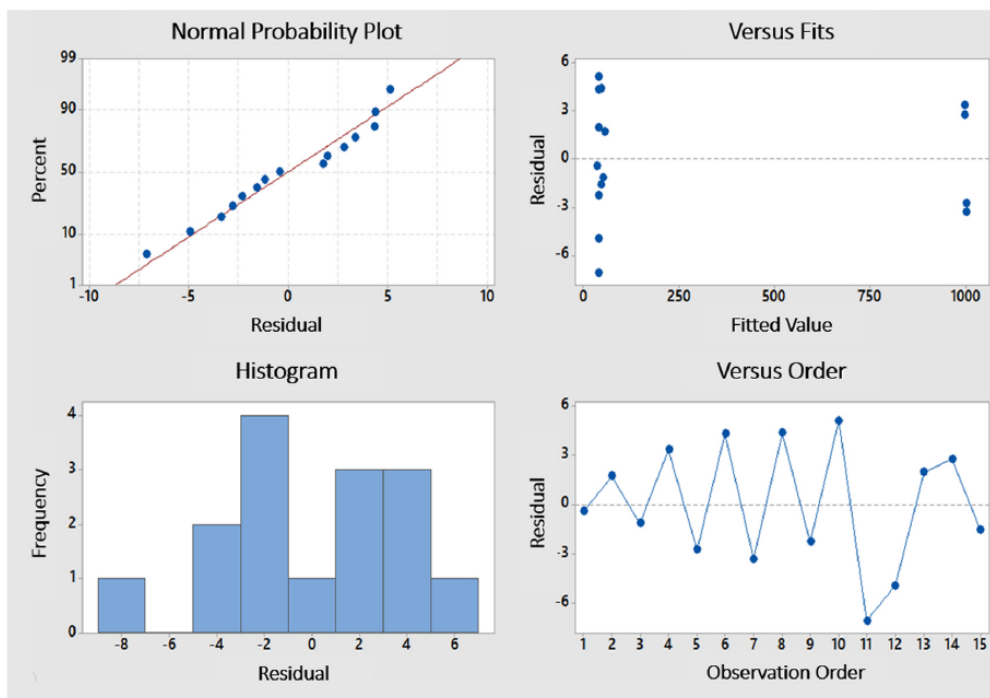
Figure 2.2: Residual graphs for composition variable of flubendazole-loaded nanoemulsion prepared by DPE process.
Source: Minitab®

Figure 2.3 shows the graph of the main effects on MPS of FLZ-loaded nanoemulsion. The test results revealed that only the oil phase concentration contributes significantly to the reduction of MPS. The oil phase concentration has a quadratic effect on MPS and inversely proportional to the oil concentration. The concentration of glycerin and initial water does not contribute to reducing MPS.
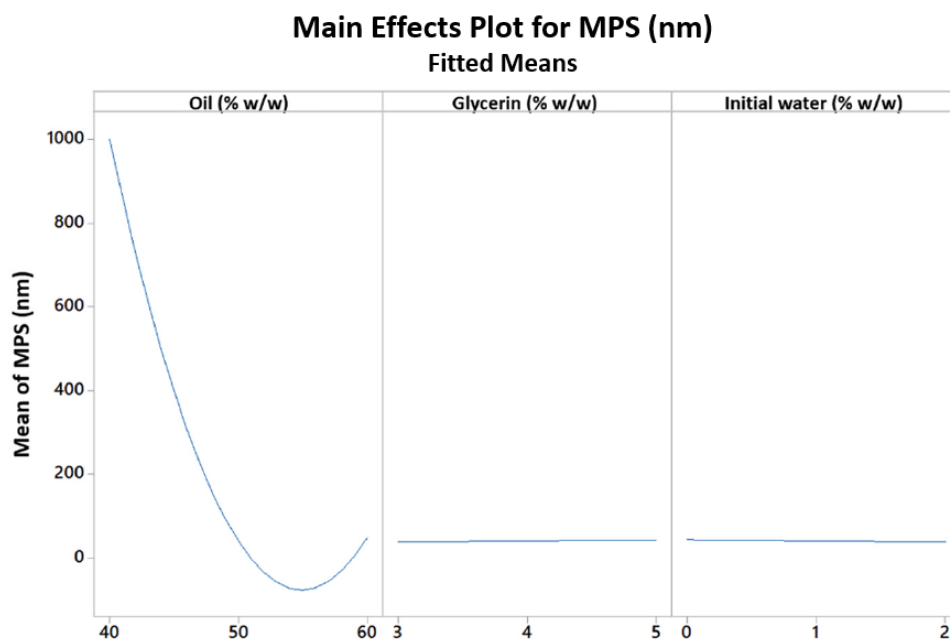
Figure 2.3: Main effects graph for the evaluation of the mean particle size (MPS) of flubendazole-loaded nanoemulsion.
Source: Minitab®

2.4.1.3. D-Phase Emulsification (DPE) process – Optimization

The process of optimization of the FLZ-loaded nanoemulsion (MAF M), based on the regression equation, indicated a condition to produce lower MPS when a higher concentration of the oil phase was used. The optimum conditions within desirability of 0.9944 were found combining a concentration of 60.0% (w / w) of oil phase, 2.0% (w / w) of glycerin, and 4.0% (w / w) of initial water, providing a theoretical MPS of 38.19 nm (**Figure 2.4**). The experimental value resulting from these conditions was MPS of 35.02 ± 1.54 nm, with a PDI of 0.452 ± 0.016. The

predicted and experimentally obtained MPS through **Equation 2.2**, as shown in **Table 2.4**, validated the proposed model.
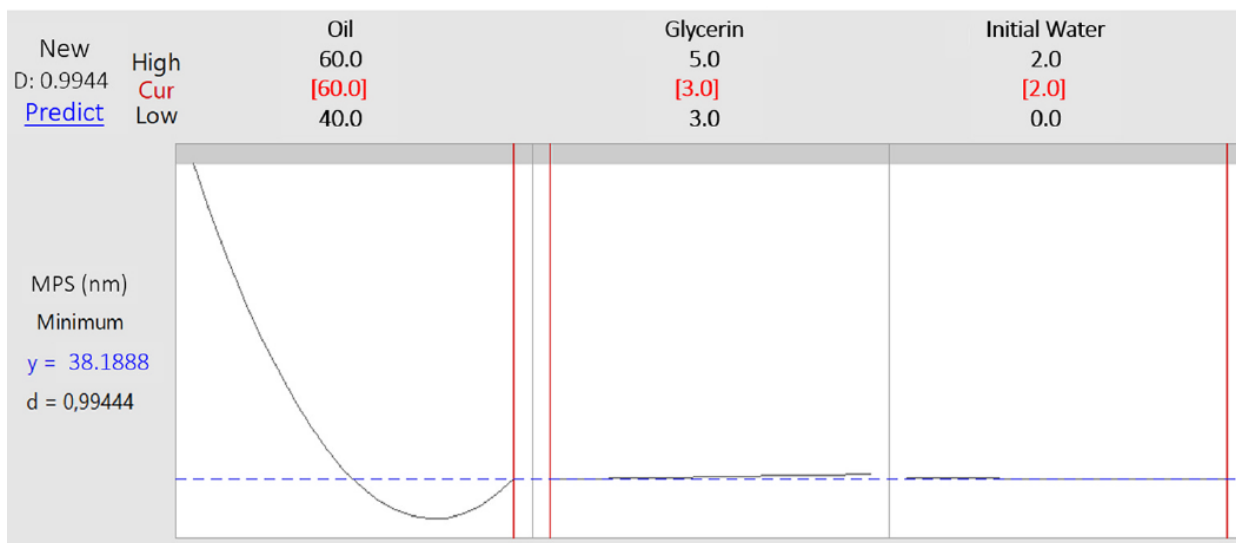
Figure 2.4: Optimization plot for flubendazole-loaded nanoemulsion for mean particle size as a function of components variables by D-Phase Emulsification process.
Source: Minitab®

Table 2.4: Theoretical and experimental value of the mean particle size (MPS) of flubendazole-loaded nanoemulsion optimized by response surface

	Oil (% w/w)	Glycerin (%w/w)	Initial water (%w/w)	Theoretical MPS (nm)	Experimental MPS (nm)	Experimental PDI
MAF M	60.0	3.0	2.0	38.19	35.02 ± 1.54	0.452 ± 0.016

*MAF M contains 20 mg flubendazole in 100 g of nanoemulsion

This MPS of the optimized nanoemulsion, MAF M, demonstrated the efficiency of the process to obtain a very small particle size structure, despite the high oil phase concentration at 60.0% (w/w). The PDI of approximately 0.450 is satisfactory, indicating a suitable particle size homogeneity.

2.4.1.4. Flubendazole entrapment efficiency of the optimized nanoemulsion

The quantification of FLZ was carried out using spectrophotometry at a wavelength of 310 nm, with the supernatant diluted in acetonitrile. The blank nanoemulsion was used to avoid interference or overlapping from the excipients of the nanoemulsion formulation. The calibration curve of FLZ concentration (x, µg/mL) versus absorbance (y) was y = 0.0372 x + 0.1121, with a correlation coefficient of 0.9929.

The FLZ-loaded nanoemulsion (MAF M) resulted in a final EE% of 97.40%.

2.4.1.5.Stability test of optimized nanoemulsion

The stability result of MAF M nanoemulsion for three months at 25.0 °C is shown in **Table 2.5**.

Despite the high oil phase concentration compared to the surfactant concentration, the nanoemulsion was stable for three months, indicating no significant variation of MPS and PDI during this period. The reduced MPS obtained by the synergistic combination of statistical optimization and the DPE process may have overcome the limitation of the Ostwald ripening phenomenon, which is considered the leading cause of nanoemulsion destabilization. The addition of Soluplus® that provides steric stabilization may also have contributed to the stability of this system.

Table 2.5: Stability of flubendazole-loaded nanoemulsion (MAF M) during three months at 25 °C

Time	MPS (nm)	PDI	Visual aspect
0 D	35.02 ± 1.54	0.452 ± 0.016	Stable
1 M	36.42 ± 2.04	0.441 ± 0.011	Stable
2 M	37.05 ± 1.33	0.451 ± 0.028	Stable
3 M	33.08 ± 1.43	0.422 ± 0.018	Stable

MPS: mean particle size; **PDI:** polydispersity index; **D:** day and **M:** month

2.4.2. *In vitro and in vivo evaluation of anticryptococcal activity*

2.4.2.1. In vitro antifungal activity

Assessing the in vitro antifungal activity of FLZ, in nanoemulsion (MAF M) and in solution (FLZ), the MIC values for both were lower than 0.1 to 0.12 µg/mL against *C. neoformans* and *C. gattii*. In contrast, standard antifungal AMB showed an expected antifungal effect (**Table 2.6**). Relevant information was that the components of nanoemulsion had no inhibitory effect against fungal growth, not even in the highest tested dilution for FLZ-free MAF (25%).

Table 2.6: Susceptibility of *Cryptococcus neoformans* H99 and *Cryptococcus gattii* ATCC 56990 to flubendazole in solution (FLZ) and in nanoemulsion (MAF M).

	MIC (µg/mL)	
Samples	*C. neoformans* H99	*C. gattii* ATCC56990
MAF M	≤0.10	≤0.10
FLZ	≤0.12	≤0.12
AMB	0.25	0.25

MIC = minimum inhibitory concentration; AMB = amphotericin B

2.4.2.2. Toxicity test in an invertebrate model of *Galleria mellonella*

Treatments using FLZ-loaded nanoemulsion 5 mg/kg (MAF M) or FLZ-free MAF (MAF M BR) did not damage the larvae. Both treatments maintained 100% larval survival, like the control group PBS. In addition, the larvae health index did not show significant differences between the treated and PBS groups (**Figure 2.5**), demonstrating that nanoemulsions have no toxic effect in an invertebrate model of *G. mellonella*.
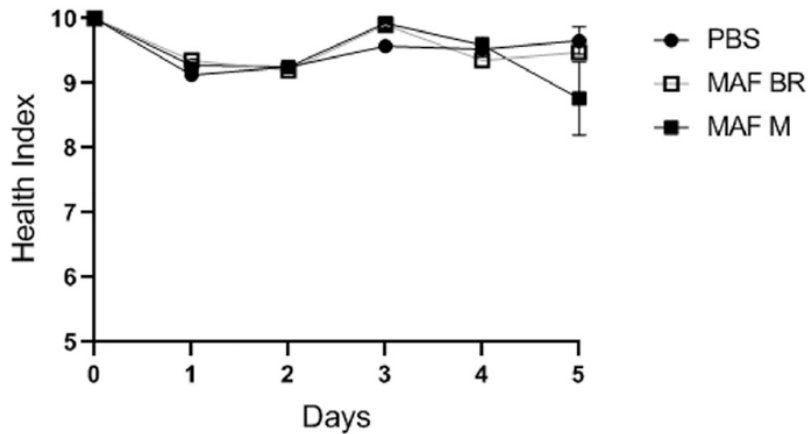
Figure 2.5: Morbidity curve of *Galleria mellonella* larvae treated with flubendazole-loaded nanoemulsion at dose of 5 mg/kg (MAF M) or flubendazole-free MAF (MAF M BR). PBS group is a control for vehicle and mechanical injury caused by needle. The morbidity curve w was analyzed by two-way ANOVA (p > 0.05).

Source: Own authorship

2.4.2.3. Antifungal efficacy of flubendazole-loaded nanoemulsion in a murine model of systemic cryptococcosis

Mice infected with *C. neoformans* H99 yeasts and treated with FLZ-loaded nanoemulsion (MAF M) or crude-free FLZ suspension (0.8 mg/Kg of FLZ for both formulations), bid for five days orally, were euthanized on the seventh day to assess the fungal burden on the brain and lungs. Treatment with the MAF nanoemulsion reduced the fungal burden on the lungs and brain compared to the untreated control, while the crude-free FLZ suspension did not show antifungal activity (**Figure 2.6**). Although FLZ-loaded nanoemulsion did not significantly reduce the fungal burden in the brain, it reduced approximately 29.3% of CFU/g, while in the lungs, this formulation reduced approximately 16.1% of the fungal burden ($P = 0.0106$) compared to the untreated group (**Figure 2.6**). In this regard, the fungal load was also reduced in the histological sections of animals treated with MAF M in contrast to the crude-free FLZ treatment, corroborating the CFU data (**Figure 2.S1**) (Supplementary Information).
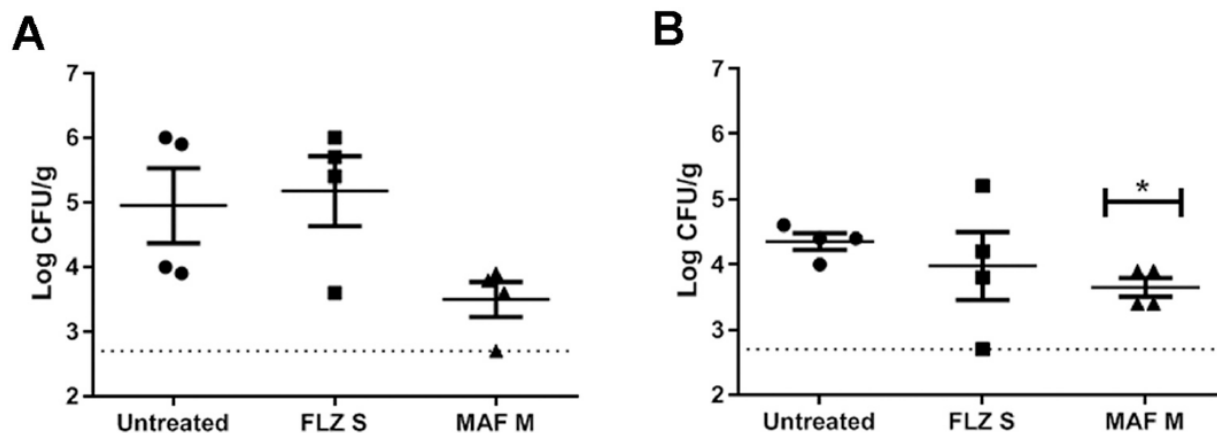
Figure 2.6: Fungal burden in the brain (A) and lungs (B) of mice infected with *Cryptococcus neoformans* H99 and treated with crude-free flubendazole in suspension (FLZ S) or flubendazole-loaded nanoemulsion (MAF M). N = 4 animals/group; *P < 0.05 compared with the untreated group (student t-test). Fungal burden data are represented by the mean ± standard deviation. Source: Own authorship

2.5. DISCUSSION

Diseases caused by cryptococcosis are a worldwide concern due to the high incidence in patients with HIV/AIDS and the increase in non-HIV patients. Currently available medications present problems of high cost, difficult administration, toxicity, or resistance. Cryptococcal meningitis has been listed among the most neglected diseases in the world, according to the 2016 Global Incentives for Neglected Diseases (G-Finder) Report [28]. Thus, the development of new safe medicine, affordable for low-income people and that offers patient compliance to fight against health emergencies and assisting neglected populations, is unquestionable.

Here, a 35-nm FLZ-loaded O/W nanoemulsion containing a high oil/surfactant ratio, administered orally and safe, has been successfully developed by the DPE process with a process temperature of 25 °C and without the need for specific equipment.

2.5.1. *D-Phase emulsification process and Design of Experiment:*

In the present work, the DPE process showed that there is no need for a well-balanced combination of hydrophilic and lipophilic surfactants, nor the use of organic solvents to obtain nanoemulsion. Moreover, in the main effect curve, we observed the inversely proportional correlation between oil concentration and MPS (**Figure 2.3**), also seen in a previous report with different composition [23]. Usually, the MPS of nanoemulsions increases with increasing oil phase concentration in conventional preparations [29]. Thus, this opposite phenomenon makes DPE a unique process: this is a low-energy process that does not require equipment based on high pressure, shear force, or cavitation; it is a physical-chemical method that reduces the interfacial tension between the oil and water phases at least, under the correct hydrophilic-lipophilic-balance (HLB) of the system. Nevertheless, unlike conventional low-energy processes, such as phase inversion temperature or composition (PIT and PIC, respectively), the DPE method does not require a strict adjustment of HLB. It requires polyol as the fourth component of the system [20]. The polyol (glycerin) seems to be a promoter of the formation of the isotropic phase in combination with surfactant and initial water, lowering the interfacial tension between the phases, which facilitates the incorporation of a large amount of oil phase and easy conversion into fine nanoemulsion, under gentle agitation [22]. The combined application of this process with the design of the experiment (DoE) allowed the obtaining of optimized O/W nanoemulsion with high oil concentration (60.0% w/w) and only 3.0% (w/w) of hydrophilic surfactants. The preparation process, possible at a temperature of 25 °C, saves time and energy on an industrial scale, and avoids problems caused by factors such as water loss through evaporation or component degradation.

2.5.2. *Flubendazole-loaded nanoemulsion to overcome gastrointestinal and blood-to-brain barriers*

Nanoemulsions can overcome the challenge of drug bioavailability administered orally. However, the blood-brain barrier (BBB) is another challenge that restricts the effective delivery of drugs to the brain. This specialized capillary network system that regulates and protects the central nervous system (CNS) is composed of a complex tight junction, a wide range of efflux transporters

(e.g., P-glycoprotein, multidrug resistance proteins, and the solute-carrier superfamily), minimizing the efficient transport of drugs into it [30]. Recent studies have demonstrated the effectiveness of nanoemulsions for drug delivery, to the CNS under oral administration: olmesartan medoxomil-loaded nanoemulsion, an angiotensin II receptor blocker, showed improved oral bioavailability with prolonged pharmacodynamic activity and reduced toxicity to the brain [31]; the nanoemulsion containing Darunavir, for treating infection by HIV, was developed for oral administration and showed 2.65-fold greater brain uptake of the drug-loaded in nanoemulsion than drug suspension [19].

This present study focuses on several well-selected elements to circumvent barriers in delivering drug from the gastrointestinal (GI) tract to the brain.

2.5.2.1. Contribution of lipid phase

The drug is loaded in the solubilized form in the lipid phase of nanoemulsion. This state may eliminate the dissolution step of drugs in aqueous fluids in the GI tract and promote its direct transfer to the membranes of the GI tract, improving the drug bioavailability [32].

Furthermore, the oil type greatly contributes to drug delivery–an exciting study of nanoemulsion of polyunsaturated fatty acids (PUFA) oils, administered orally, has shown the rapid distribution of the drug in the brain. PUFA oils are known for their rich content of omega-3 and omega-6 fatty acids, both of which are linoleic acid compounds [33]. The selective mechanism of PUFA entry explains this phenomenon due to the presence of PUFA transporters in the abluminal membrane of the BBB endothelial cells [34]. Maisine CC® is composed of linoleic mono-di and triglycerides–thus, we can hypothesize that it will be an ideal drug delivery lipid carrier to target the brain.

2.5.2.2. Contribution of surfactant

Tween 80 is indicated to favor the bioavailability of the preparations due to its activity of inhibiting the efflux mechanism. This surfactant is well known for modulating the P-gp efflux

pumps and the function of CYP450 enzymes [19]. Tween 80 is also recognized as a permeability enhancer through BBB. In addition to the inhibition activity in BBB P-gp efflux pumps [35], this surfactant generally increases the fluidization of the cell membrane and opens the tight junctions of this site [5].

2.5.2.3. Contribution of drug structure

Studies with benzimidazole derivatives have shown interesting results in recent years as anticryptococcal agents. In the study of 727 drugs tested against *C. neoformans*, the drugs fenbendazole, mebendazole and FLZ showed the highest activity, interfering with biofilm formation, fungal morphology, cell proliferation, and intracellular parasitism [10]. The in vitro antifungal test showed an inhibitory effect of FLZ against *C. neoformans* with a modal MIC of 0.078 to 0.125 µg/mL [11,36]; and similar results were obtained here for FLZ, in its crude-free form or loaded nanoemulsion. The FLZ-loaded nanoemulsion in our study demonstrated the further contribution of the solubilized state of FLZ in the form of nanoemulsion to the increase of efficiency.

Concerning the BBB bypass of FLZ loaded in nanoemulsion, several neuronal pathways are supposed to improve drug transportation. First is the physicochemical aspect of FLZ. To circumvent the BBB challenge, drugs must pass through the tight junction of this tissue, which is known to be almost 5-fold smaller than other tissues of the body. Consequently, drugs with molecular weight (MW) above 400 to 500 g/mol are not considered to have an effective BBB crossover [37]. FLZ MW is 313.29 g/mol, which favors the BBB crossing. Besides, after reaching the capillary interface of the brain, the hydrophobicity of the FLZ molecule can pass through the lipid cell membranes employing passive diffusion, unlike hydrophilic molecules that do not allow efficient permeation [30]. Second, the primary anthelmintic activity mechanism of FLZ is known as the binding of the β-subunit of tubulin, similar to the colchicine-binding site, causing microtubule disorganization and blocking cell division [38]. However, an additional target may be involved: a study using molecular dynamics simulation demonstrates that FLZ has a stable interaction with Atg4B protein [39]. An interesting study evaluating the Atg4B protein in rat tissue demonstrated the greater expression of this protein and mRNA in the brain compared to other

tissues. This protein is associated with autophagy, a degradation pathway in eukaryotic cells that may play an essential role in preserving the metabolism of neurons in the central nervous system under physiological and pathological conditions. Although the direct relationship with meningoencephalitis caused by cryptococcosis has not yet been elucidated, this affinity of FLZ with this protein may influence this treatment efficacy since autophagy seems to be involved in cellular homeostasis, neurodegenerative diseases, cancer, and bacterial and viral infections [40].

2.5.3. *Flubendazole-loaded nanoemulsion efficacy and safety*

FLZ shows limitations under oral administration due to its poor systemic bioavailability. Intramuscular administration of this drug as a suspension was performed as an alternative for onchocerciasis treatment and demonstrated high efficacy in humans. But it failed due to serious injection site reactions [18]. To overcome these problems, several oral nanosystems were developed to increase the FLZ bioavailability. For cryptococcal meningitis, an elegant test performed by Nixon et al. (2018) demonstrated the oral bioavailability of nanodispersion of the amorphous solid FLZ in mice. The dose of 12 mg of FLZ (mg/kg body weight/day) for seven days resulted in a reduction of approximately 2 log CFU/g in fungal burden compared to that of the vehicle-treated controls. There was no significant fungal burden reduction at doses below 12 mg/kg compared to the untreated mice [11].

In the present work using FLZ-loaded nanoemulsion, a reduction of the fungal burden in the brain of approximately 1.4 logs CFU/g (30%) was observed compared to the untreated animals. The total administered dose of FLZ was 1.6 mg FLZ/kg body weight/day (0.8 mg/kg b.i.d.), for five days, which corresponds to 7.5-fold lower than the dose of 12 mg in the previous nanodispersion.

Despite the emergence of these promising FLZ-based formulations, the risk/benefit profile raises concerns considering human safety. A toxicity study was carried out by Lachau-Durand et al. (2019), using oral administration of amorphous solid dispersion formulation of FLZ in rats for two weeks. The administered doses ranged from 10 to 30 mg (as a basis)/kg body weight/day (mg eq./kg/day), and results indicated several negative effects in hematological and gastrointestinal systems, also in the testis and thymus at that concentration range. However, results showed the no-

observed-adverse-effect level (NOAEL) at 5 mg eq./kg/day in males and 2.5 mg eq./kg/day in females. Based on these results, the authors reported no possible effective use of FLZ within the safe exposure dose [17]. Another study used pregnant female Sprague-Dawley rats, dosed on a gestational day (GD) 9.5 and 10.5, and embryos/fetuses were evaluated on GD 11.5, 12.5, or 20. Results showed no interference of FLZ with rat embryofetal development only at the dosage of 2 mg eq./kg/day [41].

In order to overcome these limitations established by previous studies, for the first time, we developed a nanoemulsion containing FLZ with an effective and safe dose in treating cryptococcal meningitis. Under a dose of 1.6 mg/kg/day in an in vivo assay in mice by oral administration, this nanoemulsion was able to overcome the gastrointestinal and blood-brain barriers and reduce approximately 30% of fungal burden compared to the control of the drug micronized form (suspension).

Also, we designed tests employing *Galleria mellonella* as an alternative model to using animals, offering superior ability to predict toxicity in mammals, unlike others such as in vitro tests [42,43]. Results obtained from the larvae morbidity curve showed that the FLZ-loaded nanoemulsion, at a dose of 5 mg/Kg, and the blank nanoemulsion, did not present toxicity in the *G. mellonella* larvae. This demonstrated the safe profile of the present orally administered FLZ-loaded nanoemulsion for cryptococcosis treatment, even at a dose approximately 3-fold higher than what we used in the efficacy test.

Thus, we can assume that, compared to the solid amorphous nanodispersions, the drug solubilized in the form of nanoemulsion, and the accurate selection of components may favor its bioavailability by oral route, optimizing its transport, whether through blood or lymphatic system, overcoming the BBB to achieve favorable antifungal concentration in the brain.

For future development, several approaches can be considered for further efficacy enhancement: increasing daily dosage of FLZ-loaded nanoemulsion (up to 2.0-2.5 mg eq./kg/day), or the association with other drugs, as it is conducted with the currently available drugs. Kopecká [44,45] carried out interesting studies with *C. neoformans*, indicating that treatment with a single drug, such as microtubule inhibitors (vincristine, methyl benzimidazole-2-ylcarbamate, nocodazole, thiabendazole) or the actin inhibitor latrunculin A, inhibited cell division. However, resistant cells emerged later, and only the combination of microtubule inhibitors with actin

inhibitor drugs resulted in an effective interruption of cell division in *C. neoformans*. Therefore, exploring new synergy by combining the FLZ-loaded nanoemulsion with other drugs with complementary function may be another strategy for the promising treatment of brain-targeted cryptococcosis.

Furthermore, unlike conventional development processes using the one-factor-at-a-time method, in which only one of the variables is modified, while the others remain fixed, here we used the DoE statistical design. The advantage of the DoE is that it allows the optimization of a formulation by studying the influences of multiple variables in a reduced number of experiments [46]. Additionally, the selection of the safety test using the invertebrate larvae model may help spur international trends regarding alternative methods for the use of animals.

2.6. CONCLUSIONS

The present work introduced readers to an alternative process design, with its step-by-step description aiming to develop a tailored drug-loaded nanosystem, without the need for specific tools. Using DPE process, DoE, and judicious selection of the components, a 35 nm FLZ-loaded O/W nanoemulsion with 60.0% oil phase was successfully developed.

The rationally designed nanoemulsion, with careful selection of components, oil with high FLZ solubility efficacy, and low surfactant ratio, could overcome the limitations of previous works and provide multiple benefits ranging from improving the GI and BBB crossing, increasing drug delivery in the brain, minimizing systemic side effects. Differing from current available drugs for cryptococcus treatment, this oral administered FLZ-loaded nanoemulsion also offers notable benefits including its noninvasiveness and easy administration without requiring specifically trained people, resulting in greater patient compliance. In addition to the affordable production cost, these are the key factors that highlight the present work as a promising alternative to overcome shortcomings in the current standard of care treatment for cryptococcosis.

2.7. REFERENCES

[1]   S.C.A. Chen, W. Meyer, T.C. Sorrell, Cryptococcus gattii infections, Clinical Microbiology Reviews. 27 (2014) 980–1024. https://doi.org/10.1128/CMR.00126-13.

[2]   S.C.A. Chen, M.A. Slavin, C.H. Heath, E. Geoffrey Playford, K. Byth, D. Marriott, S.E. Kidd, N. Bak, B. Currie, K. Hajkowicz, T.M. Korman, W.J.H. McBride, W. Meyer, R. Murray, T.C. Sorrell, Clinical manifestations of cryptococcus gattii infection: Determinants of neurological sequelae and death, Clinical Infectious Diseases. 55 (2012) 789–798. https://doi.org/10.1093/cid/cis529.

[3]   C.M. Hull, J. Heitman, Genetics of Cryptococcus neoformans, Annual Review of Genetics. 36 (2002) 557–615. https://doi.org/10.1146/annurev.genet.36.052402.152652.

[4]   D.S. Lawrence, T. Boyer-Chammard, J.N. Jarvis, Emerging concepts in HIV-associated cryptococcal meningitis, Current Opinion in Infectious Diseases. 32 (2019) 16–23. https://doi.org/10.1097/QCO.0000000000000514.

[5]   C. de C. Spadari, F. Wirth, L.B. Lopes, K. Ishida, New approaches for cryptococcosis treatment, Microorganisms. 8 (2020) 1–15. https://doi.org/10.3390/microorganisms8040613.

[6]   P.R. Williamson, J.N. Jarvis, A.A. Panackal, M.C. Fisher, S.F. Molloy, A. Loyse, T.S. Harrison, Cryptococcal meningitis: Epidemiology, immunology, diagnosis and therapy, Nature Reviews Neurology. 13 (2016) 13–24. https://doi.org/10.1038/nrneurol.2016.167.

[7]   C. Coelho, A.L. Bocca, A. Casadevall, The Tools for Virulence of Cryptococcus neoformans, in: Advances in Applied Microbiology, Academic Press Inc., 2014: pp. 1–41. https://doi.org/10.1016/B978-0-12-800261-2.00001-3.

[8]   R.C. May, N.R.H. Stone, D.L. Wiesner, T. Bicanic, K. Nielsen, Cryptococcus: From environmental saprophyte to global pathogen, Nature Reviews Microbiology. 14 (2016) 106–117. https://doi.org/10.1038/nrmicro.2015.6.

[9]   M.C. Fisher, D.A. Henk, C.J. Briggs, J.S. Brownstein, L.C. Madoff, S.L. McCraw, S.J. Gurr, Emerging fungal threats to animal, plant and ecosystem health, Nature. 484 (2012) 186–194. https://doi.org/10.1038/nature10947.

[10] L.S. Joffe, R. Schneider, W. Lopes, R. Azevedo, C.C. Staats, L. Kmetzsch, A. Schrank, M. Del Poeta, M.H. Vainstein, M.L. Rodrigues, The anti-helminthic compound mebendazole has multiple antifungal effects against Cryptococcus neoformans, Frontiers in Microbiology. 8 (2017) 1–14. https://doi.org/10.3389/fmicb.2017.00535.

[11] G.L. Nixon, L. McEntee, A. Johnson, N. Farrington, S. Whalley, J. Livermore, C. Natal, G. Washbourn, J. Bibby, N. Berry, J. Lestner, M. Truong, A. Owen, D. Lalloo, I. Charles, W. Hope, Repurposing and reformulation of the antiparasitic agent flubendazole for treatment of cryptococcal meningoencephalitis, a neglected fungal disease, Antimicrobial Agents and Chemotherapy. 62 (2018) 1–39. https://doi.org/10.1128/AAC.01909-17.

[12] T. Vigh, B. Démuth, A. Balogh, D.L. Galata, I. Van Assche, C. Mackie, M. Vialpando, B. Van Hove, P. Psathas, E. Borbás, H. Pataki, P. Boeykens, G. Marosi, G. Verreck, Z.K. Nagy, Oral bioavailability enhancement of flubendazole by developing nanofibrous solid dosage forms, Drug Development and Industrial Pharmacy. 43 (2017) 1126–1133. https://doi.org/10.1080/03639045.2017.1298121.

[13] K.T. Savjani, A.K. Gajjar, J.K. Savjani, Drug Solubility: Importance and Enhancement Techniques, ISRN Pharmaceutics. 2012 (2012) 1–10. https://doi.org/10.5402/2012/195727.

[14] U.S. Food & Drug Administration, Guidance for industry considering whether an FDA-regulated product involves the application of nanotechnology, Biotechnology Law Report. 30 (2014) 613–616. https://doi.org/10.1089/blr.2011.9814.

[15] M.A. Bazán Henostroza, K.J. Curo Melo, M. Nishitani Yukuyama, R. Löbenberg, N. Araci Bou-Chacra, Cationic rifampicin nanoemulsion for the treatment of ocular tuberculosis, Colloids and Surfaces A: Physicochemical and Engineering Aspects. 597 (2020) 124755. https://doi.org/10.1016/j.colsurfa.2020.124755.

[16] S. Tiwari, M. Amiji, A Review of Nanocarrier-Based CNS Delivery Systems, Current Drug Delivery. 3 (2006) 219–232. https://doi.org/10.2174/156720106776359230.

[17] S. Lachau-Durand, L. Lammens, B.J. van der Leede, J. van Gompel, G. Bailey, M. Engelen, A. Lampo, Preclinical toxicity and pharmacokinetics of a new orally bioavailable flubendazole

formulation and the impact for clinical trials and risk/benefit to patients, PLoS Neglected Tropical Diseases. 13 (2019). https://doi.org/10.1371/journal.pntd.0007026.

[18]   A. Dominguez-Vazquez, H.R. Taylor, A.M. Ruvalcaba-Macias, R.P. Murphy, B.M. Greene, A.R. Rivas-Alcala, F. Beltran-Hernandez, COMPARISON OF FLUBENDAZOLE AND DIETHYLCARBAMAZINE IN TREATMENT OF ONCHOCERCIASIS, The Lancet. 321 (1983) 139–143. https://doi.org/10.1016/S0140-6736(83)92753-8 (accessed September 20, 2021).

[19]   J. Desai, H. Thakkar, Enhanced oral bioavailability and brain uptake of Darunavir using lipid nanoemulsion formulation, Colloids and Surfaces B: Biointerfaces. 175 (2019) 143–149. https://doi.org/10.1016/j.colsurfb.2018.11.057.

[20]   H. Sagitani, Formation of o/w emulsions by surfactant phase emulsification and the solution behavior of nonionic surfactant system in the emulsification process, Journal of Dispersion Science and Technology. 9 (1988) 115–129. https://doi.org/10.1080/01932698808943980.

[21]   M.N. Yukuyama, E.T.M. Kato, G.L.B. de Araujo, R. Löbenberg, L.M. Monteiro, F.R. Lourenço, N.A. Bou-Chacra, Olive oil nanoemulsion preparation using high-pressure homogenization and D-phase emulsification – A design space approach, Journal of Drug Delivery Science and Technology. 49 (2019) 622–631. https://doi.org/10.1016/j.jddst.2018.12.029.

[22]   H. Endoo, M., Sagitani, Preparation of Triglyceride O/W Emulsions by D Phase Emulsification, J. Oil Sci. 40 (1991) 133–139. https://doi.org/10.5650/jos1956.40.133.

[23]   M.N. Yukuyama, P.L.F. Oseliero, E.T.M. Kato, R. Lobënberg, C.L.P. de Oliveira, G.L.B. de Araujo, N.A. Bou-Chacra, High internal vegetable oil nanoemulsion: D-phase emulsification as a unique low energy process, Colloids and Surfaces A: Physicochemical and Engineering Aspects. 554 (2018) 296–305. https://doi.org/10.1016/j.colsurfa.2018.06.023.

[24]   M.P. Weinstein, J.S. Lewis, A.M. Bobenchik, S. Campeau, S.K. Cullen, M.F. Galas, H. Gold, R.M. Humphries, T.J. Kirn, B. Limbago, A.J. Mathers, T. Mazzulli, S.S. Richter, M. Satlin, A.N. Schuetz, P.J. Simner, M100 Performance Standards for Antimicrobial Susceptibility Testing, 31st Edition, 31st ed., 2021.

[25]   M. Frenkel, M. Mandelblat, A. Alastruey-Izquierdo, S. Mendlovic, R. Semis, E. Segal, Pathogenicity of Candida albicans isolates from bloodstream and mucosal candidiasis assessed in

mice and Galleria mellonella, Journal de Mycologie Medicale. 26 (2016) 1–8. https://doi.org/10.1016/j.mycmed.2015.12.006.

[26]   J.M.S. Loh, N. Adenwalla, S. Wiles, T. Proft, Galleria mellonella larvae as an infection model for group A streptococcus, Virulence. 4 (2013) 419–428. https://doi.org/10.4161/viru.24930.

[27]   S.M. Dordević, N.D. Cekić, M.M. Savić, T.M. Isailović, D. V. Randelović, B.D. Marković, S.R. Savić, T.T. Stamenić, R. Daniels, S.D. Savić, Parenteral nanoemulsions as promising carriers for brain delivery of risperidone: Design, characterization and in vivo pharmacokinetic evaluation, International Journal of Pharmaceutics. 493 (2015) 40–54. https://doi.org/10.1016/j.ijpharm.2015.07.007.

[28]   N. Chapman, L. Abela-Oversteegen, A. Doubell, V. Chowdhary, U. Gurjav, M. Ong, NEGLECTED DISEASE RESEARCH AND DEVELOPMENT: A PIVOTAL MOMENT FOR GLOBAL HEALTH, 2017.

[29]   H. Choudhury, M. Pandey, B. Gorain, B. Chatterjee, T. Madheswaran, S. Md, K.-K. Mak, M. Tambuwala, M.K. Chourasia, P. Kesharwani, Nanoemulsions as Effective Carriers for the Treatment of Lung Cancer, Elsevier Inc., 2019. https://doi.org/10.1016/b978-0-12-815720-6.00009-5.

[30]   S. Ganta, D. Deshpande, A. Korde, M. Amiji, A review of multifunctional nanoemulsion systems to overcome oral and CNS drug delivery barriers, Molecular Membrane Biology. 27 (2010) 260–273. https://doi.org/10.3109/09687688.2010.497971.

[31]   B. Gorain, S.K. Bhattamishra, H. Choudhury, U. Nandi, M. Pandey, P. Kesharwani, Overexpressed Receptors and Proteins in Lung Cancer, Elsevier Inc., 2019. https://doi.org/10.1016/b978-0-12-815720-6.00003-4.

[32]   S.B. Tiwari, M.M. Amiji, Improved oral delivery of paclitaxel following administration in nanoemulsion formulations, Journal of Nanoscience and Nanotechnology. 6 (2006) 3215–3221. https://doi.org/10.1166/jnn.2006.440.

[33]   T.K. Vyas, A. Shahiwala, M.M. Amiji, Improved oral bioavailability and brain transport of Saquinavir upon administration in novel nanoemulsion formulations, International Journal of Pharmaceutics. 347 (2008) 93–101. https://doi.org/10.1016/j.ijpharm.2007.06.016.

[34] J. Edmond, Essential polyunsaturated fatty acids and the barrier to the brain: The components of a model for transport, Journal of Molecular Neuroscience. 16 (2001) 181–193. https://doi.org/10.1385/JMN:16:2-3:181.

[35] J. Kreuter, Nanoparticulate systems for brain delivery of drugs, Advanced Drug Delivery Reviews. 64 (2012) 213–222. https://doi.org/10.1016/j.addr.2012.09.015.

[36] M. Truong, L.G. Monahan, D.A. Carter, I.G. Charles, Repurposing drugs to fast-track therapeutic agents for the treatment of cryptococcosis, PeerJ. 2018 (2018) 1–18. https://doi.org/10.7717/peerj.4761.

[37] W.M. Pardridge, Blood-brain barrier drug targeting: the future of brain drug development., Molecular Interventions. 3 (2003) 90–105. https://doi.org/10.1124/mi.3.2.90.

[38] P.A. Spagnuolo, J. Hu, R. Hurren, X. Wang, M. Gronda, M.A. Sukhai, A. Di Meo, J. Boss, I. Ashali, R.B. Zavareh, N. Fine, C.D. Simpson, S. Sharmeen, R. Rottapel, A.D. Schimmer, The antihelmintic flubendazole inhibits microtubule function through a mechanism distinct from Vinca alkaloids and displays preclinical activity in leukemia and myeloma, Blood. 115 (2010) 4824–4833. https://doi.org/10.1182/blood-2009-09-243055.

[39] L. Zhang, M. Guo, J. Li, Y. Zheng, S. Zhang, T. Xie, B. Liu, Systems biology-based discovery of a potential Atg4B agonist (Flubendazole) that induces autophagy in breast cancer, Molecular BioSystems. 11 (2015) 2860–2866. https://doi.org/10.1039/c5mb00466g.

[40] K. Yoshimura, M. Shibata, M. Koike, K. Gotoh, M. Fukaya, M. Watanabe, Y. Uchiyama, Effects of RNA interference of Atg4B on the limited proteolysis of LC3 in PC12 cells and expression of Atg4B in various rat tissues, Autophagy. 2 (2006) 200–208. https://doi.org/10.4161/auto.2744.

[41] M. Longo, S. Zanoncelli, M. Messina, I. Scandale, C. Mackenzie, T. Geary, K. Marsh, D. Lindley, G. Mazué, In vivo preliminary investigations of the effects of the benzimidazole anthelmintic drug flubendazole on rat embryos and fetuses, Reproductive Toxicology. 49 (2014) 33–42. https://doi.org/10.1016/j.reprotox.2014.06.009.

[42] E. Allegra, R.W. Titball, J. Carter, O.L. Champion, Galleria mellonella larvae allow the discrimination of toxic and non-toxic chemicals, Chemosphere. 198 (2018) 469–472. https://doi.org/10.1016/j.chemosphere.2018.01.175.

[43] O.L. Champion, S. Wagley, R.W. Titball, Galleria mellonella as a model host for microbiological and toxin research, Virulence. 7 (2016) 840–845. https://doi.org/10.1080/21505594.2016.1203486.

[44] M. Kopecká, Effects of microtubule and actin inhibitors on cryptococcus neoformans examined by scanning and transmission electron microscopy, Chemotherapy. 60 (2014) 99–106. https://doi.org/10.1159/000371413.

[45] M. Kopecká, Microtubules and Actin Cytoskeleton of Cryptococcus neoformans as Targets for Anticancer Agents to Potentiate a Novel Approach for New Antifungals, Chemotherapy. 61 (2016) 117–121. https://doi.org/10.1159/000437134.

[46] J.M. Gutiérrez, C. González, A. Maestro, I. Solè, C.M. Pey, J. Nolla, Nano-emulsions: New applications and optimization of their preparation, Current Opinion in Colloid and Interface Science. 13 (2008) 245–251. https://doi.org/10.1016/j.cocis.2008.01.005.

2.8.SUPPLEMENTARY INFORMATION
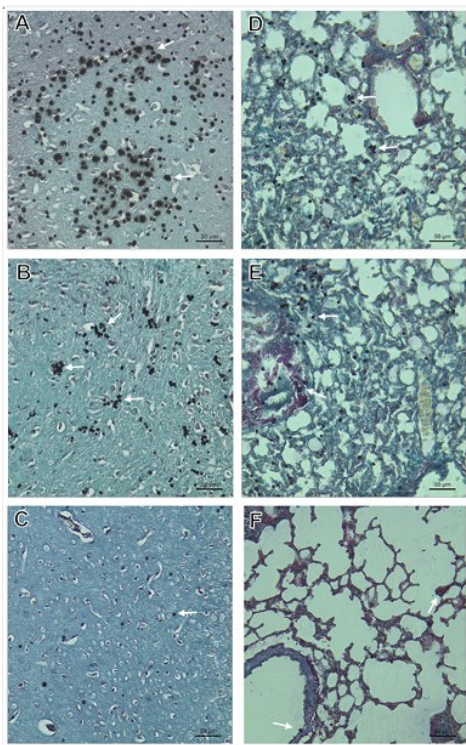
Figure 2.S1. Histopathological sections of brain (A, B and C) and lungs (D, E and F) of mice infected with *Cryptococcus neoformans* H99 and treated with flubendazole at dose of 0.8 mg/kg, in suspension (FLZ S) or in nanoemulsion (MAF M). **A and D)** untreated group. **B and E)** treated with FLZ S. **C and F**) treated with MAF M. White arrows indicate yeasts. Bars: 50 µm.

Source: Own authorship

CHAPTER 3 – UNVEILING MICROTUBULE DYNAMICS IN LUNG CANCER: RECENT FINDINGS AND PROSPECTS FOR DRUG DELIVERY TREATMENT

I am the first author and was responsible for Conceptualization, Investigation, Resources, Data Curation, Project administration, Writing - Original Draft and Funding acquisition

3.1. Introduction

Microtubules are a dynamic and extensive network of hollow and cylindrical structures, comprising heterodimers of α- and β-tubulin proteins. The binding of the plus and minus ends of these heterodimers form protofilaments that can be associated laterally to generate microtubules. Microtubules have a distinct polarity: the α-tubulin proteins represent the minus end, and β-tubulin proteins represent the plus end, which is capped in the GTP-bound state (Pecqueur et al., 2012) (**Figure 3.1**). Microtubules' continuous shrinkage or growth occurs by removing or adding tubulin heterodimers, respectively. These shrinkage (catastrophe phase) and growth (rescue phase) phases are highly dynamic in the plus end, where β-tubulin proteins are exposed. Microtubules are essential for determining cell shape, cell motility, cell differentiation, intracellular transport of proteins and organelles, and creation of the mitotic spindle for accurate chromosomal segregation during the cell division (Nasedkin et al., 2021). For intracellular transport of compounds, microtubules recruit motor proteins kinesin and dynein via acetylation on lysine 40 of α-tubulin. Kinesin *walks* on the minus ends of the microtubule tracks and dynein on the plus end to carry their cargo by protein-to-protein interactions with other adaptor proteins (Ong et al., 2020; Parker et al., 2017; Vona et al., 2021).
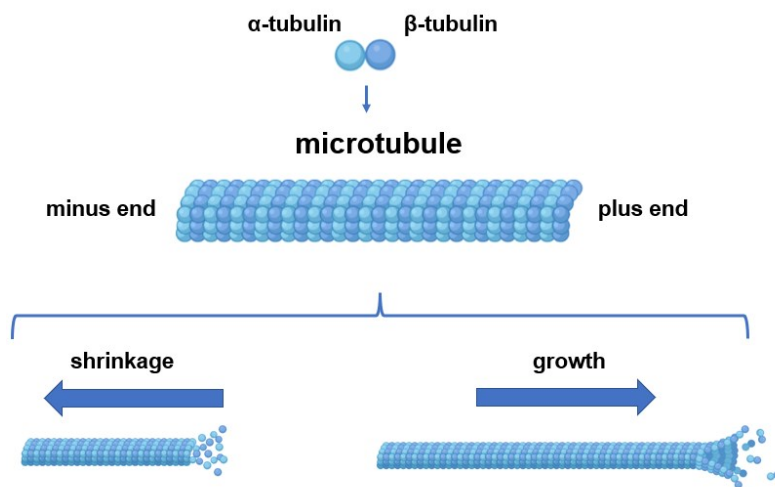
Figure 3.1: Structure of microtubule with polymerization (growth) and depolymerization (shrinkage) processes

Source: Own authorship

The development and assembly of microtubules occur in the G2 segment as well as the mitosis prophase of cells (G2/M phase) (Sharifi-Rad et al., 2021). During the mitotic phase, microtubules are nucleated at the centrosome, an organelle that acts as the main microtubule organizing center. Polymerization of microtubules promotes elongation that expands them towards the cell periphery, resulting in the formation of mitotic spindle fibers. These spindle fibers pull chromosomes to opposite ends of the cell, allowing the correct chromosome segregation. The error in segregation due to impaired spindle formation leads to the spindle assembly checkpoint, causing cell arrests and apoptotic cell death (Kanakkanthara and Miller, 2021). Moreover, the dysfunction of microtubules may induce several diseases, including cancer.

Lung cancer is one of the main causes of death worldwide, alongside breast cancer in women and prostate cancer in men (World Health Organization). Among patients diagnosed with this type of cancer, approximately 17.8% have a 5-year survival, and nearly 50% die within the first year due to poor cancer diagnosis, which may progress to advanced stages of the disease (Thakur, 2019).

Histologically, lung cancer is classified into two groups: non-small cell lung cancer (NSCLC) and small cell lung cancer (SCLC). The former is the most frequent type, and it accounts for approximately 90% of all lung cancer occurrences. The following subtypes comprise NSCLC: adenocarcinoma, squamous cell carcinoma, and large cell carcinoma, and they are preferentially located in the peripheral lungs. SCLC is responsible for about 10% of total lung cancer and is preferentially located in the bronchi, the central airways. SCLC grows and spreads faster than NSCLS, so it tends to respond better to chemotherapy and radiation therapy (Chen et al., 2022; Choudhury et al., 2019; Wong, 2020).

Several factors, including those of external or internal origin, can lead to the development of lung cancers. External factors include, for example, cigarette smoke, air pollutants, and ionizing radiation, in which smoking is responsible for nearly 85% of cancer cases. According to studies, long-term smokers have a possibility of developing lung cancer 10 to 30 times greater than nonsmokers, indicating the risk of these components in the initiation, progression, and malignancy of lung cancer (Thakur, 2019). Internal factors are attributed to the genetic and epigenetic changes that involve the onset and development of lung cancer (Choudhury et al., 2019; Thakur, 2019).

Several enzymes and cancer cell receptors can interact with the normal biological functions of cells and promote angiogenesis, which consists of the formation of new blood vasculature, diffusion of this vasculature to invade surrounding tissues, migration of cancer cells and their spread to distant organs (Pasquier et al., 2006). In the case of lung adenocarcinoma, several oncogenic factors are possibly involved, such as anaplastic lymphoma kinase (ALK), mesenchymal to epithelial transition (MET), epidermal growth factor receptor (EGFR) v-Raf murine sarcoma viral oncogene homolog B1 (BRAF), and oncogene Kirsten rat sarcoma virus (KRAS) (Thakur, 2019) .

Since several high-quality reviews on microtubules are already available, this review aims to focus on the most recent findings related to interactions between microtubules and lung cancer to support development of future delivery treatments. In this regard, we divided this manuscript into the following items: (1) current treatment based on microtubule-targeted therapy; (2) microtubule subtypes and their influence on lung cancer; (3) new findings of microtubule functions and interactive agents for future clinical applications, which involve bioelectrical function, kinetochore interaction, mitochondria dynamics, and ciliogenesis; (4) new biomarkers or microtubule-based therapy for lung cancer; and (5) nano-based therapies.

3.2. Current treatment of lung cancer in microtubule-based therapy

Current lung cancer treatment involves complicated processes from chemotherapy to surgery, radiotherapy, radiofrequency/microwave ablation, and immunotherapy (Imran et al., 2020; Sharifi-Rad et al., 2021). Unfortunately, patients have undergone surgery with NSCLC showed reoccurrence in 33% of cases, and 26% presented reoccurrence within 10 years (Fink-Neuboeck et al., 2020). The first-line agents for lung cancer treatments include crizotinib, platinum-based chemotherapy, pembrolizumab, cisplatin combined with, eg, paclitaxel (PTX), and others, and second-line ones include osimertinib, alectinib, immunotherapy, platinum-based chemotherapy, docetaxel (DTX) combined with other agents. In most cases, these treatments are used in combination (Shah et al., 2022).

Since the key feature of cancer cell growth is rapid cell proliferation, microtubules are strategic targets for treating various cancer diseases, including lung cancer. Microtubule-targeting

agents (MTA) have been used for several years, and they are one of the most widely used chemotherapeutics. They are categorized into two types: microtubule-stabilizing agents (MSAs) and microtubule-destabilizing agents (MDA). MSAs attach to the tubulin heterodimers and, by increasing their lateral interactions, lead to increased microtubule polymerization and stabilization. MDAs, in contrast, decrease the interactions of heterodimers and lead to microtubule depolymerization. Generally, these effects are reached when the MTAs are applied at high concentrations (Tangutur et al., 2017). The MSAs include taxanes, and MDAs include eg, vinca alkaloids, colchicines, which are all plant-derived drugs (Garcia-Oliveira et al., 2021). The interference of these MTAs on microtubule dynamics during cell mitosis affects the mitotic spindle formation, leading to cell proliferation blockage, activation of metaphase-spindle-assembly-checkpoint (SAC)—also known as the metaphase-to-anaphase transition, the mechanism that prevents chromosome segregation errors, resulting in so-called *mitotic catastrophe*, which induces apoptotic cell death (Hevia and Fanarraga, 2020). MTAs also affect the intracellular transport of organelles and proteins along microtubule fiber tracks during cell interphase (Serpico et al., 2020).

Paclitaxel (PTX) belongs to taxane groups and enhances the microtubule stability by linking to the β-subunit of tubulin and hampering the microtubule depolymerization process, affecting the G2/M phase. Thus, PTX prevents cell replication. More specifically, PTX has the taxane ring and homochiral ester side chains at C13 that have important affinity to the microtubules, both crucial for stabilizing microtubules. They generate disorder of microtubules in a guanosine triphosphate-independent manner (Sharifi-Rad et al., 2021). One study indicates the synergistic interaction with the combination of gemcitabine, a conventional drug, and PTX, suppressing tumor growth by modulating polymerization and acetylation of tubulin in NSCLC cell lines (Effendi et al., 2019).

Docetaxel (DTX) is another taxane derivative with a similar structure and mechanism of action as PTX (Das et al., 2021). It also induces apoptotic cell death by supressing the expression of the anti-apoptotic gene Bcl-2 and promoting the expression of cell cycle inhibitor p27. DTX presents a 2-fold higher binding affinity to tubulin than PTX, faster tubulin polymerization rate, and improved tumor inhibition capability by in vitro test (Imran et al., 2020). Moreover, DTX offers improved efficacy over DNA-damaging chemotherapies such as alkylating agents, topoisomerase inhibitors, platinum, and others which are correlated with wild-type p53. NSCLC

often shows loss of functional p53; therefore, DTX presents clinical advantages over these therapies in tumors with the loss of functional p53 (Souquet and Geriniere, 2001).

Despite PTX and DTX being widely used for cancer therapy, they present some limitations. Although DTX has better solubility than PTX, both have limited water solubility, toxicity problems, nonspecific targeted behavior, and adverse effects such as neurotoxicity, hepatotoxicity, genotoxicity, hypersensitivity, and hair loss (Imran et al., 2020; Serpico et al., 2020; Sharifi-Rad et al., 2021). They also have production bottlenecks because they are derived from a natural source (Garcia-Oliveira et al., 2021).

Among the MDA group, colchicine and vinca alkaloids are the earliest discovered MTAs. Both are of plant origin and inhibit microtubule formation by causing cell cycle arrest at the G2/M phase. They are used as a base structure for generating new potential anticancer drugs, and they have different domain-binding sites from each other (colchicine- and vinca-domain, respectively). Colchicine presents a few drawbacks, such as high toxicity and low specificity, limiting its application in cancer treatments (Garcia-Oliveira et al., 2021). Vinca alkaloids include vincristine, vinblastine, and the semisynthetic vinca alkaloid, vinorelbine, and they are currently used as chemotherapeutic agents, including lung cancer (Liu et al., 2020).

However, one of the main drawbacks of these drugs is intrinsic or acquired multiple-drug resistance (Wijdeven et al., 2016). Several mechanisms are implicated in drug resistance, ranging from overexpression of the ABC transmembrane efflux transporters, including P-glycoprotein, mutation of microtubule-binding proteins, *mitotic slippage*, tumor microenvironment alteration that enhances cancer cell survival, alteration of apoptotic protein or anti-apoptotic proteins, and modulation of signal transduction pathways that include cytokines, chemokines, and transcription factors (Das et al., 2021; Serpico et al., 2020). More descriptions of these resistance mechanisms are detailed by Das *et al.* (Das et al., 2021).

In the subsequent sessions, we present several topics that highlight the relationship of microtubules with lung cancers, as well as recent discoveries related to new mechanisms or elements that play a role in these interactions.

3.3. New findings of microtubule functions and interaction agents for future clinical application

The recent findings of microtubule function show that better understanding of tubulin isotypes, bioelectrical function, kinetochore interactions, mitochondria dynamics, and ciliogenesis can improve diagnosis, treatment, and prognosis of cancer progression.

3.3.1. *Microtubule isotypes*

Cytoskeletal proteins are responsible for multiple functions, including regulating cellular structure, trafficking, organization, and motility in proper functioning and biochemical processes of cells, connecting directly or indirectly with the plasma membrane and several intracellular organelles. There are mainly three types of cytoskeletal proteins: microtubules (Steinmetz and Prota, 2018), microfilaments (Rao and Li, 2004), and intermediate filaments (Dutour-Provenzano and Etienne-Manneville, 2021). The subtypes, based on their respective function and molecular type, are as follows: The microtubules have tubulin isotypes and microtubule-associated proteins (MAP) (Khwaja et al., 2021); the microfilaments have actin (Suresh and Diaz, 2021), myosin (Peckham, 2016), and others; and intermediate filaments have Type I and II (keratins), Type III (vimentin and desmin), Type IV (neurofilaments), Type V (lamins) and Type VI (nestins) (Ong et al., 2020). Here we will focus on tubulin isotypes.

There are four isotypes of α-tubulins in human cells, which are classified as αI, αIII, αIV, and αVIII. Some subtypes of α-tubulins are tissue-specific, and others are widely distributed. However, the role of α-tubulin isotypes in microtubule activities is not well known (Borys et al., 2020).

In mammalian cells, there are eight different isotypes of β-tubulin, including classes I and IVb, that are essentially expressed. In contrast, classes II, III, V, VI, and VII are generally tissue specific (Lyu et al., 2020). Studies indicate that the βIII isotype in mammals consists of 25% of all tubulins (Banerjees et al., 1992) and has a higher homologous structure than other β-tubulin isotypes (Ludueña, 2013). Several studies demonstrate that the alteration in tubulin isotype composition influences the regulation of cancer biology and chemotherapy resistance, resulting in aggressive and treatment-refractory cancers (Prassanawar and Panda, 2019). These different

compositions include overexpression or decreased expression of some tubulin isotypes in cancer cells compared to the healthy tissue (Parker et al., 2017). Studies reported that a greater level of βIII isotypes is correlated with resistance to taxanes and vinca alkaloids in several cancer cell lines, including NCI-H460 (lung cancer) cells (Das et al., 2021). Cell-free studies using isolated tubulin demonstrated that microtubules composed of βIII isotypes are more active compared to microtubules composed of βII or IV isotypes, suggesting a higher contribution of βIII isotype in the resistance to the chemotherapeutics (Parker et al., 2017). Moreover, it has been shown that high βIII isotype expression is strongly correlated with aggressive clinical behavior, progression to metastatic disease and poor patient outcome in NSCLC (Sève and Dumontet, 2008), and lymph node metastases from primary adenocarcinoma NSCLC (Katsetos et al., 2003). Since cell motility and migration are strongly correlated with tumor growth and metastasis, the overexpression of the βIII isotype may increase microtubule dynamics, which is correlated with increased cell motility and migration (Sobierajska et al., 2016). In cancer cells, βIII isotype may also be responsible for regulating the caspase-mediated apoptotic cascade. The study demonstrated an increased sensitivity to cisplatin in NSCLC cells by knockdown of the βIII isotype (McCarroll et al., 2010). Various studies of βIII isotype in lung cancer and other cancer cells are summarized by Kanakkanthara and Miller (Kanakkanthara and Miller, 2021).

Therefore, microtubule dynamics seem to be highly influenced by the ratio of tubulin isotypes within the cell, their intrinsic properties, and the expression of specific isotypes (Borys et al., 2020).

3.3.2. Bioelectrical function of microtubules

Another function of microtubules is electrical signal propagation. Signal transfer between the inside and outside microtubules may influence cells to external stimuli and drive cell division and organization (Ilan, 2022). Microtubules seem to be a leading player in the mechanotransduction process, whereby mechanical forces are converted into biochemical signals in cells. Microtubules can be associated by minus-end and plus-end microtubule-motor proteins (dynein and kinesin, respectively), and form different shapes and geometries. In this regard, Jafari et al. investigated the wave propagation patterns in various directions and frequencies to

understand the dynamic responses of the microtubule-based bio-nano-architected networks (Jafari et al., 2019). The same authors also analyzed the damping effects of microtubule-based metamaterials on elastic wave-propagation characteristics. The damping effect is a phenomenon that influences the oscillatory system, working to reduce this oscillation. Thus, Jafari et al. modeled the interplay between the microtubule structures and their neighboring media with drag forces (a force that resists a body's motion with fluid) and viscous damping. Results of the analytical model showed that the damping effect on the dispersion curve differed depending on the different architected structures of microtubules. Also, the propagation of out-of-plane and in-plane waves was independent, and the equations of motions for the general linear wave propagations were not linked. It is known that the malfunctioning of the transduction process by the microtubule network may result in several diseases, including cancer. Their work aims to pave the way to create and model microtubule-based bio-nano-filters with unique wave-filtering properties and higher biocompatibility (Jafari et al., 2020).

Another exciting study regarding the electrical conductivity of microtubules was carried out by using doped silicon nanowires to be used as electrodes to measure the electrical resistance of microtubules. Microtubules have semiconductive behavior; hence an electrical measurement was performed in breast cancer cells upon administration of mebendazole (MBZ) as a microtubule destabilizing agent and PTX as a microtubule stabilizing agent. As a result, the former led to an electrical resistance decrease and the latter to an electrical resistance increase. Those modifications in the cytoskeletal network organization disturb the mechanical characteristics of the cells, affecting the proliferative ability and invasiveness of tumor cells. Thus, this study may open an opportunity to create a label-free method for controlling the drug resistance of tumor cells (Gharooni et al., 2019).

Kalra et al. succeeded in measuring the pH in the immediate surrounding of the microtubules by using a direct nanometer-scale chemical probe. The authors designed a double-functional fluorescent tag that changes from teal to orange at the time of full protonation. Microtubules have electrical properties due to the highly negative electrostatic charge and significant dipole moment of tubulin dimers. Thus, it can operate as ion-selective conduits for transport and charge storage. Hence, for the first time the attraction of protons to the surrounding area of microtubules in solution was experimentally demonstrated. They found that microtubule-dense regions have lower pH values than the other regions, demonstrating that microtubules have

a charge storage function inside the cell through cations. Knowing that cancer cells cause pH perturbations, this new method may allow testing the efficacy of several drugs by measuring alterations in local pH, or using it as a diagnostic tool to measure malignancy and cancer progression (Kalra et al., 2022).

3.3.4.   *Kinetochore functions on microtubule dynamics*

Kinetochores are protein complexes that play an essential role in attaching chromosomes to microtubules by assembling with the centromere during cell division. The centromere holds two sister chromatids generated from chromosomes during mitosis, and each sister chromatid is attached with its own kinetochores on the opposite sides (Alexander et al., 2015). Then these kinetochores bind to the mitotic spindle poles (microtubule spindles emanating from the opposite poles), and a bundle of microtubules, also called kinetochore-fiber or k-fiber, is formed. The attachment of each sister kinetochore to the spindle from the opposite poles in a bioriented way is termed amphitelic attachment. Later, these sister chromatids are pulled apart to opposite poles in the cell division process. To this extent, k-fibers are key elements for biorientation and segregation during mitosis (Castrogiovanni and Meraldi, 2022) (**Figure 3.2**).
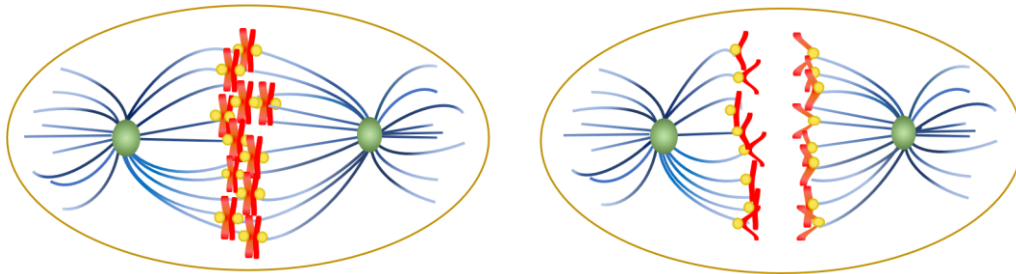
Figure 3.2: Schematic illustration of a human cell division showing microtubules (k-fibers) in blue, sister chromatids in red, kinetochores in yellow and centrosome in green
Source: Own authorship

Since discovering microtubule dynamic instability, the elegant search-and-capture hypothesis has been the mechanism underlying chromosome biorientation and segregation during cell division. It was hypothesized that growing and shrinking bundles of microtubule spindles, generated from the centrosome, search for kinetochores in the centromeric region of the chromosomes, capture them, stabilize them, and generate the k-fiber. However, recent discoveries gave rise to an understanding of the more accurate k-fiber arrangement and chromosome biorientation mechanisms (Soares-de-Oliveira and Maiato, 2022). Using high-resolution live-cell tracking of microtubules and kinetochores in human RPE-1 cells, Renda, Miles et al. provided new insights to establish when, where, and how chromosome biorientation is realized. According to the authors, noncentrosomal short microtubules emanate from kinetochores, and they connect with centrosomal long microtubule bundles of antiparallel spindles. Soon after the interaction, these short microtubules rapidly convert into nascent k-fibers. When the microtubule spindle reaches approximately 80% of its maximum length, most amphitelic attachments rapidly form in the defined space (where short microtubules emanating from the kinetochores interact with the spindles). During the interaction, dynein binds the short microtubule minus-end with the long microtubule spindle minus-ends, forming k-fibers that finally pull the chromosome. The authors also determined by a computational model that the optimal biorientation condition occurs when the number of short microtubules emanating from the kinetochores is approximately twenty and when the ratio of microtubules with opposite polarity within the bundle does not exceed 3:1 (Renda et al., 2022). This exciting discovery of Renda, Miles et al. may also explain the possibility of a significant reduction of error frequency by biorientation during spindle assembly (Soares-de-Oliveira and Maiato, 2022) (**Figure 3.3**).
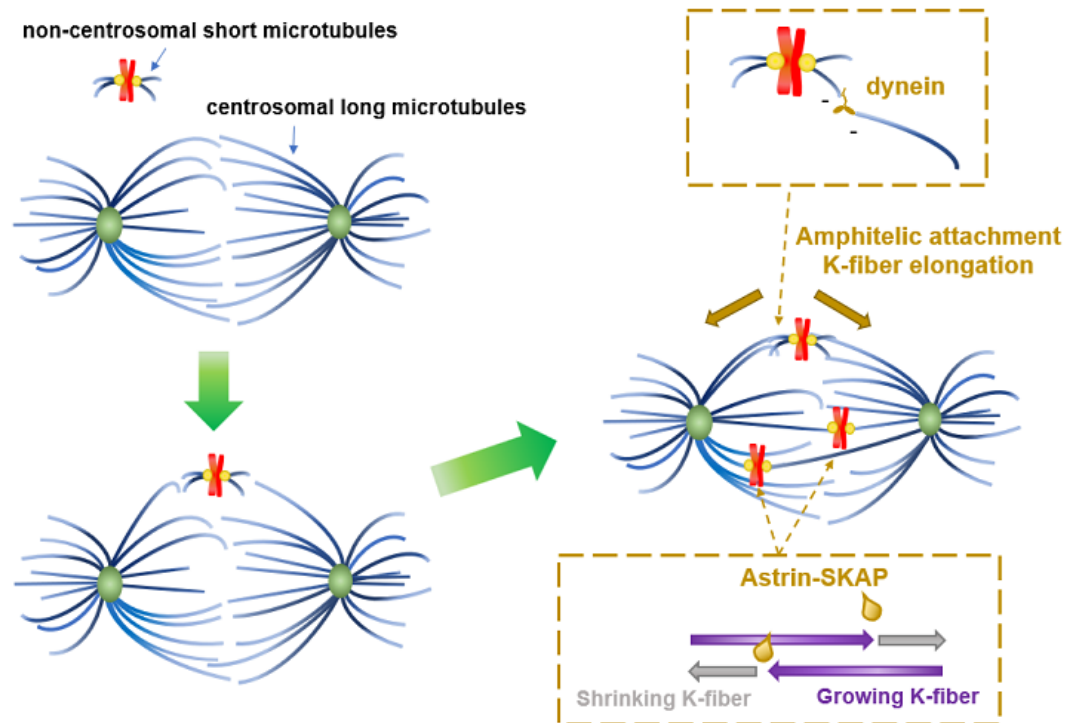
Figure 3.3: Schematical model of k-fiber spindle elongation and amphitelic attachment after interaction between non-centrosomal short microtubules and centrosomal long microtubules driven by dynein. The Astrin-SKAP complex acts as a lubricant to reduce friction at the kinetochore-microtubule interface.

Source: Own authorship

Another interesting finding addressing the kinetochore-microtubule interface dynamic is reported in a recent study (Rosas-Salvans et al., 2022). The authors describe the mechanism behind the rapid frictionless movement in the kinetochore-microtubule interface that ensures efficient segregation. NDC80 and SKA complexes are well known for playing an essential role in attaching kinetochore-microtubules and biorienting/increasing their attachment stability, respectively. Many researchers have carried out extensive studies on attachment in recent years. However, questions remain: an excessive binding force of kinetochores with microtubules is unfavorable to keep the chromosomes in the center position, which oscillates along the dynamic instability of k-fibers due to their constant shrinkage and growth (Castrogiovanni and Meraldi, 2022).

Thus, a complex was identified for the first time, namely the Astrin-SKAP complex, which is responsible for decreasing the grip at the interface of kinetochore and microtubule and reducing friction. This complex, that acts as a lubricant in the interface, helps to promote accurate chromosome segregation during cell division. To understand the mechanical role of this complex, researchers carried out live-cell imaging of metaphase chromosome movements in human retinal pigment epithelial-1, GFP-CenpA, and centrin 1-GFP cells. The results demonstrated that SKAP enhances kinetochore mobility and velocity in polymerizing and depolymerizing microtubules, making them more force-responsive. Furthermore, SKAP reduces the kinetochore-microtubule interface tension, lowering friction and making this interface more dynamic without losing grip and attachment stability. Thus, this recent discovery reveals that not only components that grip the interface but also components that facilitate sliding are essential for rapid, flexible, and effective chromosome segregation during mitosis (Rosas-Salvans et al., 2022) (**Figure 3.3**).

It is reported that disorders of the kinetochore-microtubule interface can perturb microtubule dynamics and disrupt chromosome segregation (Thompson and Compton, 2011). Also, mutation or alterations in SKAP expression are often observed in human cancers (Castrogiovanni and Meraldi, 2022; Rosas-Salvans et al., 2022) .

3.3.5. *Mitochondrial dynamics and microtubules*

Mitochondria are dynamic organelles located at the front edges of cells. In addition to providing cellular energy, they have several functions, such as cell cycle regulation and cell growth control under metabolic and environmental stress responses (Altieri, 2017) . The balance between fission and fusion mechanisms plays a vital role in keeping the dynamic network of mitochondria (Chan, 2012; Vyas et al., 2016). Existing mitochondria can divide or segregate in the fission process to generate new mitochondria (Rehman et al., 2012). Fusion is the process whereby partially damaged mitochondria fuse with healthy ones to restore the impaired mitochondria (Ong et al., 2020). Microtubules play essential roles in mitochondria, such as regulating fission and fusion balance and the intracellular distribution of mitochondria during the cell division process (Vona et al., 2021).

Mitochondria travel from one area to another in the cell, and this is an essential operation during the separation or merging process. Studies suggested that impaired mitochondrial motility mediated by nocodazole or vasopressin inhibits the fusion process (Yi et al., 2004). The mitochondrial motility mediated by microtubules is crucial during fission and fusion processes (Vona et al., 2021): the microtubule-mitochondria binding protein (Mmb1p) is responsible for the interaction and stability between the microtubule and mitochondria. Mmbp1 seems to inhibit the GTPase dynamin-related protein DRP1, a cytosolic protein, reducing mitochondrial fragmentation. Since DRP1 favors the fission process, its inhibition stabilizes the microtubule network. Thus, it favors longer contact time between mitochondria and microtubules, which contributes to mitochondrial elongation (namely, fusion) (Li et al., 2015; Vona et al., 2021).

In tumorigenesis, the mitochondrial fusion and fission processes are essential activities in the disease progression. The former has been associated with tumor cell resistance and apoptosis, and the latter with increased invasiveness. DRP1 seems to be involved in mitochondrial trafficking in tumor cells. Since this protein induces the fission process, it generates quicker transfer and redistribution of mitochondria along the microtubules, which may influence tumor invasiveness (Pathak et al., 2010).

It is also reported that microtubules and microtubule-associated motor proteins, kinesin and dynein, are crucial in transporting mitochondria along their tracks (Boldogh and Pon, 2007; Wang et al., 2021). These proteins traffic and distribute mitochondria through axons and dendrites to energy-intensive areas, producing adenosine triphosphate and guanosine triphosphate. The acetylation on lysine 40 of α-tubulin is responsible for the interaction between kinesin and tubulin, increasing cell motility and affecting the mitochondria motility, distribution, and morphology (Saxton and Hollenbeck, 2012). Studies suggest that the βIII-tubulin C-terminal tail alters kinesin-1 force production and causes abnormal mitochondrial trafficking (Vona et al., 2021).

Moreover, microtubules are known to participate in the regulation of voltage-dependent anion channels (VDAC) within the outer membrane of mictochondria (Fang and Maldonado, 2018). VDAC is essential for the cell's energy state (Shoshan-Barmatz and Ben-Hail, 2012), and the mitochondrial tubulins interact with VDAC to regulate channel opening and closure. Thus, tubulins play essential roles in controlling the permeability of the mitochondrial membrane, in the flow exchange of ions and metabolites in the mitochondria, the regulation of ATP, and multiple

cellular processes (Rovini, 2019). By regulating the mitochondrial membrane potential, VDAC influences oxidative phosphorylation, glycolysis, and apoptotic cell death (Ong et al., 2020; Parker et al., 2017). βIII-tubulin seems to suppress glycolytic metabolism, and its expression causes cell viability and proliferation in glucose-starved NSCLC cells (Parker et al., 2016).

Studies mention several other mechanisms involving the role of microtubule cytoskeletons in the mitochondria transport, such as mitochondrial Rho GTPases (MIRO 1 and 2), motor proteins kinesin-1/3 and dynein, trafficking adapter proteins that combine to kinesin (TRAK1 and TRAK2), and calcium fluxes, which are well described by Vona et al. (Vona et al., 2021).

Intracellular oxidative, mitochondrial, and endoplasmic reticulum stress occurs in normal cells but also in cancer cells. However, reorganization and associated signaling pathways of cytoskeletal proteins by such stress in cancer cells may promote increased tumor aggressiveness leading to tumor metastasis (Roberts and Thomas, 2013).

3.3.6. *Ciliogenesis and lung cancer*

In addition to the diverse functions that microtubules have, as described above, they play a crucial role in air exchange during breathing (Kratzer et al., 2012). Thus, they critically impact several respiratory diseases (Livraghi and Randell, 2007), including lung cancer (Jiang et al., 2013).

Cilium is a tiny hair-like structure generally composed of nine microtubules with a cilium core called an axoneme. Cilia can be classified into two types: primary (immotile) and motile cilia (Tilley et al., 2015). Primary cilia have a photo-, chemo-, and mechanosensory function (Hu et al., 2014), while motile cilia have a role in cell movement of fluid flow. Motile cilia are located in large numbers in airway epithelium and function in mucociliary clearance, in addition to the mechano- and chemosensory function in other cells (Jain et al., 2012). They function as mechanical nanomachines in the respiratory system, generating a high-speed beating motion to effectively move endogenous mucus, toxicants, and pathogens out of the airways (Wallmeier et al., 2020). The human lung has approximately three billion motile cilia. Dynein is located in the axoneme, bridging adjacent microtubule doublets, and by *walking* along the microtubule doublet, it generates a force that promotes the cilia beating motion (Ishikawa, 2017). The dysfunction of

this system may lead to several chronic diseases, mainly when associated with cigarette smoke (Wijesekara et al., 2022). Cigarette smoke constitutes more than a thousand chemical components, several of which have been identified as carcinogens by the FDA, increasing the risk of lung cancer (Xiong et al., 2021).

Studies demonstrated the impact of cigarette smoke on the respiratory system (Alexander et al., 2015), such as a decrease in α-tubulin acetylation resulting in microtubule depolymerization of pulmonary endothelial cells and a consequent increase of lung endothelial barrier permeability by decreasing this barrier integrity (Borgas et al., 2016; Lu et al., 2018). Xiong et al. carried out the transcriptomics-based approach integrated with the pathophysiological measurements in an in vitro human air-liquid interface airway tissue model to show the irregularities observed in the airways of smokers caused by cigarette smoke. These abnormalities include impaired ciliary structures, decreased number of cilia and their functions, squamous cell differentiation, mucin secretion dysfunction, oxidative stress induction, and increased release of proinflammatory cytokine and matrix metalloproteinases. The ciliary damage was positively correlated with cigarette smoke concentration, and a 20-day recovery only partially reversed the abnormalities observed by the high concentration. Also, by GO enrichment analysis, it was demonstrated that lung disease-associated pathways were increased even after the recovery phase. These estimated lung diseases include lung carcinoma, chronic obstructive pulmonary disease, non-small cell lung carcinoma, lung adenocarcinoma, small cell lung carcinoma, pulmonary emphysema, lung squamous cell carcinoma, interstitial lung disease, and pulmonary fibrosis (Xiong et al., 2021).

Considering the increasing number of electronic cigarette (EC) users replacing tobacco cigarette smokers in recent years, Pozuelos et al. compared three different groups using RNA-seq analysis. The first group consisted of former smokers who entirely replaced to second-generation ECs for at least six months (EC group), the second group of current tobacco cigarette smokers (CS group), and the third of nonsmokers and former smokers who quit cigarettes (NS group). Both EC and CS smoker groups presented increased oxidative stress, dysregulation of cilia, and reduced ciliogenesis, with significantly increased inflammation in the EC group. ECs are battery-operated devices that aerosolize liquids containing nicotine or non-nicotine flavored chemicals, which can cause the downregulation of genes involved in ciliary biogenesis (Pozuelos et al., 2022). In contrast, the NS group showed restored respiratory epithelium, which agrees with other studies

(Lu et al., 2018), indicating reversible pulmonary endothelial cells in healthy smokers who quit smoking. Thus, this study brought new insights showing that the ciliogenesis was not recovered after replacing cigarettes with ECs (Pozuelos et al., 2022).

Some recent exciting research may open possibilities to measure the cilia beating frequency for future modeling and developing therapies for genetic and environmental ciliopathies. Wijesekara et al. engineered a rotating apical-out airway organoid (AOAO) from a fixed number of cells. AOAO consists of a ciliated airway spheric organoid with cilia beating on the external surface, which presented a stable rotational motion in Matrigel-embedded suspension culture. The authors developed a visual computational framework to track algorithms by conducting real-time analysis and measuring organoid rotational movement from video data. They successfully registered and evaluated the angular speed of the same AOAOs pre- and post-treatment with cilia-beating inhibitors. These findings may enable the evaluation of abnormal cilia motility under pathophysiological conditions using patient-derived cells for future development of analysis for therapeutic screening and personalized disease management (Wijesekara et al., 2022) (**Figure 3.4**).
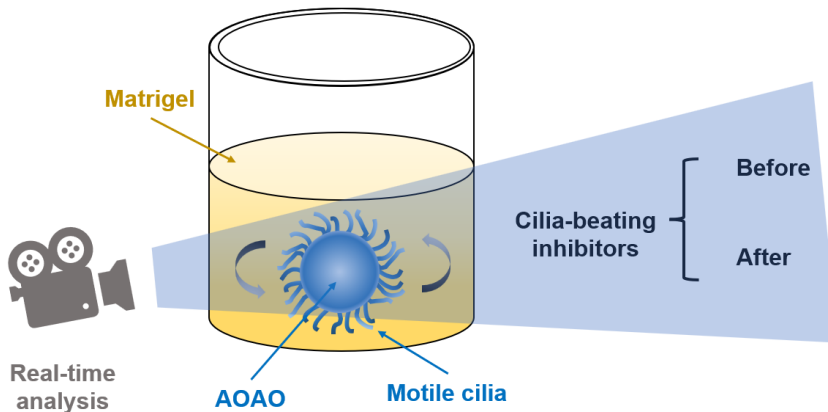
Figure 3.4: Schematical model of rotating apical-out airway organoid (AOAO) in Matrigel suspension and measurement of cilia motility.
Source: Own authorship

3.4. New players in lung cancer and microtubule-based therapy

The never-in-mitosis (NIMA)-related kinase 2 (NEK2) was determined as a novel target for treating several cancers. NEK2 is overexpressed in several cancers, including NSCLC. This serine/threonine kinase protein's primary role is regulating mitotic processes, such as microtubule organization and stabilization, centrosome duplication and separation, kinetochore attachment, and spindle assembly checkpoint. The abnormality of NEK2 activity in NSCLC cells resulted in aneuploidy, premature centrosome separation, nuclear defects, and abnormal proliferation of cells. NEK2 is also important for controlling the disassembly of cilia through phosphorylation, and it may also control invasion/metastasis and inhibit apoptosis through dysregulation of Rho1-Rac1 balance. Therefore, NEK2 may be a potential biomarker for lung cancers, also opening possibilities for NEK2 inhibitors as a candidate for treating resistant lung cancers (Shah et al., 2022).

Another recently reported biomarker for NSCLC is the transforming acidic coiled-coil-containing protein 3 (TACC3). The TACC family interacts with tubulin and microtubules and regulates microtubule and centrosome dynamics, taking part in the arrangement of cell growth, apoptosis, development, and differentiation. TACC3 plays a crucial role in microtubule assembly and organization, chromosome alignment in during mitosis, structuring the nuclear envelope maintenance, regulation of gene transcription, as well as cell growth and differentiation. Overexpression of TACC3 was found in lung cancer, leading to tumorigenesis by fibroblast growth factor receptor (FGFR)1-TACC1 and FGFR3-TACC3 gene fusions. Thus, this protein may be indicated as a novel biomarker and provide a basis to support the development of an innovative immunotherapy target (Y. Chen et al., 2022).

Heat shock proteins (HSP), essential chaperone proteins, are greatly expressed in various cancers, including lung adenocarcinoma (LUAD). Among them, chaperonin-containing T-complex protein-1 subunit 3 (CCT3), a part of the HSP60 family group II, was significantly expressed in LUAD cells, and identified as crucial for tumor growth and metastasis. Suppression of CCT3 highly impacted the energy supply and protein synthesis pathways, inhibiting the proliferation of LUAD cells, promoting apoptosis and cell cycle arrest, and preventing migration and invasion of these cells. Silencing CCT3 decreased intracellular ATP levels in LUAD cells by hindering glycolysis. In addition, CCT3 knockdown caused tubulin deficiency, which may explain

the inhibition of cell motility and induction of cell cycle arrest. This work demonstrated that restriction of CCT3 may be a potential therapeutic approach for LUAD treatment (S. Chen et al., 2022).

Chalcone is a natural product consisting of two aryl groups and an α-, β-unsaturated alkenone that can bind to microtubule proteins and lead to microtubule inhibition and disruption of its homeostasis. The advantage of chalcone is its simple structure and chemical synthesis, allowing it to produce diverse derivatives as an antitumor agent. Liu et al. summarized recent works on chalcone derivatives and their biological activities as tubulin polymerization inhibitors. Several chalcone derivatives with antitumor activity in A549 cells (adenocarcinomic human alveolar basal epithelial cells) are cited, such as indole-chalcones, benzoxazole-chalcones, Combrestastatin A-4-based chalcones, carbonyl modification, rigidified chalcone derivatives, platinum-chalcone hybrids, nitrogen mustard-chalcone hybrids, and benzothiazole-chalcone hybrids (W. Liu et al., 2022).

A combination of acridanone derivative 5-dimethylaminopropylamino-8-hydroxytriazoloacridinone (C-1305) with paclitaxel (PTX) demonstrated synergic tumor-suppressive effects in cancer cells. The authors identified C-1305 as the first microtubule-stabilizing molecule that presents additional topoisomerase II inhibiting effect. The binding site of this molecule was different from that of PTX. In A549-tumor-bearing mice, the tendency toward increased α-tubulin and no considerable changes in βIII-tubulin expression were observed by this combined treatment. Signaling pathways related to the angiogenic process were evaluated, demonstrating that the PDGF level was significantly decreased and the plasma level of CCL2 was enhanced. Despite the encouraging in vitro results, the in vivo antitumor experiments of this molecule in combination with PTX were restrictive and equivalent to the modulation of tumor angiogenesis (Świtalska et al., 2022).

2-methoxy-5((3,4,5-trimethosyphenyl) seleninyl) phenol (SQ), a vinylogous Combretastatin A-4 analog, prevented the proliferation of A549 cells and H460 cells (epithelial cell from large cell lung carcinoma) in time- and dose-dependent ways. In vitro tests demonstrated that SQ disturbs microtubule polymerization, induces G2/M phase arrest, which is related to microtubule depolymerization, downregulates cyclin B1 and CDK7, results in apoptosis, enhances the Bax levels, cleaves caspase-3 and downregulates the level of Bcl-2 and caspase-3, which is

potentially the cause of cell death through a mitochondrial apoptotic pathway. This new microtubule inhibitor with enhanced stability may be a potential antitumor drug in NSCLC (Y. Liu et al., 2022).

Furthermore, to overcome the limitation of cancer chemotherapies due to multidrug resistance (MDR), Park et al. developed 5-(N-methylmaleimid-3-yl)-chromone (SPC-160002), a unique microtubule inhibitor effective for various human cancers, including A549 lung cancer cells and multidrug-resistant cell lines. SPC-160002 mediated mitotic arrest of the cell cycle at the G2/M phase, promoting and stabilizing microtubule polymerization with a mechanism similar to taxane-based drugs. This new anticancer agent did not affect P-gp expression or drug efflux function. It also restricted the survival and sphere-forming activity of cancer stem cells. There is no clear explanation of the maleimide group activity on microtubule stabilization. It was hypothesized that the interaction between the microtubule and this group occur by the Michael-type addition reaction on the sulfhydryl-rich heterodimer site of tubulin. Although the potency of SPC-16002 is weaker than paclitaxel, this is a novel microtubule-targeting drug for several human cancer cells, including MDR cancer cells (Park et al., 2021).

Another elegant agent aiming to overcome drug resistance in diverse cancer cells is the peptide-based rotor molecule, driven by the multicomponent-targeting feature of molecular self-assembly (MSA). The synthesized MSA is an environmentally responsive molecule that can self-adjust morphologically in return for the variations of pH and viscosity during Golgi-endosome trafficking. It demonstrated to evade trafficking cargos and physically combine to the microtubule array in a nonspecific way. The observation of the tubulin polymerization mixture by electron microscopy imaging indicates that this polymerization is suppressed by MSA-induced aggregation. Cell viability tests, including A549 cells, indicated effective toxicity of synthesized MSA, with good anticancer selectivity. It also demonstrated its potential as a non-neurotoxic antimitotic agent. Thus, this regional tubulin polymerization suppressor is a promising anticancer drug that overcomes the problem of MDR and the neurotoxicity of current microtubule agents (Li et al., 2021).

3.5. Nano-based therapy using microtubules-targeting agents for lung cancer

Nanotechnologies have been highlighted as an innovative technology to overcome several limitations of conventional drugs or delivery systems in cancer treatments. The nano-ranged particles may allow more accessible interactions of these particles with the intracellular environment, promote a modified drug release, enhance drug stability during storage, protect the drug from enzymatic or chemical degradation, escape from reticuloendothelial system uptake, and enhance the bioavailability of poorly water-soluble drugs. They can reach tumor sites through passive or active targeting (physicochemical or specific target site delivery, respectively). Nanotechnology can be administered through different routes, such as intravenous, oral, or intranasal, and customized according to the patient's needs. In addition, they are applicable for both the diagnosis and treatment of cancers, opening several doors for creating new promising therapies, which are described below (Imran et al., 2020; Wang et al., 2018).

In an elegant review, Imran et al. summarized the recent development of nanotechnology-based DTX for cancer treatments (Imran et al., 2020). Several studies regarding lung cancer treatments were cited by them, as follows: Biodegradable core-shell lipid-polymer hybrid nanoparticles (LPNs) were conjugated with epidermal growth factor (EGF) to co-deliver DTX and resveratrol. Epidermal growth factor receptor (EGFR) was the targeted site since it is known to be overexpressed in NSCLC cells. The authors performed in vitro and in vivo studies using HCC827 cells (epithelial cell isolated from the lung adenocarcinoma) and NCIH2135 (NSCLC lung adenocarcinoma cell), and results revealed a notable synergy in delivering these drugs in the mitochondria of tumor cells, overcoming multidrug resistance, with high tumor suppression ability and low systemic toxicity (Z. Song et al., 2018). Huang et al. synthesized ephrin A2-targeted liposomal prodrug incorporating pH-sensitive paclitaxel and DTX prodrugs. This nanoliposomal prodrug presented high stability, high encapsulation efficiency, long circulation pharmacokinetics, efficient drug release, and greater antitumor activity than DTX alone in A549 cells and other cancer xenograft cell models (Huang et al., 2019). DTX-loaded hyaluronic acid nanocapsules were developed by a simple self-assembling process by Cadete et al. This process did not require heat, high shear forces, or organic solvents. These nanocapsules demonstrated high drug encapsulation efficiency, adequate stability in plasma, and effective intracellular delivery of DTX in in vitro studies using A549 cells (Cadete et al., 2019). Gong et al. prepared DTX-loaded N-(tert-

butoxycarbonyl)-L-phenylalanine end-capped methoxy-poly(ethylene glycol)-block-poly(D,L-lactide) (mPEG-b-PLA-Phe(Boc)) micelles (DTX-PMs) and compared them to the marketed DTX formulation Taxotere®. DTX-PMs showed high aqueous stability, and in vivo evaluation revealed a higher drug concentration in blood and plasma than Taxotere®. Moreover, it presented a similar therapeutic effect as this marketed formulation with only half of the DTX dosage by an in vivo study using A549 tumor-bearing mice (Gong et al., 2020).

An interesting summary of nanotherapy employing another currently approved drug for lung cancer, paclitaxel (PTX), was done by Sharifi-Rad et al. (Sharifi-Rad et al., 2021). Some recent studies refer to development of a new mitochondria-targeting and glutathione-sensitive PTX-ss-berberine nanoparticle (NP) that is self-assembled in water. Berberine (BBR) is known to be selectively accumulated in tumor cell mitochondria for cancer cell growth inhibition by a different mechanism from PTX. The synergistic effects of PTX-ss-BBR NPs resulted in successful drug and mitochondria-targeting delivery, in vitro antitumor efficacy, elevated apoptosis-inducing effect, ROS production, and promoted apoptosis in A549 cells (Cheng and Ji, 2020). Song et al. prepared PTX-loaded redox-sensitive NPs based on hyaluronic acid-vitamin E succinate conjugates (HA-SS-VES, HSV). Results showed enhanced in vitro cytotoxicity and apoptosis-inducing ability of HSV against CD44 overexpressed A549 cells than redox-insensitive NPs and Taxol®. In vivo A549 mouse xenograft model study also showed higher antitumor efficacy and an improved safety profile (Y. Song et al., 2018). Wang et al. designed a combined therapy of PTX and Osimertinib (AZD9291) nanoformulations to target EGFR T790M and treat EGFR-mutant NSCLC patients. These nanoformulations presented strong synergistic effects, glutathione-responsive drug release, promoting cell cycle arrest and apoptosis in a dose-dependent way, by in vitro study using H1975 cells (cell line exhibiting epithelial morphology from NSCLC). This apoptosis was promoted by the downregulation of IKBa, increased p65 (NF-κB) activity, and downregulation of Bcl-2 when treated with these nanoformulations. In vivo evaluation using H1975 xenografts in mice demonstrated superior cancer eradication with decreased hematological toxicity than the single drugs (Wang et al., 2018).

Carbon nanotubes (CNTs) are nanometric cylinder-shaped tubes composed of carbon atoms with unique physicochemical properties. Due to the mechanical and morphological similarities, CNTs can interact with the microtubule cytoskeleton, which causes the nucleation of

acentrosomal microtubules, centrosome disassembly, and migration defects, leading to general cellular malfunctions and apoptosis. Among different types of CNTs, the multi-walled CNTs (MWCNTs) seem to interfere more with actin and tubulin, providing intracellular hybrid disorganized microtubules with enhanced stability. Hevia and Fanarraga did a brilliant review of the application of CNTs in cancer therapy. Unlike conventional microtubule stabilizing agents such as PTX or DTX, CNTs can overcome several drug resistance mechanisms, such as drug efflux pumps or mutation in the drug binding site, since CNTs are not secreted out of the cells, and they do not have a specific binding site (Hevia and Fanarraga, 2020). Intravenously administered CNTs were subjected to tissue biodistribution analysis, and found in several tissues, including the lung (Deng et al., 2007; Hevia and Fanarraga, 2020; Singh et al., 2006). Although some toxicity concerns remain due to the high affinity and stability of CNTs in tissues (Ema et al., 2016), they can be an exciting component to boost the efficacy of conventional drugs to offer synergistic effects, administered in parallel or as carriers (Hevia and Fanarraga, 2020).

Gao et al. developed a nanoradiosensitizer by loading nitrosylated maytansinoid DM1(DM1-NO) onto poly(lactide-co-glycolic)-*block*-poly(ethylene glycol) (PLGA-b-PEG) nanoparticles (NPs). Radiosensitizers are agents often used to improve sensitivity during radiotherapy in cancer treatments. DM1 is an antibody-drug conjugate of maytansinoids (a potent and high-toxicity radiosensitizer), delivered to cancer cells with better pharmacokinetics and pharmacodynamics due to the conjugation. Additionally, the PLGA encapsulation and S-nitrosylation suppressed the DM1's toxicity and delivered the drug systematically to tumors through enhanced permeation and retention effects. They showed that the consecutive radiation caused the release of DM1 and NO by cleavage of the S-N bond, where the former led to cell enrichment at the G2/M phase and mitotic arrest, and the latter formed free radicals by reactive oxygen species to oxidize lipids. DM1 also interfered with tubulin polymerization. In vitro and in vivo tests using H1299 cells (human NSCLC cells) demonstrated a very efficient cell proliferation suppressing effect and lower toxicity of DM1-NO-NPs than non-nanosized components (Gao et al., 2020).

Flubendazole (FLU) is an anthelmintic drug with destabilization activity of microtubules, and it is a repositioning drug candidate for several cancer treatments. FLU is a Class II drug in biopharmaceutical classification. Thus, Gonçalves et al. designed a FLU nanocrystal using a

combination of microfluidization method followed by a freeze-dried method with statistical design. The final stable FLU nanocrystal showed an increased saturation solubility when compared to crude-free-FLU. An in vivo study using the A549 xenograft mouse model resulted in a 40% reduction in tumor size from day 53 in comparison to the control group (de Souza Gonçalves et al., 2022). A FLU-loaded nanoemulsion was developed in combination with a high content linoleic acid derived oil, using D-Phase emulsification method (Yukuyama et al., 2021). Although there was no efficacy on tumor development in an A549 xenograft mouse model, this nanoemulsion demonstrated an effective inhibition of malignant wound development. Malignant wound affects up to 15% of cancer patients in advanced stage, leading to detrimental effects such as extreme malodor and tissue deformity. Oral administration of this nanoemulsion sample resulted in nonappearance of malignant wound even after 80 days of treatment, unlike other samples such as FLU in suspension and another oil, which presented malignant wound in 40% of animals after 38 and 52 days, respectively (Yukuyama et al., 2022).

Therefore, several exciting nano-based drug developments are already ongoing as prospective delivery therapies for lung cancers.

3.6. Summary and future perspectives

Microtubules are dynamic and fascinating proteins that play key roles in various living cell activities in maintaining their normal functions and reproduction. In contrast, their malfunctions may cause several complications that can lead to cancer. Lung cancer, one of the main causes of cancer-related deaths worldwide, still lacks accurate earlier diagnosis and effective treatment. Growing evidence indicated that microtubules strongly correlate with the development of lung cancer and its resistance against current therapeutic agents.

After briefly introducing the general description of the fundamental structures and functions of microtubules, this review highlighted the recently discovered mechanisms of microtubules and their interactions with lung cancer. Although the influence of βIII isotype on tumors has been known for years, recent studies reinforced this assumption in lung cancer. Bioelectrical properties of microtubules paved the way to develop an alternative analysis for future cancer detection or evaluation of the efficacy of new treatment agents. Understanding kinetochore-

microtubule interactions led to better understanding of cell division and chromosome segregation in cancer development and progression, which may illuminate the intriguing hypothesis of how these segregation errors are reduced. Recent discoveries of the mitochondria-microtubule interactions allow for elaborating on the generation of energy as well as the correct regulation of cell functions, including fusion and fission processes. A better understanding of ciliogenesis and the influence of external factors such as cigarette smoking on lung cancer is another area to consider and create an alternative mechanistic mode to evaluate and develop treatments. Current studies of novel biomarkers and agents in lung cancer prognosis or treatments updated the relevance of the subject reported in this review. Finally, nanotechnology-based drugs targeting microtubules for lung cancer treatments align with the current trends and needs, to support future development of nano systems.

Although problems such as neurotoxicity and specificity may remain, microtubule-targeting agents are an interesting strategy to overcome the limitations of current therapies. These recent studies of new agents and new mechanisms of microtubules may drive future developments of more specific, less toxic, and more effective drug delivery, as well as new evaluation tools for the early diagnosis of lung cancer.

3.7. References

Alexander, L.E.C., Shin, S., Hwang, J.H., 2015. Inflammatory diseases of the lung induced by conventional cigarette smoke a review. Chest 148, 1307–1322. https://doi.org/10.1378/chest.15-0409

Altieri, D.C., 2017. Mitochondria on the move: Emerging paradigms of organelle trafficking in tumour plasticity and metastasis. Br J Cancer. https://doi.org/10.1038/bjc.2017.201

Banerjees, A., Roach, M.C., Trcka, P., Luduena, R.F., 1992. Preparation of a Monoclonal Antibody Specific for the Class IV Isotype of βTubulin. Journal of Biological Chemistry 267, 5625–5630.

Boldogh, I.R., Pon, L.A., 2007. Mitochondria on the move. Trends Cell Biol. https://doi.org/10.1016/j.tcb.2007.07.008

Borgas, D., Chambers, E., Newton, J., Ko, J., Rivera, S., Rounds, S., Lu, Q., 2016. Cigarette smoke disrupted lung endothelial barrier integrity and increased susceptibility to acute lung injury via histone deacetylase 6. Am J Respir Cell Mol Biol 54, 683–696. https://doi.org/10.1165/rcmb.2015-0149OC

Borys, F., Joachimiak, E., Krawczyk, H., Fabczak, H., 2020. Intrinsic and Extrinsic Factors Affecting Microtubule Dynamics in Normal and Cancer Cells. Molecules. https://doi.org/10.3390/molecules25163705

Cadete, A., Olivera, A., Besev, M., Dhal, P.K., Gonçalves, L., Almeida, A.J., Bastiat, G., Benoit, J.P., de la Fuente, M., Garcia-Fuentes, M., Alonso, M.J., Torres, D., 2019. Self-assembled hyaluronan nanocapsules for the intracellular delivery of anticancer drugs. Sci Rep 9. https://doi.org/10.1038/s41598-019-47995-8

Castrogiovanni, C., Meraldi, P., 2022. Cell division: The science friction of chromosome attachment. Current Biology. https://doi.org/10.1016/j.cub.2022.05.045

Chan, D.C., 2012. Fusion and fission: Interlinked processes critical for mitochondrial health. Annu Rev Genet 46, 265–287. https://doi.org/10.1146/annurev-genet-110410-132529

Chen, S., Tian, Y., Ju, A., Li, B., Fu, Y., Luo, Y., 2022. Suppression of CCT3 Inhibits Tumor Progression by Impairing ATP Production and Cytoplasmic Translation in Lung Adenocarcinoma. Int J Mol Sci 23. https://doi.org/10.3390/ijms23073983

Chen, Y., Zhou, M., Gu, X., Wang, L., Wang, C., 2022. High Expression of TACC3 Is Associated with the Poor Prognosis and Immune Infiltration in Lung Adenocarcinoma Patients. Dis Markers 2022. https://doi.org/10.1155/2022/8789515

Cheng, Y., Ji, Y., 2020. Mitochondria-targeting nanomedicine self-assembled from GSH-responsive paclitaxel-ss-berberine conjugate for synergetic cancer treatment with enhanced cytotoxicity. Journal of Controlled Release 318, 38–49. https://doi.org/10.1016/j.jconrel.2019.12.011

Choudhury, H., Pandey, M., Gorain, B., Chatterjee, B., Madheswaran, T., Md, S., Mak, K.-K., Tambuwala, M., Chourasia, M.K., Kesharwani, P., 2019. Nanoemulsions as Effective Carriers for the Treatment of Lung Cancer, in: Nanotechnology-Based Targeted Drug Delivery Systems for Lung Cancer. Elsevier, pp. 217–247. https://doi.org/10.1016/b978-0-12-815720-6.00009-5

Das, T., Anand, U., Pandey, S.K., Ashby, C.R., Assaraf, Y.G., Chen, Z.S., Dey, A., 2021. Therapeutic strategies to overcome taxane resistance in cancer. Drug Resistance Updates 55. https://doi.org/10.1016/j.drup.2021.100754

de Souza Gonçalves, D., Yukuyama, M.N., Miyagi, M.Y.S., Silva, T.J.V., Lameu, C., Bou-Chacra, N.A., de Araujo, G.L.B., 2022. Revisiting Flubendazole Through Nanocrystal Technology: Statistical Design, Characterization and Its Potential Inhibitory Effect on Xenografted Lung Tumor Progression in Mice. J Clust Sci. https://doi.org/10.1007/s10876-022-02220-x

Deng, X., Jia, G., Wang, H., Sun, H., Wang, X., Yang, S., Wang, T., Liu, Y., 2007. Translocation and fate of multi-walled carbon nanotubes in vivo. Carbon N Y 45, 1419–1424. https://doi.org/10.1016/j.carbon.2007.03.035

Dutour-Provenzano, G., Etienne-Manneville, S., 2021. Intermediate filaments. Current Biology R522–R529.

Effendi, W.I., Nagano, T., Tachihara, M., Umezawa, K., Kiriu, T., Dokuni, R., Katsurada, M., Yamamoto, M., Kobayashi, K., Nishimura, Y., 2019. Synergistic interaction of gemcitabine and paclitaxel by modulating acetylation and polymerization of tubulin in non-small cell lung cancer cell lines. Cancer Manag Res 11, 3669–3679. https://doi.org/10.2147/CMAR.S193789

Ema, M., Gamo, M., Honda, K., 2016. A review of toxicity studies of single-walled carbon nanotubes in laboratory animals. Regulatory Toxicology and Pharmacology 74, 42–63. https://doi.org/10.1016/j.yrtph.2015.11.015

Fang, D., Maldonado, E.N., 2018. VDAC Regulation: A Mitochondrial Target to Stop Cell Proliferation, in: Advances in Cancer Research. Academic Press Inc., pp. 41–69. https://doi.org/10.1016/bs.acr.2018.02.002

Fink-Neuboeck, N., Lindenmann, J., Porubsky, C., Fediuk, M., Anegg, U., Maier, A., Smolle, J., Lamont, E., Smolle-Juettner, F.M., 2020. Hazards of Recurrence, Second Primary, or Other Tumor at Ten Years After Surgery for Non–Small-Cell Lung Cancer. Clin Lung Cancer 21, 333–340. https://doi.org/10.1016/j.cllc.2020.02.011

Gao, S., Zhang, W., Wang, R., Hopkins, S.P., Spagnoli, J.C., Racin, M., Bai, L., Li, L., Jiang, W., Yang, X., Lee, C., Nagata, K., Howerth, E.W., Handa, H., Xie, J., Ma, Q., Kumar, A., 2020. Nanoparticles Encapsulating Nitrosylated Maytansine to Enhance Radiation Therapy. ACS Nano 14, 1468–1481. https://doi.org/10.1021/acsnano.9b05976

Garcia-Oliveira, P., Otero, P., Pereira, A.G., Chamorro, F., Carpena, M., Echave, J., Fraga-Corral, M., Simal-Gandara, J., Prieto, M.A., 2021. Status and challenges of plant-anticancer compounds in cancer treatment. Pharmaceuticals. https://doi.org/10.3390/ph14020157

Gharooni, M., Alikhani, A., Moghtaderi, H., Abiri, H., Mashaghi, A., Abbasvandi, F., Khayamian, M.A., Miripour, Z.S., Zandi, A., Abdolahad, M., 2019. Bioelectronics of the cellular cytoskeleton: Monitoring cytoskeletal conductance variation for sensing drug resistance. ACS Sens 4, 353–362. https://doi.org/10.1021/acssensors.8b01142

Gong, F., Wang, R., Zhu, Z., Duan, J., Teng, X., Cui, Z.K., 2020. Drug-interactive mPEG-b-PLA-Phe(Boc) micelles enhance the tolerance and anti-tumor efficacy of docetaxel. Drug Deliv 27, 238–247. https://doi.org/10.1080/10717544.2020.1718245

Hevia, L.G., Fanarraga, M.L., 2020. Microtubule cytoskeleton-disrupting activity of MWCNTs: applications in cancer treatment. J Nanobiotechnology. https://doi.org/10.1186/s12951-020-00742-y

Hu, Q., Wu, Y., Tang, J., Zheng, W., Wang, Q., Nahirney, D., Duszyk, M., Wang, S., Tu, J.C., Chen, X.Z., 2014. Expression of polycystins and fibrocystin on primary cilia of lung cells. Biochemistry and Cell Biology 92, 547–554. https://doi.org/10.1139/bcb-2014-0062

Huang, Z.R., Tipparaju, S.K., Kirpotin, D.B., Pien, C., Kornaga, T., Noble, C.O., Koshkaryev, A., Tran, J., Kamoun, W.S., Drummond, D.C., 2019. Formulation optimization of an ephrin A2 targeted immunoliposome encapsulating reversibly modified taxane prodrugs. Journal of Controlled Release 310, 47–57. https://doi.org/10.1016/j.jconrel.2019.08.006

Ilan, Y., 2022. Microtubules as a potential platform for energy transfer in biological systems: a target for implementing individualized, dynamic variability patterns to improve organ function. Mol Cell Biochem. https://doi.org/10.1007/s11010-022-04513-1

Imran, M., Saleem, S., Chaudhuri, A., Ali, J., Baboota, S., 2020. Docetaxel: An update on its molecular mechanisms, therapeutic trajectory and nanotechnology in the treatment of breast, lung and prostate cancer. J Drug Deliv Sci Technol. https://doi.org/10.1016/j.jddst.2020.101959

Ishikawa, T., 2017. Axoneme structure from motile cilia. Cold Spring Harb Perspect Biol 9. https://doi.org/10.1101/cshperspect.a028076

Jafari, H., Yazdi, M.H., Fakhrabadi, M.M.S., 2020. Damping effects on wave-propagation characteristics of microtubule-based bio-nano-metamaterials. Int J Mech Sci 184. https://doi.org/10.1016/j.ijmecsci.2020.105844

Jafari, H., Yazdi, M.R.H., Fakhrabadi, M.M.S., 2019. Wave propagation in microtubule-based bio-nano-architected networks: A lesson from nature. Int J Mech Sci 164. https://doi.org/10.1016/j.ijmecsci.2019.105175

Jain, R., Javidan-Nejad, C., Alexander-Brett, J., Horani, A., Cabellon, M.C., Walter, M.J., Brody, S.L., 2012. Sensory functions of motile cilia and implication for bronchiectasis. Front Biosci 4, 1088–1098.

Jiang, H., Yu, X.M., Zhou, X.M., Wang, X.H., Su, D., 2013. Correlation between microtubule-associated gene expression and chemosensitivity of patients with stage II non-small cell lung cancer. Exp Ther Med 5, 1506–1510. https://doi.org/10.3892/etm.2013.1007

Kalra, A.P., Eakins, B.B., Vagin, S.I., Wang, H., Patel, S.D., Winter, P., Aminpour, M., Lewis, J.D., Rezania, V., Shankar, K., Scholes, G.D., Tuszynski, J.A., Rieger, B., Meldrum, A., 2022. A Nanometric Probe of the Local Proton Concentration in Microtubule-Based Biophysical Systems. Nano Lett 22, 517–523. https://doi.org/10.1021/acs.nanolett.1c04487

Kanakkanthara, A., Miller, J.H., 2021. βIII-tubulin overexpression in cancer: Causes, consequences, and potential therapies. Biochim Biophys Acta Rev Cancer. https://doi.org/10.1016/j.bbcan.2021.188607

Katsetos, C.D., Herman, M.M., Mörk, S.J., 2003. Class III β-tubulin in human development and cancer. Cell Motil Cytoskeleton. https://doi.org/10.1002/cm.10116

Khwaja, S., Kumar, K., Das, R., Negi, A.S., 2021. Microtubule associated proteins as targets for anticancer drug development. Bioorg Chem. https://doi.org/10.1016/j.bioorg.2021.105320

Kratzer, E., Tian, Y., Sarich, N., Wu, T., Meliton, A., Leff, A., Birukova, A.A., 2012. Oxidative stress contributes to lung injury and barrier dysfunction via microtubule destabilization. Am J Respir Cell Mol Biol 47, 688–697. https://doi.org/10.1165/rcmb.2012-0161OC

Li, G., Hu, X., Wu, X., Zhang, Y., 2021. Microtubule-Targeted Self-Assembly Triggers Prometaphase-Metaphase Oscillations Suppressing Tumor Growth. Nano Lett 21, 3052–3059. https://doi.org/10.1021/acs.nanolett.1c00233

Li, T., Zheng, F., Cheung, M., Wang, F., Fu, C., 2015. Fission yeast mitochondria are distributed by dynamic microtubules in a motor-independent manner. Sci Rep 5. https://doi.org/10.1038/srep11023

Liu, H., Fu, Q., Lu, Y., Zhang, W., Yu, P., Liu, Z., Sun, X., 2020. Anti-tubulin agent vinorelbine inhibits metastasis of cancer cells by regulating epithelial-mesenchymal transition. Eur J Med Chem 200. https://doi.org/10.1016/j.ejmech.2020.112332

Liu, W., He, M., Li, Y., Peng, Z., Wang, G., 2022. A review on synthetic chalcone derivatives as tubulin polymerisation inhibitors. J Enzyme Inhib Med Chem. https://doi.org/10.1080/14756366.2021.1976772

Liu, Y., Meng, Y., Bian, J., Liu, B., Li, X., Guan, Q., Li, Z., Zhang, W., Wu, Y., Zuo, D., 2022. 2-Methoxy-5((3,4,5-trimethosyphenyl) seleninyl) phenol causes G2/M cell cycle arrest and apoptosis in NSCLC cells through mitochondrial apoptotic pathway and MDM2 inhibition. J Biochem Mol Toxicol 36. https://doi.org/10.1002/jbt.23066

Livraghi, A., Randell, S.H., 2007. Cystic Fibrosis and Other Respiratory Diseases of Impaired Mucus Clearance. Toxicol Pathol 35, 116–129. https://doi.org/10.1080/01926230601060025

Lu, Q., Gottlieb, E., Rounds, S., 2018. Effects of cigarette smoke on pulmonary endothelial cells. Am J Physiol Lung Cell Mol Physiol 314, 743–756. https://doi.org/10.1152/ajplung.00373.2017.-Cigarette

Ludueña, R.F., 2013. A Hypothesis on the Origin and Evolution of Tubulin, in: International Review of Cell and Molecular Biology. Elsevier Inc., pp. 41–185. https://doi.org/10.1016/B978-0-12-407699-0.00002-9

Lyu, J., Yang, E.J., Zhang, B., Wu, C., Pardeshi, L., Shi, C., Mou, P.K., Liu, Y., Tan, K., Shim, J.S., 2020. Synthetic lethality of RB1 and aurora A is driven by stathmin-mediated disruption of microtubule dynamics. Nat Commun 11. https://doi.org/10.1038/s41467-020-18872-0

McCarroll, J.A., Gan, P.P., Liu, M., Kavallaris, M., 2010. βIII-tubulin is a multifunctional protein involved in drug sensitivity and tumorigenesis in non-small cell lung cancer. Cancer Res 70, 4995–5003. https://doi.org/10.1158/0008-5472.CAN-09-4487

Nasedkin, A., Ermilova, I., Swenson, J., 2021. Atomistic molecular dynamics simulations of tubulin heterodimers explain the motion of a microtubule. European Biophysics Journal 50, 927–940. https://doi.org/10.1007/s00249-021-01553-1

Ong, M.S., Deng, S., Halim, C.E., Cai, W., Tan, T.Z., Huang, R.Y.J., Sethi, G., Hooi, S.C., Kumar, A.P., Yap, C.T., 2020. Cytoskeletal proteins in cancer and intracellular stress: A therapeutic perspective. Cancers (Basel). https://doi.org/10.3390/cancers12010238

Park, M., Hwang, J.W., Cho, Y., Kim, S., Han, S.H., Yu, J., Ha, S., Kim, W.Y., Kim, S.N., Kim, I.S., Kim, Y.K., 2021. A novel synthetic microtubule inhibitor exerts antiproliferative effects in multidrug resistant cancer cells and cancer stem cells. Sci Rep 11. https://doi.org/10.1038/s41598-021-90337-w

Parker, A.L., Teo, W.S., McCarroll, J.A., Kavallaris, M., 2017. An emerging role for tubulin isotypes in modulating cancer biology and chemotherapy resistance. Int J Mol Sci. https://doi.org/10.3390/ijms18071434

Parker, A.L., Turner, N., McCarroll, J.A., Kavallaris, M., 2016. βIII-Tubulin alters glucose metabolism and stress response signaling to promote cell survival and proliferation in glucose-starved non-small cell lung cancer cells. Carcinogenesis 37, 787–798. https://doi.org/10.1093/carcin/bgw058

Pasquier, E., Honoré, S., Braguer, D., 2006. Microtubule-targeting agents in angiogenesis: Where do we stand? Drug Resistance Updates 9, 74–86. https://doi.org/10.1016/j.drup.2006.04.003

Pathak, D., Sepp, K.J., Hollenbeck, P.J., 2010. Evidence that myosin activity opposes microtubule-based axonal transport of mitochondria. Journal of Neuroscience 30, 8984–8992. https://doi.org/10.1523/JNEUROSCI.1621-10.2010

Peckham, M., 2016. How myosin organization of the actin cytoskeleton contributes to the cancer phenotype. Biochem Soc Trans 44, 1026–1034. https://doi.org/10.1042/BST20160034

Pecqueur, L., Duellberg, C., Dreier, B., Jiang, Q., Wang, C., Plückthun, A., Surrey, T., Gigant, B., Knossow, M., 2012. A designed ankyrin repeat protein selected to bind to tubulin caps the microtubule plus end. Proc Natl Acad Sci U S A 109, 12011–12016. https://doi.org/10.1073/pnas.1204129109

Pozuelos, G.L., Kagda, M., Rubin, M.A., Goniewicz, M.L., Girke, T., Talbot, P., 2022. Transcriptomic Evidence That Switching from Tobacco to Electronic Cigarettes Does Not Reverse Damage to the Respiratory Epithelium. Toxics 10. https://doi.org/10.3390/toxics10070370

Prassanawar, S.S., Panda, D., 2019. Tubulin heterogeneity regulates functions and dynamics of microtubules and plays a role in the development of drug resistance in cancer. Biochemical Journal. https://doi.org/10.1042/BCJ20190123

Rao, J., Li, N., 2004. Microfilament Actin Remodeling as a Potential Target for Cancer Drug Development, Current Cancer Drug Targets.

Rehman, J., Zhang, H.J., Toth, P.T., Zhang, Y., Marsboom, G., Hong, Z., Salgia, R., Husain, A.N., Wietholt, C., Archer, S.L., 2012. Inhibition of mitochondrial fission prevents cell cycle progression in lung cancer. The FASEB Journal 26, 2175–2186. https://doi.org/10.1096/fj.11-196543

Renda, F., Miles, C., Tikhonenko, I., Fisher, R., Carlini, L., Kapoor, T.M., Mogilner, A., Khodjakov, A., 2022. Non-centrosomal microtubules at kinetochores promote rapid chromosome biorientation during mitosis in human cells. Current Biology 32, 1049-1063.e4. https://doi.org/10.1016/j.cub.2022.01.013

Roberts, E.R., Thomas, K.J., 2013. The role of mitochondria in the development and progression of lung cancer, in: Computational and Structural Biotechnology Journal. Research Network of Computational and Structural Biotechnology, p. e201303019. https://doi.org/10.5936/csbj.201303019

Rosas-Salvans, M., Sutanto, R., Suresh, P., Dumont, S., 2022. The Astrin-SKAP complex reduces friction at the kinetochore-microtubule interface. Current Biology 32, 2621-2631.e3. https://doi.org/10.1016/j.cub.2022.04.061

Rovini, A., 2019. Tubulin-VDAC interaction: Molecular basis for mitochondrial dysfunction in chemotherapy-induced peripheral neuropathy. Front Physiol 10. https://doi.org/10.3389/fphys.2019.00671

Saxton, W.M., Hollenbeck, P.J., 2012. The axonal transport of mitochondria. J Cell Sci 125, 2095–2104. https://doi.org/10.1242/jcs.053850

Serpico, A.F., Visconti, R., Grieco, D., 2020. Exploiting immune-dependent effects of microtubule-targeting agents to improve efficacy and tolerability of cancer treatment. Cell Death Dis. https://doi.org/10.1038/s41419-020-2567-0

Sève, P., Dumontet, C., 2008. Is class III β-tubulin a predictive factor in patients receiving tubulin-binding agents?

Shah, D., Joshi, M., Patel, B.M., 2022. Role of NIMA-related kinase 2 in lung cancer: Mechanisms and therapeutic prospects. Fundam Clin Pharmacol. https://doi.org/10.1111/fcp.12777

Sharifi-Rad, J., Quispe, C., Patra, J.K., Singh, Y.D., Panda, M.K., Das, G., Adetunji, C.O., Michael, O.S., Sytar, O., Polito, L., Živković, J., Cruz-Martins, N., Klimek-Szczykutowicz, M., Ekiert, H., Choudhary, M.I., Ayatollahi, S.A., Tynybekov, B., Kobarfard, F., Muntean, A.C., Grozea, I., Daştan, S.D., Butnariu, M., Szopa, A., Calina, D., 2021. Paclitaxel: Application in Modern Oncology and Nanomedicine-Based Cancer Therapy. Oxid Med Cell Longev. https://doi.org/10.1155/2021/3687700

Shoshan-Barmatz, V., Ben-Hail, D., 2012. VDAC, a multi-functional mitochondrial protein as a pharmacological target. Mitochondrion. https://doi.org/10.1016/j.mito.2011.04.001

Singh, R., Pantarotto, D., Lacerda, L., Pastorin, G., dric Klumpp, C., Prato, M., Bianco, A., Kostarelos, K., 2006. Tissue biodistribution and blood clearance rates of intravenously administered carbon nanotube radiotracers.

Soares-de-Oliveira, J., Maiato, H., 2022. Mitosis: Kinetochores determined against random search-and-capture. Current Biology. https://doi.org/10.1016/j.cub.2022.02.003

Sobierajska, K., Wieczorek, K., Ciszewski, W.M., Sacewicz-Hofman, I., Wawro, M.E., Wiktorska, M., Boncela, J., Papiewska-Pajak, I., Kwasniak, P., Wyroba, E., Cierniewski, C.S., Niewiarowska, J., 2016. β-III tubulin modulates the behavior of Snail overexpressed during the epithelial-to-mesenchymal transition in colon cancer cells. Biochim Biophys Acta Mol Cell Res 1863, 2221–2233. https://doi.org/10.1016/j.bbamcr.2016.05.008

Song, Y., Cai, H., Yin, T., Huo, M., Ma, P., Zhou, J., Lai, W., 2018. Paclitaxel-loaded redox-sensitive nanoparticles based on hyaluronic acid-vitamin E succinate conjugates for improved lung cancer treatment. Int J Nanomedicine 13, 1585–1600. https://doi.org/10.2147/IJN.S155383

Song, Z., Shi, Y., Han, Q., Dai, G., 2018. Endothelial growth factor receptor-targeted and reactive oxygen species-responsive lung cancer therapy by docetaxel and resveratrol encapsulated lipid-polymer hybrid nanoparticles. Biomedicine and Pharmacotherapy 105, 18–26. https://doi.org/10.1016/j.biopha.2018.05.095

Souquet, P.J., Geriniere, L., 2001. Docetaxel and non small-cell lung cancer. Prescrire Int 10, 43–45. https://doi.org/10.2217/14750708.3.5.579

Steinmetz, M.O., Prota, A.E., 2018. Microtubule-Targeting Agents: Strategies To Hijack the Cytoskeleton. Trends Cell Biol. https://doi.org/10.1016/j.tcb.2018.05.001

Suresh, R., Diaz, R.J., 2021. The remodelling of actin composition as a hallmark of cancer. Transl Oncol. https://doi.org/10.1016/j.tranon.2021.101051

Świtalska, M., Filip-Psurska, B., Milczarek, M., Psurski, M., Moszyńska, A., Dąbrowska, A.M., Gawrońska, M., Krzymiński, K., Bagiński, M., Bartoszewski, R., Wietrzyk, J., 2022. Combined anticancer therapy with imidazoacridinone analogue C-1305 and paclitaxel in human lung and colon cancer xenografts—Modulation of tumour angiogenesis. J Cell Mol Med 26, 3950–3964. https://doi.org/10.1111/jcmm.17430

Tangutur, A.D., Kumar, D., Krishna, K.V., Kantevari, S., 2017. Microtubule Targeting Agents as Cancer Chemotherapeutics: An Overview of Molecular Hybrids as Stabilizing and Destabilizing Agents. Curr Top Med Chem 17, 2523–2537. https://doi.org/10.2174/1568026617666170104

Thakur, C., 2019. An Overview, Current Challenges of Drug Resistance, and Targeting Metastasis Associated With Lung Cancer, in: Nanotechnology-Based Targeted Drug Delivery Systems for Lung Cancer. Elsevier, pp. 21–38. https://doi.org/10.1016/b978-0-12-815720-6.00002-2

Thompson, S.L., Compton, D.A., 2011. Chromosome missegregation in human cells arises through specific types of kinetochore-microtubule attachment errors. Proc Natl Acad Sci U S A 108, 17974–17978. https://doi.org/10.1073/pnas.1109720108

Tilley, A.E., Walters, M.S., Shaykhiev, R., Crystal, R.G., 2015. Cilia dysfunction in lung disease. Annu Rev Physiol 77, 379–406. https://doi.org/10.1146/annurev-physiol-021014-071931

Vona, R., Mileo, A.M., Matarrese, P., 2021. Microtubule-based mitochondrial dynamics as a valuable therapeutic target in cancer. Cancers (Basel). https://doi.org/10.3390/cancers13225812

Vyas, S., Zaganjor, E., Haigis, M.C., 2016. Mitochondria and Cancer. Cell. https://doi.org/10.1016/j.cell.2016.07.002

Wallmeier, J., Nielsen, K.G., Kuehni, C.E., Lucas, J.S., Leigh, M.W., Zariwala, M.A., Omran, H., 2020. Motile ciliopathies. Nat Rev Dis Primers 6. https://doi.org/10.1038/s41572-020-0209-6

Wang, H., Zeng, X., Zhang, X., Liu, H., Xing, H., 2021. Ammonia exposure induces oxidative stress and inflammation by destroying the microtubule structures and the balance of solute carriers in the trachea of pigs. Ecotoxicol Environ Saf 212. https://doi.org/10.1016/j.ecoenv.2021.111974

Wang, X.S., Zhang, L., Li, X., Kong, D.J., Hu, X.C., DIng, X.Z., Yang, J.Q., Zhao, M.Q., He, Y., Lam, K.S., Gao, S.G., Lin, T.Y., Li, Y., 2018. Nanoformulated paclitaxel and AZD9291 synergistically eradicate non-small-cell lung cancers in vivo. Nanomedicine 13, 1107–1120. https://doi.org/10.2217/nnm-2017-0355

Wijdeven, R.H., Pang, B., Assaraf, Y.G., Neefjes, J., 2016. Old drugs, novel ways out: Drug resistance toward cytotoxic chemotherapeutics. Drug Resistance Updates 28, 65–81. https://doi.org/10.1016/j.drup.2016.07.001

Wijesekara, P., Yadav, P., Perkins, L.A., Stolz, D.B., Franks, J.M., Watkins, S.C., Reinoso Jacome, E., Brody, S.L., Horani, A., Xu, J., Barati Farimani, A., Ren, X., 2022. Engineering rotating apical-out airway organoid for assessing respiratory cilia motility. iScience 25. https://doi.org/10.1016/j.isci.2022.104730

Wong, T.W., 2020. Choice of nanocarrier for pulmonary delivery of cancer therapeutics. Expert Opin Drug Deliv. https://doi.org/10.1080/17425247.2020.1702021

World Health Organization, n.d. Cancer [WWW Document]. URL https://www.who.int/health-topics/cancer#tab=tab_1 (accessed 11.27.22).

Xiong, R., Wu, Y., Wu, Q., Muskhelishvili, L., Davis, K., Tripathi, P., Chen, Y., Chen, T., Bryant, M., Rosenfeldt, H., Healy, S.M., Cao, X., 2021. Integration of transcriptome analysis with pathophysiological endpoints to evaluate cigarette smoke toxicity in an in vitro human airway tissue model. Arch Toxicol 95, 1739–1761. https://doi.org/10.1007/s00204-021-03008-0

Yi, M., Weaver, D., Hajnóczky, G., 2004. Control of mitochondrial motility and distribution by the calcium signal: A homeostatic circuit. Journal of Cell Biology 167, 661–672. https://doi.org/10.1083/jcb.200406038

Yukuyama, M.N., Ferreira Guimaraes, L.M., Segovia, R.S., Lameu, C., de Araujo, G.L.B., Löbenberg, R., de Souza, A., Bazán Henostroza, M.A., Folchini, B.R., Peroni, C.M., Saito Miyagi, M.Y., Oliveira, I.F., Rinaldi Alvarenga, J.F., Fiamoncini, J., Bou-Chacra, N.A., 2022. Malignant wound – The influence of oil components in flubendazole-loaded nanoemulsions in A549 lung cancer xenograft-bearing mice. J Drug Deliv Sci Technol 103963. https://doi.org/10.1016/j.jddst.2022.103963

Yukuyama, M.N., Ishida, K., de Araujo, G.L.B., Spadari, C. de C., de Souza, A., Löbenberg, R., Henostroza, M.A.B., Folchini, B.R., Peroni, C.M., Peters, M.C.C., de Oliveira, I.F., Miyagi, M.Y.S., Bou-Chacra, N.A., 2021. Rational design of oral flubendazole-loaded nanoemulsion for brain delivery in cryptococcosis. Colloids Surf A Physicochem Eng Asp 630. https://doi.org/10.1016/j.colsurfa.2021.127631

CHAPTER 4 – MALIGNANT WOUND – THE INFLUENCE OF OIL COMPONENTS IN FLUBENDAZOLE-LOADED NANOEMULSIONS IN A549 LUNG CANCER XENOGRAFT-BEARING MICE

I am the first author and was responsible for conceptualization, investigation, resources, data curation, project administration, writing - original draft, project administration, funding acquisition.

4.1. INTRODUCTION

Malignant wound (MW), also known as a malignant fungating wound, is a chronic disease commonly occurring in uncontrolled cancer. It is caused by aggressive infiltration of malignant cells into the skin, blood, and lymph vessels, afflicting up to 15% of advanced stage cancer patients [1,2].

MW is reported to be generated among patients with breast, head, and neck, gynecological and lung cancers [3]. The symptoms related to MW are multiple; an extensive review by Tilley et al. (2020) revealed that pain was the most frequent symptom (31.3-77.3%), followed by exudate occurrence (17.9%), malodor (11.9%) and bleeding (6%) [4]. This is a frequent, persistent, and spontaneously occurring disease, with scarce research reported in the world literature.

The malignant evolution of MW may progress to necrosis, putrefaction of tissues, and the generation of strong malodor and exudate, which are considered the main factors that seriously reduce the quality of life in the patients [3]. MW patients already suffer from symptoms of cancer itself, in addition to side effects from chemotherapy and palliative radiation [2]. Moreover, when MW affects these patients' lives, it also affects their family members who care for them daily. Despite its low prevalence compared to other chronic wounds, such as diabetic foot ulcers, venous leg ulcers and pressure ulcers [5] it is an important health problem that affects patients with advanced cancer during the last 6 to 12 months of life, when the cancer becomes uncontrollable. Given MW severity, numerous symptoms, and prolonged treatment time, comprehensive assessment and treatment of patients suffering from MW symptoms become crucial [4].

Because skin is an essential organ that protects the human body against external stresses, wound healing is considered an innate process to reestablish skin from the damages caused by these stresses [6]. Necrotic tissues originating from cancerous wounds are due to the easy proliferation of anaerobic and aerobic bacteria, which are favored by the reduced immunity of cancer patients. Wound debridement can diminish these necrotic tissues that produce strong malodor, mainly caused by anaerobic bacteria. However, mechanical debridement can lead to bleeding and pain. Thus, autolytic and biological debridement are frequently used as a topical treatment for wound healing [7,8]. Calcium alginate, nonadherent coatings (e.g., regenerated oxidized cellulose), and cauterizing substances (e.g., silver nitrate) are the most frequent

therapeutic approaches [1]. Nevertheless, they show limitations for intense, pulsating bleeding resulting from the rupture of larger blood vessels [5].

Despite a lack of studies reported in the literature, the use of oils and fatty acids for open wound treatments is an effective and affordable-cost approach [9]. Several recent studies have demonstrated the efficacy of wound healing properties of oils, specifically fatty acids.

Tanideh et al. (2016) evaluated the effect of fish oil in combination with honey on wound healing in rats. The topical treatment with this combination showed the best improvement in wound contraction and epithelialization of animals after 14 consecutive days. Fish oil has a high content of omega-3 fatty acids, which are known to inhibit arachidonic acid synthesis and reduce dermatitis and platelet aggregation [10]. *Opuntia ficus indica L. inermis* (OFI), a natural bioactive compound rich in unsaturated free fatty acids (linoleic and oleic acids), was investigated by employing an excisional wound healing model in rats. After the ninth day of consecutive topical application, a significant wound contraction was observed, followed by better dermis extracellular matrix organization in OFI-treated rats than in normal saline-treated rats [6]. Bardaa et al. (2016) analyzed cold-pressed oil from pumpkin seed (*Cucurbita* pepo L.) for wound healing properties. This oil, containing a high amount of linoleic acid ($\approx$ 50% of total fatty acids), showed full re-epithelialization and well-organized collagen fibers and no inflammatory cells after topical treatment compared to untreated animals [11]. Additionally, Poljšak et al. (2019) summarized the wound healing properties of several vegetable butters and oils including black cumin, cranberry, grape, green coffee, lucuma, pumpkin oils and others rich in linoleic acid. These components demonstrated, in many cases, more effective wound healing properties than synthetic compounds used as topical wound-healing controls [12]. Additionally, topically delivered ionic polymeric micelles were developed by combining chitosan and linoleic or oleic acids for wound healing purposes. The results demonstrated these micelles as promising carriers for loading low-water-soluble drugs, aiming to improve dermal regeneration and tissue repair during wound healing [13].

In addition to oil components, our previous study applying FLZ nanocrystals for lung tumor inhibition reported the absence of necrotic spots on the tumor. This MW was detected in the control group without FLZ application [14]. FLZ is an anthelmintic drug in Class II of the Biopharmaceutical Classification System and has demonstrated several antitumor effects in recent works [15–17].

Considering the implications of MW symptoms in topical treatments - such as daily care by trained healthcare workers and risk of bleeding and pain during treatment - a more convenient administration route, mainly oral administration, might be a promising approach for greater patient compliance. However, a limitation of the oral route is reduced bioavailability, especially for low-water-soluble drugs, such as FLZ. Thus, a nanostructure approach is recommended to overcome this limitation. Among nanostructures, nanoemulsions are one of the best options for associating low-water-soluble drugs with oil components. Nevertheless, the high oil content makes it challenging to obtain a nanosized emulsion. The D-phase emulsification (DPE) process offers several advantages due to the lack of dependency on specific equipment, such as a high-pressure homogenizer and the lack of need for strict adjustment of hydrophilic-lipophilic-balance of the emulsion system [18].

To the best of our knowledge, there is no reported work comparing different oils in a drug-loaded nanoemulsion with high oil content prepared by the D-phase emulsification process and administered by the oral route. In the present work, we propose a new oral treatment alternative for MW, comparing the effect of two different oils in FLZ-loaded-nanoemulsion and FLZ in suspension and evaluating the synergy of FLZ and oil in an A549 xenograft animal model.

4.2. MATERIALS

FLZ was obtained from Changzhou Yabang—QH Pharmachem CO., LTD (Jiangsu, China). Maisine CC® (glyceryl monolinoleate) was a gift from Gattefossée (Sao Paulo, Brazil) and Mcassab (Sao Paulo, Brazil); Capmul® MCM was kindly provided by ABITEC Corp. (Columbus, OH, US); glycerin and polysorbate 80 were purchased from Sigma-Aldrich (Brazil) and Soluplus® was kindly donated from BASF (Brazil). Milli-Q® ultrapure water was used.

4.3. METHODS

4.3.1. Development of flubendazole-loaded nanoemulsions: preparation and optimization

The preparation of FLZ-loaded nanoemulsion containing Capmul MCM as the main oil phase was carried out using the DPE process and DoE statistical analysis.

FLZ was solubilized in oil (1 mg FLZ/2 g total oil) by constant mixing using a magnetic bar at 90 ± 0.5 °C and cooled to 25 ± 0.5 °C to form the oil phase. For preparation by the DPE process, first, an isotropic phase consisting of initial water, glycerin, and polysorbate 80 was mixed. Then, the oil phase containing FLZ was added dropwise with constant homogenization at 300 rpm (all at 25 ± 0.5 °C) and the mixture was kept for 20 minutes under the same condition. Then, the remaining water was added dropwise at the same temperature with constant agitation at 300 rpm to form the final oil-in-water (O/W) nanoemulsion.

The composition of the preparations was determined by the DoE statistical method. The initial water, glycerin, and oil phase concentrations were selected as independent variables, and mean particle size (MPS) was selected as the dependent variable or response. The generation of matrices of experiments was carried out using Minitab software, version 18 (State College, PA, US).

For optimization of the FLZ-loaded nanoemulsion, a desirability composite function method was used to optimize the response with Minitab 18 statistical software. The desirability was used to identify the lowest MPS of the nanoemulsion with the highest oil phase concentration. The desirability of compound (d) ranges from 0 to 1, where 1 represents the lowest MPS, and 0 represents the largest MPS.

The preparation of an FLZ-loaded nanoemulsion containing Maisine CC® as the only oil phase (MF nanoemulsion) was carried out using the same process obtained in our previous work [19].

4.3.2. Determination of mean particle size and polydispersity index

The evaluation of mean particle size (MPS) and polydispersity index (PI) was carried out by the dynamic light scattering method using Zetasizer Nano ZS90 equipment (Malvern Inst. Malvern, UK). The FLZ-loaded nanoemulsions were properly diluted with Milli-Q ultrapure water. The results correspond to the means of three determinations at a 90° angle.

4.3.3. Flubendazole entrapment efficiency

The entrapment efficiency of the FLZ-loaded nanoemulsion was assessed by Centrifuge 5424-11, Eppendorf® equipment, centrifuging with an ultrafilter (Amicon®Ultra 50 kDa - 0.5 mL) at 5000 rpm and 25 °C for 10 minutes. FLZ was extracted using Milli-Q water with an appropriate dilution. The free FLZ in the supernatant was analyzed by the Evolution 201 spectrophotometer at 310 nm (Thermo Fisher Scientific Inc., Waltham, MA, USA).

The entrapment efficiency (EE%) was calculated using Equation (4.1):

$$EE\ (\%) = (W_T - W_F) / W_T \times 100 \qquad \text{(Equation 4.1)}$$

where W_T refers to the total amount of FLZ, and W_F refers to the FLZ amount in the supernatant.

4.3.4. Stability of the optimized flubendazole-loaded nanoemulsion

The sample was stored in a borosilicate glass bottle at 25 ± 0.5 °C for three months. MPS, PDI analyses, and visual inspection of the nanoemulsion were carried out immediately after their preparation and at 30-day intervals.

4.3.5. Lung cancer xenograft murine model

4.3.5.1. A-549 lung cancer cell culture

The human lung cancer cell line A-549 (CCL-185) was used in this study. The A-549 cells were cultivated in cell plus culture flasks (Sarstedt) in size T-75 at 37 °C in an incubator with an atmosphere composed of 5% CO_2 in a maintenance medium consisting of RPMI (LGC-Biotechnology) supplemented with 10% fetal bovine serum (FBS -LGC-Biotechnology) and penicillin/streptomycin (1%). The culture medium was changed every 2 days.

4.3.5.2. Tumorsphere formation

After the cells reached 80% confluence in the flask and washed with PBS, 5 mL of trypsin (Gibco) was added, and the flask was kept in an CO2 incubator at 37 °C for 5 minutes. Cell counting was performed using a Neubauer chamber. Then, the cells were transferred to new flasks, which were previously treated with 2% pluronic acid for 24 hours, to form tumorspheres. A total of $10X10^6$ cells were used for the 175 cm^2 hydrophobic flasks (T-175) with a defined medium containing RPMI, penicillin, streptomycin (1%), epidermal growth factor EGF (Sigma–Aldrich - 20 ng/mL), basic fibroblast growth-b FGF (Sigma–Aldrich - 20 ng/mL) and a set of N2 supplements (1x - Life Technologies). The cells were kept for four days without changing the medium for the formation of tumorspheres and monitored under a microscope daily.

4.3.5.3. A549 cell subcutaneous injection in mice

BALB/c nude male mice were kept in a controlled environment with a central air conditioning system for ventilation and exhaustion, controlled lighting of 12 hours light/12 hours dark, and a temperature maintained at 22 °C with food and water ad libitum. The tumorspheres were centrifuged at low speed at 1100 rpm for 10 minutes; the medium was discarded, and the pellet was resuspended in 1X phosphate-buffered saline (PBS) for cell counting in a Neubauer chamber. These cells were resuspended in 50 µL of PBS and 50 µL of Matrigel®, and

approximately $2X10^6$ cells were injected into the subcutaneous region of the lower right flank per mouse to monitor tumor growth and finally compare the different treatments.

Forty-eight hours after the injection of tumor cells, the first administration of samples via gavage was performed in the mice. After that, samples were administered three times a week, and animal weight and tumor size were monitored twice a week. The mice were divided into 6 groups of 5 animals as follows:

(C): no xenotransplantation or treatment
(XC): bearing A549 cell line xenografts, no treatment
(FS): bearing A549 cell line xenografts treated with FLZ in suspension (micronized)
(NE CM): bearing A549 cell line xenografts treated drug-free nanoemulsion containing Capmul MCM and Maisine CC® as oil phase (CM nanoemulsion)
(NE MF): bearing A549 cell line xenografts treated with FLZ-loaded nanoemulsion containing Maisine CC® as oil phase (MF nanoemulsion)
(NE CMF): bearing A549 cell line xenografts treated with FLZ-loaded nanoemulsion containing Capmul MCM and Maisine CC® as oil phase (CMF nanoemulsion)

The nanoemulsions were previously diluted with Milli-Q water to facilitate flow through the gavage needle, and the final dose of FLZ administered in each nanoemulsion was 0.8 mg FLZ/kg per animal three times a week. The FLZ suspension (micronized FLZ) was administered at the same drug concentration as in the nanoemulsions.

This experiment is in accordance with the Ethical Principles in Animal Experimentation adopted by the National Institutes of Health guide for the care and use of Laboratory animals (NIH Publications No. 8023, revised 1978), which was followed, and was approved by the Ethics Committee on Animal Use, from IQ-USP, on February 18th, 2020 (Certificate number 164/2020).

For monitoring and endpoints, the general appearance and behavior of the animals were constantly monitored to assess their health conditions in the entire experimental stages. Based on this assessment, the early interruption of the experiments occurs in the following cases: a situation of threat to the health and well-being of the animals; excessive weight loss in a short period of time; impossibility of using medication to relieve distress or suffering; loss of stitches with opening of the incision; or even when the physical conditions of the animals make it impossible to obtain

reliable experimental data for the study. Once these occurrences are verified, the animals must be euthanized. All conditions and manifestations related to the progress of the experiment and the well-being of the animals were monitored, along the IACUC "Scoring and endpoints in tumor studies in rats and mice". Accordingly, 3 points were evaluated in the animals under experiment, daily: general appearance of the animal, size and degree of necrosis of the tumor and changes in the animal's weight. These 3 aspects were analyzed for each animal and, according to its score, it remained in the experiment or euthanized, thus minimizing the suffering of the animals. (https://research.utsa.edu/_files/pdfs/compliance-integrity-pdf-folder/iacuc-forms/IACP-Policy-012-Revision-2-Approved-02-07-19-Scoring-and-Endpoints-in-Tumor-Studies-in-Rats-and-Mice.pdf)

4.3.5.4. Statistical analysis

Changes in the volume of the tumor or animal weight as a function of the segment days of the experiment were evaluated using unilateral analysis of variance (ANOVA). P-values below 5% (p-value < 0.05) were considered statistically significant.

4.4. RESULTS

4.4.1. Preparation and optimization of nanoemulsions with statistical design

A screening test was performed to find the ratio between Capmul MCM and Maisine CC® that offered the best stability (data not shown). The 10:0 ratio for Capmul MCM:Maisine CC showed separation within one month at 25.0 °C. The 8:2 ratio for Capmul MCM:Maisine CC showed the best stability and therefore was selected to assess the influence of independent variables (oil phase concentration, glycerin, and initial water) on the MPS characteristics. The test matrix (**Table 4.1**) presents the concentrations of the variables: 40.0, 50.0 and 60.0% (w/w) for the oil phase, 2.0, 3.0 and 4.0% (w/w) for glycerin and 2.0, 3.0 and 4.0% (w/w) for initial water. Matrix construction and analysis of the results were carried out by the Box–Behnken response surface with 3 central point using Minitab 18 software.

Table 4.1: Test matrix for preparing nanoemulsions containing flubendazole using Capmul MCM:Maisine CC (8:2 ratio) as the oil phase, and experimental results of mean particle size (MPI) and podispersity index (PI)

	Oil phase (% w/w)	Glycerin (%w/w)	Initial water (%w/w)	MPS (nm)	PI
1	60.0	3.0	4.0	70.15±2.44	0.367±0.101
2	50.0	3.0	3.0	83.88±9.90	0.219±0.070
3	40.0	4.0	3.0	117.00 ±10.60	0.285±0.154
4	50.0	4.0	4.0	84.52±10.30	0.242±0.182
5	60.0	3.0	2.0	72.20±2.32	0.403±0.058
6	50.0	3.0	3.0	86.03±4.91	0.350±0.086
7	40.0	3.0	2.0	112.40±12.02	0.207±0.138
8	50.0	3.0	3.0	85.88±2.55	0.391±0.089
9	50.0	4.0	2.0	88.81±6.03	0.326±0.133
10	50.0	2.0	4.0	65.06±3.32	0.391±0.006
11	50.0	2.0	2.0	85.24±2.18	0.427±0.011
12	60.0	4.0	3.0	76.21±1.53	0.441±0.011
13	40.0	2.0	3.0	109.20±2.75	0.472±0.026
14	60.0	2.0	3.0	73.92±1.62	0.425±0.004
15	40.0	3.0	4.0	99.98±12.97	0.200±0.120

MPS: mean particle size; **PI:** polydispersity index

The surfactants were used at fixed concentrations of 2.0% (w/w) polysorbate 80 and 4.5% (w/w) Soluplus:H_2O (1:2), and the remaining water to complete 100.0% (w/w).

The MPS of the prepared nanoemulsions ranged between 65.06 and 117.0 nm, and PI ranged between 0.200 and 0.472. A PI below 0.500 indicates good homogeneity of the prepared nanoemulsion system.

Table 4.2 shows analysis of variance (ANOVA) of resulting quadratic polynomial models for MPS of FLZ-loaded nanoemulsion. This analysis was done to identify significant factors (independent variables) and conduct a statistical analysis of the regression model [20]. Effects corresponding to investigated independent variables (concentration of oil, glycerin, and initial water) for MPS were evaluated. The "p value" represents the significance of the regression coefficients for a polynomial equation, where a "p value" less than 0.05 ($\alpha = 0.05$) indicates that the corresponding coefficient was significant [21,22] The significant independent variables were oil concentration ("p value" equal to 0.000 and 0.003), glycerin ("p value" equal to 0.016) and initial water ("p value" equal to 0.007 and 0.039). The lack of adjustment was not significant ("p value" equal to 0.071, greater than 0.05), indicating minimal pure errors (such as experimental errors) [23]. This result indicates adequacy of the proposed quadratic polynomial model.

Table 4.2: Analysis of variance to evaluate the significance of the regression of data obtained for evaluating mean particle size (MPS) of flubendazole nanoemulsion containing the following variables: concentration of oil, glycerin and initial water (all % w/w)

Source	DF	SS (adj)	MS (adj)	f value	p-value
Model	5	3360.82	672.16	43.41	0.000
Linear	3	2994.27	998.09	64.47	0.000
Oil (% w/w)	1	2667.42	2667.42	172.29	**0.000**
Glycerin (%w/w)	1	137.12	137.12	8.86	**0.016**
Initial water (%w/w)	1	189.74	189.74	12.25	**0.007**
Square	2	366.55	183.27	11.84	0.003
Oil (%w/w)*Oil (%w/w)	1	253.39	253.39	16.37	**0.003**
Initial water (%w/w)* Initial water (%w/w)	1	89.74	89.74	5.80	**0.039**
Error	9	139.34	15.48		
Lack of fit	7	136.46	19.49	13.53	**0.071**
Pure error	2	2.88	1.44	*	*
Total	14	3500.16			

$R^2 = 96.02\%$; $R^2_{(adj)} = 93.81$ 5; $R^2_{(pred)} = 87.34\%$)

DF: degrees of freedom; **SS $_{(adj)}$:** sequential sums of squares; **MS $_{(adj)}$:** adjusted sequential mean square; **f value:** value on the F distribution; **p value:** lack-of-fit adjustment; R^2**:** multiple correlation coefficient; R^2 $_{(adj)}$**:** adjusted multiple correlation coefficient; R^2 $_{(pred)}$**:** predicted correlation coefficient.

The quadratic regression model demonstrated a multiple correlation coefficient (R_2) for the MPS of 96.02%, indicating that this response value can be attributed to the identified independent variables. The adjusted multiple correlation coefficient (R_2 adj), which reflects the correlation between the experimental and predicted values, was 93.81%. This value is close to R_2, indicating a good statistical model. The predicted correlation coefficient (R_2 pred) was 87.34%, indicating how well the model predicts responses to new observations (**Table 4.2**).

The quadratic model for MPS of FLZ-loaded nanoemulsion (containing Capmul MCM and Maisine CC® as oil phase) was generated, as shown in the regression equation, in noncoded factor units (**Equation 4.2**):

MPS (nm) = 341.3 - 10.09 Oil + 4.14 Glycerin + 24.6 Initial water + 0.0826 Oil *Oil – 4.92 Initial water * Initial water   (**Equation 4.2**)

Figure 4.1 plots the main effects on MPS of the nanoemulsion. This result revealed that the oil concentration significantly contributes to reducing MPS. The oil and initial water concentrations have a quadratic effect on the MPS, being inversely proportional to the oil. The glycerin concentration has a linear effect, which is directly proportional to MPS.
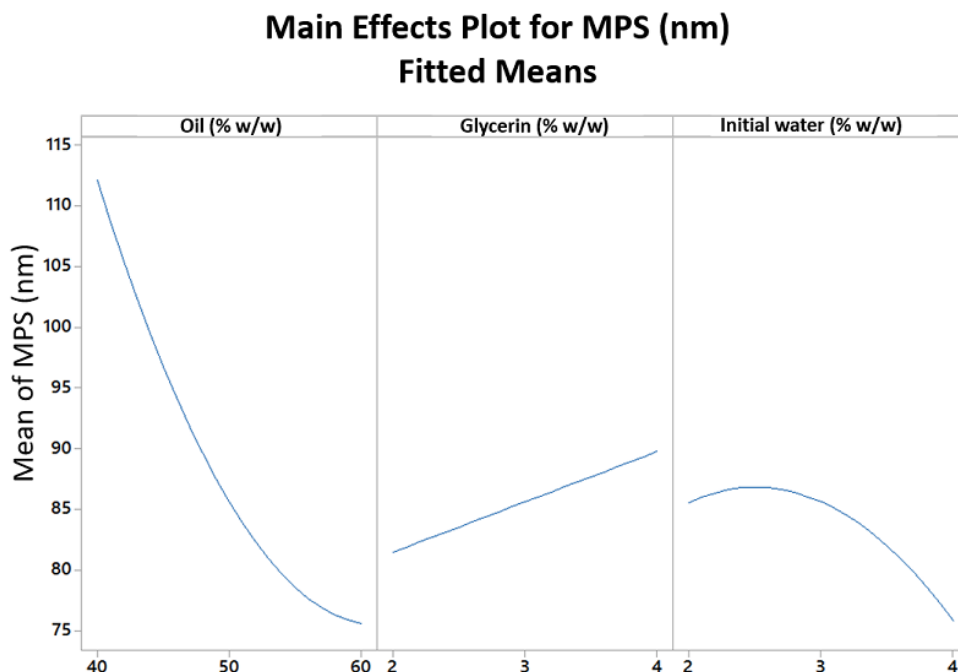
Figure 4.1: Main effects graph for evaluating the mean particle size of nanoemulsions containing flubendazole, Capmul MCM and Maisine CC (8:2) as the oil phase

Source: Minitab®

The nanoemulsion optimization process based on the regression equation indicated a condition to produce a lower MPS and a higher oil phase concentration, composed of Capmul MCM:Maisine CC at a ratio of 8:2. Optimal conditions within a desirability of 1,000 were found by combining a concentration of 60.0% (w/w) of oil, 2.0% (w/w) of glycerin, and 4.0% (w/w) of initial water, giving a theoretical MPS of 61.66 nm (**Figure 4.2**). The experimental value resulting from these conditions was a MPS of 61.07 ± 3.07 nm, with a PI of 0.375 ± 0.077 (CMF nanoemulsion). As shown in **Table 4.3**, the predicted MPS obtained experimentally through **Equation 4.2** validated the proposed model.

Table 4.3: Theoretical and experimental value of MPS of response surface optimized preparation

Oil (% w/w)	Glycerin (%w/w)	Initial water (%w/w)	Theoretical MPS	Experimental MPS (nm)	Experimental PI

			(nm)		
60.0	2.0	4.0	61.66	61.07±3.07	0.375±0.077

4.4.2. Stability of the optimized nanoemulsion

The stability of the optimized CMF nanoemulsion for 3 months at 25.0 ± 0.5 °C is shown in **Table 4.4**. There was no phase separation, and the MPS and PI values were practically unaltered during the 3 months of stability.

Table 4.4: Results of the optimized nanoemulsion containing flubendazole and Capmul MCM: Maisine CC (8:2) as the oil phase for three months stability evaluation at 25 ± 0.5 °C.

Time	MPS (nm)	PI	Visual aspect
0 D	61.07±3.07	0.375±0.077	No separation
1 M	72.66±2.66	0.370±0.083	No separation
2 M	58.83±2.82	0.394±0.024	No separation
3 M	65.82±2.48	0.376±0.081	No separation

MPS: mean particle size; **PI:** polydispersity index; **D:** day and **M:** month

4.4.3. Entrapment efficacy of flubendazole-loaded nanoemulsions

FLZ quantification was carried out using UV spectrophotometry at a wavelength of 310 nm. The collected supernatant containing FLZ was diluted in acetonitrile. The free drug nanoemulsion was used as a blank to avoid overlapping or interference from the excipients in this nanoemulsion. The calibration curve of FLZ concentration (x, µg/mL) versus absorbance (y) was y = 0.0372 x + 0.1121, with a correlation coefficient of 0.9929.

The optimized CMF nanoemulsion resulted in a final EE (%) of 99.9%.

4.4.4. *Efficacy of treatments for MWs of BALB/c nude mice bearing A549 lung cancer xenografts*

Aiming at evaluating the efficacy of treatments for MWs, the present study was sequenced according to the following aims: first, to evaluate the effect on MWs of FLZ at micronized size as a suspension; second, to evaluate the effect of oil components in nanoemulsion without FLZ; and finally, to study the effects of two different oils – medium-chain oil (Capmul MCM) and long-chain oil (Maisine CC®) in FLZ-loaded nanoemulsion - both approved for oral administration.

The treatments were administered orally. Aiming at verifying the influence of the gavage process and stress on MW development in BALB/c nude mice, the MW development in untreated tumor xenograft-bearing mice that were not assayed with the gavage procedure (group: positive control) was also evaluated. The MW treatment efficacy results are shown in **Figures 4.3a** to 4.**3e**.

When the animals reached the total acceptance score limit, they were euthanized immediately.
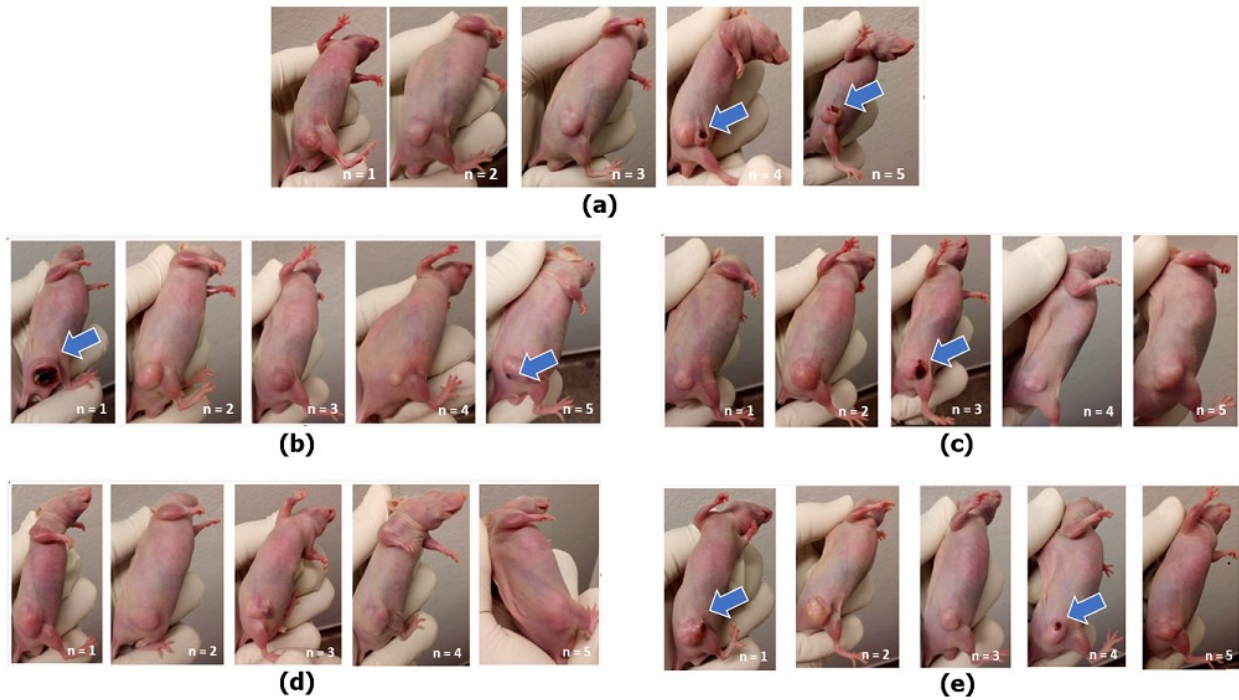
Figure 4.3: Malignant wounds of A-549 tumor xenograft-bearing mice with (a) no treatment, (b) flubendazole in suspension, (c) drug-free nanoemulsion, (d) flubendazole-loaded nanoemulsion

with Maisine CC and (e) flubendazole-loaded nanoemulsion with Capmul MCM: Maisine CC (8:2), after 80-day sample treatment date. The blue arrow shows the malignant wound emergence and its size. Total of 5 animals (from n=1 to n=5).

Source: Own authorship

Untreated mice: **Figure 4.3a** shows the MW results in untreated mice. As noted, 40% of mice presented MWs that comprised approximately half of the tumor area. Open wounds and exudation were observed after 38 days of test sample treatment date.

Animals treated with FLZ in suspension: as observed in **Figure 4.3b**, MWs with open wounds and exudate occurred in 40% of mice treated with FLZ in suspension (micronized form). One mouse showed an apparent open wound covering almost the entire tumor. These MWs appeared after 38 days of treatment.

Animals treated with drug-free nanoemulsion: **Figure 4.3c** shows open wound and exudate in 20% of mice treated with the drug-free nanoemulsion. This MW comprised approximately half of the tumor area and emerged after 38 days of treatment.

Animals treated with FLZ-loaded nanoemulsions with Maisine CC®: as demonstrated in **Figure 4.3d**, none of the animals treated with the MF nanoemulsion presented MW with exudate or bleeding after 80 days of treatment.

Animals treated with FLZ-loaded nanoemulsions with Capmul MCM:Maisine CC (8:2): **Figure 4.3e** shows the presence of open wounds and exudate in 40% of animals treated with CMF nanoemulsion. However, the size of the MW represents less than half of the tumor area. These MWs appeared after 52 days of treatment.

4.4.5. *Tumor growth in A-549 tumor cell xenograft – untreated and treated animals*

Figure 4.4 demonstrates no significant improvement in tumor size reduction when FLZ-loaded nanoemulsions or drug suspension were applied in the present work. The group of mice treated with drug-free nanoemulsion was not included in this tumor size evaluation, but only for

MW evaluation. The weight of the mice was also followed for 80 days, and there was no significant difference among the tested animals (Supplementary material, **Figure 4.S1**).
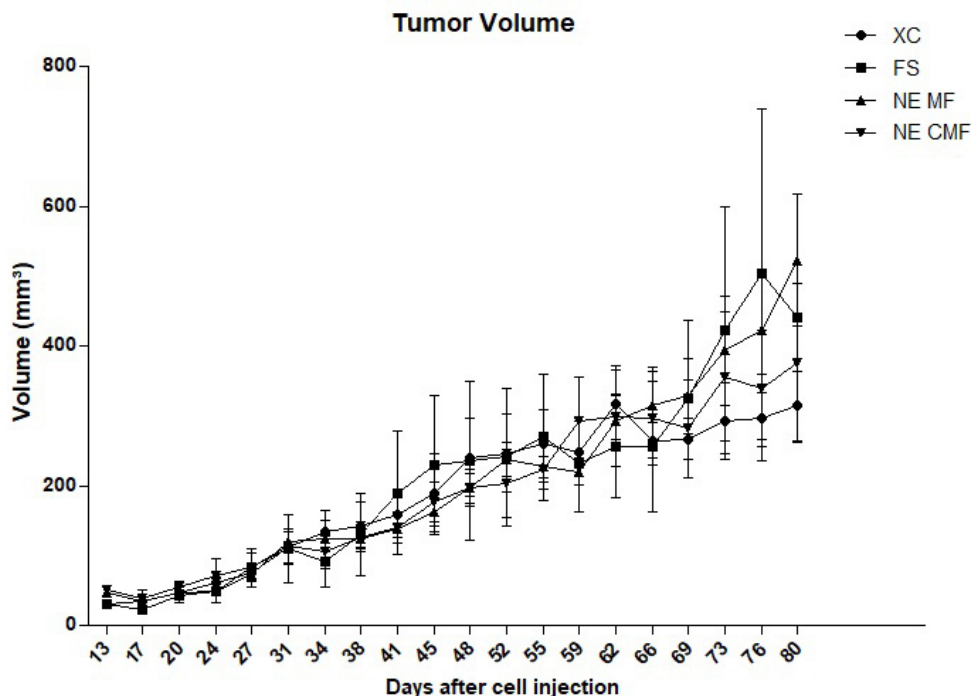
Figure 4.4: Tumor growth in lung cancer murine model. XC: xenograft-bearing untreated mice (without gavage); FS: xenograft-bearing mice treated with flubendazole in suspension (0.8 mg of flubendazole/kg animal); NE MF: xenograft-bearing mice treated with flubendazole-loaded nanoemulsion containing Maisine CC (0.8 mg of flubendazole/kg animal); NE CMF: xenograft-bearing mice treated with flubendazole-loaded nanoemulsion containing Capmul CC:Maisine CC (8:2) (0.8 mg of flubendazole/kg animal)

Source: Own authorship

4.5. DISCUSSION

MW, a disease with devastating effects throughout the final months of cancer patients' lives affects the physical, social, and psychological aspects of these patients and their families. Despite its severe impact, few studies have been reported in the literature until now, and treatment alternatives are lacking for this illness. We evaluated a poorly water-soluble drug, FLZ, solubilized in two different oils to enhance the MW healing effect. The oral route was selected as an easy and

cost-effective alternative for treatment administration to ameliorate patients' quality of life and support those caring for them. Moreover, we developed an FLZ-loaded nanoemulsion to overcome the limitation of bioavailability by this route. The DPE process was used in association with the DoE statistical tool to provide a high oil content nanoemulsion with a low surfactant concentration. Consequently, we successfully obtained an optimized oil-in-water FLZ-loaded nanoemulsion with 60.0% (w/w) medium-chain oil as the main oil phase at a 25 °C processing temperature, without the need for specific equipment, using only 3.5% (w/w) hydrophilic surfactants.

DPE is a low-energy process that differs from other conventional low-energy processes, such as phase inversion temperature (PIT) or phase inversion composition (PIC) methods, which require strict adjustment of the HLB of the system. In the DPE process, creating an isotropic phase enables incorporating high content of the oil phase, forming an oil-in-surfactant (O/D) phase. Then, by water phase addition, this O/D phase is converted into an O/W nanoemulsion [24,25]. The combination of DPE with a statistical approach resulted in a high-oil content CMF nanoemulsion with 61.07±3.07 nm, which was stable for three months at 25 °C.

According to the results obtained in this study, the system consisting of only Capmul MCM as the oil phase did not present good stability. Compared with Maisine CC®, this compound has high polarity, resulting in greater affinity for the external aqueous phase. This affinity allows the diffusion of the internal oil phase from smaller to larger micelles through the external aqueous phase with greater ease. This diffusion caused by the Laplace pressure difference between micelles of different sizes, called the Ostwald ripening phenomenon, is mainly responsible for the instability of nanoemulsions [26]. Several attempts are presented in studies to overcome the instability of nanoemulsions caused by this phenomenon. Adding an oil phase with a lower affinity for the external phase, even at low concentrations, is one of the proposals observed [27,28]. Thus, the addition of Maisine CC® at a minimum ratio of 20% (w/w) of total oil contributed to the stability improvement of this nanoemulsion.

This nanoemulsion was compared to another FLZ-loaded nanoemulsion, consisting of Maisine CC® (MF nanoemulsion) as the only oil component, developed in our previous study [19].

From the results of the in vivo test, it was possible to verify that lung cancer xenograft-bearing mice from the five groups - untreated, treated with micronized FLZ, treated with FLZ nanoemulsions, and free drug nanoemulsion - presented different profiles of MW development

over time (**Figure 3a to 3b**). Additionally, all treated mice were compared to the positive control group (untreated tumor xenograft-bearing animals) that was not subjected to possible stress by the gavage process.

4.5.1. *Effectiveness of flubendazole in suspension on malignant wounds*

Micronized FLZ (suspension in water) was applied by oral administration and the results demonstrated that 40% of treated animals presented MWs, with a notable large open wound in one of the animals compared to the others. One reason for this gap may be due to the nonhomogeneous size of FLZ when applied as a suspension. Herein, the FLZ suspension could not retard MW development at an administration dose of 0.8 mg FLZ/kg of mice, 3 times per week by gavage. This dose is equivalent to 2.4 mg FLZ/kg of animal per week. In previous work by our group [14], we observed no development of MWs in animals treated with nanocrystals (administration doses of 14 mg FLZ/kg of animal) once a week by intraperitoneal administration. Nevertheless, this effect was not observed when the same dose (14 mg FLZ/kg of animal) was administered as FLZ suspension, which agrees with our present results.

4.5.2. *Malignant wound in A-549 tumor cell xenografts – mice treated with drug-free nanoemulsion*

Drug-free nanoemulsion composed of a combination of Capmul CMC:Maisine CC (8:2) presented a reduced number of MW occurrences (20% of total occurrence) after 38 days of treatment. It did not reduce the time of occurrence, but it seems to be promising for reducing MW frequency when compared to the untreated group that showed 40% of total occurrence. Capmul CC is derived from medium-chain fatty acids, and Maisine CC® is derived from linoleic acid, a long-chain fatty acid.

The oral administration of fatty acids has been reported to have wound healing effects: in rats, oral ingestion of oleic and linoleic acids was carried out, and the results demonstrated that both fatty acids accelerate the inflammatory phase of wound healing. However, these mechanisms were different. Both oleic and linoleic acids reduced the concentrations of IL-1, IL-6, and

macrophage inflammatory protein-3 and decreased NF-kB activation at 24-hours post-wounding. However, at 1-hour post-wounding, linoleic acid increased the concentration of hydrogen peroxide and cytokine-induced neutrophils, the influx of inflammatory cells, and the activation of transcription factor activator protein-1 in the wound. In contrast, oleic acid increased the concentration of TNF- and NF-kB activation [9], different effects from different fatty acids are expected for wound treatment.

4.5.3. *Effectiveness of flubendazole-loaded nanoemulsions on malignant wounds*

An interesting result was demonstrated when we compared FLZ-loaded nanoemulsions with different oil contents in combination with FLZ. Even if it was impossible to impede tumor growth, nanoemulsion containing only Maisine CC® (MF nanoemulsion) prevented the development of MW in 100% of cases (n=5) after 80 days of treatment.

On the other hand, 40% of the animals treated with nanoemulsion containing Capmul CMC:Maisine CC (8:2) (CMF nanoemulsion) developed MWs. Although the percentage of occurrence was equal to that of the xenografted untreated animals without the gavage and higher than that of animals treated with the drug-free nanoemulsion, two improvements were observed. The MW in both untreated animals and treated with drug-free nanoemulsion represented approximately half the size of the tumor. The MWs of animals treated with FLZ-loaded nanoemulsions containing this combination of oils were less than half the size of the tumor. Another difference is the timing of MW emergence. Both untreated animals and animals treated with drug-free nanoemulsions developed MWs within 38 days. In contrast, the animals treated with these combined oils and FLZ developed MWs after 52 days, showing a significant delay of two weeks in MW emergence.

As a matter of dosage comparison, in the previous work [14], FLZ nanocrystals showed a positive result on MW by intraperitoneal administration applying 14 mg FLZ/kg of animal, once a week. In the present work, we observed the MW treatment efficacy by administering a dose of 0.8 mg FLZ/kg of the animal as a nanoemulsion three times per week by gavage. This dose is equivalent to 2.4 mg FLZ/kg of the animal per week, which corresponds to a 6-fold lower concentration of FLZ than FLZ in the nanocrystal.

Thus, using the suitable oil component, mainly derived from linoleic acid, in combination with FLZ loaded in nanoemulsion presented a significant improvement of MW treatment by oral administration.

As a sequence, to better understand the possible mechanism of wound healing, these four sequential steps are generally involved in the wound healing process: (1) hemostasis to stop bleeding; (2) inflammation with the recruitment of immune cells and delivery of inflammatory mediators; (3) proliferation with vascular proliferation (angiogenesis) and granulation tissue formation; and (4) remodeling with wound closure [6,9,12]. The vascular proliferation step seems to cause a greater risk of bleeding [29].

It has also been reported that the angiogenesis and inflammatory phases seem to play essential roles in the wound healing process. Angiogenesis, the formation of new vessels from pre-existing vessels, promotes the migration of immune cells and mediators and restores the supply of nutrients and oxygen to the wound area. This process is upregulated by growth factors (e.g., VEGF and ANGPT-2) and downregulated by angiostatin and tumor growth factor-β (TGF-β). Several mediators and cells (e.g., neutrophils, macrophages, endothelial cells) are involved in the wound healing process, and the duration or intensity of the inflammatory phase influences the onset of the next phase and may impair angiogenesis progression [30].

Maisine CC® is derived from linoleic acid, an essential omega-6 fatty acid. This component is found in ceramides in the stratum corneum and in the phospholipids of human cell membranes [12]. Linoleic acid plays a key role in the inflammatory process since it is the precursor of arachidonic acid that generates essential inflammatory mediators (prostaglandins, thromboxane, and leukotrienes). These mediators enhance local neovascularization, remodel the extracellular matrix, and enhance the migration of cells and fibroblastic differentiation to accelerate the dynamics of wound healing [31]. It also activates peroxisome proliferator-activated receptor alpha (PPARα), a nuclear receptor expressed by keratinocytes involved in keratinocyte proliferation, lipid barrier homeostasis, and inflammation [12].

It should be noted that linoleic acid plays an essential role in enhancing fibroblast mitogenesis by influencing the epidermal growth factor-regulated sequence of biochemical events, inducing early formation of granulation tissue [32]. An interesting study carried out by Manosalva et al. (2020) evaluated the possible mechanism of linoleic acid on keratinocytes through FFA1, the

free fatty acid receptor 1, in which linoleic acid is its natural ligand. FFA1 is a G protein-coupled receptor that modulates the inflammatory process. Using a human keratinocyte cell line that expresses the FFA1 receptor, HaCaT cells, they showed that through FFA1, linoleic acid increased HaCaT cell migration by activating the ERK12 and p38 signaling pathways. In addition, it increased MMP-9 activity and the expression of IL-8, which contribute to neutrophil chemotaxis and could accelerate wound healing processes [33].

Concerning FLZ, two pathways are regulated by this drug: the STAT3 (signal transducer and activator of transcription 3) axis and the NF-kB (a crucial transcription factor in the signal transduction cascade of inflammatory signaling) axis. STAT3 has been linked to cell proliferation and differentiation, apoptosis, angiogenesis, metastasis, immune responses, and therapeutic resistance [34,35]. It is a multifunctional protein that is upregulated in the inflammatory process and induces anti-inflammatory activity when downregulated [36]. Short-term activation of STAT3 is a determinant of wound healing, but its persistent activation is a recurring characteristic of many epithelial tumors [35]. FLZ is known to inhibit STAT3 activity [37]. In oncogenesis, NF-kB plays a fundamental role in the development and progression of cancer, such as proliferation, migration, and apoptosis. Patients with small-cell lung cancer (SCLC) and non-small-cell lung cancer (NSCLC) with high expression of NF-kB have worse prognosis than patients with low levels of expression [38,39]. The silencing of NF-kB inhibits lung cancer cell survival and proliferation [40,41]. A study showed that FLZ inhibited NF-κB signaling in esophageal squamous cell carcinoma [42]. On the other hand, a study mentioned the influence of quick activation of the NF-kB pathway on the increase in HaCaT cell proliferation, thus a positive effect on keratinocyte proliferation, suggesting a close relationship between the first immune response and wound healing onset [43].

Despite these contradictions and that further studies are needed to better understand the action of FLZ on wound healing, in the present study, we suggest that FLZ positively modulates the wound healing process by synergizing with oil derived from linoleic acid when solubilized and loaded in a nanoemulsion.

4.6. CONCLUSION

Physical and psychological stresses caused by MW make this disease one of the most complex and challenging to treat, which is often undervalued. In the present work, the comparison between different preparations - FLZ in suspension, free drug nanoemulsion, and FLZ-loaded nanoemulsions with different oils - showed distinct results in the percentage of occurrence, time, and extent of MW. Results of in vivo test in mice suggested that FLZ-loaded nanoemulsion containing only Maisine CC® as oil phase prevented the development of MW in 100% of cases even after 80 days of treatment. Other mice treated with different samples suggested MW occurrence in 20% to 40% of the cases after 37 or 52 days of treatment, indicating that FLZ, combined with an oil derived from linoleic acid, can significantly improve treatment or prevention of MW in lung cancer. This result corroborates several studies in the literature concerning linoleic acid efficacy in wound healing. Moreover, for the first time, we demonstrated the combined effect of this oil component with FLZ in an oral nanoemulsion.

Although further studies are needed to better understand the mechanism of components in wound healing, our study suggested that oil derived from linoleic acid positively modulates wound healing by dynamic orchestrated interactions with FLZ solubilized and loaded in a nanoemulsion.

4.7. REFERENCES

[1]   F. Firmino, D.L. Villela-Castro, J. dos Santos, V.L. Conceição de Gouveia Santos, Topical Management of Bleeding From Malignant Wounds Caused by Breast Cancer: A Systematic Review, Journal of Pain and Symptom Management. 61 (2021) 1278–1286. https://doi.org/10.1016/j.jpainsymman.2020.10.020.

[2]   C. Tilley, J. Lipson, M. Ramos, Palliative Wound Care for Malignant Fungating Wounds: Holistic Considerations at End-of-Life, Nursing Clinics of North America. 51 (2016) 513–531. https://doi.org/10.1016/j.cnur.2016.05.006.

[3]   L. Peng, Y. Dai, Effect of metronidazole combined with autolytic debridement for the management of malignant wound malodor, Journal of International Medical Research. 48 (2019). https://doi.org/10.1177/0300060519889746.

[4]   C.P. Tilley, M.R. Fu, J. van Cleeve, B.L. Crocilla, C.P. Comfort, Symptoms of Malignant Fungating Wounds and Functional Performance among Patients with Advanced Cancer: An Integrative Review from 2000 to 2019, Journal of Palliative Medicine. 23 (2020) 848–862. https://doi.org/10.1089/jpm.2019.0617.

[5]   F. Firmino, K.C. Meira, V.A. Junior, V.L.C. de G. Santos, Regenerated oxidised cellulose versus calcium alginate in controlling bleeding from malignant breast cancer wounds: randomised control trial study protocol, Journal of Wound Care. 29 (2020) 52–60. https://doi.org/10.12968/jowc.2020.29.1.52.

[6]   I. Khémiri, B. Essghaier Hédi, N. Sadfi Zouaoui, N. ben Gdara, L. Bitri, The Antimicrobial and Wound Healing Potential of Opuntia ficus indica L. inermis Extracted Oil from Tunisia, Evidence-Based Complementary and Alternative Medicine. 2019 (2019). https://doi.org/10.1155/2019/9148782.

[7]   K. Watanabe, A. Shimo, K. Tsugawa, Y. Tokuda, H. Yamauchi, E. Miyai, K. Takemura, A. Ikoma, S. Nakamura, Safe and effective deodorization of malodorous fungating tumors using topical metronidazole 0.75 % gel (GK567): a multicenter, open-label, phase III study (RDT.07.SRE.27013), Supportive Care in Cancer. 24 (2016) 2583–2590. https://doi.org/10.1007/s00520-015-3067-0.

[8]   L. Woodward, M.E. Haisfield-Wolfe, Management_of_a_Patient_With_a_Malignant_Cutaneous_2003, Journal of Wound Ostomy & Continence Nursing . 30 (2003) 231–236. https://doi.org/10.1067/mjw.2003. 138.

[9]   H.G. Rodrigues, M.A.R. Vinolo, J. Magdalon, K. Vitzel, R.T. Nachbar, A.F.M. Pessoa, M.F. dos Santos, E. Hatanaka, P.C. Calder, R. Curi, Oral administration of oleic or linoleic acid accelerates the inflammatory phase of wound healing, Journal of Investigative Dermatology. 132 (2012) 208–215. https://doi.org/10.1038/jid.2011.265.

[10]   N. Tanideh, E. Abdordideh, S.L.A. Yousefabad, S. Daneshi, O.K. Hosseinabadi, S.M. Samani, A comparison of the effects of honey, fish oil and their combination on wound healing in rat, Journal of Coastal Life Medicine. 4 (2016) 683–688. https://doi.org/10.12980/jclm.4.2016j6-93.

[11] S. Bardaa, N. ben Halima, F. Aloui, R. ben Mansour, H. Jabeur, M. Bouaziz, Z. Sahnoun, Oil from pumpkin (Cucurbita pepo L.) seeds: Evaluation of its functional properties on wound healing in rats, Lipids in Health and Disease. 15 (2016). https://doi.org/10.1186/s12944-016-0237-0.

[12] N. Poljšak, S. Kreft, N. Kočevar Glavač, Vegetable butters and oils in skin wound healing: Scientific evidence for new opportunities in dermatology, Phytotherapy Research. 34 (2020) 254–269. https://doi.org/10.1002/ptr.6524.

[13] M.C. Bonferoni, G. Sandri, E. Dellera, S. Rossi, F. Ferrari, M. Mori, C. Caramella, Ionic polymeric micelles based on chitosan and fatty acids and intended for wound healing. Comparison of linoleic and oleic acid, European Journal of Pharmaceutics and Biopharmaceutics. 87 (2014) 101–106. https://doi.org/10.1016/j.ejpb.2013.12.018.

[14] D. de Souza Gonçalves, M.N. Yukuyama, M.Y.S. Miyagi, T.J.V. Silva, C. Lameu, N.A. Bou-Chacra, G.L.B. de Araujo, Revisiting Flubendazole Through Nanocrystal Technology: Statistical Design, Characterization and Its Potential Inhibitory Effect on Xenografted Lung Tumor Progression in Mice, Journal of Cluster Science. (2022). https://doi.org/10.1007/s10876-022-02220-x.

[15] Z.-J. Hou, X. Luo, W. Zhang, F. Peng, B. Cui, S.-J. Wu, F.-M. Zheng, J. Xu, L.-Z. Xu, Z.-J. Long, X.-T. Wang, G.-H. Li, X.-Y. Wan, Y.-L. Yang, Q. Liu, Flubendazole, FDA-approved anthelmintic, targets breast cancer stem-like cells, n.d. www.impactjournals.com/oncotarget.

[16] V. Králová, V. Hanušová, P. Staňková, K. Knoppová, K. Čáňová, L. Skálová, Antiproliferative effect of benzimidazole anthelmintics albendazole, ricobendazole, and flubendazole in intestinal cancer cell lines, Anti-Cancer Drugs. 24 (2013) 911–919. https://doi.org/10.1097/CAD.0b013e3283648c69.

[17] M. Michaelis, B. Agha, F. Rothweiler, N. Löschmann, Y. Voges, M. Mittelbronn, T. Starzetz, P.N. Harter, B.A. Abhari, S. Fulda, F. Westermann, K. Riecken, S. Spek, K. Langer, M. Wiese, W.G. Dirks, R. Zehner, J. Cinatl, M.N. Wass, J. Cinatl, Identification of flubendazole as potential anti-neuroblastoma compound in a large cell line screen, Scientific Reports. 5 (2015). https://doi.org/10.1038/srep08202.

[18] M. ENDOO, H. Sagitani, Preparation of Triglyceride O/W Emulsions by D Phase Emulsification, Japan Oil Chemists' Society. 40 (1991) 133–139. https://doi.org/10.5650/jos1956.40.133.

[19] M.N. Yukuyama, K. Ishida, G.L.B. de Araujo, C. de C. Spadari, A. de Souza, R. Löbenberg, M.A.B. Henostroza, B.R. Folchini, C.M. Peroni, M.C.C. Peters, I.F. de Oliveira, M.Y.S. Miyagi, N.A. Bou-Chacra, Rational design of oral flubendazole-loaded nanoemulsion for brain delivery in cryptococcosis, Colloids and Surfaces A: Physicochemical and Engineering Aspects. 630 (2021). https://doi.org/10.1016/j.colsurfa.2021.127631.

[20] G. Choi, T.H. Le, S. Shin, A new multidimensional design space identification method for a quality-oriented drug development process, Total Quality Management and Business Excellence. 27 (2016) 804–817. https://doi.org/10.1080/14783363.2016.1187999.

[21] S.M. Dordević, N.D. Cekić, M.M. Savić, T.M. Isailović, D. v. Randelović, B.D. Marković, S.R. Savić, T.T. Stamenić, R. Daniels, S.D. Savić, Parenteral nanoemulsions as promising carriers for brain delivery of risperidone: Design, characterization and in vivo pharmacokinetic evaluation, International Journal of Pharmaceutics. 493 (2015) 40–54. https://doi.org/10.1016/j.ijpharm.2015.07.007.

[22] S. Kotta, A.W. Khan, S.H. Ansari, R.K. Sharma, J. Ali, Formulation of nanoemulsion: A comparison between phase inversion composition method and high-pressure homogenization method, Drug Delivery. 22 (2015) 455–466. https://doi.org/10.3109/10717544.2013.866992.

[23] C.L. oong Ngan, M. Basri, F.F. ang Lye, H.R. eza Fard Masoumi, M. Tripathy, R.A. bedi Karjiban, E. Abdul-Malek, Comparison of process parameter optimization using different designs in nanoemulsion-based formulation for transdermal delivery of fullerene, Int J Nanomedicine. 9 (2014) 4375–4386. https://doi.org/10.2147/IJN.S65689.

[24] H. Sagitani, Formation of o/w emulsions by surfactant phase emulsification and the solution behavior of nonionic surfactant system in the emulsification process, Journal of Dispersion Science and Technology. 9 (1988) 115–129. https://doi.org/10.1080/01932698808943980.

[25] M.N. Yukuyama, P.L.F. Oseliero, E.T.M. Kato, R. Lobënberg, C.L.P. de Oliveira, G.L.B. de Araujo, N.A. Bou-Chacra, High internal vegetable oil nanoemulsion: D-phase emulsification as a

unique low energy process, Colloids and Surfaces A: Physicochemical and Engineering Aspects. 554 (2018) 296–305. https://doi.org/10.1016/j.colsurfa.2018.06.023.

[26] C. Solans, I. Solé, Nano-emulsions: Formation by low-energy methods, Current Opinion in Colloid and Interface Science. 17 (2012) 246–254. https://doi.org/10.1016/j.cocis.2012.07.003.

[27] S.S. Davis, T. Purewal, H.P. Round, OSTWALD RIPENING IN EMULSION SYSTEMS. THE EFFECT OF AN ADDED THIRD COMPONENT, Journal of Pharmacy and Pharmacology. 31 (1979) 4P-4P. https://doi.org/10.1111/j.2042-7158.1979.tb11552.x.

[28] A.S. Kabal'nov, A. v Pertzov, E.D. Shchukin, Ostwald Ripening in Two-Component Disperse Phase Systems: Application to Emulsion Stability, Elsevier Science Publishers B.V, 1987.

[29] F.M.Q. Schmidt, F. Firmino, N. de F.B. Lenza, V.L.C. de G. Santos, Nursing team knowledge on care for patients with fungating wounds, Rev Bras Enferm. 73 (2020) e20170738. https://doi.org/10.1590/0034-7167-2017-0738.

[30] H.G. Rodrigues, M.A.R. Vinolo, F.T. Sato, J. Magdalon, C.M.C. Kuhl, A.S. Yamagata, A.F.M. Pessoa, G. Malheiros, M.F. dos Santos, C. Lima, S.H. Farsky, N.O.S. Camara, M.R. Williner, C.A. Bernal, P.C. Calder, R. Curi, Oral administration of Linoleic acid induces new vessel formation and improves skin wound healing in diabetic rats, PLoS ONE. 11 (2016). https://doi.org/10.1371/journal.pone.0165115.

[31] S. Bardaa, N. Chabchoub, M. Jridi, D. Moalla, M. Mseddi, T. Rebai, Z. Sahnoun, The effect of natural extracts on laser burn wound healing, Journal of Surgical Research. 201 (2016) 464–472. https://doi.org/10.1016/j.jss.2015.11.052.

[32] W.C. Glasgow, T.E. Eling, Epidermal growth factor stimulates linoleic acid metabolism in BALB/c 3T3 fibroblasts, Mol Pharmacol. 38 (1990) 503–510.

[33] C. Manosalva, P. Alarcón, K. González, J. Soto, K. Igor, F. Peña, G. Medina, R.A. Burgos, M.A. Hidalgo, Free Fatty Acid Receptor 1 Signaling Contributes to Migration, MMP-9 Activity, and Expression of IL-8 Induced by Linoleic Acid in HaCaT Cells, Frontiers in Pharmacology. 11 (2020). https://doi.org/10.3389/fphar.2020.00595.

[34] Y. Chen, T. Li, Cellular Uptake Mechanism of Paclitaxel Nanocrystals Determined by Confocal Imaging and Kinetic Measurement, AAPS Journal. 17 (2015) 1126–1134. https://doi.org/10.1208/s12248-015-9774-0.

[35] J. Huynh, A. Chand, D. Gough, M. Ernst, Therapeutically exploiting STAT3 activity in cancer — using tissue repair as a road map, Nature Reviews Cancer. 19 (2019) 82–96. https://doi.org/10.1038/s41568-018-0090-8.

[36] H.M. Han, S. Ko, M.-J. Cheong, J.K. Bang, C.H. Seo, T. Luchian, Y. Park, Myxinidin2 and myxinidin3 suppress inflammatory responses through STAT3 and MAPKs to promote wound healing, Oncotarget,. 8 (2017) 87582–87597. https://doi.org/10.18632/oncotarget.20908.

[37] S. Lin, L. Yang, Y. Yao, L. Xu, Y. Xiang, H. Zhao, L. Wang, Z. Zuo, X. Huang, C. Zhao, Flubendazole demonstrates valid antitumor effects by inhibiting STAT3 and activating autophagy, Journal of Experimental and Clinical Cancer Research. 38 (2019). https://doi.org/10.1186/s13046-019-1303-z.

[38] X. Jin, Z. Wang, L. Qiu, D. Zhang, Z. Guo, Z. Gao, C. Deng, F. Wang, S. Wang, C. Guo, Potential biomarkers involving IKK/RelA signal in early stage non-small cell lung cancer, Cancer Science. 99 (2008) 582–589. https://doi.org/10.1111/j.1349-7006.2007.00713.x.

[39] M. Karin, F.R. Greten, NF-κB: Linking inflammation and immunity to cancer development and progression, Nature Reviews Immunology. 5 (2005) 749–759. https://doi.org/10.1038/nri1703.

[40] X. Wang, W. Ju, J. Renouard, J. Aden, S.A. Belinsky, Y. Lin, 17-Allylamino-17-demethoxygeldanamycin synergistically potentiates tumor necrosis factor-induced lung cancer cell death by blocking the nuclear factor-κB pathway, Cancer Research. 66 (2006) 1089–1095. https://doi.org/10.1158/0008-5472.CAN-05-2698.

[41] X. Wang, W. Chen, Y. Lin, Sensitization of TNF-induced cytotoxicity in lung cancer cells by concurrent suppression of the NF-κB and Akt pathways, Biochemical and Biophysical Research Communications. 355 (2007) 807–812. https://doi.org/10.1016/j.bbrc.2007.02.030.

[42] J. Tao, H. Zhao, X. Xie, M. Luo, Z. Gao, H. Sun, Z. Huang, The anthelmintic drug flubendazole induces cell apoptosis and inhibits NF-κb signaling in esophageal squamous cell carcinoma, OncoTargets and Therapy. 12 (2019) 471–478. https://doi.org/10.2147/OTT.S193206.

129

[43]   S. Tonello, M. Rizzi, M. Migliario, V. Rocchetti, F. Renò, Low concentrations of neutrophil extracellular traps induce proliferation in human keratinocytes via NF-kB activation, Journal of Dermatological Science. 88 (2017) 110–116. https://doi.org/10.1016/j.jdermsci.2017.05.010.

4.8. SUPPLEMENTARY MATERIAL
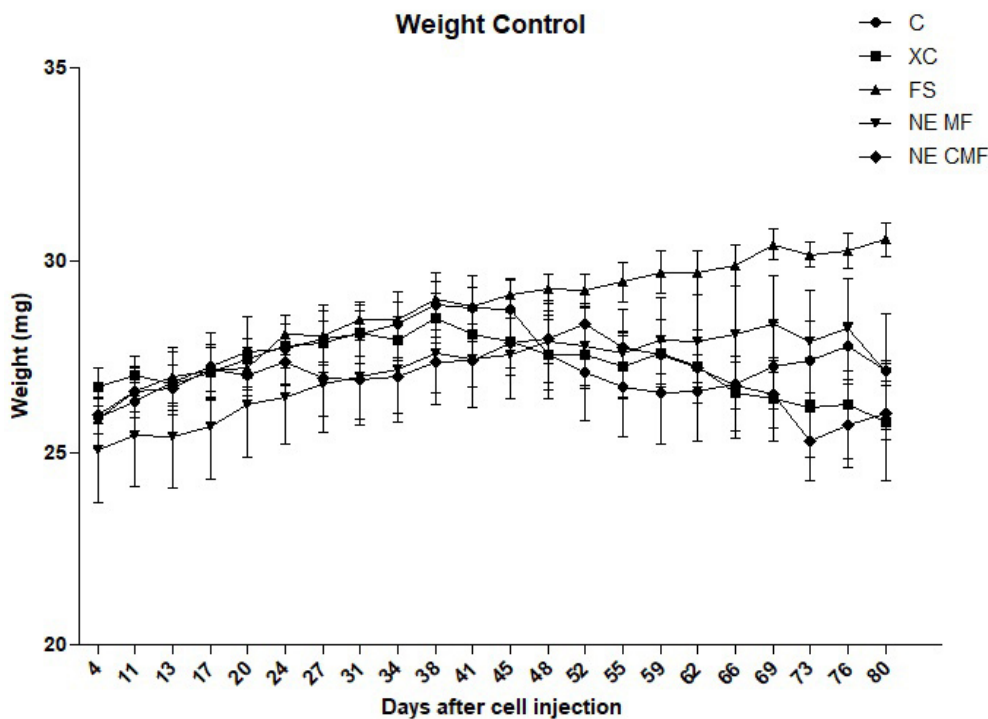
Figure 4.S1: Weight evaluation in lung cancer animal models. **C:** no xenotransplantation or treatment; **XC:** xenograft-bearing untreated animals (without gavage); **FS:** xenograft-bearing animals treated with flubendazole in suspension (0.8 mg of flubendazole/kg animal); **NE MF:** xenograft-bearing animals treated with flubendazole-loaded nanoemulsion containing Maisine CC (0.8 mg of flubendazole/kg animal); **NE CMF:** xenograft-bearing animals treated with flubendazole-loaded nanoemulsion containing Capmul CC:Maisine CC (8:2) (0.8 mg of flubendazole/kg animal)

Source: Own authorship

CHAPTER 5 - CANCER TREATMENT IN THE LYMPHATIC SYSTEM: A PROSPECTIVE TARGETING EMPLOYING NANOSTRUCTURED SYSTEMS

.

I am the first author and was responsible for conceptualization, investigation, writing - original draft.

5.1. Introduction

Lymphatic vessels circulate through most of the body including the central nervous system (Yoshimatsu et al., 2016) and they are responsible for three main activities: (1) maintaining fluid balance, (2) absorbing dietary lipids and returning them to the bloodstream, and (3) supporting immune defenses. This third function is important in transporting pathogens from peripheral tissues, or from antigen-presenting cells (APCs), which encompass the pathogens, to the lymph nodes (LNs), triggering the adaptive immunity process (Liao and von der Weid, 2015).

Cancer is the second leading cause of death in the world, with an estimated value of US$1.16 trillion of the total annual economic costs in 2010. In 2018, this disease accounted for approximately 9.6 million deaths worldwide, corresponding to about 1 in 6 of all deaths (World Health Organisation, 2018).

Although other terms like malignant tumors and neoplasms are also used, cancer is a large and heterogeneous group of diseases. Initiated by the development of abnormal cell growth, these tumor cells have the potential for gradual invasion or dissemination to other parts of the body (Gao et al., 2016; Leong and Tseng, 2014). This progression from the primary tumor to the metastatic tumor involves several mechanisms, in which the lymphovascular system is considered the first site of metastasis for most malignant cancers (Leong and Tseng, 2014; Xie et al., 2009). Micrometastatic cancer cells, in some solid tumors, are recognized as having a critical and strategic position in initiating the process of leaving the primary tumor's microenvironment, colonizing, and establishing metastatic diseases. In this process, the sentinel lymph nodes (SLNDs) may be a viable gateway for distant organ metastasis (Leong and Tseng, 2014).

Understanding the involvement of lymphatic systems in cancer metastasis and the detection of the micrometastasis in the first stage of tumor processes is one of the key elements in preventing this global disease. Cancer therapy and immunotherapy based on nanomaterials have improved in recent decades. However, new discoveries and challenges continue to arise reflecting the complexity and persistence of this disease.

This review describes recent advances in developing nanostructured systems in cancer therapy associated with the lymphatic system. The specific topics involving nanodevices for cancer mapping, in-depth descriptions of different factors or modulators of lymphatic cancer, discussion of the specific surface interactions of these components and tumors have been deeply revised over time. Therefore, this substantial body of work is not the focus of this review. We begin by briefly

132

revisiting the lymphatic vascular system structure and nanostructured systems, followed by the introduction of emerging strategies on the design of nanomaterials aimed at lymphatic systems for cancer therapy, their challenges and future perspectives.

5.2. Lymphatic system and cancer dynamics

The lymphatic system is a highly organized system of vessels and nodules, which differ from the blood system. Lymphatic vessels are composed of three morphologically distinct types: lymphatic (or initial lymphatic) capillaries, precollecting vessels, and lymphatic collecting vessels. Capillaries consist of blind-ended vessels, composed of a single-cell layer of lymphatic endothelial cells (LEC) formed by discontinuous junctions. These discontinuous junctions are attached to the anchoring filaments of the surrounding extracellular matrix. Under conditions of high pressure, caused, for example, by stress, these filaments induce the opening of the junctions allowing the capture of macromolecules and lymphatic fluid leading them unidirectionally in the lumen of the lymphatic capillaries to the pre-collecting vessel. The latter, is scarcely covered by smooth muscle cells (SMCs), and transports fluids to the large collecting vessels. The collecting vessels are composed of SMCs, continuous basement membrane, and lumen valves, responsible for preventing reflux of the lymph. Contractions of SMCs, together with skeletal muscles, propel the lymphatic fluid to return to the bloodstream through the connection of the subclavian veins (Karnezis et al., 2012; Martinez-Corral and Makinen, 2013) (**Figure 5.1**).
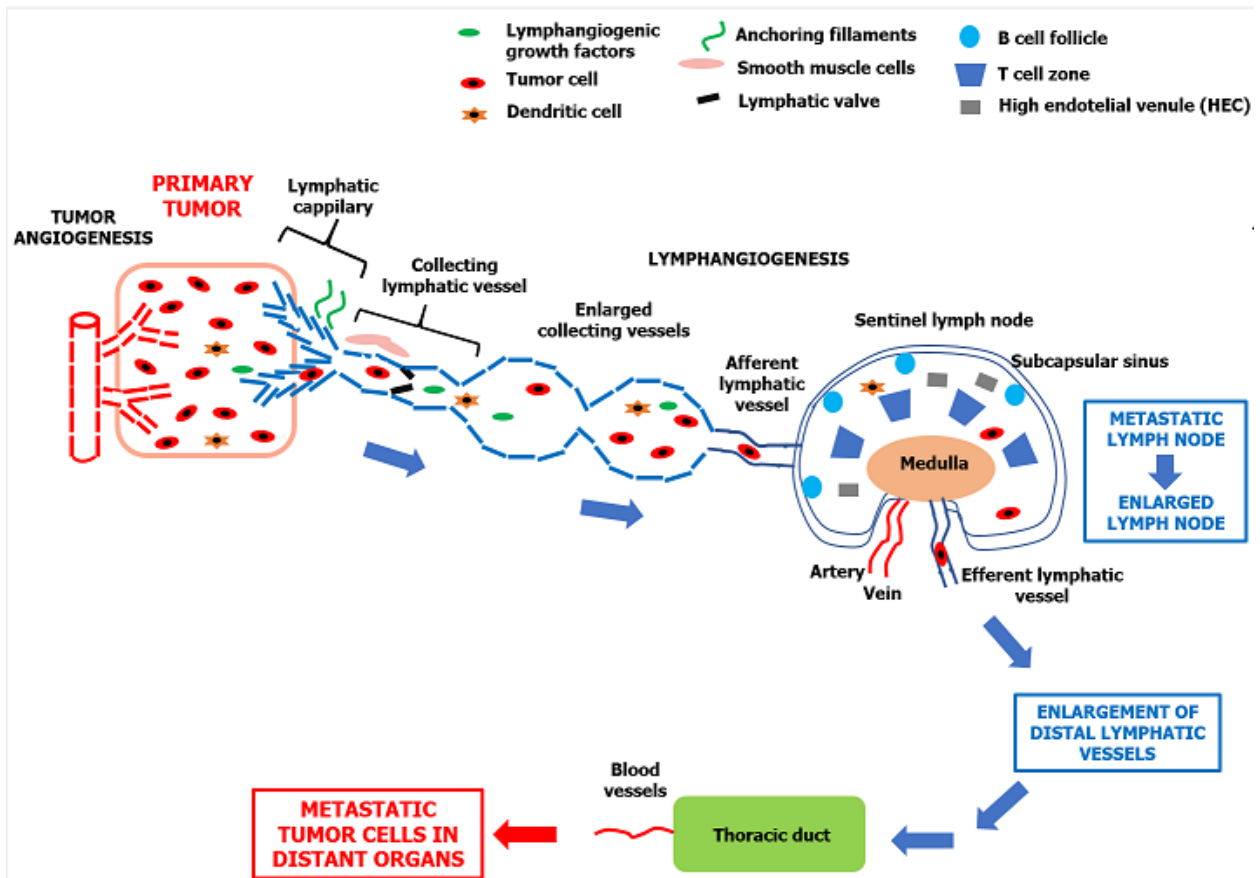
Figure 5.1: Schematic illustration of the lymphatic system and development of lymphangiogenesis.

Source: Own authorship

Lymphatic capillaries are composed of discontinuous cell junctions and connected to the interstitium by means of anchoring filaments. Lymph fluids enter the lymphatic capillaries and are driven to collecting lymphatic vessels that show continuous junction molecules and covered by smooth muscle cells. The contraction of smooth muscle cells and the lymphatic valve deliver fluids unidirectionally to the lymph nodes, through the afferent lymph vessel. The lymphangiogenic growth factors promote the enlargement of the lymphatic vessels and increase in number, which facilitates the transport of tumor cells to the lymph nodes. In the advanced stage of lymphangiogenesis, there is a process of enlargement and remodelling of the lymph nodes: modifications in high endothelial venules, chemokines and cytokines and immune cell

134

composition. The impairment of the adaptive immune system caused by metastatic lymph nodes facilitates the dissemination of tumor cells to distant organs. Lymphatic vessels may drain tumor cells into the systemic circulation through the thoracic duct.

However, recent discoveries with several LEC markers in the early 21st century have spurred progress in lymphangiogenesis-related research (Yoshimatsu et al., 2016). This, defined as abnormal growth of the lymphatic vessel's diameter and their number, implies the evolution of several types of cancer, e.g., colorectal, breast, lung, head, neck and melanoma cancer. Different factors have been identified in the onset of these diseases, such as LYVE-1, Prox1, podoplanin (gp38), VEGF-C / D, neuropilin-2, angiopoietin-1 and CCL21 (Lohela et al., 2009). The expansion of the diameter of the lymphatic vessels caused by lymphangiogenesis occurs at the primary tumor and can also extend to lymph nodes and sentinel lymph nodes (SLNDs) (Ryan et al., 2014). The lymph nodes are an ovoid organ present in different parts of the body in the lymphatic system, and act as central trafficking hubs of immune cells, residing T-cells and B-cells (Braun et al., 2011). The SLNDs are defined as lymph nodes that drain solid tumors and are functionally involved in conducting anti-tumor immune response and suppression (Thomas and Schudel, 2015).

Through the expanded lymphatic vessels, cancer cells migrate easily from primary tumors to local lymph nodes that act as a reservoir. Then they continue to migrate through lymphatic vessels to blood vessels to reach final sites, inducing metastasis in distant organs, as seen in **Figure 5.1** (Dieterich and Detmar, 2016; Liao and von der Weid, 2015; Yoshimatsu et al., 2016). Several circumstances promote the advantage of metastatic diffusion of the lymphatic system over blood vessels: the larger diameter and the higher permeability of the lymphatic vessels than the blood vessels, the reduced pressure and lower flow rates in the lymphatic system that may generate less damage to tumor cells than blood circulation, and the possible higher cell viability in the lymph due to the similarities of its components with the interstitial fluid (Ryan et al., 2014; Swartz, 2001). Thus, the lymphatic system is one of the key gateways for the diffusion of cancer cells prior to the final stage of cancer.

5.3. Nanostructured systems and the lymphatic system

Nanostructured systems have brought significant attention and progress to developing nanomedicine and immunotherapy in treating cancers. Carriers based on nanostructured systems

may offer efficient, selective and high uptake of drugs into the lymphatic system and lymph nodes (Xie et al., 2009), and subsequently into the tumor cells. They also decrease risks of debilitating side effects on patients caused by toxic or non-specific chemotherapies (Mousa and Bharali, 2011). Since the conventional intravenous or subcutaneous injections of drugs do not access the lymphatic system, several approaches are proposed to improve the delivery of drugs to this system. The surface charge interferes with access to the lymphatic site: under subcutaneous administration, the negatively charged interstitial area below the skin dermis due to the presence of glycosaminoglycans favors neutrally charged nanomaterials (McLennan et al., 2005). On other hand, cationic materials are preferably retained at the injection site (Ryan et al., 2014). Specific bindings or conjugations on the surface of nanomaterials may enhance the interaction of nanomaterials with APCs such as dendritic cells and their subsequent maturation (Hamdy et al., 2011). Under oral administration, the composition of nanomaterials affects their transport into the lymphatic system by intestinal enterocytes: long-chain triglycerides show higher uptake compared to short-chain triglycerides. This process of intestinal lymphatic drug transport is regulated by chylomicrons, a specific intestinal lipoprotein. High-affinity triglycerides get assembled into the core of chylomicrons, forwarded to the lymphatic system, avoiding the first-pass metabolism of poorly absorbed drugs under oral administration (Chaudhary et al., 2014). Although several factors regulate the uptake of nanomaterials in lymphatics, size is considered the main one to control this process. Particulates below 10 nm are primarily absorbed by the blood system, between 10-80 nm are taken up by the lymphatic system, and above 100 nm remain preferentially at the injection site (Xie et al., 2009). It is also reported that particles between 20 to 200 nm are drained into the lymph nodes, and 500 nm or less are taken up by dendritic cells or macrophages (Oyewumi et al., 2010). Different types of nanocarriers have been developed so far. Doxil was the first drug delivery system approved in the 1990s for cancer treatment, which consists of a liposomal nanostructure. In addition to the liposome, other technologies such as dendrimers, polymers, lipids, inorganic and organic nanoparticles have been developed to target the lymphatic system. We review below some examples of these developments.

A solid lipid nanoparticle (SLN) composed of Gelucire 44/14, Compritol 888 ATO, Lipoid S 75 and Poloxamer 188 was produced by hot homogenization and ultrasonication. The particle size of the solid lipid nanoparticle (SLN) obtained was 168 nm, and the zeta potential was -35.55 mV. The study of lymphatic transport and tissue distribution in rats showed the uptake of this SLN

in the lymph by the chylomicron mechanism and in spleen, considered the major lymphatic organ (Makwana et al., 2015).

Another SLN was prepared by the hot self-nano-emulsification technique, under the mixture of stearic acid, poloxamer and polyethylene glycol. A poor oral bioavailable drug, lopinavir, was loaded into this nanocarrier, yielding an SLN of 180.6 ± 2.32 nm and a zeta potential of -13.4 ± 0.56 mV. This final lopinavir-loaded SLN demonstrated significantly higher lymphatic transport compared to this drug solution in in vivo tests using rats (Negi et al., 2013).

Cabral et al. (2015) investigated the influence of systemically administered nanocarriers with different sizes on the lymph node metastatic disease. Polymeric micelles loading platinum anticancer drugs were evaluated in syngeneic melanoma models, in primary orthoptic melanoma and after this removal, in their LN metastasis. According to the results, sub-50 nm nanoparticles of this system successfully targeted and accumulated in LN metastasis. This is possibly due to the size-related abilities of this nanocarrier to extravasate from the blood vessel and penetrate within the metastatic mass, in metastasis (Cabral et al., 2015).

Aiming at an enhanced permeability and retention (EPR) effect at the melanoma draining lymph node (dLN), an evaluation of different bionanomaterial-based formulations was performed by intradermal administration. To compare the differences in structures, dextran was used as a flexible macromolecule and the polystyrene spheres as rigid particulates. Different hydrodynamic sizes of both materials were prepared to evaluate the influence of size. Except for the 5 nm dextran, which was quickly cleared from the injection site, dextran demonstrated relative greater accumulation in dLN compared to polystyrene spheres, in all tested sizes. The hypothesized mechanism of accumulation is passive transportation, since there was no difference in accumulation between 24 and 72 h post-injection. However, a significant increase of dLN accumulation of the largest polystyrene spheres (500 nm) was observed at 72 h, suggesting that this rigid structure may be impacted by cell-mediated transport (active transportation). Thus, this interesting study demonstrated that, in addition to size, the flexibility of the carrier influences the diffusion in the skin and the lymphatic uptake (Rohner and Thomas, 2017).

As shown, nanostructured systems are very promising in strategic delivery of drugs in the lymphatic system. The following topics focus on two different directions: (1) imaging therapy and (2) immunotherapy, in the development of nanostructures for treating lymphatic metastatic cancer (**Table 5.1, Table 5.2**).

Table 5.1: Nanostructured systems targeting lymphatic systems for cancer treatment

Proposal	Target/Outcome	Nanostructure	Characterization	Author	Publication year
THERANOSTICS					
Sonoporation					
Lymph node delivery of multifunctional polymer microbubbles for imaging and therapy	Squamous carcinoma cell, lymph nodes metastasis	Poly(lactic-co-glycolic acid) (PLGA) microbubbles loaded with co-encapsulated iron oxide nanoparticles and doxorubicin	868.0 ± 68.73 nm	Niu, C. et al.	2013
Intralymphatic administration of chemotherapy combined with ultrasound and nano-/ microbubbles	Sarcoma cells, lymph nodes metastasis	Acoustic liposomes composed of 1,2-distearoyl-sn-glycero-3-phosphatidylcholine and 1,2-distearoyl-*sn*-glycero-3-phosphoethanolaminemethoxy-polyethyleneglycol, containing C3F8 gas, combined to ultrasound and *cis*-diamminedichloroplatinum (II) (CDDP)	Particle size of 199 ± 84.4 nm, zeta potential of −2.10 ± 0.90 mV	Sato, T. et al.	2014
Intralymphatic drug delivery with nano/ microbubbles (NMBs) and ultrasound	Breast carcinoma cells, lymph node metastasis using MXH10/Mo-lpr/lpr mice exhibiting lymphadenopathy	Acoustic liposomes composed of 1,2-distearoyl-sn-glycero-3-phosphatidylcholine and 1,2-distearoyl-*sn*-glycero-3-phosphoethanolaminemethoxy-polyethyleneglycol, containing C3F8 gas, combined to ultrasound and *cis*-diamminedichloroplatinum (II) (CDDP)	~200 nm and neutral zeta potential	Sato, T. et al.	2015
Intralymphatic drug delivery into subiliac lymph nodes of MXH10/Mo-lpr/lpr mice	Head and neck cancer, lymph nodes metastasis	Acoustic liposomes composed of 1,2-distearoyl-sn-glycero-3-phosphatidylcholine and 1,2-distearoyl-*sn*-glycero-3-phosphoethanolaminemethoxy-polyethyleneglycol, containing C3F8 gas, combined to ultrasound and fluorophores	199 ± 84.4 nm	Kato, S. et al.	2015
Subiliac lymph node injection using MXH10/Mo-lpr/lpr mice	Three different tumor cell lines (malignant fibrous histiocytoma-like cells, osteosarcoma cell and bladder tumor cell	Acoustic liposomes composed of 1,2-distearoyl-sn-glycero-3-phosphatidylcholine and 1,2-distearoyl-*sn*-glycero-3-phosphoethanolaminemethoxy-polyethyleneglycol, containing C3F8 gas, combined to ultrasound and doxorubicin	< 100 nm	Kato, S. et al.	2015
Photothermal therapy					
Subcutaneous, intratumor or intravenous administration of MoS2-PEG nanosheets combined with photothermal and chemotherapy.	Breast cancer cells	Two-dimensional MoS2-PEG nanosheets with lipoic acid conjugated PEG (LA-PEG) containing a disulfide group on the PEG terminal, and loaded with doxorubicin.	~ 50 nm	Liu, T. et al.	2014
Tail vein injection combined to imaging and photodynamic therapy	Gastric cancer, draining LN metastasis	Nanoparticles loaded with the indocyanine green -loaded lactosome, a micelle assembled from block copolymers, PS–PLLA	Particle size of 40–50 nm, zeta potential of −0.51 mV.	Tsujimoto, H. et al.	2015
Delivery from an accessory axillary lymph node of polymeric gold nanorods (PAuNRs) combined to near-infrared laser irradiation and skin temperature controlled by cooling	Mammary carcinoma cells, lymph node metastasis	Polymeric gold nanorods (PAuNRs) functionalized with mPEG-SH	10.1 ± 0.35 nm	Oladipo, A.O. et al.	2017
Injection into the proper axillary lymph node, using MXH10/Mo-lpr/lpr mice and near-infrared laser light with controlled surface cooling	Malignant fibrous histiocytoma-like cells, lymph node metastasis	Neutravidin polymer-conjugated gold nanorods (GNRs) combined to near-infrared (NIR) laser light	Aspect ratio, 6.7; surface plasmon resonance peak, 1,065 nm; axial diameter, 10 nm; and length, 67 nm; zeta potential of −13.79 ± 1.33 mV	Sugiura, T. et al.	2015
Magnetic resonance imaging therapy					
Tail vein injection to achieve upconversion luminescent/magnetic particles for both optical and magnetic resonance imaging (MRI) of tumors	Gastric carcinoma cells, lymph node metastasis	Core@shell structured NaGdF4:Yb, Er@NaGdF4 upconversion nanoparticles coated with polyethylene glycol (PEG)	< 100 nm	Qiao, R. et al.	2015
Injection of nanopeptide into the primary tumor of mouse, followed by photothermal heating	Primary tumors and sentinel lymph nodes lung metastasis	PEG-functionalized gold shelled iron oxide nanoclusters as the magnetic-responsive photothermal agent	~100 nm	Liang, C. et al.	2015
Fluorescence imaging therapy					
Subcutaneous injection of nanoparticles for direct lymph node targeting and imaging	RFP-expressing melanoma tumor	Genetic modification of subunit protein of human ferritin heavy chain (hFTN) as a surface carrier of the model TSA [red fluorescence protein (RFP)]	22.0 ± 0.7 nm	Lee, B. et al.	2016
Injection of nanoparticles on an IVIS Lumina XR III *in vivo* imaging system, enabling both non-invasive multimodality imaging and targeting photothermal therapy	Metastatic gastric cancer cells in lymph node	fluorescent copper sulfide (CuS) nanoparticle (RGD-CuS-Cy5.5)	~21 nm	Shi, H. et al.	2018

Table 5.2: Nanostructured systems targeting lymphatic systems for cancer treatment - Immunotherapy.

Proposal	Target/Outcome	Nanosctruture	Characterization	Author	Publication year
IMMUNOTHERAPY					
Macrophages					
In vitro primary and secondary cytotoxicity of nanoparticles mediated by alveolar macrophages for anti-tumor response	Th1 cytokines secreted by alveolar macrophage caused a significant secondary cytotoxicity effect on lung cancer cells	Doxorubicin-loaded poly (isobutyl cyanoacrylate) nanoparticles	Particle size of 140 ± 1.98 nm, zeta potential of 21.56 ± 0.32 mV	Al-Hallak, K.M.H.D. *et al.*	2010
Administration via inhalation of nanoparticles for alveolar macrophages targeting	Fewer and reduced-size tumors, and better survival in human non-small cell lung carcinoma model	Doxorubicin-loaded nanoparticles incorporated into inhalable effervescent carrier particles	Particle size of 137.22 ± 1.53 nm, zeta potential of −23.5 ± 0.41 mV	Roa, W.H. *et al.*	2011
Subcutaneous injection of nanogel-based vaccine targeting medullary macrophages	The immunologically stealth nanoparticulate delivery system was efficiently transported to draining lymph node and inhibited tumor growth in colon epithelial tumor cells	Nanoparticulate cancer vaccine of synthetic long peptide antigen ancapsulated within nanoparticulate hydrogel of cholesteryl pullulan	~50 nm and uncharged surface	Muraoka, D. *et al.*	2014
Secondary cytotoxicity of nanoparticles for antitumor effect in the microclimate of the coculture model	Nanoparticles presented secondary cytotoxic effect on lung cancer cells and reduced cell viability. This effects were reduced after macrophages exposition to anti-inflammatory drugs	Gelatin nanoparticles and poly (isobutylcyanoacrylate) nanoparticles containing doxorubicin, in combination with anti-inflammatory drugs	Particle size from 170 to 316 nm, zeta potential of ~14 mV	Sarfraz, M. *et al.*	2016
Dendritic cells					
Pulmonary instillation of nanoparticles to target draining lymph nodes	Internalization of nanoparticles by alveolar macrophages	Amine-containing hydrogel rod-shaped cationic and anionic nanoparticles, fabricated by continuous roll-to-roll PRINTmethod	80 nm × 80 nm × 320 nm	Fromen, C.A. *et al*	2016
Subcutaneous injection of AF488-labeled nanoparticles into the footpad of mice to target limph node	Lymph node dendritic cells and T cells	PEGlated poly(methacrylic acid) nanoparticles	~200 nm	Koker, S.D. *et al.*	2016
Toll-like receptors					
Transcutaneous antigen delivery of nanoparticles	Increased uptake of nanoparticles by skin antigen-presenting cells and their enhanced migration to the surrounding lymph nodes (transcutaneous vaccine delivery)	Gp100 (melanocyte-associated antigen gp100 protein) or ovalbumin-loaded chitosan (CS)-sodium tripolyphosphate (TPP)-grafted NPs. Imiquimod was used together with the antigen.	258 nm ± 15 nm, zeta potential of 27.6 mV ± 4.7 mV	Li, N. *et al.*	2014
Subcutaneous injection or topical application of nanoparticles to a 2 cm × 2 cm skin area for anticancer immunotherapy	Innate activation in the draining lymph node; inducing potent T-cell responses and antibody responses	Covalent ligation of a small-molecule imidazoquinoline-based TLR7/8 agonist to degradable polymeric nanogels	~50 nm	Nuhn, L. *et al.*	2016
Subcutaneous injection of nanoparticles at the tail base, targeting lymph nodes	CpG's lymph node accumulation, enhanced CD8 + T cell responses and improvement of antitumor immunotherapy in TC-1 tumor cells	Covalent link of oligonucleotide agonist (CpG DNA, a TLR9 agonist) to dextran polymer	6.5 nm	Zhang, W. *et al.*	2017
Subcutaneous injection of nanoparticles to target draining lymph nodes and uptake by dendritic cells	Increase of antigen specific cytotoxic T lymphocytes and a strong anti-tumor effect in a lung metastatic melanoma model	Polymeric hybrid micelles loaded with melanoma antigen peptide Trp2 and Toll-like receptor-9 agonist CpG ODN	sub-30 nm	Zeng, Q. *et al.*	2017
T Cells					
Intradermal or intratumoral injection of nanoparticles, targeting tumor-draining lymph node	Promoted anti-tumor immunity and hinder tumor growth in B16–F10 melanoma	Incorporation of toll-like receptor ligands CpG oligonucleotide (a TLR-9 agonist) or paclitaxel (a TLR-4 agonist) in pluronic-stabilized poly(propylene) sulfide-core nanoparticles	30 nm	Thomas, S.N. *et al.*	2014
Lymph nodes delivery of nanoparticles and induction of CD8 + T-cell responses	Induction of poly-functional T-cell responses to eliminate tumors in mouse lymphoma tumor model	Gold nanoparticle-based vaccines conjugated with recombinant ovalbumin	between 10 nm and 22 nm	Kang, S. *et al.*	2017
Injection of nanoparticles in tail base of mice, targeting lymph nodes	High antitumor immunity induction and tumor growth inhibition in EL-4 thymoma cells	Surface character (amination) of poly(γ-glutamic acid)-based synthetic vaccine nanoparticles incorporated with ovalbumin and toll-like receptor 3 agonist (poly (I:C))	20–70 nm	Kim, S-Y. *et al.*	2017
B Cells			10 nm	Sharma *et al.*	2013
CH12.LX B-cell line derived from the murine CH12 B cell lymphoma for evaluation of cellular uptake, interaction with IKK signal transduction proteins and activation of the NF-kB pathway.	Au-NPs activate the canonical NF-kB pathway, increase IgA production and 30IghRR activity, support a direct interaction between IKK altering NF-kB signaling and leading to B lymphocyte dysfunction	Gold nanoparticle (Au-NP) synthesized by the modified Turkevich method, from tetrachloroauric(III) acid monohydrate (52% Au) and sodium citrate			
Evaluation of *in vivo* anti-tumor efficacy in BALB/c mice.	DOX/VCR NLCs showed the synergistic effect and the excellent delivery ability compared with drug solutions and single-drug NLCs.	A mixture of 65 ℃ lipid phase composed of COMPRITOL 888ATO Stearic acid, Cremophor ELP, doxorubicin (DOX) base and vincristine (VCR) (DOX versus VCR¼1:1, w/w) was rapidly injected into the aqueous phase, followed by dialyzed method, centrifugation, washing and filtration through a 0.45-mm membrane	96 nm	Dong *et al.*	2016
Treatment of B-cell lymphoma through *in vivo* treatment to a lymph cancer animal model (BALB/c mice).	DOX–GEM VCR NLCs showed the highest antitumor effect in *in vitro* and *in vivo* test when compared with the single-drug NLCs and the drug solutions	Doxorubicin (DOX)–gemcitabine(GEM) prodrug was synthesized and combined to vincristine (VCR) to develop DOX–GEM VCR NLCs by the solvent diffusion method	112.6 nm, zeta potential of −39.7 mV	Ni *et al.*	2017
Exosomes					
Subcutaneous injection of nanoparticles and M1 exosomes for melanoma growth inhibition	Uptake of M1 exosomes by macrophages and dendritic cells in the lymph nodes and tumor growth inhibition immunopotentiator for a cancer vaccine in murine melanoma cell line	Lipid calcium phosphate nanoparticle-encapsulated Trp2 vaccine combined with exosomes derived from M1-polarized, proinflammatory macrophages	< 100 nm (exosomes)	Cheng, L. *et al.*	2017

5.3.1. *Imaging Therapy for lymphatic cancer*

Sentinel lymph nodes (SLNDs) are the first few lymph nodes that drain tumor cells through the lymphatic vessels (Kodama et al., 2016). They can act as a reservoir for these tumor cells, for the future dissemination of metastatic cells to the secondary nodes and so on, towards distant sites. Thus, SLND biopsy is often used to predict and identify malignancies (Ryan et al., 2014). Treatment via axilla lymph node (LN) dissection for breast cancer associated with lymphatic metastases is also frequently employed. However, this anatomical rupture can result in adverse effects such as nerve damage and lymphedema, additionally to the risk of micrometastasis already disseminated in non-dissected lymph nodes (Kodama et al., 2016). The same risk is considered for neck dissection for head and neck cancer, which can generate injuries of nerve and scar fibrosis (Kato et al., 2015b).

Unfortunately for most patients, conventional methods of detecting cancer at an early or ideal stage before metastasis are still restricted, leading to late diagnosis for effective treatment (Kodama et al., 2016). Therefore, the development of alternative methods capable of identifying and eliminating cancers in the lymphatic system is a fundamental treatment strategy for a variety of cancers and a determining factor in a patient's prognosis (Ryan et al., 2014).

Development of "theranostic" nanoagents have attracted attention, targeting to minimally invasive treatment of metastatic cancer. They consist of a combination of rational and multifunctional components, simultaneously allowing diagnosis, therapy, dose adjustments and monitoring of therapeutic responses (Björnmalm et al., 2017; Song et al., 2015; Tsujimoto et al., 2015) (**Figure 5.2**).
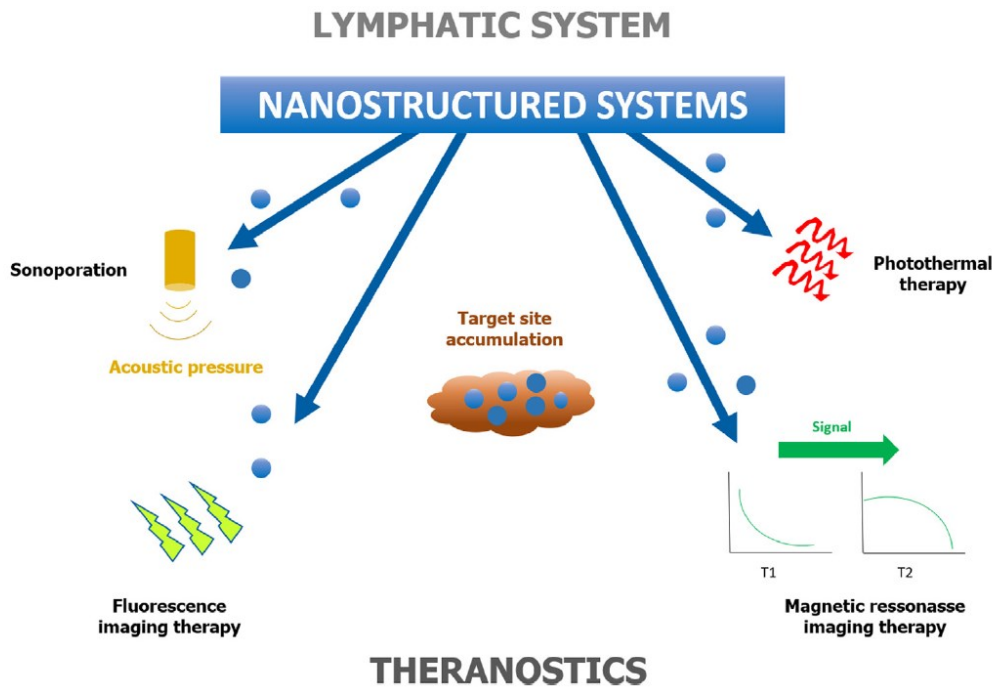
Figure 5.2: Theranostic methods based on nanostructured systems for direct targeting of lymphatic system

Source: Own authorship

3.1.1. Sonoporation

Several imaging procedures such as computer tomography, positron emission tomography, ultrasound (US) and magnetic resonance imaging are applied in combination with histological biopsy for identification of cancer cells (Kato et al., 2015b). Nevertheless, small size metastatic LNs with micrometastasis, which have disseminated from dissected areas soon after surgery, are not detectable by these conventional procedures (Kato et al., 2015a). Moreover, there are limitations in terms of sensitivity and image resolution in conventional methods to be overcome (Niu et al., 2013).

Aiming at efficient targeting and imaging of LN, methods associating US with contrast agents (such as microbubbles) have been developed (Sato et al., 2015, 2014). The sonoporation method is defined as delivery of exogenous molecules into target cells or tissues by use of US. Briefly, in the presence of nano-/microbubbles, a temporary and reversible increase in permeability of target cells occurs due to the two sequential processes: stable and inertial cavitation. The first process consists of a cascade of local shear force generated by a certain size of stable bubbles.

Under higher acoustic pressures, the second process occurs by expansion and collapse of these bubbles, causing several phenomena such as shock waves, generation of free radicals and local heat, and consequently, cell membrane disruption (Sato et al., 2014).

Polymeric microbubbles of poly(lactic-co-glycolic acid) (PLGA) were applied to co-encapsulate Fe_3O_4 nanoparticles and a chemotherapeutic agent doxorubicin (DOX). This resulted in Fe_3O_4 nanoparticles and DOX co-encapsulated PLGA microbubbles, named multifunctional polymer microbubbles (MPMBs), which were filled with perfluorocarbon gas. These MPMBs showed improved US/magnetic resonance imaging in tumor lymph nodes, and the highest apoptotic index of tumor cells after associated treatment of MPMBs with sonication (Niu et al., 2013).

Interesting studies using MXH10/Mo-*lpr*/*lpr* mice have been carried out by several authors, aiming at improving monitoring tumor growth and therapeutic intervention with small changes in the LN internal structures. This recombinant inbred strain of mice exhibits systemic lymphadenopathy generating enlarged peripheral LNs diameter, similar to human LNs. Thus, it made possible a more precise and reproducible administration of agents into the lymphatic system, allowing to obtain minimal information about the alterations and detailed monitoring of the internal structure of lymphatic systems (Kato et al., 2015a, 2015b; Sato et al., 2015, 2014). For example, intravenously administered chemotherapy in LN metastasis has limitations due to the fact that small molecules are easily re-absorbed into the blood capillaries. To overcome this, a combination of intralymphatic injection of chemotherapeutic agent *cis*-Diamminedichloroplatinum (II) (CDDP) with US and nano-/micro-bubbles were applied to treat LN metastasis. The intralymphatically administered combined system showed increased drug delivery to LN tumors and anti-tumor activity. The information about alterations in the volume and blood vessel density of tumor-bearing LNs with CE-HFUS imaging was successfully obtained by using this MXH10/Mo-lpr/lpr mice model (Sato et al., 2014). Other studies, including this animal model and drug delivery system combining nano/microbubbles (NMBs) with ultrasound (US), demonstrated outstanding results on breast carcinoma cells (Sato et al., 2015), head and neck cancer (Kato et al., 2015b), and in three different tumor cell lines (sarcoma cell line established from the spleen, osteosarcoma cell line and bladder tumor cell line) (Kato et al., 2015a), showing promising application of these methods in future research and development.

5.3.2. Photothermal therapy

In addition to sonoporation, another approach has attracted attention in theranostics for the cancer treatments. Photothermal therapy (PTT) is based on the use of light-induced heating agents to destroy cancer cells. The identification of PTT components that provide strong absorbance and photostability in the near-infrared (NIR) region, combined with the high efficiency of photothermal conversion, are the main elements of the success of this therapy. The NIR region, which consists of a wavelength between 700-900 nm, has low absorption by biological tissues, blood and aqueous systems. Thus, under good accumulation of PTT agents in the tumor sites, mainly by passive diffusion, it is possible to burn them up and avoid damage to the surrounding healthy tissues (Liang et al., 2015; Song et al., 2015).

Several nanostructured systems with PTT agents have been developed until now, and imaging-guided PTT systems for lymphatic system-based cancer treatment have also been reported in recent studies.

In a study by Liu et al. (2014), MoS_2 nanosheets functionalized with polyethylene glycol were used to load doxorubicin, providing combined photothermal and chemotherapy for cancer. MoS_2 is a transition metal dichalcogenide, a two-dimensional (2D) nanomaterial with physical and chemical properties that allows the diagnosis and therapy of the disease. The resulting MoS_2-PEG/DOX with NIR irradiation showed approximately 95% cancer cell deaths and dramatically inhibited tumor growth in the tested animals (Liu et al., 2014).

Indocyanine green (ICG) is an NIR dye approved by the US Food and Drug Administration for clinical use. However, this dye has several limitations when used alone, such as instability in the aqueous medium due to the concentration-dependent aggregation, lack of specificity for targeting the tumor, and low stability under continuous irradiation with high potency (Song et al., 2015). To overcome these problems, ICG-loaded lactosome nanoparticles (ICGm) were developed. The experimental model of draining LN metastasis from human gastric cancer showed, by image-guided PTT, a significantly lower increase in popliteal LNs and visible cell apoptosis in the metastatic LNs of mice, after intravenous ICGm administration (Tsujimoto et al., 2015).

Gold nanostructures offer unique properties, such as high biocompatibility and flexible surface chemistry. Oladipo et al. (2017) prepared polymeric gold nanorods (PAuNRs) to efficiently deliver them from the accessory axillary LN to a tumor-containing proper axillary LN, to prevent LN metastasis. This direct injection of a PTT agent into the LN allowed rapid delivery

of PAuNRs in high concentration compared to intravenous injection. An effective block of tumor growth was observed with less morphological changes in the LNs, when the combination of lymphatic system-delivered PAuNRs with laser irradiation (with cooling of skin surface) was used (Oladipo et al., 2017). Another intriguing study concerns the application of PTT using NIR laser light and gold nanorods (GNRs). Using the temperature control system, the skin was kept at 45 °C in order to avoid damage to the skin. Although further improvement is required for better distribution of GNRs in tumor cells, the results showed a significant reduction in LN tumor progression in treated animals (Sugiura et al., 2015).

3.1.3. Magnetic resonance imaging (MRI) therapy

MRI is a noninvasive method that offers powerful imaging ability for diagnosis of tumors and other diseases. This method relies on detecting relaxation signals of hydrogen atom (such as water in the human body) proton spins. Radio-frequency signals of these atoms are detected under strong external magnetic field, and the variation of pulse sequence parameters differentiate the tissues in the body. Two types of relaxation processes of proton spins occur: the longitudinal relaxation (T_1) and transverse relaxation (T_2). T_1 contrast agents (CAs) are chemical agents that increase the T_1 signal intensity, and T_2 CAs are related to the T_2 signal (Gao et al., 2016). T_1 CAs have shorter relaxation process time than T_2 CAs, but are quickly excreted by the kidney due to their relatively small molecules. T_2 CAs are more stable under physiological conditions than T_1 CAs, but they show limitation to distinguish from low-level background magnetic resonance signals. T_1 CAs have a high signal for fat, but low signal for water. T_2 CAs have a high signal for both water and fat. Thus, $T_1 - T_2$ dual imaging offer benefits by easily distinguishing signals from different tissue components (bright or dark), owing to their sensitivity to each CA (Li et al., 2018). Some examples of T_1 contrast nanoparticle (NP) agents are gadolinium (Gd)-based NPs, manganese-based NPs, and the iron oxide NPs are largely used as T_2 contrast agents (Gao et al., 2016).

Quiao et al. (2015) developed core@shell structured $NaGdF_4$:Yb,Er@$NaGdF_4$ upconversion nanoparticles coated with polyethylene glycol (PEG) as a sensitive detection tool of lymphatic dissemination. A gastric-cancer specific probe was injected through a tail vein into tumor-bearing mice, followed by upconversion luminescence imaging, to successfully detect small

lymphatic metastasis (< 1 mm). This study offers a very sensitive and specific diagnosis at the primary and lymphatic metastatic site of gastric cancer (Qiao et al., 2015).

Aiming at theranostics, gold-shelled iron oxide nanoclusters with polyethylene glycol coatings were developed as the magnetic-responsive PTT agent. Being monitored by magnetic resonance imaging (MRI) followed by NIR laser, these nanoparticles were accumulated in the SLNDs, and burned up both primary tumors and SLNDs. Mice treated by this system showed remarkably prolonged animal survival, without weight loss or lung metastasis. This is a very promising treatment for superficial tumors (Liang et al., 2015).

3.1.4. Fluorescence imaging therapy

Some of recent developments in optimal fluorescence imaging systems include the application of human ferritin heavy chain (hFTN) as a carrier. The subunit protein of hFTN was genetically modified to densely present on its surface, the red fluorescence protein (RFP), a model tumor-specific antigen (TSAs) to LNs. The resulted hFTN-RFP nanoparticle was injected into healthy mice resulting in rapid LN targeting and accumulation. This can be due to the high affinity of human ferritin to T cell immunoglobulin and mucin domain-2 (TIM-2), which regulates cellular immunity. The vaccination of mice by hFTN-RFP significantly increased the T cell population in LN, and also the number of IFN-ɣ-secreting CD8+ T cells in their spleen. Thus, this nanoparticle can be used as a fluorescence imaging contrast, combined with its TSA-carrying vaccine platform for immunotherapy (Lee et al., 2016).

Another study concerning fluorescence imaging aimed at a proper diagnosis of NL metastasis to guide lymphadenectomy in gastric cancer. The fluorescent copper sulfide (CuS) nanoparticle (RGD-CuS-Cy5.5) had been developed by Shi et al. (2018). After injection into primary tumors, this nanoparticle demonstrated high selectivity to metastatic gastric MNK45 tumor cells and accumulation. The NIR fluorescence and computed tomography could significantly differentiate the metastatic SLNDs to normal SLNDs of gastric cancers, allowing appropriate irradiation of tumor site with localized PTT and elimination of metastatic gastric tumor cells in SLNDs (Shi et al., 2018).

Cancer is one of the major causes of mortality worldwide, affecting people of all ages, countries and sex. However, between 30% to 50% of cancer diseases are preventable by following

a healthy lifestyle, such as avoiding tobacco, exercising and preventing infection; in addition, early detection and treatment of cancer is considered a critical issue to avoid mortality from this disease (World Health Organisation, 2018). Therefore, new theranostic methods based on nanostructured systems combined with lymphatic system direction is a promising alternative for preventing and treating cancer.

5.3.3. *Immunotherapy for lymphatic cancer*

Cancer immunotherapy is an emerging and promising treatment to induce or support the body's adaptive immune system for antitumor responses. Several specific antigens expressed by tumor cells can be key elements in developing cancer vaccines, and balancing the cascades of immune stimulatory and inhibitory signals. Therefore, the recognition of malignant antigens by the adaptive immune system should be effective to produce cells and antibodies to kill tumor cells, preserve healthy cells, and generate memory to provide long-lasting protection to the body (Björnmalm et al., 2017; Lee et al., 2016).

The lymphatic system plays an important role in this process, since the lymphatic vessels are responsible for transporting antigens and immune cells from the afferent lymphatic vessels to draining lymph nodes (dLNs), initiating the cascade process for adaptive immune protection (Liao and von der Weid, 2015). Lymph nodes (LNs) are lymphoid tissues that accommodate the population of resident dendritic cells (DCs), plasmacytoid DCs, and macrophages. During the antigen transportation, these populations are activated into antigen-presenting cells (APCs) to cross-present antigens to lymphocytes (T and B cells), converting naive lymphocytes to mature ones, critical for killing tumor cells (Lee et al., 2016).

Although several mechanisms are involved in the lymphatic metastatic process and some are still unclear, different proposals of nanostructured systems have been developed targeting this site. Some recent developments are shown in the following items (**Figure 5.3**).
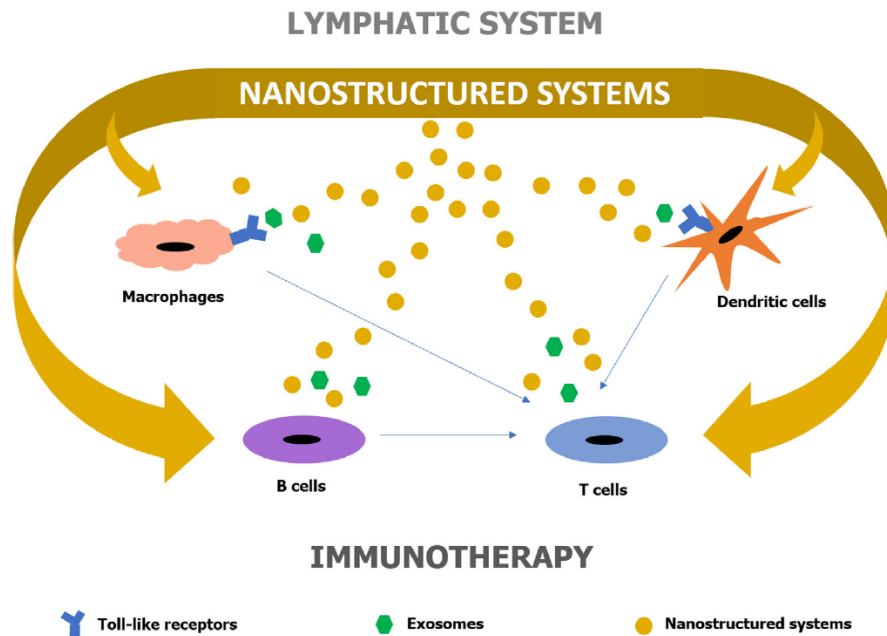
Figure 5.3: Nanostructured systems for targeting cancer factors associated with lymphatic system. Source: Own authorship

5.3.3.1. Macrophages

As part of the APC group, macrophages process antigens of endogenous and exogenous origin. Their main function is known to internalize, sequester and completely degrade tissue-invading pathogens, being less effective in presenting antigens and capable of taking larger particles than DCs (Fromen et al., 2016; Hamdy et al., 2011). However, some recent papers well-summarized by Komohara et al. (2017) showed a significant role of lymph node (LN) sinus macrophages in inducing anti-tumor immunity in several diseases (e.g. colorectal tumor, endometrial tumor and malignant melanoma). LN sinus is a lymphatic fluid-filled and macrophage-rich region, located in the central medullary part of lymph nodes. Macrophages detected in this region express the surface antigen CD169. Although no mechanism of CD169 in this immunological effect has been revealed yet, it has been proposed that LN sinus macrophages engulf antigens by various receptors and present antigen-derived peptides to B- and T-lymphocytes. The high percentage of CD169-positive LN macrophages seems to be linked to higher density of infiltrating CD8+ lymphocytes in primary tumor tissues. This evidence

encouraged development of possible vaccines, targeting macrophages (Komohara et al., 2017). In order to transport antigens to professional APCs (macrophages and DCs) in draining LNs to increase immunogenicity, a synthetic long peptide antigen was encapsulated within an immunologically inert nanoparticulate hydrogel (nanogel) of cholesteryl pullulan (CHP). By subcutaneous injection, the CHP nanogel reached the medulla, a central area of LN, where it was entirely engulfed by LN sinus macrophages. This behavior of the CHP nanogel is called "immunological stealth mode" by the authors. These macrophages definitely cross-primed the vaccine-specific CD8+ T cells in LNs and inhibited tumor growth in vivo. Even though the mechanism of this interaction of macrophages with the CHP nanogel in the immune response has not been elucidated, a strong antitumor response of T cells dependent on these cells has been observed (Muraoka et al., 2014).

Furthermore, studies report the presence of tumor-associated macrophages (TAMs) categorized into M1 and M2 cells, having yin-yang influence on the performance of chemotherapy and radiotherapy. The former produces proinflammatory cytokines to eradicate malignant agents, and the latter acts as a suppressor of immune responses. TAMs regulate cancer-related inflammation by common inflammatory pathways to support several cancer treatments. Nonetheless, according to the disease stage, tissue type, and the host microbiota, they can coordinate a tumor-promoting repair response to tissue damage, contributing to the anti-tumor activity. Thus, several efforts have been made to promote activation and redirect macrophages to potentially support current anti-cancer therapies. Details of these mechanisms are well-described by Mantovani et al.(2017) (Mantovani et al., 2017). Al-Hallak et al. (2010) developed inhaled doxorubicin (DOX)-loaded nanoparticles (NPs) to investigate their role in activation of alveolar macrophages and this result in H460 lung cancer cells. Usually, the dynamic migration of alveolar macrophages between the lung tissues and the lymphatic system turn them into TAM, after infiltration into the lung tumor tissue. Results showed that the fragments of DOX-loaded NPs after phagocyting by macrophages induced increased excretion of Th1-type cytokines. These cytokines are known to induce acute inflammation and cell-mediated immune response. The induced cytokines proportion were, in order of magnitude, monocyte chemoattractant protein-1 (MCP-1), macrophage inflammatory protein-1 (MIP-1), tumor necrosis factor α (TNF-α), and interferon gamma (IFN-γ), and this result was not observed by naive macrophages (Al-Hallak et al., 2010). Later, studies performed by the same group showed in vivo results using DOX-loaded NPs

integrated into inhalable effervescent carrier particles using a spray–freeze drying technique. Animals treated with these particle carriers showed smaller lung tumors and longer survival times. This is probably due to the prevention of NP agglomeration and enhanced dispersion of NPs for better uptake by alveolar macrophages compared to the non-effervescent powder (Roa et al., 2011). Other interesting research includes the drug interaction of ordinally anti-inflammatory agents with nanoparticles in a macrophage-lung cancer coculture model. Anti-inflammatory agents, such as NSAIDs (ibuprofen, celecoxib), methotrexate, and GCs (prednisolone and dexamethasone) are commonly used in current anti-cancer treatments. However, results showed that these agents, in combination with NPs, significantly enhanced (up to around 30%) cancer cell viability compared to NPs alone. These results may be due to the negative influence of these agents over the acutely inflamed state of the macrophages, reducing their secondary toxicity for cancer nanotherapy (Sarfraz et al., 2016).

5.3.3.2. Dendritic cells

In addition to the role of APC, DCs have several functions in regulating the recirculation of T cells from the blood to LNs through the lymphatic vessels. DCs modulate the phenotype of high endothelial venules (HEVs), the blood vessels responsible for recruiting lymphocytes (T or B cells). Thus, in the presence of DCs, HEV is maturated and lymphocytes are recruited to LNs. Lymphotoxin derived from DCs also works to control lymphocyte entry into LNs (Moussion and Girard, 2011). Another interesting study by Braun et al. (2011) describes the role of mature DCs in secondary LNs, located downstream from primary LNs. The chain organization of the LNs suggest that the lymphocytes that leave the peripheral primary LN through efferent lymphatics, enter the subcapsular sinus (SCS) of more central secondary LN through its afferent lymphatic vessel. The activated DCs in the secondary SCS promote changes in the morphology of this SCS floor, which supports the direct entry of the T cells. Thus, DCs have a privileged role over T cell transportation during immune response (Braun et al., 2011).

Targeting DCs for vaccination strategies with nanoparticles (NPs) and preventing the clearance by macrophage uptake, Fromen et al. (2016) investigated the influence of the nanoparticle surface charge on immune responses in the lung. The authors prepared hydrogel-based NPs using particle replication in non-wetting templates (PRINT) technique, which allowed the preparation of NPs with the same size, shape and antigen loading, except for the surface charge

(anionic and cationic). After pulmonary instillation, preferential associations of anionic NPs with alveolar macrophages (AMs) and cationic NPs with DCs were observed. The cationic NPs resulted in increased expression of *Ccl2* and *Cxc10*, which are important chemo-attractants that act in recruiting DC into the lung. A high accumulation of CD11b DCs, a subtype of DCs in the lung, that play an important role in the production of soluble protein mediators, chemokines and cytokines has been demonstrated. These cationic NPs can be a potential carrier as pulmonary vaccine NPs for diverse diseases, to promote the recruitment and maturation of lung DCs (Fromen et al., 2016).

PEGylation is known to increase the mobility of particles in the extracellular matrix after systemic injection, due to the decreased interaction with macrophages and serum proteins. PEGylated polymer hydrogel nanoparticles of modified poly(methacrylic acid) were developed to target multiple immune cell subsets in the draining LNs. The results showed extensive internalization of these nanoparticles by DCs, high interaction of them in the LN DCs and B cells, followed by an increase in the antigen presentation and the priming of antigen-specific T cells (De Koker et al., 2016).

5.3.3.3. Toll-like receptors

Toll-like receptors (TLRs) are expressed on the membranes of populations such as DCs, macrophages, lymphocytes T and B cells. They play important roles in recognizing malignant molecules and, by binding with these molecules, initiate a cascade of processes involved in innate immune responses and, especially, in the adaptive immune system. This cascade recruits a considerable number of proteins, including protein kinases and cytokines, for later upregulation or suppression of defense responses. In anticancer immunotherapy, the use of TLRs agonists have a significant impact on the development of a promising adjuvant, with more specific and effective treatment (Nuhn et al., 2016; Zhang et al., 2017).

However, the systemic administration of these agonists in the pure state generally presents restrictions such as a lack of response due to a lack of recognition by the immune system, problems of solubility and inflammatory toxicity at high doses when attempting sustained signaling of TLR in the immune system (Hamdy et al., 2011; Nuhn et al., 2016). Overcoming these limitations, the targeting strategy using nanocarriers revealed a dramatic improvement in adjuvant efficacy, resulting in greater LN accumulation, higher stability, sustained release and activation of immune

responses, avoiding T$_{reg}$-mediated immune suppression in T-cell responses (Hamdy et al., 2011; Zhang et al., 2017).

Promising carriers for transcutaneous vaccine delivery were developed using chitosan nanoparticles (CS-NPs) in anti-tumor therapy. The antigen-incorporated CS-NP with gp100, a tumor-associated melanoma antigen, showed tumor growth reduction and increased survival rates in treated mice. This suggests that this NP may provide increase uptake of NP by APS such as Langerhans cells, inducing their activation, maturation and migration from the epidermis to the dermis and surrounding LNs, for stimulation of immune cells. Another CS-NPs loaded with ovalbumin (OVA) as a model antigen was combined with imiquimod, a synthetic TLR7 ligand that can be used as an adjuvant for transcutaneous immunization. This combination resulted in enhanced transcutaneous immune responses, possibly due to the activation of skin immune cells through TLR7 and TLR8 by imiquimod, and induction of the migration of Langerhans cells (Li et al., 2014).

A small-molecule imidazoquinoline-based TLR7/8 agonist was covalently linked to pH-degradable polymeric nanogels. TLR7/8 is localized in the endosomal membrane of DCs, and analysis revealed a greater internalization of nanogels by DCs, compared to soluble polymer. In vitro cultured dendritic cell tests demonstrated a high preservation of agonist potency to activate TLR7/8. Increases in nanogel-positive B cells, nanogel-positive DCs, nanogel-positive macrophages, nanogel-positive Ly6 chimonocytes in the draining LN were also demonstrated. The inflammatory toxicity associated with soluble TLR agonists was limited, and an increase in the induction of T-cell responses and antibody responses was observed under this administration of nanogel (Nuhn et al., 2016).

A covalently linked oligonucleotide agonist (CpG DNA) to the dextran polymer provided a 6.5-nm nanostructure to target the LN to effectively activate LN-resident APCs. Class B CPG DNA is a TLR9 agonist capable of prime potent CD8+ T cell responses. The Dextran-CpG Conjugate increased LN uptake, CD8+ T-cell immune responses, long-term memory T-cells to prevent tumor recurrence and efficiently combined with whole necrotic tumor cells, providing high adaptive immunity to draining LN (Zhang et al., 2017).

Zeng et al. (2017) (Z5) developed polymeric hybrid micelles (HMs) that encapsulated the melanoma antigen peptide Trp2 and the agonist of TLR-9, CpG ODN. The HMs are self-assembled through hydrophobic and electrostatic interactions of two amphiphilic diblock

copolymers, poly-(ethylene glycol) phosphoethanolamine (PEG-PE) and polyethylenimine-stearic acid conjugate (PSA). Under the adjustment of the molar ratio of PEG-PE and PSA, the equal ratio of these copolymers proved to be the best ratio to potently target the proximal LNs and efficiently internalize the antigen/agonist in the DCs. This nanocarrier greatly increases the antigen-specific cytotoxic T cells, providing a strong anti-tumor result in a lung metastatic melanoma model (Zeng et al., 2017).

5.3.3.4. T cells

T cells play a fundamental role in a range of immune responses as described previously. T cells can be activated by antigen stimulation by acute or chronic infections or cancer, and can trigger adaptive immune mechanisms. LNs are the main site where these mechanisms take effect: T cells are primed and maturated for immune protection for defense against cancer. However, in parallel, sentinel LNs are considered to be the first LNs that drain tumor cells, which favor their subsequent diffusion to the distant organs, named metastasis. An intriguing question is: how does the function of T cells in LNs differ in the immune defense against primary cancer, and in facilitating the dissemination of cancer?

During an acute infection, mature T cells clear malignant antigens and some T cells transform to memory T cells for future protection of the body. During cancer disease, the complex tumor microenvironment releases several inhibitory signals. This repeated exposure of T cells to malignant signals causes exhaustion, generating dysfunction of T cells. The co-expression of multiple inhibitory receptors seems to be associated with this acquired dysfunction of T cells, which includes PD-1, cytotoxic T lymphocyte antigen 4 (CTLA-4), T-cell immunoglobulin domain and mucin domain-3 (Tim-3), and others. Then, it leads to the failure of the effective elimination of tumor cells due to these dysfunctional T cells. Several new trials to repair these dysfunctions are being studied, such as single or combined immune checkpoint blockage, where the description of the mechanisms of dysfunctions and preventions has been well detailed by Xia et al. (2019) (Xia et al., 2019).

Aiming at the activation or maturation of T cells, we briefly present some specific research for target LNs using nanostructured systems. Some of them are closely associated with TLR interaction.

Under intradermal administration, targeted delivery of adjuvant to the tumor-draining LN (TDLN) was accomplished by developing polymeric nanoparticles (NPs) that effectively target DCs within the TDLNs. The NPs were loaded with adjuvants CpG oligonucleotide (TLR9 agonist) or paclitaxel (TLR4 agonist), and administered to the ipsilateral limb to target TDLN in a B16-F10 melanoma. DC maturation was observed in TDLN, the remodeling of CD4+ helper T cell distribution and also an increase in the frequency of antigen-specific CD8+ T cells in the tumor. CD8+ T cells are known to play an important role due to their cytotoxic response to clear cancer cells. Therefore, this nanosystem has shown effective results for promoting anti-tumor immunity and reducing tumor growth (Thomas et al., 2014).

The size effect of gold nanoparticle (GNP)-based vaccines was evaluated on their ability to deliver to LNs and to induce CD8+ T cell responses. Under conjugation with recombinant ovalbumin (OVA) as a model antigen, OVA-GNPs with hydrodynamic diameter ranging from ~10 to 33 nm were prepared. It was suggested that the OVA-GNPs be drained directly into the LNs, instead of being transported by the DCs present at the injection site. This may be related to the particle size of these nanoparticles. The uptake of OVA-GNPs in LN DCs was comparable for nanoparticles of sizes 22- and 33-nm by in vivo delivery. Also in vivo, when compared to 10nm, the 22 nm OVA-GNPs showed greater recognition and killing effect of their corresponding antigen-bearing target cancer cells. This is possibly related to the better quality of the corresponding cytotoxic T-lymphocyte responses of this nanoparticle (Kang et al., 2017).

Nanoparticles of synthetic vaccine based on poly(γ-glutamic acid) (SVNPs) were developed to load the model tumor antigen (OVA) and the TLR 3 agonist (poly (I:C)) to target immune cells in the lymph nodes. This resulted in the efficient uptake of antigen and agonist loaded in SVNPs, both by the same DC cells derived from bone marrow, and the increased secretion of inflammatory cytokines TNF-α and IL-6. When SVNP-OVA and SVNP-IC were injected simultaneously in vivo, the IFN-ɣ (produced by CD8+ T cells and important to induce a specific cytotoxic response) was highly secreted, and tumor growth was dramatically inhibited in the treated mice (Kim et al., 2017).

5.3.3.5. B Cells

One of key element for antibody production (the immunoglobulins, i.e. IgA, IgM), is the B cell. B cells are generated in bone marrow in immature form, and some subsets are matured after

entering secondary lymphoid organs such as lymph nodes. These cells detect and produce more specific antibodies to antigens, even in the presence of small amounts of antigens in the environment, which differs from other APCs (Sharma et al., 2013). Although B cells' role in presenting antigen to T cells for innate response, it is pointed their role in the regulation of anti-tumor immunity, inhibiting the cytotoxic response of T cell, in addition to inducing lymphangiogenesis. Studies demonstrated the activation of B cells in metastatic lymph nodes (Zirakzadeh et al., 2013), the preferential accumulation of regulatory B cells in the tumor-draining lymph nodes, promoting melanoma tumor growth (Ganti et al., 2015), the activation of NF-κB pathway by stimulating B-cell receptor signaling in lymph nodes and promoting proliferation of tumor in chronic lymphocytic leukemia. NF-κB pathway is involved in cell-cycle regulation, inhibition of apoptosis, sign transduction and chemotaxis (Herishanu et al., 2011). It was also described the sentinel lymph node as site where B cells are maturated (or educated) under chronic exposure to tumor antigens to increase systemic IgG anticancer antibodies and antitumor immune responses, in breast cancer patients (McDaniel et al., 2018). A recent work by Gu et al (2019) demonstrated the accumulation of B cells in draining lymph node induced by primary tumors in a breast cancer mouse model of lymph node metastasis. Pathogenic IgG was produced by these B cells, activating the HSPA4 (Heat Shock Protein Family A (Hsp70) Member 4) and consequently the NF-κB pathway to selectively promote lymph node metastasis (Gu et al., 2019). Therefore, several studies indicated the role of tumor-educated B cells in promoting cancer progression.

Gold compounds were known to inhibit NF-κB pathway and IKK (inhibitory kB kinase, which is responsible to promote large number of signaling cascades including activation of this pathway). However, Sharma et al. (2013) demonstrated the induction of 'canonical' NF-kB signaling pathway using a gold nanoparticle (Au-NP) of 10 nm (Sharma et al., 2013). This canonical pathway mediates inflammatory responses (Shih et al., 2011) related to B cells antibody production. Evaluation using murine B-lymphocyte cell line (CH12.LX) indicated that Au-NPs crossed the cellular membrane, physically connected to cellular proteins, inhibiting IKKs activation and causing prolonged NF-kB activation. Thus, authors emphasize the importance of understanding the nano-bio interactions which are dependent on each specific material properties of nanosystems (Sharma et al., 2013). Other authors developed nanostructured lipid carriers (NLCs) loading doxorubicin (DOX) and vincristine (VCR) (Dong et al., 2016), and also the combination of DOX, VCR and gemcitabine (GEM) to treat B-cell lymphoma (Ni et al., 2017).

Results showed enhanced antitumor effect of these synergistic combination, when compared with the drug solutions or the single drug-loaded NLCs.

5.3.3.6. Exosomes

Exosomes are nano-sized (40-100 nm) membrane-bound extracellular vesicles produced by most eukaryotic cells. They can be present in various extracellular fluids, such as serum, blood, lymph, urine, saliva, cerebrospinal fluids, ascites fluids, etc. Exosomes originate from several cells and are enriched by various sources of parental cells (such as lipids, mRNAs, protein, micro-RNAs and carbohydrates) that are packaged in their vesicles during their origin. Thus, each exosome differs from the others, carrying different information from the parent cells. They play an important role in mediating cell-to-cell communication, and recent studies have shown their role in the inflammatory and immunomodulatory effects on target cells (Cheng et al., 2017; Kojima et al., 2018).

Tumor-derived exosomes seem to be involved in the progression of metastasis, promoting angiogenesis and remodeling stroma. But other studies have also demonstrated their role as an immunosuppressor, impairing the tight junctions and the stability of the microvascular barrier of the metastatic site (Kojima et al., 2018). In addition to this immunomodulatory function, exosomes are lipidic membrane vesicles that are promptly uptaken by the cells by membrane fusion. This physical-chemical property makes them excellent carriers, including drug delivery in cancer immunotherapy (Cheng et al., 2017).

One of the main target cells of exosomes are macrophages, which in addition to cytokines and chemokines, can also excrete exosomes. Cheng et al.(2017) evaluated exosomes derived from M1 macrophages on the vaccine platform based on lipid calcium phosphate (LCP). This nanoparticulate vaccine showed LNs targeting properties after subcutaneous injection in mice, induced the expression of pro-inflammatory cytokines and a T cell immune response, and showed more potent inhibition of tumor growth when compared to CpG ODNs with LCP or LCP alone, via induction of the Th1 cytokine adaptive immune response (Cheng et al., 2017).

In summary, nanostructured systems targeting the lymphatic system are an interesting strategy not only due to the recent discoveries concerning lymphangiogenesis compared to angiogenesis,

but also for evoking new strategies for treating cancer. Nonetheless, this is a complicated disease that involves activation and suppression of multiple factors, with unpredictable time and site of recurrence. Thus, the recent recommendations for the eradication of advanced tumors, even if impossible to be complete, are the combined therapies that employ both innate and adaptive immune systems, by different administration sites (Björnmalm et al., 2017; Wang et al., 2017). This makes sense when thinking about the associated interactions of different immune cells and their cascading actions to respond to multiple stimuli in the dynamic environment where these cells are found.

5.4. Final Discussions and Perspectives

The lymphatic system plays an essential role in diffusing metastatic cancer cells to distinct organs and different tumors. However, several challenges remain in developing advanced methods for prognosis of micrometastasis and its treatment, as well developing immunotherapies to target specific cells in lymphangiogenesis. In this context, nanostructured systems associated with the lymphatic system showed to be emerging and intriguing strategies for combating specific cancers. Treating already established solid tumors is much more challenging than preventing this establishment. The direct introduction of therapeutic agents into the lymph nodes or the lymphatic system may generate substantial benefits, providing more effective targeting, activation of the key elements of the adaptive immune system through direct interactions of the drug with these immune systems, or passive transportation and activation of the innate immune system. In addition, by avoiding clearance due to direct uptake via the blood system, this strategy may reduce the risk of toxicity and provide better recovery for patients.

Several imaging therapy methods associated with specific test models have been designed to conduct nanostructured systems through the lymphatic system to treat cancer. These intelligent methods, namely theranostics, include sonoporation, photothermal therapy, magnetic resonance and fluorescence imaging therapy. These methods guide and accumulate nanomaterials to the tumor site to finally destroy them, causing less damage to the surrounding healthy tissues. Consequently, keeping in mind the main role of immune defense cells in the regression or progression of tumors, focusing on them is an unquestionable choice. Antigen-presenting cells, T cells, toll-like receptors, and exosomes are some of the strategic approaches using nanostructured

156

systems. The selection of the right materials to 'switch on' the defense system has been shown as a prospective approach to immunotherapy through the lymphatic system. Even in the progression stage, the combination of these therapies are promising approaches that open doors for synergic and multi-variant solutions for specific cancers.

We offered in this review a general understanding of the involvement of the lymphatic system in the progression of cancer, and the scopes of different nanostructured systems for specific targeting. Therefore, we provided readers a clearer vision of trends that may support future development and selection of therapies, aiming at combined treatment for recovering from various types of cancers.

5.5. References

Al-Hallak, K.M.H.D., Azarmi, S., Anwar-Mohamed, A., Roa, W.H., Löbenberg, R., 2010. Secondary cytotoxicity mediated by alveolar macrophages: A contribution to the total efficacy of nanoparticles in lung cancer therapy? Eur. J. Pharm. Biopharm. 76, 112–119. https://doi.org/10.1016/j.ejpb.2010.05.002

Björnmalm, M., Thurecht, K.J., Michael, M., Scott, A.M., Caruso, F., 2017. Bridging Bio-Nano Science and Cancer Nanomedicine. ACS Nano 11, 9594–9613. https://doi.org/10.1021/acsnano.7b04855

Braun, A., Worbs, T., Moschovakis, G.L., Halle, S., Hoffmann, K., Bölter, J., Münk, A., Förster, R., 2011. Afferent lymph-derived T cells and DCs use different chemokine receptor CCR7-dependent routes for entry into the lymph node and intranodal migration. Nat. Immunol. 12, 879–887. https://doi.org/10.1038/ni.2085

Cabral, H., Makino, J., Matsumoto, Y., Mi, P., Wu, H., Nomoto, T., Toh, K., Yamada, N., Higuchi, Y., Konishi, S., Kano, M.R., Nishihara, H., Miura, Y., Nishiyama, N., Kataoka, K., 2015. Systemic targeting of lymph node metastasis through the blood vascular system by using size-controlled nanocarriers. ACS Nano 9, 4957–4967. https://doi.org/10.1021/nn5070259

Chaudhary, S., Garg, T., Murthy, R.S.R., Rath, G., Goyal, A.K., 2014. Recent approaches of lipid-based delivery system for lymphatic targeting via oral route. J. Drug Target. 22, 871–882. https://doi.org/10.3109/1061186X.2014.950664

Cheng, L., Wang, Y., Huang, L., 2017. Exosomes from M1-Polarized Macrophages Potentiate the

Cancer Vaccine by Creating a Pro-inflammatory Microenvironment in the Lymph Node. Mol. Ther. 25, 1665–1675. https://doi.org/10.1016/j.ymthe.2017.02.007

De Koker, S., Cui, J., Vanparijs, N., Albertazzi, L., Grooten, J., Caruso, F., De Geest, B.G., 2016. Engineering Polymer Hydrogel Nanoparticles for Lymph Node-Targeted Delivery. Angew. Chemie - Int. Ed. 55, 1334–1339. https://doi.org/10.1002/anie.201508626

Dieterich, L.C., Detmar, M., 2016. Tumor lymphangiogenesis and new drug development. Adv. Drug Deliv. Rev. 99, 148–160. https://doi.org/10.1016/j.addr.2015.12.011

Dong, X., Wang, W., Qu, H., Han, D., Zheng, J., Sun, G., 2016. Targeted delivery of doxorubicin and vincristine to lymph cancer: evaluation of novel nanostructured lipid carriers in vitro and in vivo. Drug Deliv. 23, 1374–1378. https://doi.org/10.3109/10717544.2015.1041580

Fromen, C.A., Rahhal, T.B., Robbins, G.R., Kai, M.P., Shen, T.W., Luft, J.C., DeSimone, J.M., 2016. Nanoparticle surface charge impacts distribution, uptake and lymph node trafficking by pulmonary antigen-presenting cells. Nanomedicine Nanotechnology, Biol. Med. 12, 677–687. https://doi.org/10.1016/j.nano.2015.11.002

Ganti, S.N., Albershardt, T.C., Iritani, B.M., Ruddell, A., 2015. Regulatory B cells preferentially accumulate in tumor-draining lymph nodes and promote tumor growth. Sci. Rep. 5, 1–8. https://doi.org/10.1038/srep12255

Gao, Z., Ma, T., Zhao, E., Docter, D., Yang, W., Stauber, R.H., Gao, M., 2016. Small is Smarter: Nano MRI Contrast Agents - Advantages and Recent Achievements. Small 12, 556–576. https://doi.org/10.1002/smll.201502309

Gu, Y., Liu, Y., Fu, L., Zhai, L., Zhu, J., Han, Y., Jiang, Y., Zhang, Y., Zhang, P., Jiang, Z., Zhang, X., Cao, X., 2019. Tumor-educated B cells selectively promote breast cancer lymph node metastasis by HSPA4-targeting IgG. Nat. Med. 25, 312–322. https://doi.org/10.1038/s41591-018-0309-y

Hamdy, S., Haddadi, A., Hung, R.W., Lavasanifar, A., 2011. Targeting dendritic cells with nano-particulate PLGA cancer vaccine formulations. Adv. Drug Deliv. Rev. 63, 943–955. https://doi.org/10.1016/j.addr.2011.05.021

Herishanu, Y., Pérez-Galán, P., Liu, D., Biancotto, A., Pittaluga, S., Vire, B., Gibellini, F., Njuguna, N., Lee, E., Stennett, L., Raghavachari, N., Liu, P., McCoy, J.P., Raffeld, M., Stetler-Stevenson, M., Yuan, C., Sherry, R., Arthur, D.C., Maric, I., White, T., Marti, G.E., Munson, P., Wilson, W.H., Wiestner, A., 2011. The lymph node microenvironment promotes

B-cell receptor signaling, NF-κB activation, and tumor proliferation in chronic lymphocytic leukemia. Blood 117, 563–574. https://doi.org/10.1182/blood-2010-05-284984

Kang, S., Ahn, S., Lee, J., Kim, J.Y., Choi, M., Gujrati, V., Kim, H., Kim, J., Shin, E.C., Jon, S., 2017. Effects of gold nanoparticle-based vaccine size on lymph node delivery and cytotoxic T-lymphocyte responses. J. Control. Release 256, 56–67. https://doi.org/10.1016/j.jconrel.2017.04.024

Karnezis, T., Shayan, R., Caesar, C., Roufail, S., Harris, N.C., Ardipradja, K., Zhang, Y.F., Williams, S.P., Farnsworth, R.H., Chai, M.G., Rupasinghe, T.W.T., Tull, D.L., Baldwin, M.E., Sloan, E.K., Fox, S.B., Achen, M.G., Stacker, S.A., 2012. VEGF-D Promotes Tumor Metastasis by Regulating Prostaglandins Produced by the Collecting Lymphatic Endothelium. Cancer Cell 21, 181–195. https://doi.org/10.1016/j.ccr.2011.12.026

Kato, S., Mori, S., Kodama, T., 2015a. A novel treatment method for lymph node metastasis using a lymphatic drug delivery system with nano/microbubbles and ultrasound. J. Cancer 6, 1282–1294. https://doi.org/10.7150/jca.13028

Kato, S., Shirai, Y., Kanzaki, H., Sakamoto, M., Mori, S., Kodama, T., 2015b. Delivery of Molecules to the Lymph Node via Lymphatic Vessels Using Ultrasound and Nano/Microbubbles. Ultrasound Med. Biol. 41, 1411–1421. https://doi.org/10.1016/j.ultrasmedbio.2014.12.014

Kim, S.Y., Noh, Y.W., Kang, T.H., Kim, J.E., Kim, S., Um, S.H., Oh, D.B., Park, Y.M., Lim, Y.T., 2017. Synthetic vaccine nanoparticles target to lymph node triggering enhanced innate and adaptive antitumor immunity. Biomaterials 130, 56–66. https://doi.org/10.1016/j.biomaterials.2017.03.034

Kodama, T., Matsuki, D., Tada, A., Takeda, K., Mori, S., 2016. New concept for the prevention and treatment of metastatic lymph nodes using chemotherapy administered via the lymphatic network. Sci. Rep. 6, 1–8. https://doi.org/10.1038/srep32506

Kojima, M., Gimenes-Junior, J.A., Chan, T.W., Eliceiri, B.P., Baird, A., Costantini, T.W., Coimbra, R., 2018. Exosomes in postshock mesenteric lymph are key mediators of acute lung injury triggering the macrophage activation via Toll-like receptor 4. FASEB J. 32, 97–110. https://doi.org/10.1096/fj.201700488R

Komohara, Y., Ohnishi, K., Takeya, M., 2017. Possible functions of CD169-positive sinus macrophages in lymph nodes in anti-tumor immune responses. Cancer Sci. 108, 290–295.

https://doi.org/10.1111/cas.13137

Lee, B.R., Ko, H.K., Ryu, J.H., Ahn, K.Y., Lee, Y.H., Oh, S.J., Na, J.H., Kim, T.W., Byun, Y., Kwon, I.C., Kim, K., Lee, J., 2016. Engineered Human Ferritin Nanoparticles for Direct Delivery of Tumor Antigens to Lymph Node and Cancer Immunotherapy. Sci. Rep. 6, 1–12. https://doi.org/10.1038/srep35182

Leong, S.P.L., Tseng, W.W., 2014. Micrometastatic cancer cells in lymph nodes, bone marrow, and blood: Clinical significance and biologic implications. CA. Cancer J. Clin. 64, 195–206. https://doi.org/10.3322/caac.21217

Li, J., You, J., Wu, C., Dai, Y., Shi, M., Dong, L., Xu, K., 2018. T 1 –T 2 molecular magnetic resonance imaging of renal carcinoma cells based on nano-contrast agents. Int. J. Nanomedicine 13, 4607–4625. https://doi.org/10.2147/IJN.S168660

Li, N., Peng, L.H., Chen, X., Zhang, T.Y., Shao, G.F., Liang, W.Q., Gao, J.Q., 2014. Antigen-loaded nanocarriers enhance the migration of stimulated Langerhans cells to draining lymph nodes and induce effective transcutaneous immunization. Nanomedicine Nanotechnology, Biol. Med. 10, 215–223. https://doi.org/10.1016/j.nano.2013.06.007

Liang, C., Song, X., Chen, Q., Liu, T., Song, G., Peng, R., Liu, Z., 2015. Magnetic Field-Enhanced Photothermal Ablation of Tumor Sentinel Lymph Nodes to Inhibit Cancer Metastasis. Small 11, 4856–4863. https://doi.org/10.1002/smll.201501197

Liao, S., von der Weid, P.Y., 2015. Lymphatic system: An active pathway for immune protection. Semin. Cell Dev. Biol. 38, 83–89. https://doi.org/10.1016/j.semcdb.2014.11.012

Liu, T., Wang, C., Gu, X., Gong, H., Cheng, L., Shi, X., Feng, L., Sun, B., Liu, Z., 2014. Drug delivery with PEGylated MoS2 nano-sheets for combined photothermal and chemotherapy of cancer. Adv. Mater. 26, 3433–3440. https://doi.org/10.1002/adma.201305256

Lohela, M., Bry, M., Tammela, T., Alitalo, K., 2009. VEGFs and receptors involved in angiogenesis versus lymphangiogenesis. Curr. Opin. Cell Biol. 21, 154–165. https://doi.org/10.1016/j.ceb.2008.12.012

Makwana, V., Jain, R., Patel, K., Nivsarkar, M., Joshi, A., 2015. Solid lipid nanoparticles (SLN) of Efavirenz as lymph targeting drug delivery system: Elucidation of mechanism of uptake using chylomicron flow blocking approach. Int. J. Pharm. 495, 439–446. https://doi.org/10.1016/j.ijpharm.2015.09.014

Mantovani, A., Marchesi, F., Malesci, A., Laghi, L., Allavena, P., 2017. Tumour-associated

macrophages as treatment targets in oncology. Nat. Rev. Clin. Oncol. 14, 399–416. https://doi.org/10.1038/nrclinonc.2016.217

Martinez-Corral, I., Makinen, T., 2013. Regulation of lymphatic vascular morphogenesis: Implications for pathological (tumor) lymphangiogenesis. Exp. Cell Res. 319, 1618–1625. https://doi.org/10.1016/j.yexcr.2013.01.016

McDaniel, J.R., Pero, S.C., Voss, W.N., Shukla, G.S., Sun, Y., Schaetzle, S., Lee, C.H., Horton, A.P., Harlow, S., Gollihar, J., Ellefson, J.W., Krag, C.C., Tanno, Y., Sidiropoulos, N., Georgiou, G., Ippolito, G.C., Krag, D.N., 2018. Identification of tumor-reactive B cells and systemic IgG in breast cancer based on clonal frequency in the sentinel lymph node. Cancer Immunol. Immunother. 67, 729–738. https://doi.org/10.1007/s00262-018-2123-2

McLennan, D.N., Porter, C.J.H., Charman, S.A., 2005. Subcutaneous drug delivery and the role of the lymphatics. Drug Discov. Today Technol. 2, 89–96. https://doi.org/10.1016/j.ddtec.2005.05.006

Mousa, S.A., Bharali, D.J., 2011. Nanotechnology-based detection and targeted therapy in cancer: Nano-bio paradigms and applications. Cancers (Basel). 3, 2888–2903. https://doi.org/10.3390/cancers3032888

Moussion, C., Girard, J.P., 2011. Dendritic cells control lymphocyte entry to lymph nodes through high endothelial venules. Nature 479, 542–546. https://doi.org/10.1038/nature10540

Muraoka, D., Harada, N., Hayashi, T., Tahara, Y., Momose, F., Sawada, S.I., Mukai, S.A., Akiyoshi, K., Shiku, H., 2014. Nanogel-based immunologically stealth vaccine targets macrophages in the medulla of lymph node and induces potent antitumor immunity. ACS Nano 8, 9209–9218. https://doi.org/10.1021/nn502975r

Negi, J.S., Chattopadhyay, P., Sharma, A.K., Ram, V., 2013. Development of solid lipid nanoparticles (SLNs) of lopinavir using hot self nano-emulsification (SNE) technique. Eur. J. Pharm. Sci. 48, 231–239. https://doi.org/10.1016/j.ejps.2012.10.022

Ni, S., Qiu, L., Zhang, G., Zhou, H., Han, Y., 2017. Lymph cancer chemotherapy: Delivery of doxorubicin-gemcitabine prodrug and vincristine by nanostructured lipid carriers. Int. J. Nanomedicine 12, 1565–1576. https://doi.org/10.2147/IJN.S120685

Niu, C., Wang, Z., Lu, G., Krupka, T.M., Sun, Y., You, Y., Song, W., Ran, H., Li, P., Zheng, Y., 2013. Doxorubicin loaded superparamagnetic PLGA-iron oxide multifunctional microbubbles for dual-mode US/MR imaging and therapy of metastasis in lymph nodes.

Biomaterials 34, 2307–2317. https://doi.org/10.1016/j.biomaterials.2012.12.003

Nuhn, L., Vanparijs, N., De Beuckelaer, A., Lybaert, L., Verstraete, G., Deswarte, K., Lienenklaus, S., Shukla, N.M., Salyer, A.C.D., Lambrecht, B.N., Grooten, J., David, S.A., De Koker, S., De Geest, B.G., 2016. PH-degradable imidazoquinoline-ligated nanogels for lymph node-focused immune activation. Proc. Natl. Acad. Sci. U. S. A. 113, 8098–8103. https://doi.org/10.1073/pnas.1600816113

Oladipo, A.O., Oluwafemi, O.S., Songca, S.P., Sukhbaatar, A., Mori, S., Okajima, J., Komiya, A., Maruyama, S., Kodama, T., 2017. A novel treatment for metastatic lymph nodes using lymphatic delivery and photothermal therapy. Sci. Rep. 7, 1–10. https://doi.org/10.1038/srep45459

Oyewumi, M.O., Kumar, A., Cui, Z., 2010. Nano-microparticles as immune adjuvants: Correlating particle sizes and the resultant immune responses. Expert Rev. Vaccines 9, 1095–1107. https://doi.org/10.1586/erv.10.89

Qiao, R., Liu, Changhao, Liu, M., Hu, H., Liu, Chunyan, Hou, Y., Wu, K., Lin, Y., Liang, J., Gao, M., 2015. Ultrasensitive in vivo detection of primary gastric tumor and lymphatic metastasis using upconversion nanoparticles. ACS Nano 9, 2120–2129. https://doi.org/10.1021/nn507433p

Roa, W.H., Azarmi, S., Al-Hallak, M.H.D.K., Finlay, W.H., Magliocco, A.M., Löbenberg, R., 2011. Inhalable nanoparticles, a non-invasive approach to treat lung cancer in a mouse model. J. Control. Release 150, 49–55. https://doi.org/10.1016/j.jconrel.2010.10.035

Rohner, N.A., Thomas, S.N., 2017. Flexible Macromolecule versus Rigid Particle Retention in the Injected Skin and Accumulation in Draining Lymph Nodes Are Differentially Influenced by Hydrodynamic Size. ACS Biomater. Sci. Eng. 3, 153–159. https://doi.org/10.1021/acsbiomaterials.6b00438

Ryan, G.M., Kaminskas, L.M., Porter, C.J.H., 2014. Nano-chemotherapeutics: Maximising lymphatic drug exposure to improve the treatment of lymph-metastatic cancers. J. Control. Release 193, 241–256. https://doi.org/10.1016/j.jconrel.2014.04.051

Sarfraz, M., Roa, W., Bou-Chacra, N., Löbenberg, R., 2016. Inflammation caused by nanosized delivery systems: Is there a benefit? Mol. Pharm. 13, 3270–3278. https://doi.org/10.1021/acs.molpharmaceut.6b00530

Sato, T., Mori, S., Arai, Y., Kodama, T., 2014. The combination of intralymphatic chemotherapy

with ultrasound and nano-/microbubbles is efficient in the treatment of experimental tumors in mouse lymph nodes. Ultrasound Med. Biol. 40, 1237–1249. https://doi.org/10.1016/j.ultrasmedbio.2013.12.012

Sato, T., Mori, S., Sakamoto, M., Arai, Y., Kodama, T., 2015. Direct delivery of a cytotoxic anticancer agent into the metastatic lymph node using nano/microbubbles and ultrasound. PLoS One 10, 1–16. https://doi.org/10.1371/journal.pone.0123619

Sharma, M., Salisbury, R.L., Maurer, E.I., Hussain, S.M., Sulentic, C.E.W., 2013. Gold nanoparticles induce transcriptional activity of NF-κB in a B-lymphocyte cell line. Nanoscale 5, 3747–3756. https://doi.org/10.1039/c3nr30071d

Shi, H., Yan, R., Wu, L., Sun, Y., Liu, S., Zhou, Z., He, J., Ye, D., 2018. Tumor-targeting CuS nanoparticles for multimodal imaging and guided photothermal therapy of lymph node metastasis. Acta Biomater. 72, 256–265. https://doi.org/10.1016/j.actbio.2018.03.035

Shih, V.F.S., Tsui, R., Caldwell, A., Hoffmann, A., 2011. A single NFκB system for both canonical and non-canonical signaling. Cell Res. 21, 86–102. https://doi.org/10.1038/cr.2010.161

Song, X., Chen, Q., Liu, Z., 2015. Recent advances in the development of organic photothermal nano-agents. Nano Res. 8, 340–354. https://doi.org/10.1007/s12274-014-0620-y

Sugiura, T., Matsuki, D., Okajima, J., Komiya, A., Mori, S., Maruyama, S., Kodama, T., 2015. Photothermal therapy of tumors in lymph nodes using gold nanorods and near-infrared laser light with controlled surface cooling. Nano Res. 8, 3842–3852. https://doi.org/10.1007/s12274-015-0884-x

Swartz, M.A., 2001. The physiology of the lymphatic system. Adv. Drug Deliv. Rev. 50, 3–20. https://doi.org/10.1016/S0169-409X(01)00150-8

Thomas, S.N., Schudel, A., 2015. Overcoming transport barriers for interstitial-, lymphatic-, and lymph node-targeted drug delivery. Curr. Opin. Chem. Eng. 7, 65–74. https://doi.org/10.1016/j.coche.2014.11.003

Thomas, S.N., Vokali, E., Lund, A.W., Hubbell, J.A., Swartz, M.A., 2014. Targeting the tumor-draining lymph node with adjuvanted nanoparticles reshapes the anti-tumor immune response. Biomaterials 35, 814–824. https://doi.org/10.1016/j.biomaterials.2013.10.003

Tsujimoto, H., Morimoto, Y., Takahata, R., Nomura, S., Yoshida, K., Hiraki, S., Horiguchi, H., Miyazaki, H., Ono, S., Saito, D., Hara, I., Ozeki, E., Yamamoto, J., Hase, K., 2015. Theranostic Photosensitive Nanoparticles for Lymph Node Metastasis of Gastric Cancer.

Ann. Surg. Oncol. 22, 923–928. https://doi.org/10.1245/s10434-015-4594-0

Wang, Y., Xie, Y., Li, J., Peng, Z.H., Sheinin, Y., Zhou, J., Oupický, D., 2017. Tumor-Penetrating Nanoparticles for Enhanced Anticancer Activity of Combined Photodynamic and Hypoxia-Activated Therapy. ACS Nano 11, 2227–2238. https://doi.org/10.1021/acsnano.6b08731

World Health Organisation, 2018. Cancer [WWW Document]. World Heal. Organ. URL https://www.who.int/news-room/fact-sheets/detail/cancer (accessed 4.3.20).

Xia, A., Zhang, Y., Xu, J., Yin, T., Lu, X.J., 2019. T Cell Dysfunction in Cancer Immunity and Immunotherapy. Front. Immunol. 10, 1719. https://doi.org/10.3389/fimmu.2019.01719

Xie, Y., Bagby, T.R., Cohen, M.S., Forrest, M.L., 2009. Drug delivery to the lymphatic system: importance in future cancer diagnosis and therapies. Expert Opin. Drug Deliv. 6, 785–792.

Yoshimatsu, Y., Miyazaki, H., Watabe, T., 2016. Roles of signaling and transcriptional networks in pathological lymphangiogenesis. Adv. Drug Deliv. Rev. 99, 161–171. https://doi.org/10.1016/j.addr.2016.01.020

Zeng, Q., Li, H., Jiang, H., Yu, J., Wang, Y., Ke, H., Gong, T., Zhang, Z., Sun, X., 2017. Tailoring polymeric hybrid micelles with lymph node targeting ability to improve the potency of cancer vaccines. Biomaterials 122, 105–113. https://doi.org/10.1016/j.biomaterials.2017.01.010

Zhang, W., An, M., Xi, J., Liu, H., 2017. Targeting CpG Adjuvant to Lymph Node via Dextran Conjugate Enhances Antitumor Immunotherapy. Bioconjug. Chem. 28, 1993–2000. https://doi.org/10.1021/acs.bioconjchem.7b00313

Zirakzadeh, A.A., Marits, P., Sherif, A., Winqvist, O., 2013. Multiplex B Cell Characterization in Blood, Lymph Nodes, and Tumors from Patients with Malignancies. J. Immunol. 190, 5847–5855. https://doi.org/10.4049/jimmunol.1203279

CHAPTER 6 – BIPHASIC DISSOLUTION COMBINED WITH MODIFIED CYLINDER METHOD—A NEW PROMISING METHOD FOR DISSOLUTION TEST IN DRUG-LOADED NANOEMULSIONS

6.1. INTRODUTION

Oral drug delivery provides advantages, mainly ease of administration that results in high patient acceptance and compliance. Thus, dissolution testing to evaluate a drug release profile is a key factor to establish the effective bioavailability of orally administered drugs. Accordingly, two factors—solubility and gut permeability—are responsible for bioavailability of the drug (Löbenberg et al., 2020). Flubendazole (FLZ) is an anthelmintic drug that belongs to Class II of the Biopharmaceutics Classification System (BCS) and is indicated as a potential candidate in drug repositioning in treating several types of cancer (Králová et al., 2013) and meningoencephalitis (Nixon et al., 2018). Although FLZ has high permeability, its low water solubility limits dissolution, absorption, and consequently its exposure and distribution in the blood or lymphatic systems. The development of a nanoemulsion (NE) is a promising alternative to overcome these limitations. In our previous work, we developed a FLZ-loaded NE containing 60.0% (w/w) oil (glycerol/glyceryl monolinoleate), which resulted in high solubility of the drug. In vivo testing by oral administration in mice showed that its antifungal efficacy was approximately 30% higher in the brain, when compared to FLZ in suspension (Yukuyama et al., 2021). Another in vivo test carried out with this same FLZ-loaded NE resulted in 100% prevention of a malignant wound in mice with A549 lung cancer (Yukuyama et al., 2022). These results may be attributed to the increased bioavailability of FLZ-loaded NEs.

The in vitro bioavailability of a drug loaded in NE has been evaluated by several authors: Xu et al. (2019) developed NEs containing berberine (BBR), a natural alkaloid of Berberis for diarrhea treatment (Xu et al., 2017), and Khames (2019), developed an NE loaded with eplerenone, a class-II drug for blood pressure and the cardiovascular system (Khames, 2019). Both studies demonstrated an increased bioavailability via an in vitro release experiment, using dialysis bags in 1000- and 500-mL dissolution media, respectively, at 37 °C, at different pH and different time points.

However, due to the limitations of the dialysis bag and compendial methods to discriminate between the differences of the formulations and preparation method (Gao et al., 2013), innovative methods have been proposed to evaluate in vitro drug release of drug carriers. Recently, Silva et al. (2020) carried out a method using low-buffer capacity media combined with an absorptive phase, named the biphasic dissolution method (1-octanol and water phase). This system showed to be more discriminative to drug formulation differences compared to conventional dissolution

test (Silva et al., 2020). Moreover, the biphasic dissolution method attracted attention in recent years not only due to the improved discriminatory power of minor formulation variations: a better in vitro-in vivo correlation (IVIVC) has been observed by the biphasic method compared to compendial ones. The release profile using organic phase (1-octanol) may indicate the in vivo drug absorption mimicking the in vivo environment. Thus, this in vitro assay has the potential to present clinical relevance (Silva et al., 2020; Xu et al., 2019). The same research group also developed a modified cylinder method, which enables differentiating release profiles and the release mechanism of the drug loaded nanoparticles. In contrast to this method, the dialysis bag technique has not shown an adequate discriminating power to identify differences between nanoparticle systems (Gao et al., 2013). The modified cylinder method was able to distinguish between the release from different preparations loaded with poorly water-soluble drugs, enabling to overcome the limitations of the current standardized pharmaceutical tests. Nonetheless, to the best of our knowledge, presently, there is no specific discriminatory dissolution test for drug-loaded NE systems. Hence, there is an evident need to develop a new dissolution method for drug-loaded NEs, and better explore the mechanistic basis behind this phenomenon.

Herein, for the first time, we developed an innovative test by combining biphasic dissolution with modified cylinder (BP + MC) method for drug-loaded NE. We conducted a dissolution study comparing FLZ in three different forms (micronized form as a suspension, loaded in nanoemulsion and solubilized in oil) by using a dialysis bag, modified cylinder method and this new BP + MC method, to evaluate their discriminatory power for different preparations, and to describe mechanistic behavior of FLZ-loaded NEs during this drug release process.

6.2. MATERIAL AND METHODS

6.2.1. *Material*

Flubendazole was purchased from the company Changzhou (Changzhou China); the Maisine CC® (glycerol/glyceryl monolinoleate) was gifted from the company Gattefossé (Sao Paulo, Brazil), the Soluplus® (polyvinyl caprolactam-polyvinyl acetate-polyethylene glycol graft copolymer (PCL-PVAc-PEG)) was gifted from the company BASF (Sao Paulo, Brazil); the glycerin and polysorbate 80 were purchased from Sigma-Aldrich (Sao Paulo, Brazil). The 1-

octanol 99% pure was purchased from Acros Organics (Thermo Fisher Scientific, Fair Lawn, NJ, USA).

6.2.2. *Preparation of samples for dissolution tests*

All samples for dissolution testing were prepared on the same date, immediately before the start of the test, in order to avoid interference due to precipitation or sample separation.

Flubendazole suspension: 0.02% of FLZ and 0.2% of polysorbate 80 (all %w/w) were added to distilled water (amount to complete 100% w/w) and mixed under magnetic stirrer at 500 rpm and 25.0 ± 0.5 °C for 1 minute.

Flubendazole in oil: FLZ was added to Maisine CC® (1 mg FLZ: 3 g Maisine CC®) at 90 ± 5 °C and 500 rpm using a magnetic stirrer for 30 minutes to guarantee complete solubilization of drug. After complete solubilization, this mixture was cooled down to 25.0 ± 0.5 °C.

Flubendazole-loaded nanoemulsion and free-drug nanoemulsion by D-Phase Emulsification process: the nanoemulsions were prepared following description by Yukuyama, MN et al. (2021), as shown in **Figure 6.1** (Yukuyama et al., 2021) . Briefly, in a beaker, 2.0% of Tween 80®, 3.0% of glycerin, 2.0% of distilled water and 3.0% of a mixture of Soluplus® in water (1:2) (all %w/w) was added and homogenized by magnetic bar at 25.0 ± 0.5 °C. Then, the oil phase (0.02% FLZ solubilized in 60.0% of Maisine CC®, both w/w) was added dropwise under stirring at 300 rpm at the same temperature. The remaining water to complete 100.0% (w/w) was added dropwise in the previous mixture, at the same condition. The physico-chemical properties of this nanoemulsion are described in **Table 6.1**.

For all drug dissolution tests, the nanoemulsions were diluted with the dissolution medium at a weight ratio of 2:1 (nanoemulsion: medium), by dropwise addition of the nanoemulsion in the dissolution medium, and kept under stirring for 1 minute before starting the dissolution test.
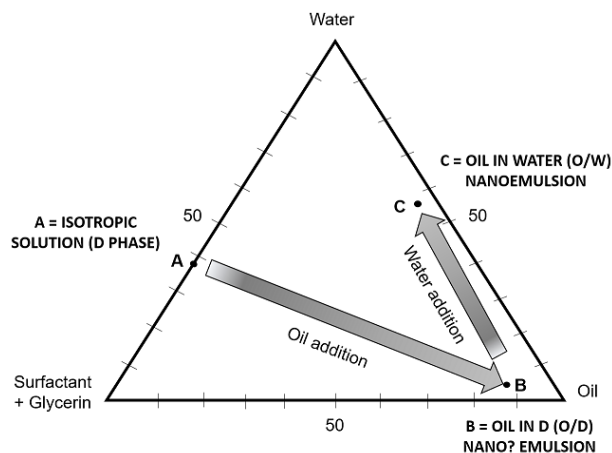
Figure 6.1: Preparation of nanoemulsion by DPE process

Source: Own authorship

6.2.3. *Drug concentration analysis – sample preparation and calibration curve*

The stock standard solution of FLZ was prepared by adding 0.0125 g of FLZ in 25 ml volumetric flask and solubilized in DMSO (Sigma-Aldrich, Steinheim, Germany), to obtain 500 µg FLZ/ml DMSO. Then, the working standard solutions were prepared by serial dilution of stock standard solution using acetonitrile (Thermo Fisher Chemical, Ottawa, Canada).

The concentration of FLZ were analyzed by UV-Spectrophotometer Genesys 10 Bio (Thermo Fisher, Germany) at 225 nm. The linearity curve was obtained at a concentration range with 3 replicates.

The calibration curve of FLZ was generated from six sample concentrations (**Figure 6.S1**). The calibration curve of concentration of FLZ (x, µg/mL) versus absorbance (y) was as follows in **Equation 6.S1** (See **Supplementary Material**).

6.2.4. *Evaluation of flubendazole diffusion behavior*

The drug diffusion behavior according to the formulation variation was established using three different methods: dialysis bag, modified cylinder, and combined method of biphasic and modified cylinder as a new dissolution method.

Considering the reported intestinal fluid volume of 77 mL (77 +/- 15 mL) (Mudie et al., 2014), a volume of 100 mL was used as aqueous phase to increase the physiologic relevance. The same quantity of aqueous media was used at pH 1.2 as a matter of comparison.

The drug concentrations of all samples were measured using Spectrophotometer Genesys 10 Bio (Thermo Fisher, Germany). For all methods, the drug-free NE and the drug-free oil were used to eliminate interference from the excipients. The tests were performed in replicates of three.

6.2.4.1. Drug Diffusion Behavior through the Modified Cylinder

The Modified Cylinder Method was performed following adaptation and optimization of Gao et al (2013) (Gao et al., 2013). Briefly, a sample containing FLZ, or FLZ-free sample were placed into a flat-bottom cylinder with internal diameter of 2 cm and the open bottom covered with dialysis membrane of MWCO: 12 to 14 kD (Thermo Fischer Scientific, Canada) previously soaked in distilled water to remove impurities. The in vitro dissolution study was performed using a dissolution Apparatus (Erweka DT6, Heusenstam, Germany) by fixing the modified cylinder onto a shaft. A sample containing equivalent to 2000 µg of FLZ or an FLZ-free sample were placed into the modified cylinders, and submerged in a conical dissolution vessel containing a 100-ml aliquot of dissolution media kept at 37.0 ± 0.5 °C and constant stirring at 100 rpm. The release media were a simulated gastric fluid (HCl buffer of pH 1.2) and simulated intestinal fluid (phosphate buffer solution of pH 6.8). At designated time intervals (0.25, 0.50, 1, 2, 4, 6 and 24 h), an aliquot of 1mL was collected with a syringe and replaced after each sampling time point with fresh medium.

6.2.4.2. FLZ diffusion behavior through the dialysis membrane bag

Dialysis tubing of MWCO 12 to 14 kD, surface area of 18 cm^2 (Thermo Fisher Scientific, Rancho Domingues, Canada) was previously soaked in distilled water to remove impurities. Sample containing equivalent to 2000 µg of FLZ, or FLZ-free sample, was placed in the dialysis bag and submerged in a beaker containing 100 ml of dissolution medium and kept at constant stirring at 100 rpm, 37.0 ± 0.5 °C. The release mediums were a simulated gastric fluid (HCl buffer of pH 1.2) and simulated intestinal fluid (phosphate buffer solution of pH 6.8). At designated time

intervals (0.25, 0.50, 1, 2, 4, 6 and 24 h), an aliquot of 1mL was collected and replaced with fresh medium after each sampling time point.

6.2.4.3. FLZ diffusion behavior using Biphasic Dissolution with Low-Buffer Capacity Medium combined with Modified Cylinder method

The new Biphasic dissolution combined with the Modified Cylinder method (BP+MC) was carried out by combining the methods of Silva et al. (2020) (Silva et al., 2020) and Gao et al. (2013) (Gao et al., 2013). BP+MC dissolution test was performed in simulated intestinal fluid pH 6.8, with 50 mL of n-octanol on top of each aqueous medium. The aqueous layer mimics the intestinal fluids, and the organic layer mimics the absorption compartment. Sample containing equivalent to 2000 µg of FLZ, or FLZ-free sample, was placed into a flat-bottom cell (internal diameter 2 cm) with the opening covered using a dialysis membrane (MWCO: 12–14 kDa). This modified cylinder was fixed onto the shaft and operated by dissolution Apparatus (Erweka DT6, Heusenstam, Germany) at 100 rpm and at 37.0 ± 0.5 °C. Aliquots from the aqueous phase (1 mL) and the organic phase (1 mL) were collected at specific time points (0.25, 0.50, 1, 2, 4, 6 and 24 h) and replaced with fresh medium or organic phase after each sampling time point.

6.2.5. Statistical Analysis

The drug release data was computed using the Excel Add-In DDSolver, following studies of Gao et al. (Gao et al., 2013) and Silva et al. (Silva et al., 2020). The results of FLZ release profile of the drug loaded in different preparations were collected; all data were expressed as means ± standard deviation.

6.3. RESULTS

6.3.1. Dissolution behavior of drug-loaded and drug-free samples

The discrimination of drug release from different preparations is complicated due to potential presence of different colloidal structures and drug precipitation, which can occur at the same time as absorption (Jankovic et al., 2019). Thus, in the current work, we started with simple steps of in vitro dissolution method development, to progress in the future to more meticulous tests.

The dissolution profile of FLZ in all preparation samples by all methods showed a very low dissolution rate. In some samples, the absorbance value was below the sensitivity of the method (<0.100) (See **Supplementary Material**). The final concentrations of released FLZ are shown in ng/ml.

The absorbance values of the NE and oil samples in all methods were deducted from the values of their respective blanks (drug-free samples), in order to eliminate the interference of their excipients.

6.3.1.1. Dissolution behavior through the modified cylinder method

The absorbances of FLZ-loaded NE and FLZ in suspension, at each time point at 225 nm and released in dissolution media of pH 1.2 and pH 6.8 by modified cylinder method, are shown in **Table 6.S1** to **Table 6.S4**.

The release profiles of FLZ-loaded NE and FLZ in suspension by modified cylinder method at pH 1.2 and pH 6.8 were treated by DDSolver, and the concentrations are shown in **Figure 6.2**.
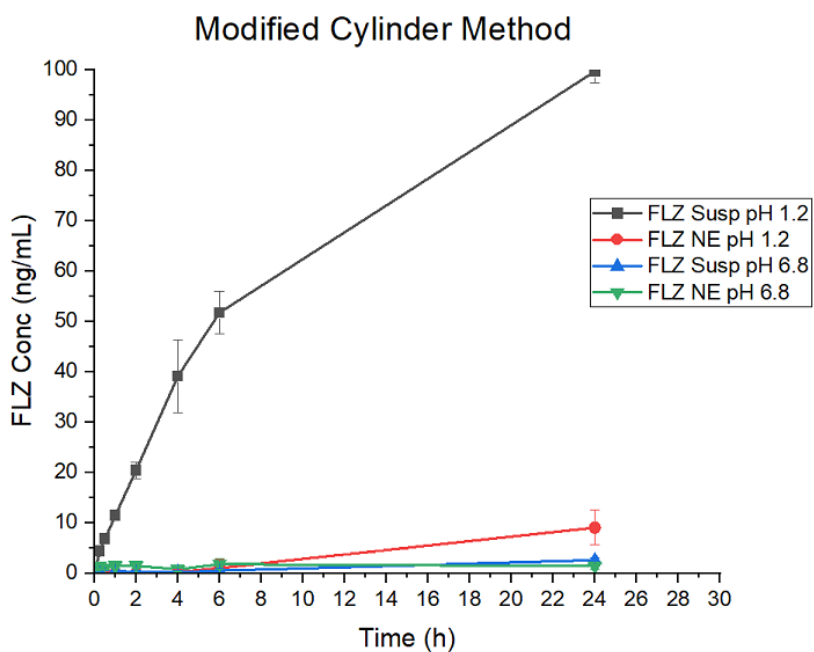
Figure 6.2: Dissolution profile of flubendazole in dissolution media at pH 1.2 and pH 6.8 by modified cylinder method. FLZ NE: flubendazole-loaded nanoemulsion; FLZ Susp: flubendazole in suspension.

6.3.1.2. Dissolution behavior through the dialysis membrane bag method

The absorbances of FLZ-loaded NE, FLZ in oil and FLZ in suspension at each time point at 225 nm and released in dissolution media of pH 1.2 and pH 6.8 by modified cylinder method are shown in **Table 6.S5 to Table 6.S10,** respectively.

The release profiles of FLZ-loaded NE, FLZ-in-oil and FLZ in suspension by dialysis bag method at pH 1.2 and pH 6.8 were treated by DDSolver, and the concentrations are shown in **Figure 6.3**.
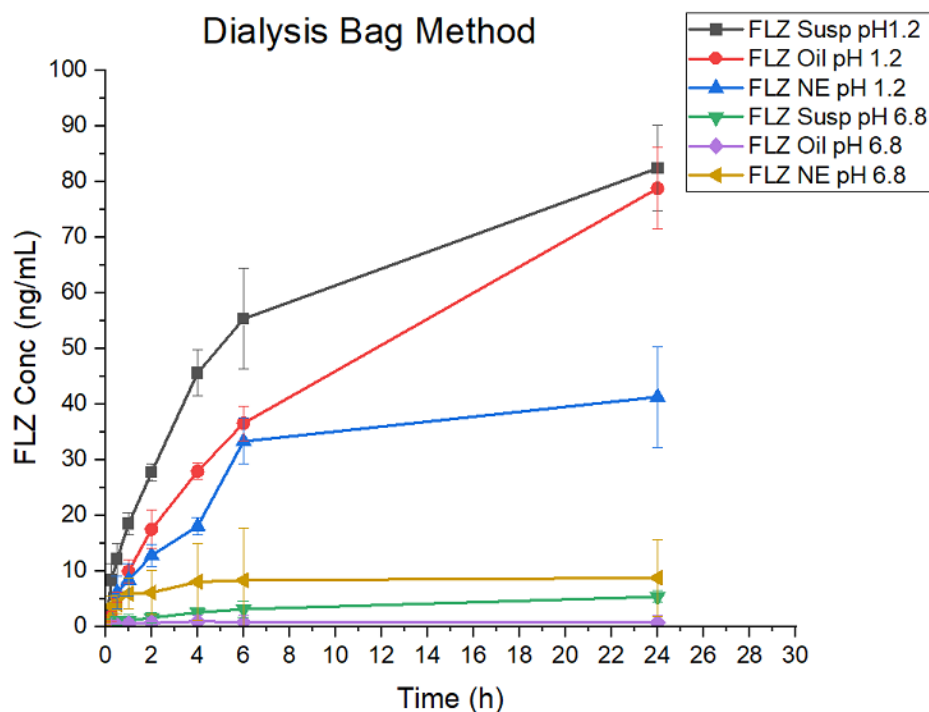
Figure 6.3: Dissolution profile of flubendazole in dissolution media at pH 1.2 and pH 6.8 by dialysis bag method. FLZ NE: flubendazole-loaded nanoemulsion; FLZ Susp: flubendazole in suspension; FLZ Oil: flubendazole solubilized in oil.

6.3.1.3. Biphasic Dissolution with Low Buffer Capacity Medium combined with Modified Cylinder method

6.3.1.3.1. Development of the combined biphasic-modified cylinder

The combined biphasic-modified cylinder method was developed by combining the method of Silva et al. (Silva et al., 2020) and the optimized modified cylinder method adopted in the present work.

To maintain the same conditions in the modified cylinder and dialysis bag methods, we used a dissolution medium of 100 ml at pH 6.8, at a temperature of 37.0 ± 0.5 °C and 100 rpm.

The height of the modified cylinder in the aqueous medium was maintained, and the amount of 50 ml of octanol was introduced on the top of the conical flask. The use of modified cylinder allows for maintaining the same rotation speed for both the aqueous and octanol phase during entire test period and for preserving the liquid state samples, such as nanoemulsions, without direct contact of the release site with the upper phase during the entire dissolution process (**Figure 6.4**).
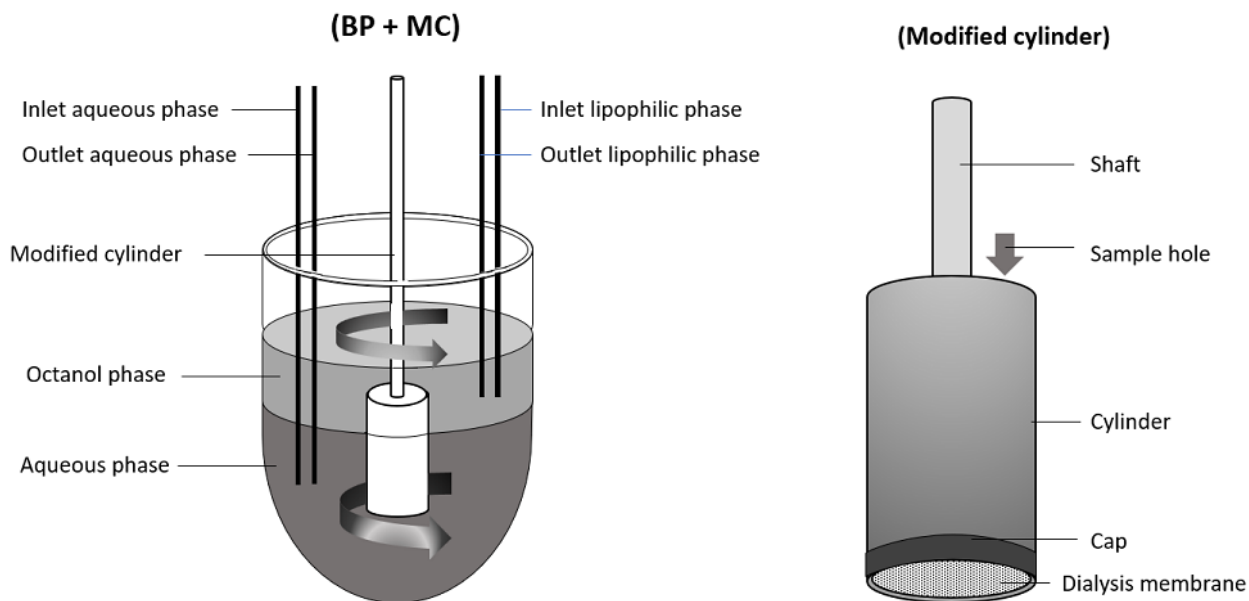
Figure 6.4: Schematic illustration of combined biphasic + modified cylinder dissolution (BP + MC) method setup

Source: Own authorship

174

6.3.1.3.2. Diffusion behavior of samples through the combined biphasic-modified cylinder (BP + MC) at pH 6.8 – aqueous and octanol phase

The absorbances of FLZ-loaded NE, FLZ in oil and FLZ in suspension, at each time point at 225 nm and released in aqueous and octanol dissolution media of pH 6.8 by BP + M.C. method, are shown in **Table 6.S11** to **Table 6.S16**.

The release profiles of FLZ-loaded NE, FLZ-in-oil and FLZ in suspension by BP + MC method in aqueous and octanol phases were treated by DDSolver, and the concentrations are shown in **Figure 6.5**.
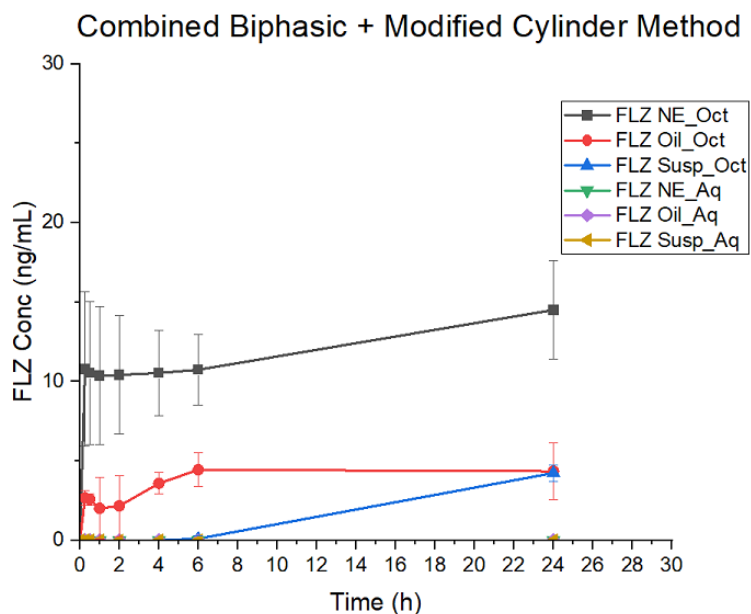
Figure 6.5: Dissolution profile of flubendazole in aqueous and octanol dissolution media at pH 6.8 by combined biphasic + modified cylinder method. FLZ NE: flubendazole-loaded nanoemulsion; FLZ Susp: flubendazole in suspension; FLZ Oil: flubendazole solubilized in oil.

Source: Own authorship

6.3.1.4. Dissolution behavior of components using Biphasic Dissolution with Low-Buffer Capacity Medium combined with Modified Cylinder method – addition of surfactant

Attempting to increase the sensitivity of the method for FLZ in the present work, an assay was performed adding 0.1% of polysorbate 80 in the dissolution medium.

The absorbances of FLZ from FLZ in suspension at each time point at 225 nm, released in dissolution media of pH 6.8 (aqueous and octanol phases) by combined biphasic-modified cylinder method with surfactant, are shown in the **Table 6.S17**.

The release profiles of FLZ in suspension by BP + MC method with surfactant in aqueous and octanol phases were treated by DDSolver, and the concentrations are shown in **Figure 6.6**.
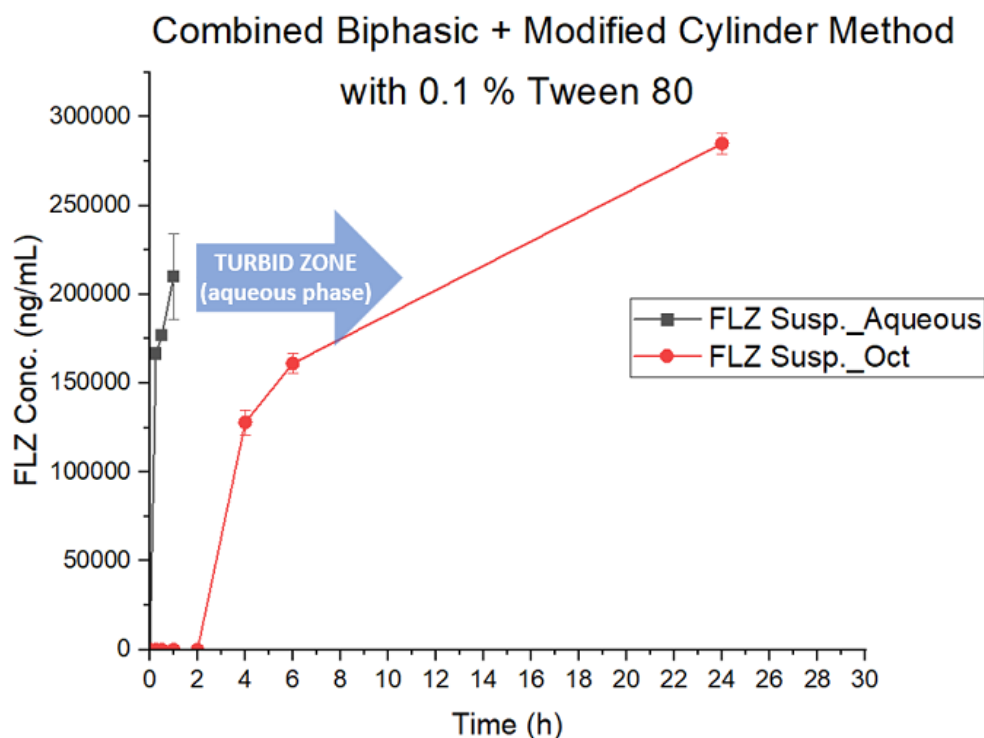
Figure 6.6: Dissolution profile of flubendazole in suspension (FLZ Susp.) in aqueous and octanol dissolution medias at pH 6.8 by combined biphasic + modified cylinder method (BP + MC) with surfactant

Source: Own authorship

6.3.2. Flubendazole release profile

Although at low concentration, both modified cylinder and dialysis bag methods in the dissolution medium at pH 1.2 showed that the dissolution rate of FLZ in suspension was superior when compared to FLZ-loaded NE (**Figure 6.7**). The highest dissolution rate of FLZ in suspension form at pH 1.2 is likely due to ionization of the drug at low pH, due to its pKa of 3.32 (de Assis et al., 2022), in addition to the free state of the drug compared to the drug solubilized in oil and loaded in NE. As shown in **Table 6.1**, studies demonstrate that the solubility of flubendazole can be approximately 32 times greater at pH 1 when compared to the medium at pH 6.75. Other physicochemical properties of FLZ, such as pKa, logP, logD, solubilities are also demonstrated in **Table 6.1** (Becelaere et al., 2022; Surov and Volkova, 2022; Vandenberge et al., 2012; Vialpando et al., 2016; Yukuyama et al., 2022).

Table 6.1: Physico-chemical properties of flubendazole and flubendazole-loaded nanoemulsion

Characteristic	Value	Reference
Flubendazole		
pKa	3.6 and 9.6	(Vialpando et al., 2016)
logP	3	(Vialpando et al., 2016)
LogD (pH = 7)	3.08	(Vandenberge et al., 2012)
Solubility [µg/ml] pH 1	25 ± 1	(Becelaere et al., 2022)
Solubility [µg/ml] pH 6.75	0.79 ± 0.27	(Becelaere et al., 2022)
Solubility S2·10^4 (M) octanol at 25°C	7.98	(Surov and Volkova, 2022)
Solubility (mg) in 15.01 g of Maisine CC$^{®}$	5.06	(Yukuyama et al., 2021)
Flubendazole-loaded Nanoemulsion		
Mean particle size (nm)	35.02 ± 1.54	(Yukuyama et al., 2021)
Polydispersity index	0.452 ± 0.016	(Yukuyama et al., 2021)

In dissolution medium at pH 6.8, both modified cylinder method and the aqueous phase of the combined BP+MC did not show a significant dissolution rate of FLZ in all samples. On the other hand, the dialysis bag method showed the superior dissolution rate for the FLZ-loaded NE. The rank order of dissolution rate by dialysis bag (pH 6.8) was FLZ-loaded NE > FLZ in suspension > FLZ in oil (**Figure 6.8**).
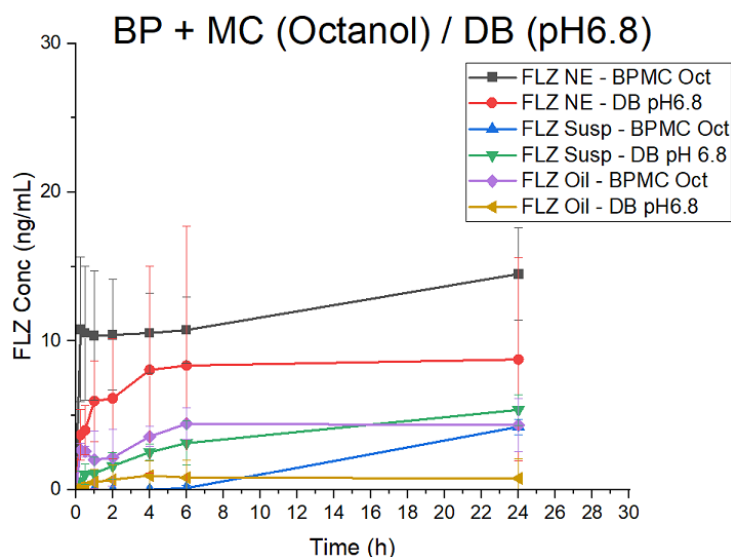
Figure 6.8: Dissolution profile of flubendazole-loaded samples by combined biphasic and modified cylinder method in octanol phase (BPMC Oct) and by dialysis bag method at pH 6.8 (DB pH 6.8). FLZ NE: flubendazole-loaded nanoemulsion; FLZ Susp: flubendazole in suspension; FLZ Oil: flubendazole solubilized in oil.

Source: Own authorship

An interesting result was observed in the octanol phase of the combined BP+MC method. Likewise in the dialysis bag method at pH 6.8, the dissolution rate of the FLZ-loaded NE in the octanol phase showed a higher value when compared to the other samples (**Figure 6.8**). However, this sample demonstrated a sudden increase in the drug release within the first 15 minutes, unlike in the dialysis bag method at pH 6.8 (**Table 6.2**). There was also a difference in the rank order of other samples. Here the order was FLZ-loaded NE > FLZ in oil > FLZ in suspension. However, due to the absorbance value below the quantification limits of the FLZ in suspension samples in

all measurements and in some points of the FLZ in oil (**Supplementary Material**), we are not able to compare the differences of the profile between these two samples.

Table 6.2: Comparison of dissolution profile of flubendazole-loaded nanoemulsion (FLZ NE), flubendazole in suspension (FLZ Susp) and flubendazole solubilized in oil (FLZ Oil) by dialysis bag method (DB) and biphasic and modified cylinder combined method in octanol phase (BP+MC Oct.)

	DB pH6.8			*BP + MC Oct.*		
	FLZ NE	FLZ Susp	FLZ Oil	**FLZ NE**	FLZ Susp	Flz Oil
	Average	Average	Average	**Average**	Average	Average
Time (h)	**(ng/mL)**	(ng/mL)	(ng/mL)	**(ng/mL)**	(ng/mL)	(ng/mL)
0.00	**0.000**	0.000	0.000	**0.000**	0.000	0.000
0.25	**3.711**	0.571	0.148	**10.775**	0.000	2.681
0.50	**4.006**	1.033	0.187	**10.539**	0.000	2.593
1.00	**5.977**	1.101	0.501	**10.363**	0.000	2.023
2.00	**6.154**	1.622	0.679	**10.421**	0.000	2.170
4.00	**8.067**	2.534	0.963	**10.539**	0.000	3.594
6.00	**8.361**	3.152	0.816	**10.745**	0.109	4.447
24.00	**8.773**	5.389	0.766	**14.512**	4.241	4.359

Regarding the comparison between these two methods, even at low values, the BP+MC method values of FLZ-loaded NE samples are approximately twice as high as the values obtained with the dialysis bag method (**Table 6.2**). The biphasic method is known to be more effective in discriminating the dissolution profile of samples with minor variations (Silva et al., 2020). The difference in value between the two methods in the same sample may be an indication of this assumption.

Comparing the results of all methods in the present study, we observed that the rate-limiting step in FLZ release is the solubility of the drug itself. The release rate is far from the maximum, but the dialysis bag method, which has a larger surface area of contact with the aqueous medium,

presented greater release value than the other methods. Thus, increasing the cylinder opening area or using a larger molecular open cut-off of the dialysis membrane would be an interesting alternative to overcome this limitation.

A complementary assay was performed to increase the sensitivity of the method for FLZ, adding surfactant to the dissolution medium of combined BP + MC method. The addition of surfactants or enzyme in the dissolution test for this drug has also been observed in several works (de Araujo et al., 2018; Farhadi et al., 2018). As observed in the dissolution profiles of the FLZ in suspension sample in aqueous phase, there was a sudden increase in drug release in the early stages of the assay (**Figure 6.6**). After 2 hours, the evaluation was impaired by the turbidity of the aqueous medium, which possibly corresponds to the formation of octanol micelles with the surfactant. In the octanol phase, a significant increase in drug release was observed, especially after two hours. Hence, with this increase in the drug dissolution values with the FLZ in suspension sample by this BP + MC combined method with surfactant, the same can be expected with the FLZ-loaded NE and FLZ in oil samples. This may lead to the increased discriminatory power compared to several methods using drug-loaded NEs. However, further studies are needed to evaluate and identify suitable surfactants or enzymes to avoid emulsification of the octanol phase.

6.4. DISCUSSION

6.4.1. *Relevance of Biphasic Dissolution method combined with Modified Cylinder method*

It is often challenging using a conventional dissolution method for a weakly acid or basic drug with poor water solubility (such as FLZ) due to its reduced reproducibility and difficulty to set up proper dissolution test conditions since conventional USP dissolution methods have, mainly, a quality control purpose (Shrivas et al., 2020). However, in the early development of a new modified drug release formulation, a dissolution method with high predictive ability is required to distinguish formulations with little differences (Deng et al., 2017; Heigoldt et al., 2010). Ideally, the method should be relatively simple, inexpensive, and mimic the physiological environment (Heigoldt et al., 2010; Phillips et al., 2012).

Several new methods have been developed in recent decades to attempt optimal biorelevant conditions in in vitro dissolution tests, such as the biphasic method, flow-through cells, three-phase dissolution-partition systems, biphasic dissolution combined with pH-gradient (Pestieau and

Evrard, 2017), two or multicompartment, in vitro dissolution test results with physiologically based pharmacokinetic (PBPK) models (Lu et al., 2017), and Caco-2 cell monolayers (Masada et al., 2021). Despite continuous implementations and improvements, some limitations or disadvantages are still observed in them. For example, the need for a large volume of dissolution media to provide sink conditions can lead to drug concentration below the detection limit (Shrivas et al., 2020), potential of plugging or blockages in the flow-through method apparatus, followed by its lengthy experiment times (Phillips et al., 2012), risk of overestimated prediction of oral bioavailability in pH-adjusted biphasic dissolution tests or similar methods (Fan et al., 2021), and a laborious time-consuming process when using Caco-2 Cells (Masada et al., 2021). These complexities may prevent carrying out quick experiments with multiple variables, or within the timeframe when developing new dosage forms. In addition, most of these methods targeted solid formulations, or else, liquid samples were placed in capsule shells. However, using capsules limits the amount of evaluated sample and may impact the drug release profile.

The combination of the modified cylinder with the biphasic dissolution method in the current work was designed to allow directly placing the liquid preparations (such as NEs) without volume problems, with no additional filling step in capsules, and be enabled to immerse the sample in the aqueous phase by preventing their direct contact with the upper oil phase during the dissolution process. Furthermore, this rotating cylinder in contact with the two phases, aqueous and oil, avoided the need for double agitation paddles or adapted paddles with attached basket. Several studies indicate the importance of the hydrodynamics of the two phases in biphasic method, since it impacts the drug release profile. The stirring speed of 100 rpm in the present work was based on the studies that suggested stirring between 75 rpm to 120 rpm (al Durdunji et al., 2016; Locher et al., 2016; O'Dwyer et al., 2020). In the present work, the speed of 100 rpm did not generate emulsification problems between aqueous and oil dissolution medium in absence of surfactant in aqueous medium.

The biphasic method is well-known for providing better discriminatory power between different drug formulations and to mimic the in vitro-in vivo correlation (IVIVC) (Pestieau and Evrard, 2017). The biphasic method simulates the dynamic interplay of drug dissolution, precipitation, and partition (al Durdunji et al., 2016). The presence of the organic phase enables the partitioning of drug to this organic compartment, which mimics absorption in the intestine. This process is very relevant for weakly basic drugs (eg, FLZ) that is unionized at dissolution

medium at pH 6.8, which simulates the pH of intestinal fluid (Jankovic et al., 2019). The dissolved drug in aqueous medium is the strict condition for its partitioning to the organic medium, and this combined effect (dissolution and partition) prevents the accumulation of drug in the aqueous medium. In this regard, the combination of the dialysis membrane at the open bottom of the modified cylinder helped to trap the undissolved drug particles inside the cylinder and their direct passage to the octanol phase.

But presently, no official dissolution method for lipid-based nanoformulation is provided by official compendia, and only a few studies have shown a possible mechanism of the drug loaded in the NE during the in vitro dissolution process. Thus, based on the current results, we described possible mechanisms in the subsequent items.

6.4.2. *Dissolution mechanism of nanoemulsions – supersaturable state*

A weakly basic drug with poor water solubility usually has high dissolution in an acidic environment such as in the stomach. The result of the current study showed a higher release profile of FLZ in pH 1.2 when compared to pH 6.8, which is in agreement with this assumption. However, after the transit of this drug solution into the small intestine, it may generate a supersaturated state due to the tendency to the drug to precipitate, as it unionizes (Okumu et al., 2008) . This happens since the drug solution from the stomach exceeds its solubility capacity after transit to the intestine. The generation of a supersaturation state in a poorly water-soluble drug is an attractive approach, due to its increased bioavailability. But since a drug solution at a high concentration has low thermodynamic stability, the maintenance of this supersaturable state is essential to improved drug absorption through intestinal mucosa before drug precipitation (Xua and Dai, 2013).

As mentioned, only a free drug is suitable to be absorbed in the intestine. Once a drug is solubilized in oils and these formulations are placed in aqueous medium, they remain as a drug solution in a supersaturated state during a certain period within the gastrointestinal tract (Xua and Dai, 2013). In nanostructures, when the partitioning of the drug into the organic phase increases, the redissolution of nanodroplets into the aqueous phase also increases, while the nanodroplet size decreases simultaneously. This size decrease of nanodroplets is explained by Ostwald ripening phenomenon. In thermodynamically unfavorable small particles, the small molecules (such as drug molecules) inside the nanodroplets detach from them and diffuse into the aqueous phase as free

molecules generating a supersaturated solution. These free molecules move to the surface of larger nanodroplets, and gradually partition into the organic phase, while the small nanodroplets are constantly shrinking (Denninger et al., 2020). Therefore, drugs in nanoaggregates or nanostructures behave as dynamic reservoirs in the aqueous medium to quickly exchange into the free drug before its absorption (Lu et al., 2017), which may explain the higher dissolution rate of FLZ-loaded NE in octanol phase when compared to other forms.

6.4.3. *Influence of nanoemulsion components in dissolution profile*

Unlike a drug in suspension or solubilized in oil, a NE is composed of several components that may cause interactions and affect the release profile of the drug.

Polysorbate 80 increases dissolution rate in biphasic method, but once exceeding its critical micelle concentration (CMC), the partitioning rate is decreased (Pestieau and Evrard, 2017). The presence of surfactant increases the solubilization of drug, increasing the free drug to partition. However, the amount of surfactant in aqueous medium above its CMC negatively affects the partitioning due to the incorporation of drug into its micelles (Thiry et al., 2016). It is reported that there are two categories of drug solubilized formulations: the supersaturable formulation and true solubilized formulation. The former is generally composed of lipid or cosolvent formulation, such as triglycerides and mixed glycerides. It generates a supersaturable state as a consequence of insufficient solubilization capacity when the formulation is exposed to an aqueous environment. The latter is generally composed of a surfactant with enough solubilization capacity in an aqueous environment. Then, it generates a micellar surfactant where the drug is completely dissolved into the micelle, not enabling free-drug formation to provide supersaturable state. As a consequence, the true solubilized formulation has lower bioavailability when compared to the supersaturable formulation (Lu et al., 2017). Generally, NEs employ lower surfactant concentration compared to self-emulsifying systems, which may ensure this supersaturable state after passage to the intestine.

Concerning Soluplus®, studies demonstrated slow release of a drug in a formulation containing a considerable amount of Soluplus®. This may be attributed to the gel effect provided by this component, which stabilizes micelles, reduces molecular mobility, and prevents drug precipitation during absorption process. It was also mentioned that nanoparticles lower than 100 nm and containing a PEG-derived component (such as Soluplus®) were found in intestinal mucosa and gut

associated lymphoid tissues (Thiry et al., 2017). The particle size of the FLZ-loaded NE of the present work is approximately 30 nm.

In attempt to further evaluate the influence of the excipients and colloidal structure in the drug dissolution profile, we compared the FLZ-free samples. The oil (Maisine CC®) used in our samples has an absorbance that interferes with the FLZ evaluation (data not shown), and both FLZ-free NE and FLZ-free oil employed the same concentration of this oil in the tests. The dialysis bag method at pH 1.2 showed that the minimum and maximum absorption value of FLZ-free NE sample was 0.041 and 0.210, respectively, while FLZ-free oil was 0.031 and 0.196, respectively at 225 nm. In the same method at pH 6.8, the minimum and maximum absorption value of the FLZ-free NE sample was 0.033 and 0.187, respectively, while FLZ-free oil was 0.024 and 0.174, respectively. According to the results, the dissolution profile in both FLZ-free NE and FLZ-free oil showed an increased release rate over time, however with a higher value in the NE (**Table 6.S18**). The synergistic effect among polysorbate 80, Soluplus® and the nanostructure, which possibly favors the supersaturable state, may explain the greater release of FLZ in NEs when compared to FLZ in oil. However, knowing how the solubilized FLZ behaves or interacts with this oil that was released into the aqueous medium is a subsequent step for future analysis.

6.5. SUBSEQUENT STEPS AND FUTURE PERSPECTIVES

The need for a simple, quick, and effective discriminatory method for dissolution profile in the early stage of the drug preparation development remains of interest, considering that presently there is no specific dissolution method for drug-loaded NEs. The results of the current work opened some perspectives for future development in this field, by using this BP + MC method, which are outlined as follows:

First, according to Jankovica et al. (2019), avoiding the high drug release in the stomach compartment and providing sustained drug release in the intestinal compartment is advantageous to maximize absorptive drug uptake (Jankovic et al., 2019). Here, we observed that the FLZ release rate at pH 1.2 (which simulates stomach conditions) was greater for FLZ in suspension than other samples, and the drug release rate in octanol phase (that simulates the intestinal compartment) was greater for FLZ-loaded NE than others, with potential sustainable release. This rationale correlates well with the treating results obtained in previous works in which the FLZ-loaded NE showed

greater efficacy in meningoencephalitis (Yukuyama et al., 2021) and cancer malignant wound treatment (Yukuyama et al., 2022), when compared to FLZ in a suspension at the same drug concentration. Although IVIVC was not carried out, this comparison demonstrated the potential predictability of the present work to discriminate FLZ preparations under oral administration.

Second, for future testing, there are other alternatives of test conditions to increase discriminative power: selection of a suitable surfactant or enzyme and its concentration in the aqueous medium to increase drug dissolution rate while preventing the emulsification problem; variation of stirrer speed to improve drug release rate; optimization of pH gradient; enlarging surface area of dialysis membrane for greater contact of drug and medium; or even changing the oil phase for greater drug partition (eg, nonanol, decanol).

Third, it would be valuable to deepen the mechanistic understanding of interactions among other potential excipients in the drug-loaded NEs upon release, especially interactions involved in partitioning of the drug from the aqueous into octanol medium. This research will potentially improve correlations of this in vitro method results with treating test results.

In sum, we can assume that this new BP + MC method may be an interesting tool to facilitate discrimination of candidate formulations and optimize selection of excipients in drug-loaded formulations of several technologies.

6.6. CONCLUSIONS

A drug-loaded NE is an interesting drug delivery system to improve drug solubility. However, there has been no specific dissolution method to discriminate the drug release profile of NEs with other preparations. Herein, for the first time, we developed a new discriminating method to evaluate the dissolution profile of drug-loaded NEs combining the biphasic method with the modified cylinder method. This combination enabled overcoming some limitations of conventional methods when evaluating the dissolution profile of NEs.

The results demonstrated a low dissolution rate of FLZ in all methods and samples, which requires future improvements. But a tendency of a higher release for FLZ in suspension at medium pH 1.2, and higher release for FLZ-loaded NE in the octanol phase were observed, when compared to the other formulations. The addition of surfactant into the aqueous medium of BP + MC method significantly increased the drug release rate in FLZ for the suspension sample, which shows that

FLZ can be solubilized. The greater absorption rate of FLZ-loaded NEs in the octanol phase is also in agreement with the previous results observed in vivo. The study provided new insights into how dissolution methods for a poorly water-solubility drug can be designed.

Further studies with other drugs still need to be conducted to deepen the understanding of the results and establish a relevant in vitro dissolution method for drug-loaded NEs. Altogether, this will pave the way for using the BP + MC method as a functionally robust method to improve the discriminatory capacity of dissolution methods when comparing drug-loaded NEs with other conventional preparations.

6.7. REFERENCES

al Durdunji, A., Alkhatib, H.S., Al-Ghazawi, M., 2016. Development of a biphasic dissolution test for Deferasirox dispersible tablets and its application in establishing an in vitro-in vivo correlation. European Journal of Pharmaceutics and Biopharmaceutics 102, 9–18. https://doi.org/10.1016/j.ejpb.2016.02.006

Becelaere, J., van den Broeck, E., Schoolaert, E., Vanhoorne, V., van Guyse, J.F.R., Vergaelen, M., Borgmans, S., Creemers, K., van Speybroeck, V., Vervaet, C., Hoogenboom, R., de Clerck, K., 2022. Stable amorphous solid dispersion of flubendazole with high loading via electrospinning. Journal of Controlled Release 351, 123–136. https://doi.org/10.1016/j.jconrel.2022.09.028

de Araujo, G.L.B., Ferreira, F.F., Bernardes, C.E.S., Sato, J.A.P., Gil, O.M., de Faria, D.L.A., Loebenberg, R., Byrn, S.R., Ghisleni, D.D.M., Bou-Chacra, N.A., Pinto, T.J.A., Antonio, S.G., Ferraz, H.G., Zemlyanov, D., Gonçalves, D.S., Minas Da Piedade, M.E., 2018. A New Thermodynamically Favored Flubendazole/Maleic Acid Binary Crystal Form: Structure, Energetics, and in Silico PBPK Model-Based Investigation. Cryst Growth Des 18, 2377–2386. https://doi.org/10.1021/acs.cgd.7b01807

de Assis, J.M.C., Barbosa, E.J., Bezzon, V.D.N., Lourenço, F.R., Carvalho, F.M.S., Matos, J.R., Araci Bou-Chacra, N., Benmore, C.J., Byrn, S.R., Costa, F.N., de Araujo, G.L.B., 2022. Hot-melt extrudability of amorphous solid dispersions of flubendazole-copovidone: An exploratory study of the effect of drug loading and the balance of adjuvants on extrudability and dissolution. Int J Pharm 614. https://doi.org/10.1016/j.ijpharm.2022.121456

Deng, J., Staufenbiel, S., Hao, S., Wang, B., Dashevskiy, A., Bodmeier, R., 2017. Development of a discriminative biphasic in vitro dissolution test and correlation with in vivo pharmacokinetic studies for differently formulated racecadotril granules. Journal of Controlled Release 255, 202–209. https://doi.org/10.1016/j.jconrel.2017.04.034

Denninger, A., Westedt, U., Rosenberg, J., Wagner, K.G., 2020. A rational design of a biphasic dissolution setup—modelling of biorelevant kinetics for a ritonavir hot-melt extruded amorphous solid dispersion. Pharmaceutics 12. https://doi.org/10.3390/pharmaceutics12030237

Fan, X., Shi, S., He, J., Deng, J., Ji, J., 2021. Development of in vivo predictive ph-gradient biphasic dissolution test for weakly basic drugs: Optimization by orthogonal design. Dissolut Technol 28, 24–29. https://doi.org/10.14227/DT280321P24

Farhadi, M., Haniloo, A., Rostamizadeh, K., Faghihzadeh, S., 2018. Efficiency of flubendazole-loaded mPEG-PCL nanoparticles: A promising formulation against the protoscoleces and cysts of Echinococcus granulosus. Acta Trop 187, 190–200. https://doi.org/10.1016/j.actatropica.2018.08.010

Gao, Y., Zuo, J., Bou-Chacra, N., Pinto, T.D.J.A., Clas, S.D., Walker, R.B., Löbenberg, R., 2013. In vitro release kinetics of antituberculosis drugs from nanoparticles assessed using a modified dissolution apparatus. Biomed Res Int 2013. https://doi.org/10.1155/2013/136590

Heigoldt, U., Sommer, F., Daniels, R., Wagner, K.G., 2010. Predicting in vivo absorption behavior of oral modified release dosage forms containing pH-dependent poorly soluble drugs using a novel pH-adjusted biphasic in vitro dissolution test. European Journal of Pharmaceutics and Biopharmaceutics 76, 105–111. https://doi.org/10.1016/j.ejpb.2010.05.006

Jankovic, S., O'Dwyer, P.J., Box, K.J., Imanidis, G., Reppas, C., Kuentz, M., 2019. Biphasic drug release testing coupled with diffusing wave spectroscopy for mechanistic understanding of solid dispersion performance. European Journal of Pharmaceutical Sciences 137. https://doi.org/10.1016/j.ejps.2019.105001

Khames, A., 2019. Formulation and characterization of eplerenone nanoemulsion liquisolids, an oral delivery system with higher release rate and improved bioavailability. Pharmaceutics 11. https://doi.org/10.3390/pharmaceutics11010040

Králová, V., Hanušová, V., Staňková, P., Knoppová, K., Čáňová, K., Skálová, L., 2013. Antiproliferative effect of benzimidazole anthelmintics albendazole, ricobendazole, and

flubendazole in intestinal cancer cell lines. Anticancer Drugs 24, 911–919. https://doi.org/10.1097/CAD.0b013e3283648c69

Löbenberg, R., Reynolds, K., Tirunellai, K., Fredro-Kumbaradzi, E., Zhang, R., Raines, K., Mathivanan, M., Davit, B.M., Laloo, A., Murti, S., Veerasingham, S., Endrenyi, L., Jamali, F., 2020. Biowaiver for Immediate and Modified Release Dosage forms Scientific summary of the CSPS workshop, J Pharm Pharm Sci (www.cspsCanada.org).

Locher, K., Borghardt, J.M., Frank, K.J., Kloft, C., Wagner, K.G., 2016. Evolution of a mini-scale biphasic dissolution model: Impact of model parameters on partitioning of dissolved API and modelling of in vivo-relevant kinetics. European Journal of Pharmaceutics and Biopharmaceutics 105, 166–175. https://doi.org/10.1016/j.ejpb.2016.06.008

Lu, E., Li, S., Wang, Z., 2017. Biorelevant test for supersaturable formulation. Asian J Pharm Sci. https://doi.org/10.1016/j.ajps.2016.10.002

Masada, T., Takagi, T., Minami, K., Kataoka, M., Takeyama, S., Fujii, Y., Takahashi, M., Yamashita, S., 2021. New biphasic system in side-by-side chambers for testing drug dissolution and permeation in vitro (BiDP system). J Drug Deliv Sci Technol 65. https://doi.org/10.1016/j.jddst.2021.102747

Mudie, D.M., Murray, K., Hoad, C.L., Pritchard, S.E., Garnett, M.C., Amidon, G.L., Gowland, P.A., Spiller, R.C., Amidon, G.E., Marciani, L., 2014. Quantification of gastrointestinal liquid volumes and distribution following a 240 mL dose of water in the fasted state. Mol Pharm 11, 3039–3047. https://doi.org/10.1021/mp500210c

Nixon, G.L., McEntee, L., Johnson, A., Farrington, N., Whalley, S., Livermore, J., Natal, C., Washbourn, G., Bibby, J., Berry, N., Lestner, J., Truong, M., Owen, A., Lalloo, D., Charles, I., Hope, W., 2018. Repurposing and reformulation of the antiparasitic agent flubendazole for treatment of cryptococcal meningoencephalitis, a neglected fungal disease. Antimicrob Agents Chemother 62. https://doi.org/10.1128/AAC.01909-17

O'Dwyer, P.J., Box, K.J., Koehl, N.J., Bennett-Lenane, H., Reppas, C., Holm, R., Kuentz, M., Griffin, B.T., 2020. Novel Biphasic Lipolysis Method to Predict in Vivo Performance of Lipid-Based Formulations. Mol Pharm 17, 3342–3352. https://doi.org/10.1021/acs.molpharmaceut.0c00427

Okumu, A., DiMaso, M., Löbenberg, R., 2008. Dynamic dissolution testing to establish in vitro/in vivo correlations for montelukast sodium, a poorly soluble drug, in: Pharmaceutical Research. pp. 2778–2785. https://doi.org/10.1007/s11095-008-9642-z

Pestieau, A., Evrard, B., 2017. In vitro biphasic dissolution tests and their suitability for establishing in vitro-in vivo correlations: A historical review. European Journal of Pharmaceutical Sciences. https://doi.org/10.1016/j.ejps.2017.03.019

Phillips, D.J., Pygall, S.R., Cooper, V.B., Mann, J.C., 2012. Overcoming sink limitations in dissolution testing: A review of traditional methods and the potential utility of biphasic systems. Journal of Pharmacy and Pharmacology. https://doi.org/10.1111/j.2042-7158.2012.01523.x

Shrivas, Meera, Khunt, D., Shrivas, Meenakshee, Choudhari, M., Rathod, R., Misra, M., 2020. Advances in In Vivo Predictive Dissolution Testing of Solid Oral Formulations: How Closer to In Vivo Performance? J Pharm Innov. https://doi.org/10.1007/s12247-019-09392-6

Silva, D.A., Al-Gousous, J., Davies, N.M., Chacra, N.B., Webster, G.K., Lipka, E., Amidon, G.L., Löbenberg, R., 2020. Biphasic dissolution as an exploratory method during early drug product development. Pharmaceutics 12. https://doi.org/10.3390/pharmaceutics12050420

Surov, A.O., Volkova, T. v., 2022. Solubility/distribution thermodynamics and permeability of two anthelmintics in biologically relevant solvents. J Mol Liq 354. https://doi.org/10.1016/j.molliq.2022.118835

Thiry, J., Broze, G., Pestieau, A., Tatton, A.S., Baumans, F., Damblon, C., Krier, F., Evrard, B., 2016. Investigation of a suitable in vitro dissolution test for itraconazole-based solid dispersions. European Journal of Pharmaceutical Sciences 85, 94–105. https://doi.org/10.1016/j.ejps.2016.02.002

Thiry, J., Kok, M.G.M., Collard, L., Frère, A., Krier, F., Fillet, M., Evrard, B., 2017. Bioavailability enhancement of itraconazole-based solid dispersions produced by hot melt extrusion in the framework of the Three Rs rule. European Journal of Pharmaceutical Sciences 99, 1–8. https://doi.org/10.1016/j.ejps.2016.12.001

Vandenberge, V., Delezie, E., Delahaut, P., Pierret, G., de Backer, P., Daeseleire, E., Croubels, S., 2012. Transfer of flubendazole and tylosin at cross contamination levels in the feed to egg matrices and distribution between egg yolk and egg white. Poult Sci 91, 1248–1255. https://doi.org/10.3382/ps.2011-02071

Vialpando, M., Smulders, S., Bone, S., Jager, C., Vodak, D., van Speybroeck, M., Verheyen, L., Backx, K., Boeykens, P., Brewster, M.E., Ceulemans, J., Novoa de Armas, H., van Geel, K., Kesselaers, E., Hillewaert, V., Lachau-Durand, S., Meurs, G., Psathas, P., van Hove, B., Verreck, G., Voets, M., Weuts, I., Mackie, C., 2016. Evaluation of Three Amorphous Drug Delivery Technologies to

Improve the Oral Absorption of Flubendazole. J Pharm Sci 105, 2782–2793. https://doi.org/10.1016/j.xphs.2016.03.003

Xu, H., Vela, S., Shi, Y., Marroum, P., Gao, P., 2017. In Vitro Characterization of Ritonavir Drug Products and Correlation to Human in Vivo Performance. Mol Pharm 14, 3801–3814. https://doi.org/10.1021/acs.molpharmaceut.7b00552

Xu, H.Y., Liu, C.S., Huang, C.L., Chen, L., Zheng, Y.R., Huang, S.H., Long, X.Y., 2019. Nanoemulsion improves hypoglycemic efficacy of berberine by overcoming its gastrointestinal challenge. Colloids Surf B Biointerfaces 181, 927–934. https://doi.org/10.1016/j.colsurfb.2019.06.006

Xua, S., Dai, W.G., 2013. Drug precipitation inhibitors in supersaturable formulations. Int J Pharm. https://doi.org/10.1016/j.ijpharm.2013.05.013

Yukuyama, M.N., Ferreira Guimaraes, L.M., Segovia, R.S., Lameu, C., de Araujo, G.L.B., Löbenberg, R., de Souza, A., Bazán Henostroza, M.A., Folchini, B.R., Peroni, C.M., Saito Miyagi, M.Y., Oliveira, I.F., Rinaldi Alvarenga, J.F., Fiamoncini, J., Bou-Chacra, N.A., 2022. Malignant wound – The influence of oil components in flubendazole-loaded nanoemulsions in A549 lung cancer xenograft-bearing mice. J Drug Deliv Sci Technol 103963. https://doi.org/10.1016/j.jddst.2022.103963

Yukuyama, M.N., Ishida, K., de Araujo, G.L.B., Spadari, C. de C., de Souza, A., Löbenberg, R., Henostroza, M.A.B., Folchini, B.R., Peroni, C.M., Peters, M.C.C., de Oliveira, I.F., Miyagi, M.Y.S., Bou-Chacra, N.A., 2021. Rational design of oral flubendazole-loaded nanoemulsion for brain delivery in cryptococcosis. Colloids Surf A Physicochem Eng Asp 630. https://doi.org/10.1016/j.colsurfa.2021.127631

6.8. SUPPLEMENTARY MATERIAL

Equation 6.S1: correlation coefficient = 0.9993.

$y = 011.326\ x + 0.0163$
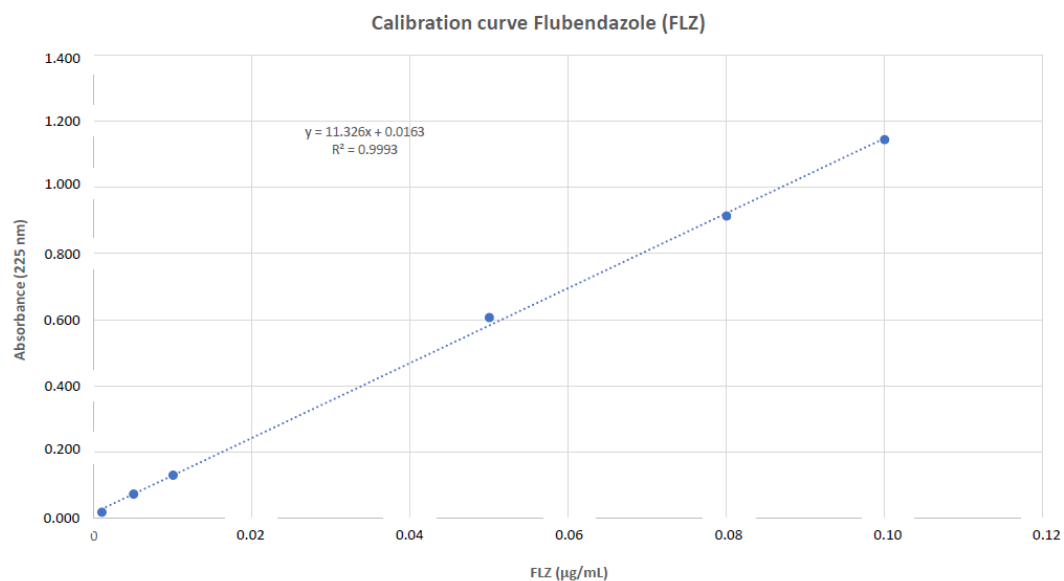
Figure 6.S1. Calibration curve of flubendazole by UV-spectrophotometer at 225 nm

Source: Own authorship

Table 6.S1. Absorbance of flubendazole-loaded nanoemulsion in dissolution media (pH 1.2) by modified cylinder method

	FLZ NE					FLZ NE – Drug free NE		
Time (h)	Abs (1)	Abs (2)	Abs (3)	AVE	STDEV	Abs (1a)	Abs (2a)	Abs (3a)
0.25	0.016	0.014	0.017	0.016	0.002	0.001	0.000	0,002
0.50	0.017	0.020	0.033	0.023	0.009	0.003	0.006	0,019
1.00	0.040	0.033	0.028	0.034	0.006	0.011	0.004	0,000
2.00	0.039	0.049	0.036	0.041	0.007	0.000	0.009	0,000
4.00	0.067	0.077	0.053	0.066	0.012	0.016	0.026	0,002
6.00	0.100	0.067	0.070	0.079	0.018	0.049	0.016	0,019
24.00	0.237	0.171	0.168	0.192	0.039	0.164	0.098	0,095

FLZ NE = flubendazole loaded nanoemulsion; Drug Free NE = flubendazole free nanoemulsion; Abs = absorbance; AVE = average; STDEV = standard deviation

Table 6.S2. Absorbance of flubendazole in suspension in dissolution media (pH 1.2) by modified cylinder method

	Flubendazole in Suspension				
Time (h)	Abs (1)	Abs (2)	Abs (3)	AVE	STDEV
0.25	0.064	0.068	0.066	0.066	0.002
0.50	0.089	0.095	0.094	0.093	0.003
1.00	0.148	0.151	0.138	0.146	0.007
2.00	0.268	0.242	0.233	0.248	0.018
4.00	0.553	0.422	0.403	0.459	0.082
6.00	0.657	0.583	0.566	0.602	0.048
24.00	1.125	1.136	1.174	1.145	0.026

Abs = absorbance; AVE = average; STDEV = standard deviation

Table 6.S3. Absorbance of flubendazole-loaded nanoemulsion in dissolution media (pH 6.8) by modified cylinder method

	FLZ NE					FLZ NE – Drug free NE		
Time (h)	Abs (1)	Abs (2)	Abs (3)	AVE	STDEV	Abs (1a)	Abs (2a)	Abs (3a)
0.25	0.020	0.028	0.018	0.022	0.005	0.015	0.023	0.013
0.50	0.022	0.021	0.015	0.019	0.004	0.015	0.014	0.008
1.00	0.029	0.023	0.019	0.024	0.005	0.022	0.016	0.012
2.00	0.030	0.029	0.018	0.026	0.007	0.021	0.020	0.009
4.00	0.029	0.024	0.021	0.025	0.004	0.014	0.009	0.006
6.00	0.045	0.025	0.027	0.032	0.011	0.033	0.013	0.015
24.00	0.045	0.046	0.059	0.050	0.008	0.011	0.012	0.025

FLZ NE = flubendazole loaded nanoemulsion; Drug Free NE = flubendazole free nanoemulsion; Abs = absorbance; AVE = average; STDEV = standard deviation

Table 6.S4. Absorbance of flubendazole in suspension in dissolution media (pH 6.8) by modified cylinder method

	Flubendazole in Suspension				
Time (h)	Abs (1)	Abs (2)	Abs (3)	AVE	STDEV
0.25	0.020	0.009	0.008	0.012	0.007
0.50	0.022	0.017	0.009	0.016	0.007
1.00	0.023	0.014	0.028	0.022	0.007
2.00	0.024	0.015	0.013	0017	0.006
4.00	0.024	0.016	0.016	0.019	0.005
6.00	0.025	0.025	0.017	0.022	0.005
24.00	0.050	0.046	0.040	0.045	0.005

Abs = absorbance; AVE = average; STDEV = standard deviation

Table 6.S5. Absorbance of flubendazole-loaded nanoemulsion in dissolution media (pH 6.8) by dialysis bag method

	FLZ NE					FLZ NE – Drug free NE		
Time (h)	Abs (1)	Abs (2)	Abs (3)	AVE	STDEV	Abs (1a)	Abs (2a)	Abs (3a)
0.25	0.119	0.139	0.075	0.111	0033	0.078	0.098	0.034
0.50	0.165	0.179	0.116	0.153	0.033	0.107	0.121	0.058
1.00	0.230	0.246	0.201	0.226	0.023	0.149	0.165	0.120
2.00	0.351	0.320	0.320	0.330	0.018	0.225	0.194	0.194
4.00	0.566	0.479	0.553	0.533	0.047	0.411	0.324	0.398
6.00	0.633	0.546	0.750	0.643	0.102	0.458	0.371	0.575
24.00	1.002	0.849	0.998	0.950	0.087	0.792	0.639	0.788

FLZ NE = flubendazole loaded nanoemulsion; Drug Free NE = flubendazole free nanoemulsion; Abs = absorbance; AVE = average; STDEV = standard deviation

Table 6.S6. Absorbance of flubendazole-in-oil in dissolution media (pH 1.2) by dialysis bag method

	FLZ Oil					FLZ Oil – Drug free Oil		
Time (h)	Abs (1)	Abs (2)	Abs (3)	AVE	STDEV	Abs (1a)	Abs (2a)	Abs (3a)
0.25	0.067	0.059	0.079	0.068	0.010	0.036	0.028	0.048
0.50	0.115	0.106	0.127	0.116	0.011	0.075	0.066	0.087
1.00	0.203	0.158	0.181	0.181	0.023	0.151	0.106	0.129
2.00	0.292	0.243	0.320	0.285	0.039	0.221	0.172	0.249
4.00	0.430	0.412	0.445	0.429	0.017	0.334	0.316	0.349
6.00	0.511	0.564	0.577	0.551	0.035	0.391	0.444	0.457
24.00	1.083	1.035	1.196	1.105	0.083	0.887	0.839	1.000

FLZ Oil = flubendazole in oil; Abs = absorbance; AVE = average; STDEV = standard deviation

Table 6.S7. Absorbance of flubendazole in suspension in dissolution media (pH 1.2) by dialysis bag method

	FLZ in suspension				
Time (h)	Abs (1)	Abs (2)	Abs (3)	AVE	STDEV
0.25	0.316	0.229	0.236	0.260	0.048
0.50	0.586	0.466	0.493	0.515	0.063
1.00	0.944	0.808	0.861	0.871	0.069
2.00	1.194	1.242	1.270	1.235	0.038
4.00	1.504	1.438	1.416	1.453	0.046
6.00	1.448	1.458	1.402	1.436	0.030
24.00	1.510	1.444	1.428	1.461	0.043

FLZ = flubendazole; Abs = absorbance; AVE = average; STDEV = standard deviation

Table 6.S8. Absorbance of flubendazole-loaded nanoemulsion in dissolution media (pH 6.8) by dialysis bag method

	FLZ NE					FLZ NE – Drug free NE		
Time (h)	Abs (1)	Abs (2)	Abs (3)	AVE	STDEV	Abs (1a)	Abs (2a)	Abs (3a)
0.25	0.082	0.079	0.114	0.092	0.019	0.049	0.046	0.081

0.50	0.115	0.078	0.103	0.099	0.019	0.078	0.041	0.066
1.00	0.167	0.108	0.123	0.133	0.031	0.118	0.059	0.074
2.00	0.223	0.145	0.143	0.170	0.046	0.139	0.061	0.059
4.00	0.299	0.187	0.147	0.211	0.079	0.196	0.084	0.044
6.00	0.364	0.195	0.168	0.242	0.106	0.233	0.064	0.037
24.00	0.389	0.280	0.239	0.303	0.078	0.202	0.093	0.052

FLZ NE = flubendazole loaded nanoemulsion; Drug Free NE = flubendazole free nanoemulsion; Abs = absorbance; AVE = average; STDEV = standard deviation

Table 6.S9. Absorbance of flubendazole-in-oil in dissolution media (pH 6.8) by dialysis bag method

	FLZ Oil					FLZ Oil – Drug free Oil		
Time (h)	Abs (1)	Abs (2)	Abs (3)	AVE	STDEV	Abs (1a)	Abs (2a)	Abs (3a)
0.25	0.045	0.027	0.025	0.032	0.011	0.021	0.003	0.001
0.50	0.054	0.037	0.036	0.042	0.010	0.023	0.006	0.005
1.00	0.078	0.052	0.058	0.063	0.014	0.033	0.007	0.013
2.00	0.103	0.069	0.084	0.085	0.017	0.037	0.003	0.018
4.00	0.128	0.091	0.116	0.112	0.019	0.039	0.002	0.027
6.00	0.153	0.108	0.132	0.131	0.023	0.041	-0.004	0.020
24.00	0.216	0.183	0.177	0.192	0.021	0.042	0,009	0.003

FLZ Oil = flubendazole in oil; Abs = absorbance; AVE = average; STDEV = standard deviation

Table 6.S10. Absorbance of flubendazole in suspension in dissolution media (pH 6.8) by dialysis bag method

	FLZ in suspension				
Time (h)	Abs (1)	Abs (2)	Abs (3)	AVE	STDEV
0.25	0.032	0.020	0.012	0.021	0.010
0.50	0.037	0.025	0.022	0.028	0.008
1.00	0.042	0.028	0.031	0.034	0.007

2.00	0.046	0.032	0.026	0.035	0.010
4.00	0.051	0.045	0.039	0.045	0.006
6.00	0.071	0.045	0.040	0.052	0.017
24.00	0.090	0.075	0.067	0.077	0.012

FLZ = flubendazole; Abs = absorbance; AVE = average; STDEV = standard deviation

Table 6.S11. Absorbance of flubendazole-loaded nanoemulsion in aqueous dissolution media (pH 6.8) by combined biphasic – modified cylinder method

	FLZ NE					FLZ NE – Drug free NE		
Time (h)	Abs (1)	Abs (2)	Abs (3)	AVE	STDEV	Abs (1a)	Abs (2a)	Abs (3a)
0.25	0.006	0.005	0.004	0.005	0.001	0.000	0.000	0.000
0.50	0.007	0.005	0.004	0.005	0.001	0.001	0.000	0.000
1.00	0.008	0.009	0.005	0.007	0.002	0.001	0.002	0.000
2.00	0.007	0.005	0.007	0.006	0.001	0.001	0.000	0.001
4.00	0.008	0.006	0.006	0.007	0.001	0.000	0.000	0.000
6.00	0.017	0.008	0.008	0.011	0.004	0.012	0.003	0.003
24.00	0.015	0.012	0.013	0.013	0.001	0.001	0.000	0.000

FLZ NE = flubendazole loaded nanoemulsion; Drug Free NE = flubendazole free nanoemulsion; Abs = absorbance; AVE = average; STDEV = standard deviation

Table 6.S12. Absorbance of flubendazole-in-oil in aqueous dissolution media (pH 6.8) by combined biphasic – modified cylinder method

	FLZ Oil					FLZ Oil – Drug free Oil		
Time (h)	Abs (1)	Abs (2)	Abs (3)	AVE	STDEV	Abs (1a)	Abs (2a)	Abs (3a)
0.25	0.017	0.010	0.008	0.012	0.004	0.012	0.005	0.003
0.50	0.012	0.006	0.007	0.008	0.002	0.008	0.002	0.003
1.00	0.010	0.010	0.005	0.008	0.002	0.003	0.003	0.000
2.00	0.009	0.007	0.005	0.007	0.001	0.003	0.001	0.000
4.00	0.017	0.008	0.006	0.010	0.004	0.011	0.002	0.000

6.00	0.009	0.014	0.007	0.010	0.003	0.002	0.007	0.000
24.00	0.011	0.014	0.017	0.014	0.002	0.002	0.005	0.008

FLZ Oil = flubendazole in oil; Abs = absorbance; AVE = average; STDEV = standard deviation

Table 6.S13. Absorbance of flubendazole in suspension in aqueous dissolution media (pH 6.8) by combined biphasic – modified cylinder method

	FLZ in suspension				
Time (h)	Abs (1)	Abs (2)	Abs (3)	AVE	STDEV
0.25	0.003	0.005	0.005	0.004	0.001
0.50	0.004	0.005	0.005	0.005	0.000
1.00	0.004	0.006	0.005	0.005	0.001
2.00	0.003	0.005	0.009	0.006	0.002
4.00	0.004	0.003	0.003	0.003	0.000
6.00	0.003	0.003	0.002	0.003	0.000
24.00	0.005	0.005	0.005	0.005	0.000

FLZ = flubendazole; Abs = absorbance; AVE = average; STDEV = standard deviation

Table 6.S14. Absorbance of flubendazole-loaded nanoemulsion in octanol dissolution media (pH 6.8) by combined biphasic – modified cylinder method

	FLZ NE					FLZ NE – Drug free NE		
Time (h)	Abs (1)	Abs (2)	Abs (3)	AVE	STDEV	Abs (1a)	Abs (2a)	Abs (3a)
0.25	0.174	0.173	0.078	0.142	0.042	0.171	0.170	0.075
0.50	0.171	0.165	0.080	0.139	0.039	0.168	0.162	0.077
1.00	0.168	0.164	0.081	0.138	0.038	0.164	0.160	0.077
2.00	0.168	0.161	0.092	0.140	0.032	0.162	0.155	0.086
4.00	0.173	0.164	0.116	0.151	0.023	0.158	0.149	0.101
6.00	0.180	0.169	0.132	0.160	0.019	0.158	0.147	0.110
24.00	0.267	0.237	0.307	0.270	0.024	0.177	0.147	0.217

FLZ NE = flubendazole loaded nanoemulsion; Drug Free NE = flubendazole free nanoemulsion; Abs = absorbance; AVE = average; STDEV = standard deviation

Table 6.S15. Absorbance of flubendazole-in-oil in octanol dissolution media (pH 6.8) by combined biphasic – modified cylinder method

	FLZ Oil					FLZ Oil – Drug free Oil		
Time (h)	Abs (1)	Abs (2)	Abs (3)	AVE	STDEV	Abs (1a)	Abs (2a)	Abs (3a)
0.25	0.056	0.045	0.051	0.051	0.004	0.052	0.041	0.047
0.50	0.055	0.047	0.050	0.051	0.003	0.050	0.042	0.045
1.00	0.065	0.047	0.053	0.055	0.007	0.060	0.042	0.000
2.00	0.063	0.054	0.067	0.061	0.005	0.058	0.049	0.000
4.00	0.076	0.065	0.061	0.067	0.006	0.066	0.055	0.051
6.00	0.091	0.074	0.068	0.078	0.009	0.080	0.063	0.057
24.00	0.187	0.165	0.147	0.166	0.014	0.086	0.064	0.046

FLZ Oil = flubendazole in oil; Abs = absorbance; AVE = average; STDEV = standard deviation

Table 6.S16. Absorbance of flubendazole in suspension in octanol dissolution media (pH 6.8) by combined biphasic – modified cylinder method

	FLZ in suspension				
Time (h)	Abs (1)	Abs (2)	Abs (3)	AVE	STDEV
0.25	0.001	0.008	0.006	0.005	0.003
0.50	0.000	0.011	0.005	0.005	0.004
1.00	0.000	0.008	0.004	0.004	0.003
2.00	0.001	0.010	0.007	0.006	0.003
4.00	0.012	0.015	0.010	0.012	0.002
6.00	0.015	0.020	0.015	0.017	0.002
24.00	0.062	0.071	0.060	0.064	0.004

FLZ = flubendazole; Abs = absorbance; AVE = average; STDEV = standard deviation

Table 6.S17. Absorbance of flubendazole in suspension in aqueous and octanol dissolution media (pH 6.8) by combined biphasic – modified cylinder method with surfactant

Time (h)	*FLZ Susp. (Aqueous Phase)*			AVE (Aqu.)	STDEV (Aqu.)	*FLZ Susp. (Octanol Phase)*			AVE (Oct.)	STDEV (Oct.)
	Abs (1)	Abs (2)	Abs (3)			Abs (1)	Abs (2)	Abs (3)		
0.25	1877.000	1897.000	1884.000	188.000	10.149	0.255	0.167	0.252	0.225	0.050
0.50	2017.000	2010.000	1988.000	2005.000	15.133	0.222	0.203	0.285	0.237	0.043
1.00	2179.000	2270.000	2686.000	2378.333	270.304	0.253	0.238	0.331	0.274	0.050
2.00	Turbid	Turbid	Turbid			0.351	0.347	0.452	0.383	0.060
4.00	Turbid	Turbid	Turbid			1385.000	1428.000	1538.000	1450.000	78.907
6.00	Turbid	Turbid	Turbid			1797.000	1785.000	1896.000	1826.000	60.918
24.00	Turbid	Turbid	Turbid			3159.000	3231.000	3291.000	3227.000	66.091

FLZ = flubendazole; Abs = absorbance; AVE = average; STDEV = standard deviation

Table 6.S18. Average absorbance value (n=3) at 225 nm of flubendazole (FLZ)-free nanoemulsion (NE) or oil in dissolution media (pH 1.2 and 6.8) by dialysis membrane method (DB)

Time (h)	DB pH1.2 FLZ free NE	DB pH1.2 FLZ free Oil	DB pH6.8 FLZ free NE	DB pH6.8 FLZ free Oil
0.25	0.041	0.031	0.033	0.024
0.50	0.058	0.040	0.037	0.031
1.00	0.081	0.052	0.049	0.045
2.00	0.126	0.071	0.084	0.066
4.00	0.155	0.096	0.103	0.089
6.00	0.175	0.120	0.131	0.112
24.00	0.210	0.196	0.187	0.174

CHAPTER 7 - GENERAL DISCUSSION, CONCLUSION, LIMITATIONS AND FUTURE DIRECTIONS

7.1. General Discussion

The increasing demand for new drugs encounters significant barriers to be overcome. Such barriers refer to safety, efficacy, compliance with regulatory requirements and the cost-effectiveness ratio. Regardless of companies' progressive efforts in research, studies demonstrate that, in the United States, only 0.1% of new drugs under development advance to the clinical trial stage. Within these, only 10% are approved. In this context, there is an urgent need for more efficient alternatives for drug developments, especially in treating specific diseases, such as neglected diseases and different types of cancer. FLZ, a drug that acts on microtubules, has potential use in different treatments, such as lymphatic filariasis, meningoencephalitis and various types of cancer, when in nanomolar concentrations. Therefore, this drug was selected as a potential candidate for drug repositioning.

There are different drug administration routes for treating comorbidities. Among them, intravenous administration is a more advantageous route because it allows the administration of large amounts of drug directly into the body. However, it may have limited effectiveness during drug circulation due to its half-life and enzymatic degradations (POUSTFOROOSH et al., 2022). In addition, this technique is invasive and requires specialized personnel for the treatment. In this sense, the oral route is a noninvasive route, with accessibility facilitated by not needing trained people, and offering better cost-effectiveness ratios. However, first-pass hepatic metabolism, the low water solubility of drugs, and the risk of drug degradation in the gastrointestinal tract, are the main barriers against better efficacy through this route of administration.

To solve this problem, nanostructured systems are a solution to overcome these limitations. Several drug-loaded nanostructured systems have been developed until now, including liposomes, dendrimers, nanopolymers, inorganic nanoparticles, nanolipids, as well as nanocrystals. Liposomes are composed of phospholipid bilayers that form vesicular structures. Dendrimers are tree-like dendritic polymers that can be freely modified according to the desired architecture and functionality. Polymeric nanoparticles have several types, such as nanogels, nanocapsules and nanospheres, according to the desired structure (gelling agent, polymeric membrane, or polymeric matrix, respectively) and have natural origin (i.e. hyaluronic acids, chitosan), synthetic biodegradable (i.e. poly(ε-caprolactone), or synthetic biocompatible (poly(lactic-co-glycolic acid)) origins. Inorganic nanoparticles can include metallic particles, such as gold, silver, metal oxide. Nanocrystals are drug-core particles usually coated by surfactants. Nanolipids include solid lipid

nanoparticles (solid lipid core), nanostructured lipid carriers (solid lipid combined with liquid lipid core), and finally, nanoemulsions in which drugs are in the liquid lipid core in a solubilized state (YUKUYAMA; ARAÚJO; BOU-CHACRA, 2020).

The low water solubility of FLZ may significantly limit its oral bioavailability. Thus, in this present work, the FLZ-loaded nanoemulsion was developed with the aim of overcoming this bioavailability limitation.

7.1.1. D-phase emulsification

Nanolipids have many advantages compared to other nanostructured systems. They are usually made of biocompatible or biodegradable lipids, have reduced risk of toxicity, ease of large-scale production, combined with potential to allow modified release of drug (NGUYEN et al., 2022).

A pertinent factor in the present work is the drug-loaded nanoemulsion preparation method. Within low energy processes, the DPE method stands out for presenting unique properties: there is no need for rigorous adjustment of HLB, no high temperatures nor high concentration of surfactants when compared to conventional phase inversion processes (PIT and PIC methods). In addition, compared to the spontaneous emulsification process, DPE allows for the formation of an NE containing a high concentration of oil internal phase, without using solvents (YUKUYAMA et al., 2018).

Consequently, we obtained a FLZ-loaded nanoemulsion with 60.0% oil phase using a significantly reduced concentration of surfactant (3.0%–3.5%w/w) and particle size below 100 nm (**Chapter 2 and Chapter 4**). These nanoemulsions with low surfactant content provide benefits compared to the microemulsion, since microemulsion requires a high surfactant content even at a low oil phase content, that may compromise the safety of patients due to potential toxicity of the surfactants.

The exploratory study allowed identifying liquid lipids with greater drug solubility, in addition to offering better safety for oral administration in future tests since they are already approved for oral use. The possible presence of the isotropic phase D in the DPE process promoted the easy dispersion of the oil phase in this medium and, consequently, obtaining nanoemulsions with reduced MPS. Statistical analysis showed an inversely proportional effect between MPS value and

oil concentration, in agreement with observations made in previous experiments. This unique characteristic of DPE method differs from other conventional low-energy methods (YUKUYAMA et al., 2018). In addition, the preparation process, enabled at 25 °C temperature, saves energy and time on an industrial scale, in addition to avoiding problems affected by factors such as degradation of components, or even water loss due to evaporation.

7.1.2. Cryptococcosis

Although several approaches have been developed for years, the delivery of drug or components to brain is still a challenge when compared to other organs of the human body. Thus, the development of drug targeting central nervous system (CNS) is more time-consuming than other types of drug delivery (POUSTFOROOSH et al., 2022).

Accordingly, there are different compartments that protect the CNS from external invasion. The most important ones are the blood brain barrier (BBB) and blood-cerebrospinal fluid barrier (BCSFB) (POUSTFOROOSH et al., 2022; SASTRI et al., 2022). BBB is a principal barrier to select passage of nutrients, lipophilic molecules and water, while blocking entrance of several harm molecules to the CNS such as toxins and bacteria (JAIN et al., 2022). BBB is composed of endothelial cells, which are tightly packed, and surrounded by a network of blood vessels to monitor the passage of substances to assure correct function of the brain (SASTRI et al., 2022). The BCSFB is composed of choroid plexus (CP), a modified cuboidal epithelium with limited fenestrations, and pia-arachnoid, which is considered a meningeal barrier. The main function of BCSFB consists of secretion of cerebrospinal fluid (CSF), and the tight junctions of these cell barriers are also limitations for several components from entering (NGUYEN et al., 2022).

Several receptors and transporter proteins are present in BBB to allow entrance of essential substances to CNS, such as transferrin and insulin receptors, glucose, glutathione, and amino acid transporters. On the other hand, some efflux transporters contribute to sending back lipophilic molecules to the systemic circulation, such as the P-gp transporters (an ATP-binding cassette family) and multidrug resistance-related proteins (FORMICA et al., 2022; SASTRI et al., 2022), which act as additional barriers for the effective drug entrance to the CNS.

In order to circumvent these barriers to achieve drug delivery to CNS, invasive and noninvasive approaches are used. Invasive approaches include intrathecal or intraparenchymal medication, intracerebral implants, injections, ultrasound-mediated BBB disruption strategy, and others. Unfortunately, these approaches may disturb the integrity of BBB and affect the barrier function against toxin and undesired molecules entering the CNS, as well as increased risk of infections (FORMICA et al., 2022; JAIN et al., 2022). In contrast, a noninvasive approach is established by the endogenous cellular transport effected by transcellular or paracellular pathway (passive or active transport, respectively) (FORMICA et al., 2022). One of the most common noninvasive delivery alternatives to the brain is oral administration.

The FLZ-loaded nanoemulsion developed in the present work is comprised of drug solubilized in oil derived from linoleic acid, a component of polyunsaturated fatty acids (PUFA). As described in **Chapter 2**, this nanoemulsion delivery may be supported by the PUFA transporter present in BBB. Furthermore, several studies indicate the contribution of polysorbate 80 (the main surfactant of this nanoemulsion), as an inhibitor of the P-gp efflux transporter, combined with its function to help open the tight junction of the BBB. Moreover, the BBB favors permeation of molecules with high lipophilicity and molecular weight below 400 g/mol, which are both specification of FLZ.

As a result, the oral application of FLZ loaded in an optimized nanoemulsion as a potent antifungal in this present work offered evidence-based support for future studies, aiming to find nanosystems that retain their anticryptococcal activity but with minimal toxicity. An in vitro study in culture medium and in vivo in *G. mellonella* larvae, indicated the nontoxicity of the developed nanoemulsion. In the test in mice, a reduction of the fungal load of 29.3% of CFU/g in the brain was observed compared with the blank nanoemulsion and FLZ in suspension, even in doses significantly lower than those of the studies found in the literature (YUKUYAMA et al., 2021).

There are several works on nanoemulsions for the brain using the oral route. However, there are few works using microtubule targeting agents for treating diseases in the brain, making the present work on nanoemulsion with oral delivery of FLZ to the brain, a unique system.

7.1.2. Lung cancer

Microtubules are dynamic proteins with crucial roles in cell division and several other activities to assure normal function of cells. The malfunction of these proteins can lead to various

diseases, including cancer. Lung cancer is one of the leading causes of global mortality by tumor diseases, originating from several limitations such as early prognosis and effective treatments. Thus, **Chapter 3** introduced the relevance of these proteins in this tumor development, including various features that promote chromosome mis-segregation, cell abnormalities and drug resistance. Different microtubule isotypes act on cell functions. The βIII isotype is known to be one of the main precursors of cell malfunctions, and this assumption was reinforced in recent studies. Microtubule bioelectrical functions generated possibilities of developing future unique evaluation methods based on electrical oscillations and pH perturbation in the vicinities of microtubules in cancer cells. New insights into the kinetochore-microtubule interaction unraveled the intriguing phenomenon of correct chromosome segregation, as well as crucial rules of mitochondrial microtubules in cell energy generation and fission-fusion processes of mitochondria. Studies on the effects of cigarette smoking on ciliogenesis demonstrated how pulmonary cells are impaired by these external factors. In addition, innovative quantification methods of motile cilia inspired new methods for boosting drug efficacy or disease progression assays. All this information consolidates the importance of microtubules and their role as a multifunctional protein. Nevertheless, the use of microtubule agents in tumor treatment requires careful attention to avoid several drawbacks that can lead to side effects, when normal cells are accidentally involved.

Several studies have shown promising findings on the use of FLZ, a microtubule destabilizing agent, as a potential alternative for cancer treatment. However, until now there has been no in vivo study on the efficacy of this drug for treating lung cancer. The results of our studies and research in partnership with another laboratory demonstrated the anticancer activity of FLZ nanocrystals in BALB/c nude mice, with subcutaneous injection of human lung cancer cell line A-549. This test showed a significant result of FLZ nanocrystal in reducing the size of tumors compared to control or drug suspension (**Appendix 4**). With this promising result, it was expected that the FLZ-loaded nanoemulsion in the present work would allow for increasing this activity, with the use of a less invasive administrative route.

In lung cancer, up to 15% of lung cancer patients with HIV suffer from a malignant wound (MW) (FIRMINO et al., 2021; TILLEY; LIPSON; RAMOS, 2016). Data indicate that by 2021, a significant number of people (38.4 million) contracted HIV/AIDS worldwide (WORLD HEALTH ORGANIZATION, 2023). Although oral administration of FLZ-loaded nanoemulsion did not reduce tumor size, significant results were observed in MW (**Chapter 4**). This study also showed

the influence of different types of oil on the effectiveness in treating this disease. FLZ-loaded nanoemulsion, which contains Maisine CC as the only oil phase, offered 100% prevention against MW even after 80 days of treatment, and FLZ-loaded nanoemulsion with mixed oil showed MW in 40% of animals but with reduced size and 14 days delay than blank nanoemulsion or FLZ in suspension.

According to studies, linoleic acid has properties to improve the wound healing effects by oral administration, under several mechanisms such as a decrease in NF-kB activation, concentrations of macrophage inflammatory protein-3 and IL-1, IL-6 (RODRIGUES et al., 2012), acceleration of wound healing dynamics by activation of fibroblastic cells differentiation and migration, local neovascularization, keratinocyte proliferation, inflammation among others (POLJŠAK; KREFT; KOČEVAR GLAVAČ, 2020). Concurrently, FLZ also influences NF-kB and STAT3, a multifunctional protein that regulates inflammatory processes (CHEN; LI, 2015; HUYNH et al., 2019). All these mechanisms may work synergistically under association of FLZ, linoleic-acid derived oil in a nanosized emulsion, which may explain the efficacy of developed nanoemulsion against MW.

With regard to the difference in tumor treatment efficacy compared to FLZ nanocrystal (**Appendix 4**), which reduced tumor size by 40%, it is important to remember the difference in the route of administration. The nanocrystal was administered intraperitonially, which results in a more direct interaction of the drug administered with the tumor site, compared to oral administration performed by the FLZ-loaded nanoemulsion, which is required to circumvent first-pass metabolism and gastrointestinal barriers. Another important factor is the final concentration of FLZ in a nanocrystal and nanoemulsion. Basically, nanocrystals have as their core the pure drug in solid or amorphous state, in nanosize, covered with a thin layer of surfactant or other stabilizing agents. In contrast, the nanoemulsion has at its core a liquid oil phase, where the drug is solubilized and which limits its concentration. Thus, nanocrystals have a loading capacity of up to 100% of drug concentration in their core, while other nanostructured systems such as nanoemulsion, other nanolipids, or nanopolymers, can vary between 5% and 30% of capacity due to the need for the presence of the carrier components in their core (FORMICA et al., 2022). Usually, the antitumor effects of microtubule targeting agents are achieved only at high concentrations (TANGUTUR et al., 2017). Controversially, studies show that less rigid nanostructures are more likely to penetrate target sites compared to more rigid nanostructures (ROHNER; THOMAS, 2016). Despite the

advantage that the nanoemulsion has a significantly more flexible core than a nanocrystal, its significantly lower drug concentration may have impaired the anticancer outcome in the current study. However, due to the difference in the route of administration and its frequency of use, for the moment it is not possible to assume this comparison.

7.1.4. Dissolution test

We conducted a dissolution study comparing FLZ in three different forms (micronized form as a suspension, loaded in nanoemulsion and solubilized in oil) by using three different methods (dialysis bag, modified cylinder method and a new combined method of modified cylinder and biphasic dissolution), to test their discriminatory power for different preparations. The aim was to develop a new discriminatory dissolution test enabling to distinguish the release profile of FLZ loaded in nanoemulsion with the drug in suspension as well as oil solution.

Several challenges were faced to optimize this drug release profile, and statistic limitations were encountered due to the low FLZ release profile in the method developed. Nevertheless, the achieved results allowed for a better understanding of possible drug release mechanisms in nanoemulsions, when compared to other forms of preparations. Modified cylinder have eased the accommodation of liquid preparations in different volumes, and the biphasic method demonstrated the relevance of the octanol phase to evaluate preparations containing oil phase, by mimicking intestinal compartments. Although at the minimum concentration detected, the drug release profile obtained by the BP+MC combined method showed a positive correlation with the efficacy results obtained by the in vivo tests for cryptococcal and lung cancer. This correlation encourages to open up new possibilities for several new hypothesis to ameliorate the present pilot test. However, it should be noted that those in vivo tests involved prolonged therapy (80 days for cancer test); thereby in vitro tests may not allow fully demonstrating the efficacy profile of these preparations. Thus, this in vitro dissolution test is a valuable test to select different drug preparations in the early stage of development, to allow pursuing the next steps.

7.2. General Conclusion

Several new agents or biomarkers for lung cancer therapy have been discovered. Oral administration of drugs may be highlighted as a preferred administration route, since it offers a better cost-effectiveness rate and patient compliance. But the water solubility problem of these new components affects their use, being one of the most limitations to obtain high treatment effectiveness. The application of a nanostructured system is an exciting alternative solution to enhance not only drug solubility, but also drug safety and stability.

The rational development of FLZ-loaded nanoemulsions through a combination of DPE with the DoE method made it possible to obtain stable nanoemulsions at 25 °C, overcoming the problem of the low solubility of this drug in water. The use of the DPE process provided developing nanoemulsions with MPS below 100 nm and with a high concentration of oil phase (60.0% w/w), which enhance the incorporation of a greater amount of solubilized drug in the nanoemulsion. The statistical design offered advantages compared to a one-factor-in-a-time experiment, by reducing the number of experiments under multiple variable factors, and also by providing a statistical view of the most influenceable variables to obtain the desired result.

In view of the needs related to the significant number of occurrences attributed to cryptococcosis worldwide, and the limitations of treatments due to the challenge of a drug's effectiveness against the BBB, the development of a new FLZ-loaded nanoemulsion is justified as an alternative to existing treatments. Although further evaluations are necessary, the present study demonstrated the potential of this nanoemulsion to reach therapeutic concentrations with greater efficacy and safety compared to conventional broad-spectrum antifungals.

This nanoemulsion also showed high expectancy to treat MW in cancer patients that suffer in the last months of life, easing their treatment in a cost-effective manner. Although this disease reaches up to 15% of late-stage cancer patients, the lack of efficient methods in the current available treatments make this discovery noteworthy.

The new way of evaluating the mechanism of oral nanoemulsion through the pilot dissolution method may support developing the next-generation dissolution method, enriching the rationale of dissolution behavior of nanoemulsions and opening discussions for several new approaches. To the best of our knowledge, this is the first study comparing dissolution behavior of a drug solubilized in oil, drug in suspension, and a drug-loaded nanoemulsion with high oil and low surfactant contents, as prepared by the DPE method.

7.3. Limitations

The visual method used to evaluate the effectiveness of FLZ solubilization of oils during the development of the nanoemulsion has a limitation such as the non-detection of possible presence of crystals. For this detection, one alternative is to filter the nanoemulsion and measure the remaining amount of drug in the filter to verify possible non visible crystallization, especially after the end of stability test. However, the limitation of the quantification method did not make it possible, requiring the future development of a more precise analytical method for amounts lower than the detection limit of the method used in this doctorate. In the present work, the UV spectrophotometry method was used, but as the UV absorption interval of Maisine CC® oil included the absorption interval of FLZ, it was necessary to measure the absorption of the sample containing the drug and subtract the value of the sample without the drug, the that could lead to errors in the final value, or effectiveness problems. In case of a trial with HPLC method, as the nanoemulsion consists of a core in liquid state, the drug concentration compared to the oil in the core is very low and it limited the use of quantification methods by HPLC. The extraction method was not successful either. Thus, more in-deep test by HPLC or other methods such as mass spectroscopy may be considered for future analysis, in addition to the quantification of FLZ metabolites for the pharmacokinetics study.

The measurement of the toxicity potential of our FLZ-loaded nanoemulsion was not performed in this work, which could open several new insights to determine the dosage of future administration. An alternative is to perform in vitro tests to assess liver toxicity, such as testing for liver enzymes in the blood, eg, aspartate aminotransferase (AST), alanine transaminase (ALT), alkaline phosphatase (ALP), where an elevated score indicates liver injury.

In **Chapter 2**, a specific detection method for the presence of FLZ in the BBB was not used. Thus, we cannot state that there was penetration of the FLZ within the BBB. The drug may have been taken via the blood or lymphatic system around the BBB, but we cannot confirm its penetration into the BBB. As the nanoemulsion is a liquid state nanosystem, it has limitations to evaluate by in vivo test the presence of the intact micelle in the brain and not just the components,

even if we use fluorescent biomarkers, unlike the solid state nanosystem. Thus, future analyzes using an in vitro BBB drug penetration test (eg 3D test) will be interesting for this assumption.

In **Chapter 4**, Malignant Wound, the result of this study suggests qualitative efficacy only. For statistical significance, a more accurate study including a statistically significant number of animals is needed.

The mechanism of action of FLZ in the treatment of malignant wound was not elucidated in this work. The action of FLZ in inhibiting STAT3 and NF-kB pathways contradicts the healing efficacy necessary for the wound healing process. Thus, a new hypothesis emerged: FLZ can act on the inhibition of neoangiogenesis that causes blood vessel growth and disruption to cause WM. In this way, FLZ can act as a prevention of MW, and the oil as a treatment for MW. However, to prove this hypothesis, future tests will be necessary.

Another limitation in this work was not having performed an in vivo test to assess the effectiveness of this nanoemulsion after tumor growth. The nanoemulsion was administered concurrently with tumor growth to assess the preventive efficacy. However, there is still a lack of a complementary in vivo test to evaluate the efficacy in post-tumor growth administration.

In addition, this work lacks information on the pharmacokinetics of the drug loaded in nanoemulsion, compared to the non-nanonized drug. Future in vitro tests could provide insight of how much the drug is contained or released, in order to obtain information about the minimum dose necessary to achieve anticancer efficacy.

The nanoemulsion containing FLZ solubilized in long-chain oil, as used in this work, may favor the targeting of this drug to the lymphatic system. An intense review on the advantage of this targeting was carried out in this work, but a practical experiment to prove this targeting of the FLZ-loaded nanoemulsion and its advantages has not yet been carried out. Future in vivo or in vitro tests for targeting the lymphatic system, including the development of quantification of metabolites of this drug, are still necessary.

7.4. Future Directions

The FLZ-loaded nanoemulsion developed in this work demonstrated 30% efficacy in cryptococcal infection, and 100% prevention against MW in A549 xenografted model with mice. Therefore, it is a potential candidate as adjuvant treatment against cryptococcus meningoencephalitis and lung cancer.

However, new directions to improve these efficacies may also be envisaged through the following approaches: (1) increase of drug administration frequency respecting the toxic limits; (2) association with synergic treatment drugs; (3) deepening the in vitro dissolution method to identify variables to improve the drug release measurement and evaluate in-vitro-in-vivo correlations; (4) development of a more accurate quantification method for the parent drug and its metabolite for future pharmacokinetic tests; and (5) due to the long-chain oil, evaluate the possible passage of this nanoemulsion to lymphatic system, which avoids the first hepatic passage of drug and decreases its degradation, toxicity, and risk of future metastasis.

As an additional task, some uncertainties remain and we should explore and elucidate in the current proposed administration route, to reduce the toxicity problem, or even to ameliorate the drug delivery to the targeted site. As mentioned previously, the use of microtubule targeting agents are based on the strategy of targeting sites with rapid cell proliferation (**Chapter 3**). However, it is well known that patients experience significant hair loss during chemotherapy treatment. This is explained by the fact that the tissues of hair follicles are one of a few adult mammal tissues that rapidly regenerate. As in hair follicles, gastrointestinal tissues also present rapid turnover time compared to others (BARKER et al., 2008; MILO; PHILLIPS, 2015). This information leads to a preoccupation and the need of specific toxicity tests to elucidate how drug concentration, frequency and treatment duration of developed oral FLZ-loaded nanoemulsion will affect a patient's gastrointestinal tract over time. In case of unfavorable assumption, another noninvasive route should also be explored.

The target site of cryptococcal meningoencephalitis is the CNS. It is also known that one of the most distal metastatic sites in lung cancer patients is the CNS (RIIHIMÄKI et al., 2014). To deliver drug to this site, the oral route is a noninvasive route of administration. However, there is another administration route to CNS that does not have the limitations of the gastrointestinal barrier and short drug half-life, which is the nose-to-brain (intranasal) route.

This minimally invasive route of drug delivery is also considered to be a direct brain delivery route, and it has several pathways: the transcellular, trigeminal nerve, olfactory, intraneural, extraneural, and glymphatic pathways. The former administration route delivers drugs from the nasal cavity to the systemic circulation to reach the CNS after they enter the respiratory epithelium region. The second internalizes drugs to peripheral trigeminal neurons through endocytosis, and delivers them to brain via trigeminal nerves. The third transports the drugs by reaching the innermost olfactory region by an intracellular, extracellular, or transcellular pathway. The intraneural one transports drugs subjected to endocytosis/pinocytosis into the olfactory bulb and releases them to different sites of the brain. The drug transport via extraneural pathway occurs in the lamina propria of the olfactory region, distributes drugs through passive diffusion or active transport, and it is considered the fastest pathway. The glymphatic pathway connects the CSF in the brain to the nasal lymphatic system by olfactory nerves. The nose-to-brain transport of drug may happen through these combinations of pathways or alone (JAIN et al., 2022; SASTRI et al., 2022). Several strategies favor intranasal drug transport, such as high lipophilicity of the drug, the combination of polymer such as hydrogels to enhance formulation viscosity to increase permanence of drug in nasal mucosa, the use of positively charged polymers to increase affinity with nasal mucosa that are negatively charged, or using a drug with a particle size lower than 400-500 nm (NGUYEN et al., 2022). However, challenges still remain due to the drug delivery limitations caused by nasal mucociliary clearance, immunological and enzymatic clearance and nasal secretions (JAIN et al., 2022). Moreover, it has been reported that the interference of the drug delivery due to the device applied (nasal and traditional spray are not effective, but a nebulizer allows better drug deposition in the nasal cavity) (SASTRI et al., 2022), and there is inconvenience as possible damage of mucosa caused by repeated use of intranasal route (POUSTFOROOSH et al., 2022).

For treating meningoencephalitis and brain metastasis as a second site of lung cancer, the use of the FLZ-loaded nanoemulsion developed in this work by intranasal administration would be an interesting new approach, due to the particle size below 400 nm and the use of surfactant polysorbate 80, that facilitate delivery to the CNS.

For the primary site of lung cancer, optimizing efficacy via the oral route, or verifying the possible targeting of the lymphatic system to eliminate the risk of passing through the liver (**Chapter 5**) is still an interesting approach.

FLZ nanocrystal is also an interesting approach to evaluate its effectiveness via intranasal administration, since nanocrystals can remain in solid form for a long time in intranasal site, allowing prolonged release of the drug when compared to other forms of preparations (FORMICA et al., 2022). Another approach would be to cover this nanocrystal with gel or mucoadhesive agents to increase affinity with the nasal mucosa.

Additional in vitro tests to evaluate the drug's toxicity, its direction to the brain and to the lymphatic system would be important to refine the knowledge and facilitate the next stage of development of in vivo efficacy tests of this nanoemulsion.

Thus, numerous new approaches arise from the nanostructured systems developed in the present work, with possibilities for improvement, both for treatment in the brain as the target site (cryptococcosis and secondary site of lung tumor), or at the primary site of a lung tumor. However, given that microtubule targeting agents aim to attack rapidly reproducing cells, and knowing that capillary and gastrointestinal cells have high regenerative features, associated with the presence of ciliary mucus in the nasal region, caution and future tests are needed to evaluate the toxicity of these agents in prolonged use, when applied orally or even intranasally.

7.5. References

BARKER, N.; VAN ES. JH; JAKS, V.; KASPER, M.; SNIPPERT, H.; TOFTGÅRD, R.; CLEVERS, H. Very long-term self-renewal of small intestine, colon, and hair follicles from cycling Lgr5+ve stem cells. **Cold Spring Harb Symp Quant Biol.**, *[S. l.]*, v. 73, p. 351–356, 2008. DOI: 10.1101/sqb.2008.72.003. PMID: 19478326.

CHEN, Yan; LI, Tonglei. Cellular Uptake Mechanism of Paclitaxel Nanocrystals Determined by Confocal Imaging and Kinetic Measurement. **AAPS Journal**, *[S. l.]*, v. 17, n. 5, p. 1126–1134, 2015. DOI: 10.1208/s12248-015-9774-0.

FIRMINO, Flavia; VILLELA-CASTRO, Diana Lima; SANTOS, Juliano Dos; CONCEIÇÃO DE GOUVEIA SANTOS, Vera Lúcia. **Topical Management of Bleeding From Malignant Wounds Caused by Breast Cancer: A Systematic Review**. **Journal of Pain and Symptom Management**Elsevier Inc., , 2021. DOI: 10.1016/j.jpainsymman.2020.10.020.

FORMICA, María L.; REAL, Daniel A.; PICCHIO, Matías L.; CATLIN, Elise; DONNELLY, Ryan F.; PAREDES, Alejandro J. **On a highway to the brain: A review on nose-to-brain drug delivery using nanoparticles**. **Applied Materials Today**Elsevier Ltd, , 2022. DOI: 10.1016/j.apmt.2022.101631.

HUYNH, Jennifer; CHAND, Ashwini; GOUGH, Daniel; ERNST, Matthias. **Therapeutically exploiting STAT3 activity in cancer — using tissue repair as a road map**. **Nature Reviews Cancer**Nature Publishing Group, , 2019. DOI: 10.1038/s41568-018-0090-8.

JAIN, Harsha; DALVI, Harshita; BHAT, Aditi; AGRAWAL, Aashruti; MADAN, Jitender; SINGH, Pankaj Kumar; MEHRA, Neelesh Kumar; SINGH, Shashi Bala; SRIVASTAVA, Saurabh. Nanomaterials in nose-to-brain delivery. *Em*: **Multifunctional Nanocarriers**. [s.l.] : Elsevier, 2022. p. 379–400. DOI: 10.1016/b978-0-323-85041-4.00016-0.

MILO, Ron; PHILLIPS, Rob. **HOW QUICKLY DO DIFFERENT CELLS IN THE BODY REPLACE THEMSELVES**. [s.l: s.n.]. Disponível em: http://book.bionumbers.org/how-quickly-do-different-cells-in-the-body-replace-themselves/. Acesso em: 16 jan. 2023.

NGUYEN, Thuy Trang; NGUYEN, Thi Thuy Dung; TRAN, Nguyen Minh An; VAN VO, Giau. **Lipid-Based Nanocarriers via Nose-to-Brain Pathway for Central Nervous System Disorders**. **Neurochemical Research**Springer, , 2022. DOI: 10.1007/s11064-021-03488-7.

POLJŠAK, Nina; KREFT, Samo; KOČEVAR GLAVAČ, Nina. **Vegetable butters and oils in skin wound healing: Scientific evidence for new opportunities in dermatology**. **Phytotherapy Research**John Wiley and Sons Ltd, , 2020. DOI: 10.1002/ptr.6524.

POUSTFOROOSH, Alireza; NEMATOLLAHI, Mohammad Hadi; HASHEMIPOUR, Hassan; PARDAKHTY, Abbas. **Recent advances in Bio-conjugated nanocarriers for crossing the Blood-Brain Barrier in (pre-)clinical studies with an emphasis on vesicles**. **Journal of Controlled Release**Elsevier B.V., , 2022. DOI: 10.1016/j.jconrel.2022.02.015.

RIIHIMÄKI, M.; HEMMINKI, A.; FALLAH, M.; THOMSEN, H.; SUNDQUIST, K.; SUNDQUIST, J.; HEMMINKI, K. Metastatic sites and survival in lung cancer. **Lung Cancer**, *[S. l.]*, v. 86, n. 1, p. 78–84, 2014. DOI: 10.1016/j.lungcan.2014.07.020.

RODRIGUES, Hosana G. et al. Oral administration of oleic or linoleic acid accelerates the inflammatory phase of wound healing. **Journal of Investigative Dermatology**, *[S. l.]*, v. 132, n. 1, p. 208–215, 2012. DOI: 10.1038/jid.2011.265.

ROHNER, Nathan Andrew; THOMAS, Susan Napier. Melanoma growth effects on molecular clearance from tumors and biodistribution into systemic tissues versus draining lymph nodes. **Journal of Controlled Release**, *[S. l.]*, v. 223, p. 99–108, 2016. DOI: 10.1016/j.jconrel.2015.12.027.

SASTRI, K. Trideva; GUPTA, N. Vishal; M, Sharadha; CHAKRABORTY, Souvik; KUMAR, Hitesh; CHAND, Pallavi; BALAMURALIDHARA, V.; GOWDA, D. V. **Nanocarrier facilitated drug delivery to the brain through intranasal route: A promising approach to transcend bio-obstacles and alleviate neurodegenerative conditions**. **Journal of Drug Delivery Science and Technology**Editions de Sante, , 2022. DOI: 10.1016/j.jddst.2022.103656.

TANGUTUR, Anjana Devi; KUMAR, Dinesh; KRISHNA, Kommalapati Vamsi; KANTEVARI, Srinivas. Microtubule Targeting Agents as Cancer Chemotherapeutics: An Overview of Molecular Hybrids as Stabilizing and Destabilizing Agents. **Current Topics in Medicinal Chemistry**, *[S. l.]*, v. 17, p. 2523–2537, 2017. DOI: 10.2174/1568026617666170104.

TILLEY, Charles; LIPSON, Jana; RAMOS, Mark. **Palliative Wound Care for Malignant Fungating Wounds: Holistic Considerations at End-of-Life**. **Nursing Clinics of North America**W.B. Saunders, , 2016. DOI: 10.1016/j.cnur.2016.05.006.

WORLD HEALTH ORGANIZATION. **HIV/AIDS**. 2023. Disponível em: https://www.who.int/health-topics/hiv-aids/#tab=tab_1. Acesso em: 4 jan. 2023.

YUKUYAMA, Megumi Nishitani et al. Rational design of oral flubendazole-loaded nanoemulsion for brain delivery in cryptococcosis. **Colloids and Surfaces A: Physicochemical and Engineering Aspects**, *[S. l.]*, v. 630, 2021. DOI: 10.1016/j.colsurfa.2021.127631.

YUKUYAMA, Megumi Nishitani; ARAÚJO, Gabriel Lima Barros De; BOU-CHACRA, Nádia Araci. Nanomaterials for hair care applications. *Em*: **Nanocosmetics**. [s.l.] : Elsevier, 2020. p. 205–225. DOI: 10.1016/b978-0-12-822286-7.00010-3.

YUKUYAMA, Megumi Nishitani; OSELIERO, Pedro Leonidas Filho; KATO, Edna Tomiko Myiake; LOBËNBERG, Raimar; DE OLIVEIRA, Cristiano Luis Pinto; DE ARAUJO, Gabriel Lima Barros; BOU-CHACRA, Nadia Araci. High internal vegetable oil nanoemulsion: D-phase emulsification as a unique low energy process. **Colloids and Surfaces A: Physicochemical and Engineering Aspects**, *[S. l.]*, v. 554, p. 296–305, 2018. DOI: 10.1016/j.colsurfa.2018.06.023.

REFERENCES

(All sources)

Akhavan, S., Assadpour, E., Katouzian, I., Jafari, S.M., 2018. Lipid nano scale cargos for the protection and delivery of food bioactive ingredients and nutraceuticals. Trends Food Sci Technol. https://doi.org/10.1016/j.tifs.2018.02.001

Alexander, L.E.C., Shin, S., Hwang, J.H., 2015. Inflammatory diseases of the lung induced by conventional cigarette smoke a review. Chest 148, 1307–1322. https://doi.org/10.1378/chest.15-0409

al Durdunji, A., Alkhatib, H.S., Al-Ghazawi, M., 2016. Development of a biphasic dissolution test for Deferasirox dispersible tablets and its application in establishing an in vitro-in vivo correlation. European Journal of Pharmaceutics and Biopharmaceutics 102, 9–18. https://doi.org/10.1016/j.ejpb.2016.02.006

Al-Hallak, K.M.H.D., Azarmi, S., Anwar-Mohamed, A., Roa, W.H., Löbenberg, R., 2010. Secondary cytotoxicity mediated by alveolar macrophages: A contribution to the total efficacy of nanoparticles in lung cancer therapy? Eur. J. Pharm. Biopharm. 76, 112–119. https://doi.org/10.1016/j.ejpb.2010.05.002

Allegra, E., Titball, R.W., Carter, J., Champion, O.L., 2018. Galleria mellonella larvae allow the discrimination of toxic and non-toxic chemicals. Chemosphere 198, 469–472. https://doi.org/10.1016/j.chemosphere.2018.01.175

Altieri, D.C., 2017. Mitochondria on the move: Emerging paradigms of organelle trafficking in tumour plasticity and metastasis. Br J Cancer. https://doi.org/10.1038/bjc.2017.201

American Cancer Society, 2013. About Lung Cancer [WWW Document]. URL https://www.cancer.org/cancer/lung-cancer/about/what-is.html (accessed 11.6.22).

An, G., Murry, D.J., Gajurel, K., Bach, T., Deye, G., Stebounova, L. V., Codd, E.E., Horton, J., Gonzalez, A.E., Garcia, H.H., Ince, D., Hodgson-Zingman, D., Nomicos, E.Y.H., Conrad, T., Kennedy, J., Jones, W., Gilman, R.H., Winokur, P., 2019. Pharmacokinetics, safety, and tolerability of oxfendazole in healthy volunteers: A randomized, placebo-controlled first-inhuman single-dose escalation study. Antimicrob Agents Chemother 63. https://doi.org/10.1128/AAC.02255-18

Arrowsmith, J., 2011. Trial watch: Phase III and submission failures: 2007-2010. Nat Rev Drug Discov. https://doi.org/10.1038/nrd3375

Arrowsmith, J., Miller, P., 2013. Trial Watch: Phase II and Phase III attrition rates 2011-2012. Nat Rev Drug Discov. https://doi.org/10.1038/nrd4090

Bardaa, S., ben Halima, N., Aloui, F., ben Mansour, R., Jabeur, H., Bouaziz, M., Sahnoun, Z., 2016a. Oil from pumpkin (Cucurbita pepo L.) seeds: Evaluation of its functional properties on wound healing in rats. Lipids Health Dis 15. https://doi.org/10.1186/s12944-016-0237-0

Bardaa, S., Chabchoub, N., Jridi, M., Moalla, D., Mseddi, M., Rebai, T., Sahnoun, Z., 2016b. The effect of natural extracts on laser burn wound healing. Journal of Surgical Research 201, 464–472. https://doi.org/10.1016/j.jss.2015.11.052

Bazán Henostroza, M.A., Curo Melo, K.J., Nishitani Yukuyama, M., Löbenberg, R., Araci Bou-Chacra, N., 2020. Cationic rifampicin nanoemulsion for the treatment of ocular tuberculosis. Colloids Surf A Physicochem Eng Asp 597, 124755. https://doi.org/10.1016/j.colsurfa.2020.124755

Banerjees, A., Roach, M.C., Trcka, P., Luduena, R.F., 1992. Preparation of a Monoclonal Antibody Specific for the Class IV Isotype of βTubulin. Journal of Biological Chemistry 267, 5625–5630.

Barker, N., van Es. JH, Jaks, V., Kasper, M., Snippert, H., Toftgård, R., Clevers, H., 2008. Very long-term self-renewal of small intestine, colon, and hair follicles from cycling Lgr5+ve stem cells. Cold Spring Harb Symp Quant Biol. 73, 351–356. https://doi.org/10.1101/sqb.2008.72.003. PMID: 19478326

Bazylińska, U., Saczko, J., 2016. Nanoemulsion-templated polylelectrolyte multifunctional nanocapsules for DNA entrapment and bioimaging. Colloids Surf B Biointerfaces 137, 191–202. https://doi.org/10.1016/j.colsurfb.2015.07.056

Becelaere, J., van den Broeck, E., Schoolaert, E., Vanhoorne, V., van Guyse, J.F.R., Vergaelen, M., Borgmans, S., Creemers, K., van Speybroeck, V., Vervaet, C., Hoogenboom, R., de Clerck, K., 2022. Stable amorphous solid dispersion of flubendazole with high loading via electrospinning. Journal of Controlled Release 351, 123–136. https://doi.org/10.1016/j.jconrel.2022.09.028

Björnmalm, M., Thurecht, K.J., Michael, M., Scott, A.M., Caruso, F., 2017. Bridging Bio-Nano Science and Cancer Nanomedicine. ACS Nano 11, 9594–9613. https://doi.org/10.1021/acsnano.7b04855

Boldogh, I.R., Pon, L.A., 2007. Mitochondria on the move. Trends Cell Biol. https://doi.org/10.1016/j.tcb.2007.07.008

Bonferoni, M.C., Sandri, G., Dellera, E., Rossi, S., Ferrari, F., Mori, M., Caramella, C., 2014. Ionic polymeric micelles based on chitosan and fatty acids and intended for wound healing. Comparison of linoleic and oleic acid. European Journal of Pharmaceutics and Biopharmaceutics 87, 101–106. https://doi.org/10.1016/j.ejpb.2013.12.018

Borgas, D., Chambers, E., Newton, J., Ko, J., Rivera, S., Rounds, S., Lu, Q., 2016. Cigarette smoke disrupted lung endothelial barrier integrity and increased susceptibility to acute lung injury via histone deacetylase 6. Am J Respir Cell Mol Biol 54, 683–696. https://doi.org/10.1165/rcmb.2015-0149OC

Borys, F., Joachimiak, E., Krawczyk, H., Fabczak, H., 2020. Intrinsic and Extrinsic Factors Affecting Microtubule Dynamics in Normal and Cancer Cells. Molecules. https://doi.org/10.3390/molecules25163705

Braun, A., Worbs, T., Moschovakis, G.L., Halle, S., Hoffmann, K., Bölter, J., Münk, A., Förster, R., 2011. Afferent lymph-derived T cells and DCs use different chemokine receptor CCR7-dependent routes for entry into the lymph node and intranodal migration. Nat. Immunol. 12, 879–887. https://doi.org/10.1038/ni.2085

Cabral, H., Makino, J., Matsumoto, Y., Mi, P., Wu, H., Nomoto, T., Toh, K., Yamada, N., Higuchi, Y., Konishi, S., Kano, M.R., Nishihara, H., Miura, Y., Nishiyama, N., Kataoka, K., 2015. Systemic targeting of lymph node metastasis through the blood vascular system by using size-controlled nanocarriers. ACS Nano 9, 4957–4967. https://doi.org/10.1021/nn5070259

Cadete, A., Olivera, A., Besev, M., Dhal, P.K., Gonçalves, L., Almeida, A.J., Bastiat, G., Benoit, J.P., de la Fuente, M., Garcia-Fuentes, M., Alonso, M.J., Torres, D., 2019. Self-assembled hyaluronan nanocapsules for the intracellular delivery of anticancer drugs. Sci Rep 9. https://doi.org/10.1038/s41598-019-47995-8

Cai, S., Yang, Q., Bagby, T.R., Forrest, M.L., 2011. Lymphatic drug delivery using engineered liposomes and solid lipid nanoparticles. Adv Drug Deliv Rev. https://doi.org/10.1016/j.addr.2011.05.017

Castrogiovanni, C., Meraldi, P., 2022. Cell division: The science friction of chromosome attachment. Current Biology. https://doi.org/10.1016/j.cub.2022.05.045

Ceballos, L., Mackenzie, C., Geary, T., Alvarez, L., Lanusse, C., 2014. Exploring the Potential of Flubendazole in Filariasis Control: Evaluation of the Systemic Exposure for Different Pharmaceutical Preparations. PLoS Negl Trop Dis 8. https://doi.org/10.1371/journal.pntd.0002838

Chalikwar, S.S., Belgamwar, V.S., Talele, V.R., Surana, S.J., Patil, M.U., 2012. Formulation and evaluation of Nimodipine-loaded solid lipid nanoparticles delivered via lymphatic transport system. Colloids Surf B Biointerfaces 97, 109–116. https://doi.org/10.1016/j.colsurfb.2012.04.027

Champion, O.L., Wagley, S., Titball, R.W., 2016. Galleria mellonella as a model host for microbiological and toxin research. Virulence 7, 840–845. https://doi.org/10.1080/21505594.2016.1203486

Chan, D.C., 2012. Fusion and fission: Interlinked processes critical for mitochondrial health. Annu Rev Genet 46, 265–287. https://doi.org/10.1146/annurev-genet-110410-132529

Chapman, N., Abela-Oversteegen, L., Doubell, A., Chowdhary, V., Gurjav, U., Ong, M., 2017. NEGLECTED DISEASE RESEARCH AND DEVELOPMENT: A PIVOTAL MOMENT FOR GLOBAL HEALTH.

Chaudhary, S., Garg, T., Murthy, R.S.R., Rath, G., Goyal, A.K., 2014. Recent approaches of lipid-based delivery system for lymphatic targeting via oral route. J. Drug Target. 22, 871–882. https://doi.org/10.3109/1061186X.2014.950664

Chen, S.C.A., Meyer, W., Sorrell, T.C., 2014. Cryptococcus gattii infections. Clin Microbiol Rev 27, 980–1024. https://doi.org/10.1128/CMR.00126-13

Chen, S.C.A., Slavin, M.A., Heath, C.H., Geoffrey Playford, E., Byth, K., Marriott, D., Kidd, S.E., Bak, N., Currie, B., Hajkowicz, K., Korman, T.M., McBride, W.J.H., Meyer, W., Murray, R., Sorrell, T.C., 2012. Clinical manifestations of cryptococcus gattii infection: Determinants of neurological sequelae and death. Clinical Infectious Diseases 55, 789–798. https://doi.org/10.1093/cid/cis529

Chen, S., Tian, Y., Ju, A., Li, B., Fu, Y., Luo, Y., 2022. Suppression of CCT3 Inhibits Tumor Progression by Impairing ATP Production and Cytoplasmic Translation in Lung Adenocarcinoma. Int J Mol Sci 23. https://doi.org/10.3390/ijms23073983

Chen, Y., Li, T., 2015. Cellular Uptake Mechanism of Paclitaxel Nanocrystals Determined by Confocal Imaging and Kinetic Measurement. AAPS Journal 17, 1126–1134. https://doi.org/10.1208/s12248-015-9774-0

Chen, Y., Zhou, M., Gu, X., Wang, L., Wang, C., 2022. High Expression of TACC3 Is Associated with the Poor Prognosis and Immune Infiltration in Lung Adenocarcinoma Patients. Dis Markers 2022. https://doi.org/10.1155/2022/8789515

Cheng, L., Wang, Y., Huang, L., 2017. Exosomes from M1-Polarized Macrophages Potentiate the Cancer Vaccine by Creating a Pro-inflammatory Microenvironment in the Lymph Node. Mol. Ther. 25, 1665–1675. https://doi.org/10.1016/j.ymthe.2017.02.007

Cheng, Y., Ji, Y., 2020. Mitochondria-targeting nanomedicine self-assembled from GSH-responsive paclitaxel-ss-berberine conjugate for synergetic cancer treatment with enhanced cytotoxicity. Journal of Controlled Release 318, 38–49. https://doi.org/10.1016/j.jconrel.2019.12.011

Choi, G., Le, T.H., Shin, S., 2016. A new multidimensional design space identification method for a quality-oriented drug development process. Total Quality Management and Business Excellence 27, 804–817. https://doi.org/10.1080/14783363.2016.1187999

Choudhury, H., Pandey, M., Gorain, B., Chatterjee, B., Madheswaran, T., Md, S., Mak, K.-K., Tambuwala, M., Chourasia, M.K., Kesharwani, P., 2019. Nanoemulsions as Effective Carriers for the Treatment of Lung Cancer, in: Nanotechnology-Based Targeted Drug Delivery Systems for Lung Cancer. Elsevier, pp. 217–247. https://doi.org/10.1016/b978-0-12-815720-6.00009-5

Chowdhary, A., Randhawa, H., Boekhout, T., Hagen, F., Klaassen, C., Meis, J., 2012. Temperate climate niche for Cryptococcus gattii in Northern Europe. Emerg Infect Dis. https://doi.org/10.3201/eid1801.111190

Coelho, C., Bocca, A.L., Casadevall, A., 2014. The Tools for Virulence of Cryptococcus neoformans, in: Advances in Applied Microbiology. Academic Press Inc., pp. 1–41. https://doi.org/10.1016/B978-0-12-800261-2.00001-3

Cohen, J.P., Sturgeon, G., Cohen, A., 2014. Measuring progress in neglected disease drug development. Clin Ther 36, 1037–1042. https://doi.org/10.1016/j.clinthera.2014.05.004

Das, T., Anand, U., Pandey, S.K., Ashby, C.R., Assaraf, Y.G., Chen, Z.S., Dey, A., 2021. Therapeutic strategies to overcome taxane resistance in cancer. Drug Resistance Updates 55. https://doi.org/10.1016/j.drup.2021.100754

Davis, S.S., Purewal, T., Round, H.P., 1979. OSTWALD RIPENING IN EMULSION SYSTEMS. THE EFFECT OF AN ADDED THIRD COMPONENT. Journal of Pharmacy and Pharmacology 31, 4P-4P. https://doi.org/10.1111/j.2042-7158.1979.tb11552.x

Dayan, A.D., 2003. Albendazole, mebendazole and praziquantel. Review of non-clinical toxicity and pharmacokinetics, in: Acta Tropica. Elsevier, pp. 141–159. https://doi.org/10.1016/S0001-706X(03)00031-7

De Araujo, G.L.B., Ferreira, F.F., Bernardes, C.E.S., Sato, J.A.P., Gil, O.M., De Faria, D.L.A., Loebenberg, R., Byrn, S.R., Ghisleni, D.D.M., Bou-Chacra, N.A., Pinto, T.J.A., Antonio, S.G., Ferraz, H.G., Zemlyanov, D., Gonçalves, D.S., Minas Da Piedade, M.E., 2018. A New Thermodynamically Favored Flubendazole/Maleic Acid Binary Crystal Form: Structure,

Energetics, and in Silico PBPK Model-Based Investigation. Cryst Growth Des 18, 2377–2386. https://doi.org/10.1021/acs.cgd.7b01807

de Assis, J.M.C., Barbosa, E.J., Bezzon, V.D.N., Lourenço, F.R., Carvalho, F.M.S., Matos, J.R., Araci Bou-Chacra, N., Benmore, C.J., Byrn, S.R., Costa, F.N., de Araujo, G.L.B., 2022. Hot-melt extrudability of amorphous solid dispersions of flubendazole-copovidone: An exploratory study of the effect of drug loading and the balance of adjuvants on extrudability and dissolution. Int J Pharm 614. https://doi.org/10.1016/j.ijpharm.2022.121456

De Koker, S., Cui, J., Vanparijs, N., Albertazzi, L., Grooten, J., Caruso, F., De Geest, B.G., 2016. Engineering Polymer Hydrogel Nanoparticles for Lymph Node-Targeted Delivery. Angew. Chemie - Int. Ed. 55, 1334–1339. https://doi.org/10.1002/anie.201508626

Deng, J., Staufenbiel, S., Hao, S., Wang, B., Dashevskiy, A., Bodmeier, R., 2017. Development of a discriminative biphasic in vitro dissolution test and correlation with in vivo pharmacokinetic studies for differently formulated racecadotril granules. Journal of Controlled Release 255, 202–209. https://doi.org/10.1016/j.jconrel.2017.04.034

Deng, X., Jia, G., Wang, H., Sun, H., Wang, X., Yang, S., Wang, T., Liu, Y., 2007. Translocation and fate of multi-walled carbon nanotubes in vivo. Carbon N Y 45, 1419–1424. https://doi.org/10.1016/j.carbon.2007.03.035

Denninger, A., Westedt, U., Rosenberg, J., Wagner, K.G., 2020. A rational design of a biphasic dissolution setup—modelling of biorelevant kinetics for a ritonavir hot-melt extruded amorphous solid dispersion. Pharmaceutics 12. https://doi.org/10.3390/pharmaceutics12030237

Desai, J., Thakkar, H., 2019. Enhanced oral bioavailability and brain uptake of Darunavir using lipid nanoemulsion formulation. Colloids Surf B Biointerfaces 175, 143–149. https://doi.org/10.1016/j.colsurfb.2018.11.057

de Souza Gonçalves, D., Yukuyama, M.N., Miyagi, M.Y.S., Silva, T.J.V., Lameu, C., Bou-Chacra, N.A., de Araujo, G.L.B., 2022. Revisiting Flubendazole Through Nanocrystal Technology: Statistical Design, Characterization and Its Potential Inhibitory Effect on Xenografted Lung Tumor Progression in Mice. J Clust Sci. https://doi.org/10.1007/s10876-022-02220-x

Dieterich, L.C., Detmar, M., 2016. Tumor lymphangiogenesis and new drug development. Adv. Drug Deliv. Rev. 99, 148–160. https://doi.org/10.1016/j.addr.2015.12.011

DiMasi, J.A., Grabowski, H.G., Hansen, R.W., 2016. Innovation in the pharmaceutical industry: New estimates of R&D costs. J Health Econ 47, 20–33. https://doi.org/10.1016/j.jhealeco.2016.01.012

Dixon, J.B., 2010. Lymphatic lipid transport: Sewer or subway? Trends in Endocrinology and Metabolism. https://doi.org/10.1016/j.tem.2010.04.003

Dominguez-Vazquez, A., Taylor, H.R., Ruvalcaba-Macias, A.M., Murphy, R.P., Greene, B.M., Rivas-Alcala, A.R., Beltran-Hernandez, F., 1983. COMPARISON OF FLUBENDAZOLE AND DIETHYLCARBAMAZINE IN TREATMENT OF ONCHOCERCIASIS. The Lancet 321, 139–143.

Dong, X., Wang, W., Qu, H., Han, D., Zheng, J., Sun, G., 2016. Targeted delivery of doxorubicin and vincristine to lymph cancer: evaluation of novel nanostructured lipid carriers in vitro and in vivo. Drug Deliv. 23, 1374–1378. https://doi.org/10.3109/10717544.2015.1041580

Dordević, S.M., Cekić, N.D., Savić, M.M., Isailović, T.M., Randelović, D. V., Marković, B.D., Savić, S.R., Stamenić, T.T., Daniels, R., Savić, S.D., 2015. Parenteral nanoemulsions as promising carriers for brain delivery of risperidone: Design, characterization and in vivo pharmacokinetic evaluation. Int J Pharm 493, 40–54. https://doi.org/10.1016/j.ijpharm.2015.07.007

Dutour-Provenzano, G., Etienne-Manneville, S., 2021. Intermediate filaments. Current Biology R522–R529.

Edmond, J., 2001. Essential polyunsaturated fatty acids and the barrier to the brain: The components of a model for transport. Journal of Molecular Neuroscience 16, 181–193. https://doi.org/10.1385/JMN:16:2-3:181

Effendi, W.I., Nagano, T., Tachihara, M., Umezawa, K., Kiriu, T., Dokuni, R., Katsurada, M., Yamamoto, M., Kobayashi, K., Nishimura, Y., 2019. Synergistic interaction of gemcitabine and paclitaxel by modulating acetylation and polymerization of tubulin in non-small cell lung cancer cell lines. Cancer Manag Res 11, 3669–3679. https://doi.org/10.2147/CMAR.S193789

Ema, M., Gamo, M., Honda, K., 2016. A review of toxicity studies of single-walled carbon nanotubes in laboratory animals. Regulatory Toxicology and Pharmacology 74, 42–63. https://doi.org/10.1016/j.yrtph.2015.11.015

Endoo, M., Sagitani, H., 1991. Preparation of Triglyceride O/W Emulsions by D Phase Emulsification. J. Oil Sci. 40, 133–139. https://doi.org/10.5650/jos1956.40.133

Evans, T.C., Gavrilovich, E., Mihai, R.C., Isbasescu, I., Thelen, D., Martin, J.A., Slane, S.S., 2014. (12) Patent Application Publication (10) Pub . No .: US 2006/0222585 A1 Figure 1.

Fan, X., Shi, S., He, J., Deng, J., Ji, J., 2021. Development of in vivo predictive ph-gradient biphasic dissolution test for weakly basic drugs: Optimization by orthogonal design. Dissolut Technol 28, 24–29. https://doi.org/10.14227/DT280321P24

Fang, D., Maldonado, E.N., 2018. VDAC Regulation: A Mitochondrial Target to Stop Cell Proliferation, in: Advances in Cancer Research. Academic Press Inc., pp. 41–69. https://doi.org/10.1016/bs.acr.2018.02.002

Farhadi, M., Haniloo, A., Rostamizadeh, K., Faghihzadeh, S., 2018. Efficiency of flubendazole-loaded mPEG-PCL nanoparticles: A promising formulation against the protoscoleces and cysts of Echinococcus granulosus. Acta Trop 187, 190–200. https://doi.org/10.1016/j.actatropica.2018.08.010

Fink-Neuboeck, N., Lindenmann, J., Porubsky, C., Fediuk, M., Anegg, U., Maier, A., Smolle, J., Lamont, E., Smolle-Juettner, F.M., 2020. Hazards of Recurrence, Second Primary, or Other Tumor at Ten Years After Surgery for Non–Small-Cell Lung Cancer. Clin Lung Cancer 21, 333–340. https://doi.org/10.1016/j.cllc.2020.02.011

Firmino, F., Meira, K.C., Junior, V.A., Santos, V.L.C. de G., 2020. Regenerated oxidised cellulose versus calcium alginate in controlling bleeding from malignant breast cancer wounds: randomised control trial study protocol. J Wound Care 29, 52–60. https://doi.org/10.12968/jowc.2020.29.1.52

Firmino, F., Villela-Castro, D.L., Santos, J. dos, Conceição de Gouveia Santos, V.L., 2021. Topical Management of Bleeding From Malignant Wounds Caused by Breast Cancer: A Systematic Review. J Pain Symptom Manage. https://doi.org/10.1016/j.jpainsymman.2020.10.020

Fisher, M.C., Henk, D.A., Briggs, C.J., Brownstein, J.S., Madoff, L.C., McCraw, S.L., Gurr, S.J., 2012. Emerging fungal threats to animal, plant and ecosystem health. Nature. https://doi.org/10.1038/nature10947

Formica, M.L., Real, D.A., Picchio, M.L., Catlin, E., Donnelly, R.F., Paredes, A.J., 2022. On a highway to the brain: A review on nose-to-brain drug delivery using nanoparticles. Appl Mater Today. https://doi.org/10.1016/j.apmt.2022.101631

Food & Drug Administration, U.S., 2014. Guidance for industry considering whether an FDA-regulated product involves the application of nanotechnology. Biotechnol Law Rep 30, 613–616. https://doi.org/10.1089/blr.2011.9814

Frenkel, M., Mandelblat, M., Alastruey-Izquierdo, A., Mendlovic, S., Semis, R., Segal, E., 2016. Pathogenicity of Candida albicans isolates from bloodstream and mucosal candidiasis assessed in

mice and Galleria mellonella. J Mycol Med 26, 1–8. https://doi.org/10.1016/j.mycmed.2015.12.006

Fromen, C.A., Rahhal, T.B., Robbins, G.R., Kai, M.P., Shen, T.W., Luft, J.C., DeSimone, J.M., 2016. Nanoparticle surface charge impacts distribution, uptake and lymph node trafficking by pulmonary antigen-presenting cells. Nanomedicine Nanotechnology, Biol. Med. 12, 677–687. https://doi.org/10.1016/j.nano.2015.11.002

Ganta, S., Singh, A., Patel, N.R., Cacaccio, J., Rawal, Y.H., Davis, B.J., Amiji, M.M., Coleman, T.P., 2014a. Development of egfr-targeted nanoemulsion for imaging and novel platinum therapy of ovarian cancer. Pharm Res 31, 2490–2502. https://doi.org/10.1007/s11095-014-1345-z

Ganta, S., Talekar, M., Singh, A., Coleman, T.P., Amiji, M.M., 2014b. Nanoemulsions in translational research - Opportunities and challenges in targeted cancer therapy. AAPS PharmSciTech. https://doi.org/10.1208/s12249-014-0088-9

Ganti, S.N., Albershardt, T.C., Iritani, B.M., Ruddell, A., 2015. Regulatory B cells preferentially accumulate in tumor-draining lymph nodes and promote tumor growth. Sci. Rep. 5, 1–8. https://doi.org/10.1038/srep12255

Gao, F., Zhang, Z., Bu, H., Huang, Y., Gao, Z., Shen, J., Zhao, C., Li, Y., 2011. Nanoemulsion improves the oral absorption of candesartan cilexetil in rats: Performance and mechanism. Journal of Controlled Release 149, 168–174. https://doi.org/10.1016/j.jconrel.2010.10.013

Gao, Y., Zuo, J., Bou-Chacra, N., Pinto, T.D.J.A., Clas, S.D., Walker, R.B., Löbenberg, R., 2013. In vitro release kinetics of antituberculosis drugs from nanoparticles assessed using a modified dissolution apparatus. Biomed Res Int 2013. https://doi.org/10.1155/2013/136590

Gao, Z., Ma, T., Zhao, E., Docter, D., Yang, W., Stauber, R.H., Gao, M., 2016. Small is Smarter: Nano MRI Contrast Agents - Advantages and Recent Achievements. Small 12, 556–576. https://doi.org/10.1002/smll.201502309

Garcia-Oliveira, P., Otero, P., Pereira, A.G., Chamorro, F., Carpena, M., Echave, J., Fraga-Corral, M., Simal-Gandara, J., Prieto, M.A., 2021. Status and challenges of plant-anticancer compounds in cancer treatment. Pharmaceuticals. https://doi.org/10.3390/ph14020157

Gharooni, M., Alikhani, A., Moghtaderi, H., Abiri, H., Mashaghi, A., Abbasvandi, F., Khayamian, M.A., Miripour, Z.S., Zandi, A., Abdolahad, M., 2019. Bioelectronics of the cellular cytoskeleton: Monitoring cytoskeletal conductance variation for sensing drug resistance. ACS Sens 4, 353–362. https://doi.org/10.1021/acssensors.8b01142

Glasgow, W.C., Eling, T.E., 1990. Epidermal growth factor stimulates linoleic acid metabolism in BALB/c 3T3 fibroblasts. Mol Pharmacol 38, 503–510.

Gong, F., Wang, R., Zhu, Z., Duan, J., Teng, X., Cui, Z.K., 2020. Drug-interactive mPEG-b-PLA-Phe(Boc) micelles enhance the tolerance and anti-tumor efficacy of docetaxel. Drug Deliv 27, 238–247. https://doi.org/10.1080/10717544.2020.1718245

Gorain, B., Bhattamishra, S.K., Choudhury, H., Nandi, U., Pandey, M., Kesharwani, P., 2019. Overexpressed Receptors and Proteins in Lung Cancer, Nanotechnology-Based Targeted Drug Delivery Systems for Lung Cancer. Elsevier Inc. https://doi.org/10.1016/b978-0-12-815720-6.00003-4

Gu, Y., Liu, Y., Fu, L., Zhai, L., Zhu, J., Han, Y., Jiang, Y., Zhang, Y., Zhang, P., Jiang, Z., Zhang, X., Cao, X., 2019. Tumor-educated B cells selectively promote breast cancer lymph node metastasis by HSPA4-targeting IgG. Nat. Med. 25, 312–322. https://doi.org/10.1038/s41591-018-0309-y

Gutiérrez, J.M., González, C., Maestro, A., Solè, I., Pey, C.M., Nolla, J., 2008. Nano-emulsions: New applications and optimization of their preparation. Curr Opin Colloid Interface Sci. https://doi.org/10.1016/j.cocis.2008.01.005

Hamdy, S., Haddadi, A., Hung, R.W., Lavasanifar, A., 2011. Targeting dendritic cells with nano-particulate PLGA cancer vaccine formulations. Adv. Drug Deliv. Rev. 63, 943–955. https://doi.org/10.1016/j.addr.2011.05.021

Han, H.M., Ko, S., Cheong, M.-J., Bang, J.K., Seo, C.H., Luchian, T., Park, Y., 2017. Myxinidin2 and myxinidin3 suppress inflammatory responses through STAT3 and MAPKs to promote wound healing. Oncotarget 8, 87582–87597. https://doi.org/10.18632/oncotarget.20908

Harris, J.R., Lockhart, S.R., Debess, E., Marsden-Haug, N., Goldoft, M., Wohrle, R., Lee, S., Smelser, C., Park, B., Chiller, T., 2011. Cryptococcus gattii in the united states: Clinical aspects of infection with an emerging pathogen. Clinical Infectious Diseases 53, 1188–1195. https://doi.org/10.1093/cid/cir723

Harris, J.R., Lockhart, S.R., Sondermeyer, G., Vugia, D.J., Crist, M.B., D'Angelo, M.T., Sellers, B., Franco-Paredes, C., Makvandi, M., Smelser, C., Greene, J., Stanek, D., Signs, K., Nett, R.J., Chiller, T., Park, B.J., 2013. Cryptococcus gattii infections in multiple states outside the US Pacific Northwest. Emerg Infect Dis 19, 1620–1626. https://doi.org/10.3201/eid1910.130441

Heigoldt, U., Sommer, F., Daniels, R., Wagner, K.G., 2010. Predicting in vivo absorption behavior of oral modified release dosage forms containing pH-dependent poorly soluble drugs using a novel

pH-adjusted biphasic in vitro dissolution test. European Journal of Pharmaceutics and Biopharmaceutics 76, 105–111. https://doi.org/10.1016/j.ejpb.2010.05.006

Herishanu, Y., Pérez-Galán, P., Liu, D., Biancotto, A., Pittaluga, S., Vire, B., Gibellini, F., Njuguna, N., Lee, E., Stennett, L., Raghavachari, N., Liu, P., McCoy, J.P., Raffeld, M., Stetler-Stevenson, M., Yuan, C., Sherry, R., Arthur, D.C., Maric, I., White, T., Marti, G.E., Munson, P., Wilson, W.H., Wiestner, A., 2011. The lymph node microenvironment promotes B-cell receptor signaling, NF-κB activation, and tumor proliferation in chronic lymphocytic leukemia. Blood 117, 563–574. https://doi.org/10.1182/blood-2010-05-284984

Hevia, L.G., Fanarraga, M.L., 2020. Microtubule cytoskeleton-disrupting activity of MWCNTs: applications in cancer treatment. J Nanobiotechnology. https://doi.org/10.1186/s12951-020-00742-y

Hou, Z.-J., Luo, X., Zhang, W., Peng, F., Cui, B., Wu, S.-J., Zheng, F.-M., Xu, J., Xu, L.-Z., Long, Z.-J., Wang, X.-T., Li, G.-H., Wan, X.-Y., Yang, Y.-L., Liu, Q., 2015. Flubendazole, FDA-approved anthelmintic, targets breast cancer stem-like cells. Oncotarget 6, 6326–6340. https://doi.org/10.18632/oncotarget.3436

Hoveizi, E., Fakharzadeh Jahromi, F., 2020. Cytotoxic Effects of Flubendazole in Human Lung Cancer Cell Line A549. Jentashapir Journal of Cellular and Molecular Biology 11. https://doi.org/10.5812/jjcmb.108923

Hu, Q., Wu, Y., Tang, J., Zheng, W., Wang, Q., Nahirney, D., Duszyk, M., Wang, S., Tu, J.C., Chen, X.Z., 2014. Expression of polycystins and fibrocystin on primary cilia of lung cells. Biochemistry and Cell Biology 92, 547–554. https://doi.org/10.1139/bcb-2014-0062

Huang, Z.R., Tipparaju, S.K., Kirpotin, D.B., Pien, C., Kornaga, T., Noble, C.O., Koshkaryev, A., Tran, J., Kamoun, W.S., Drummond, D.C., 2019. Formulation optimization of an ephrin A2 targeted immunoliposome encapsulating reversibly modified taxane prodrugs. Journal of Controlled Release 310, 47–57. https://doi.org/10.1016/j.jconrel.2019.08.006

Hull, C.M., Heitman, J., 2002. Genetics of Cryptococcus neoformans. Annu Rev Genet. https://doi.org/10.1146/annurev.genet.36.052402.152652

Huynh, J., Chand, A., Gough, D., Ernst, M., 2019. Therapeutically exploiting STAT3 activity in cancer — using tissue repair as a road map. Nat Rev Cancer. https://doi.org/10.1038/s41568-018-0090-8

Ilan, Y., 2022. Microtubules as a potential platform for energy transfer in biological systems: a target for implementing individualized, dynamic variability patterns to improve organ function. Mol Cell Biochem. https://doi.org/10.1007/s11010-022-04513-1

Imran, M., Saleem, S., Chaudhuri, A., Ali, J., Baboota, S., 2020. Docetaxel: An update on its molecular mechanisms, therapeutic trajectory and nanotechnology in the treatment of breast, lung and prostate cancer. J Drug Deliv Sci Technol. https://doi.org/10.1016/j.jddst.2020.101959

Ishikawa, T., 2017. Axoneme structure from motile cilia. Cold Spring Harb Perspect Biol 9. https://doi.org/10.1101/cshperspect.a028076

Islan, G.A., Durán, M., Cacicedo, M.L., Nakazato, G., Kobayashi, R.K.T., Martinez, D.S.T., Castro, G.R., Durán, N., 2017. Nanopharmaceuticals as a solution to neglected diseases: Is it possible? Acta Trop. https://doi.org/10.1016/j.actatropica.2017.02.019

Izquierdo, P., Esquena, J., Tadros, T.F., Dederen, J.C., Feng, J., Garcia-Celma, M.J., Azemar, N., Solans, C., 2004. Phase behavior and nano-emulsion formation by the phase inversion temperature method. Langmuir 20, 6594–6598. https://doi.org/10.1021/la049566h

Jahchan, N.S., Dudley, J.T., Mazur, P.K., Flores, N., Yang, D., Palmerton, A., Zmoos, A.F., Vaka, D., Tran, K.Q.T., Zhou, M., Krasinska, K., Riess, J.W., Neal, J.W., Khatri, P., Park, K.S., Butte, A.J., Sage, J., 2013. A drug repositioning approach identifies tricyclic antidepressants as inhibitors of small cell lung cancer and other neuroendocrine tumors. Cancer Discov 3, 1364–1377. https://doi.org/10.1158/2159-8290.CD-13-0183

Jafari, H., Yazdi, M.H., Fakhrabadi, M.M.S., 2020. Damping effects on wave-propagation characteristics of microtubule-based bio-nano-metamaterials. Int J Mech Sci 184. https://doi.org/10.1016/j.ijmecsci.2020.105844

Jafari, H., Yazdi, M.R.H., Fakhrabadi, M.M.S., 2019. Wave propagation in microtubule-based bio-nano-architected networks: A lesson from nature. Int J Mech Sci 164. https://doi.org/10.1016/j.ijmecsci.2019.105175

Jain, H., Dalvi, H., Bhat, A., Agrawal, A., Madan, J., Singh, P.K., Mehra, N.K., Singh, S.B., Srivastava, S., 2022. Nanomaterials in nose-to-brain delivery, in: Multifunctional Nanocarriers. Elsevier, pp. 379–400. https://doi.org/10.1016/b978-0-323-85041-4.00016-0

Jain, R., Javidan-Nejad, C., Alexander-Brett, J., Horani, A., Cabellon, M.C., Walter, M.J., Brody, S.L., 2012. Sensory functions of motile cilia and implication for bronchiectasis. Front Biosci 4, 1088–1098.

Jankovic, S., O'Dwyer, P.J., Box, K.J., Imanidis, G., Reppas, C., Kuentz, M., 2019. Biphasic drug release testing coupled with diffusing wave spectroscopy for mechanistic understanding of solid dispersion performance. European Journal of Pharmaceutical Sciences 137. https://doi.org/10.1016/j.ejps.2019.105001

Jiang, H., Yu, X.M., Zhou, X.M., Wang, X.H., Su, D., 2013. Correlation between microtubule-associated gene expression and chemosensitivity of patients with stage II non-small cell lung cancer. Exp Ther Med 5, 1506–1510. https://doi.org/10.3892/etm.2013.1007

Jin, G., Wong, S.T.C., 2014. Toward better drug repositioning: Prioritizing and integrating existing methods into efficient pipelines. Drug Discov Today. https://doi.org/10.1016/j.drudis.2013.11.005

Jin, X., Wang, Z., Qiu, L., Zhang, D., Guo, Z., Gao, Z., Deng, C., Wang, F., Wang, S., Guo, C., 2008. Potential biomarkers involving IKK/RelA signal in early stage non-small cell lung cancer. Cancer Sci 99, 582–589. https://doi.org/10.1111/j.1349-7006.2007.00713.x

Joffe, L.S., Schneider, R., Lopes, W., Azevedo, R., Staats, C.C., Kmetzsch, L., Schrank, A., Poeta, M. Del, Vainstein, M.H., Rodrigues, M.L., 2017. The anti-helminthic compound mebendazole has multiple antifungal effects against Cryptococcus neoformans. Front Microbiol 8, 1–14. https://doi.org/10.3389/fmicb.2017.00535

Kabal'nov, A.S., Pertzov, A. v, Shchukin, E.D., 1987. Ostwald Ripening in Two-Component Disperse Phase Systems: Application to Emulsion Stability. Elsevier Science Publishers B.V.

Kalra, A.P., Eakins, B.B., Vagin, S.I., Wang, H., Patel, S.D., Winter, P., Aminpour, M., Lewis, J.D., Rezania, V., Shankar, K., Scholes, G.D., Tuszynski, J.A., Rieger, B., Meldrum, A., 2022. A Nanometric Probe of the Local Proton Concentration in Microtubule-Based Biophysical Systems. Nano Lett 22, 517–523. https://doi.org/10.1021/acs.nanolett.1c04487

Kanakkanthara, A., Miller, J.H., 2021. βIII-tubulin overexpression in cancer: Causes, consequences, and potential therapies. Biochim Biophys Acta Rev Cancer. https://doi.org/10.1016/j.bbcan.2021.188607

Kang, S., Ahn, S., Lee, J., Kim, J.Y., Choi, M., Gujrati, V., Kim, H., Kim, J., Shin, E.C., Jon, S., 2017. Effects of gold nanoparticle-based vaccine size on lymph node delivery and cytotoxic T-lymphocyte responses. J. Control. Release 256, 56–67. https://doi.org/10.1016/j.jconrel.2017.04.024

Karin, M., Greten, F.R., 2005. NF-κB: Linking inflammation and immunity to cancer development and progression. Nat Rev Immunol. https://doi.org/10.1038/nri1703

Karnezis, T., Shayan, R., Caesar, C., Roufail, S., Harris, N.C., Ardipradja, K., Zhang, Y.F., Williams, S.P., Farnsworth, R.H., Chai, M.G., Rupasinghe, T.W.T., Tull, D.L., Baldwin, M.E., Sloan, E.K., Fox, S.B., Achen, M.G., Stacker, S.A., 2012. VEGF-D Promotes Tumor Metastasis by Regulating Prostaglandins Produced by the Collecting Lymphatic Endothelium. Cancer Cell 21, 181–195. https://doi.org/10.1016/j.ccr.2011.12.026

Kato, S., Mori, S., Kodama, T., 2015a. A novel treatment method for lymph node metastasis using a lymphatic drug delivery system with nano/microbubbles and ultrasound. J. Cancer 6, 1282–1294. https://doi.org/10.7150/jca.13028

Kato, S., Shirai, Y., Kanzaki, H., Sakamoto, M., Mori, S., Kodama, T., 2015b. Delivery of Molecules to the Lymph Node via Lymphatic Vessels Using Ultrasound and Nano/Microbubbles. Ultrasound Med. Biol. 41, 1411–1421. https://doi.org/10.1016/j.ultrasmedbio.2014.12.014

Katsetos, C.D., Herman, M.M., Mörk, S.J., 2003. Class III β-tubulin in human development and cancer. Cell Motil Cytoskeleton. https://doi.org/10.1002/cm.10116

Khames, A., 2019. Formulation and characterization of eplerenone nanoemulsion liquisolids, an oral delivery system with higher release rate and improved bioavailability. Pharmaceutics 11. https://doi.org/10.3390/pharmaceutics11010040

Khan, I., Bahuguna, A., Bhardwaj, M., Pal Khaket, T., Kang, S.C., 2018a. Carvacrol nanoemulsion evokes cell cycle arrest, apoptosis induction and autophagy inhibition in doxorubicin resistant-A549 cell line. Artif Cells Nanomed Biotechnol 46, 664–675. https://doi.org/10.1080/21691401.2018.1434187

Khan, I., Bahuguna, A., Kumar, P., Bajpai, V.K., Kang, S.C., 2018b. In vitro and in vivo antitumor potential of carvacrol nanoemulsion against human lung adenocarcinoma A549 cells via mitochondrial mediated apoptosis. Sci Rep 8. https://doi.org/10.1038/s41598-017-18644-9

Khémiri, I., Essghaier Hédi, B., Sadfi Zouaoui, N., ben Gdara, N., Bitri, L., 2019. The Antimicrobial and Wound Healing Potential of Opuntia ficus indica L. inermis Extracted Oil from Tunisia. Evidence-based Complementary and Alternative Medicine 2019. https://doi.org/10.1155/2019/9148782

Khwaja, S., Kumar, K., Das, R., Negi, A.S., 2021. Microtubule associated proteins as targets for anticancer drug development. Bioorg Chem. https://doi.org/10.1016/j.bioorg.2021.105320

Kim, S.Y., Noh, Y.W., Kang, T.H., Kim, J.E., Kim, S., Um, S.H., Oh, D.B., Park, Y.M., Lim, Y.T., 2017. Synthetic vaccine nanoparticles target to lymph node triggering enhanced innate and

adaptive antitumor immunity. Biomaterials 130, 56–66. https://doi.org/10.1016/j.biomaterials.2017.03.034

Kodama, T., Matsuki, D., Tada, A., Takeda, K., Mori, S., 2016. New concept for the prevention and treatment of metastatic lymph nodes using chemotherapy administered via the lymphatic network. Sci. Rep. 6, 1–8. https://doi.org/10.1038/srep32506

Kojima, M., Gimenes-Junior, J.A., Chan, T.W., Eliceiri, B.P., Baird, A., Costantini, T.W., Coimbra, R., 2018. Exosomes in postshock mesenteric lymph are key mediators of acute lung injury triggering the macrophage activation via Toll-like receptor 4. FASEB J. 32, 97–110. https://doi.org/10.1096/fj.201700488R

Komohara, Y., Ohnishi, K., Takeya, M., 2017. Possible functions of CD169-positive sinus macrophages in lymph nodes in anti-tumor immune responses. Cancer Sci. 108, 290–295. https://doi.org/10.1111/cas.13137

Kopecká, M., 2016. Microtubules and Actin Cytoskeleton of Cryptococcus neoformans as Targets for Anticancer Agents to Potentiate a Novel Approach for New Antifungals. Chemotherapy 61, 117–121. https://doi.org/10.1159/000437134

Kopecká, M., 2014. Effects of microtubule and actin inhibitors on cryptococcus neoformans examined by scanning and transmission electron microscopy. Chemotherapy 60, 99–106. https://doi.org/10.1159/000371413

Kotta, S., Khan, A.W., Ansari, S.H., Sharma, R.K., Ali, J., 2015. Formulation of nanoemulsion: A comparison between phase inversion composition method and high-pressure homogenization method. Drug Deliv 22, 455–466. https://doi.org/10.3109/10717544.2013.866992

Králová, V., Hanušová, V., Staňková, P., Knoppová, K., Čáňová, K., Skálová, L., 2013. Antiproliferative effect of benzimidazole anthelmintics albendazole, ricobendazole, and flubendazole in intestinal cancer cell lines. Anticancer Drugs 24, 911–919. https://doi.org/10.1097/CAD.0b013e3283648c69

Kratzer, E., Tian, Y., Sarich, N., Wu, T., Meliton, A., Leff, A., Birukova, A.A., 2012. Oxidative stress contributes to lung injury and barrier dysfunction via microtubule destabilization. Am J Respir Cell Mol Biol 47, 688–697. https://doi.org/10.1165/rcmb.2012-0161OC

Kreuter, J., 2012. Nanoparticulate systems for brain delivery of drugs. Adv Drug Deliv Rev 64, 213–222. https://doi.org/10.1016/j.addr.2012.09.015

Kronstad, J.W., Attarian, R., Cadieux, B., Choi, J., D'Souza, C.A., Griffiths, E.J., Geddes, J.M.H., Hu, G., Jung, W.H., Kretschmer, M., Saikia, S., Wang, J., 2011. Expanding fungal pathogenesis: Cryptococcus breaks out of the opportunistic box. Nat Rev Microbiol 9, 193–203. https://doi.org/10.1038/nrmicro2522

Kubíček, V., Skálová, L., Skarka, A., Králová, V., Holubová, J., Štěpánková, J., Šubrt, Z., Szotáková, B., 2019. Carbonyl reduction of flubendazole in the human liver: Strict stereospecificity, sex difference, low risk of drug interactions. Front Pharmacol 10. https://doi.org/10.3389/fphar.2019.00600

Lachau-Durand, S., Lammens, L., van der Leede, B.J., van Gompel, J., Bailey, G., Engelen, M., Lampo, A., 2019. Preclinical toxicity and pharmacokinetics of a new orally bioavailable flubendazole formulation and the impact for clinical trials and risk/benefit to patients. PLoS Neglected Tropical Diseases. 13. https://doi.org/10.1371/journal.pntd.0007026.

Lallemand, F., Daull, P., Benita, S., Buggage, R., Garrigue, J.-S., 2012. Successfully Improving Ocular Drug Delivery Using the Cationic Nanoemulsion, Novasorb. J Drug Deliv 2012, 1–16. https://doi.org/10.1155/2012/604204

Lawrence, D.S., Boyer-Chammard, T., Jarvis, J.N., 2019. Emerging concepts in HIV-associated cryptococcal meningitis. Curr Opin Infect Dis. https://doi.org/10.1097/QCO.0000000000000514

Lee, B.R., Ko, H.K., Ryu, J.H., Ahn, K.Y., Lee, Y.H., Oh, S.J., Na, J.H., Kim, T.W., Byun, Y., Kwon, I.C., Kim, K., Lee, J., 2016. Engineered Human Ferritin Nanoparticles for Direct Delivery of Tumor Antigens to Lymph Node and Cancer Immunotherapy. Sci. Rep. 6, 1–12. https://doi.org/10.1038/srep35182

Lee, W.D., Liang, Y.J., Chen, B.H., 2016. Effects of tanshinone nanoemulsion and extract on inhibition of lung cancer cells A549. Nanotechnology 27. https://doi.org/10.1088/0957-4484/27/49/495101

Leong, S.P.L., Tseng, W.W., 2014. Micrometastatic cancer cells in lymph nodes, bone marrow, and blood: Clinical significance and biologic implications. CA. Cancer J. Clin. 64, 195–206. https://doi.org/10.3322/caac.21217

Lestner, J., Mcentee, L., Johnson, A., Livermore, J., Whalley, S., Schwartz, J., Perfect, J.R., Harrison, T., Hope, W., 2017. Experimental Models of Short Courses of Liposomal Amphotericin B for Induction Therapy for Cryptococcal Meningitis. https://doi.org/10.1128/AAC

Li, G., Hu, X., Wu, X., Zhang, Y., 2021. Microtubule-Targeted Self-Assembly Triggers Prometaphase-Metaphase Oscillations Suppressing Tumor Growth. Nano Lett 21, 3052–3059. https://doi.org/10.1021/acs.nanolett.1c00233

Li, J., You, J., Wu, C., Dai, Y., Shi, M., Dong, L., Xu, K., 2018. T 1 –T 2 molecular magnetic resonance imaging of renal carcinoma cells based on nano-contrast agents. Int. J. Nanomedicine 13, 4607–4625. https://doi.org/10.2147/IJN.S168660

Li, N., Peng, L.H., Chen, X., Zhang, T.Y., Shao, G.F., Liang, W.Q., Gao, J.Q., 2014. Antigen-loaded nanocarriers enhance the migration of stimulated Langerhans cells to draining lymph nodes and induce effective transcutaneous immunization. Nanomedicine Nanotechnology, Biol. Med. 10, 215–223. https://doi.org/10.1016/j.nano.2013.06.007

Li, T., Zheng, F., Cheung, M., Wang, F., Fu, C., 2015. Fission yeast mitochondria are distributed by dynamic microtubules in a motor-independent manner. Sci Rep 5. https://doi.org/10.1038/srep11023

Liang, C., Song, X., Chen, Q., Liu, T., Song, G., Peng, R., Liu, Z., 2015. Magnetic Field-Enhanced Photothermal Ablation of Tumor Sentinel Lymph Nodes to Inhibit Cancer Metastasis. Small 11, 4856–4863. https://doi.org/10.1002/smll.201501197

Liao, S., von der Weid, P.Y., 2015. Lymphatic system: An active pathway for immune protection. Semin. Cell Dev. Biol. 38, 83–89. https://doi.org/10.1016/j.semcdb.2014.11.012

Lin, S., Yang, L., Yao, Y., Xu, L., Xiang, Y., Zhao, H., Wang, L., Zuo, Z., Huang, X., Zhao, C., 2019. Flubendazole demonstrates valid antitumor effects by inhibiting STAT3 and activating autophagy. Journal of Experimental and Clinical Cancer Research 38. https://doi.org/10.1186/s13046-019-1303-z

Liu, H., Fu, Q., Lu, Y., Zhang, W., Yu, P., Liu, Z., Sun, X., 2020. Anti-tubulin agent vinorelbine inhibits metastasis of cancer cells by regulating epithelial-mesenchymal transition. Eur J Med Chem 200. https://doi.org/10.1016/j.ejmech.2020.112332

Liu, T., Wang, C., Gu, X., Gong, H., Cheng, L., Shi, X., Feng, L., Sun, B., Liu, Z., 2014. Drug delivery with PEGylated MoS2 nano-sheets for combined photothermal and chemotherapy of cancer. Adv. Mater. 26, 3433–3440. https://doi.org/10.1002/adma.201305256

Liu, W., He, M., Li, Y., Peng, Z., Wang, G., 2022. A review on synthetic chalcone derivatives as tubulin polymerisation inhibitors. J Enzyme Inhib Med Chem. https://doi.org/10.1080/14756366.2021.1976772

Liu, Y., Meng, Y., Bian, J., Liu, B., Li, X., Guan, Q., Li, Z., Zhang, W., Wu, Y., Zuo, D., 2022. 2-Methoxy-5((3,4,5-trimethosyphenyl) seleninyl) phenol causes G2/M cell cycle arrest and apoptosis in NSCLC cells through mitochondrial apoptotic pathway and MDM2 inhibition. J Biochem Mol Toxicol 36. https://doi.org/10.1002/jbt.23066

Livraghi, A., Randell, S.H., 2007. Cystic Fibrosis and Other Respiratory Diseases of Impaired Mucus Clearance. Toxicol Pathol 35, 116–129. https://doi.org/10.1080/01926230601060025

Löbenberg, R., Reynolds, K., Tirunellai, K., Fredro-Kumbaradzi, E., Zhang, R., Raines, K., Mathivanan, M., Davit, B.M., Laloo, A., Murti, S., Veerasingham, S., Endrenyi, L., Jamali, F., 2020. Biowaiver for Immediate and Modified Release Dosage forms Scientific summary of the CSPS workshop, J Pharm Pharm Sci (www.cspsCanada.org).

Locher, K., Borghardt, J.M., Frank, K.J., Kloft, C., Wagner, K.G., 2016. Evolution of a mini-scale biphasic dissolution model: Impact of model parameters on partitioning of dissolved API and modelling of in vivo-relevant kinetics. European Journal of Pharmaceutics and Biopharmaceutics 105, 166–175. https://doi.org/10.1016/j.ejpb.2016.06.008

Loh, J.M.S., Adenwalla, N., Wiles, S., Proft, T., 2013. Galleria mellonella larvae as an infection model for group A streptococcus. Virulence 4, 419–428. https://doi.org/10.4161/viru.24930

Lohela, M., Bry, M., Tammela, T., Alitalo, K., 2009. VEGFs and receptors involved in angiogenesis versus lymphangiogenesis. Curr. Opin. Cell Biol. 21, 154–165. https://doi.org/10.1016/j.ceb.2008.12.012

Longo, M., Zanoncelli, S., Colombo, P.A., Harhay, M.O., Scandale, I., Mackenzie, C., Geary, T., Madrill, N., Mazué, G., 2013. Effects of the benzimidazole anthelmintic drug flubendazole on rat embryos in vitro. Reproductive Toxicology 36, 78–87. https://doi.org/10.1016/j.reprotox.2012.12.004

Lotfi Shahreza, M., Ghadiri, N., Mousavi, S.R., Varshosaz, J., Green, J.R., 2018. A review of network-based approaches to drug repositioning. Brief Bioinform. https://doi.org/10.1093/bib/bbx017

Lu, E., Li, S., Wang, Z., 2017. Biorelevant test for supersaturable formulation. Asian J Pharm Sci. https://doi.org/10.1016/j.ajps.2016.10.002

Lu, Q., Gottlieb, E., Rounds, S., 2018. Effects of cigarette smoke on pulmonary endothelial cells. Am J Physiol Lung Cell Mol Physiol 314, 743–756. https://doi.org/10.1152/ajplung.00373.2017.-Cigarette

Ludueña, R.F., 2013. A Hypothesis on the Origin and Evolution of Tubulin, in: International Review of Cell and Molecular Biology. Elsevier Inc., pp. 41–185. https://doi.org/10.1016/B978-0-12-407699-0.00002-9

Lyu, J., Yang, E.J., Zhang, B., Wu, C., Pardeshi, L., Shi, C., Mou, P.K., Liu, Y., Tan, K., Shim, J.S., 2020. Synthetic lethality of RB1 and aurora A is driven by stathmin-mediated disruption of microtubule dynamics. Nat Commun 11. https://doi.org/10.1038/s41467-020-18872-0

Mackenzie, C.D., Geary, T.G., 2011. Flubendazole: A candidate macrofilaricide for lymphatic filariasis and onchocerciasis field programs. Expert Rev Anti Infect Ther. https://doi.org/10.1586/eri.11.30

Makwana, V., Jain, R., Patel, K., Nivsarkar, M., Joshi, A., 2015. Solid lipid nanoparticles (SLN) of Efavirenz as lymph targeting drug delivery system: Elucidation of mechanism of uptake using chylomicron flow blocking approach. Int. J. Pharm. 495, 439–446. https://doi.org/10.1016/j.ijpharm.2015.09.014

Manosalva, C., Alarcón, P., González, K., Soto, J., Igor, K., Peña, F., Medina, G., Burgos, R.A., Hidalgo, M.A., 2020. Free Fatty Acid Receptor 1 Signaling Contributes to Migration, MMP-9 Activity, and Expression of IL-8 Induced by Linoleic Acid in HaCaT Cells. Front Pharmacol 11. https://doi.org/10.3389/fphar.2020.00595

Mantovani, A., Marchesi, F., Malesci, A., Laghi, L., Allavena, P., 2017. Tumour-associated macrophages as treatment targets in oncology. Nat. Rev. Clin. Oncol. 14, 399–416. https://doi.org/10.1038/nrclinonc.2016.217

Marrinefl, S.E., Morris, D.L., Dickson, B., Bogan, J.A., 1986. Pharmacokinetics of Albendazole in Man. Eur J Clin Pharmacol 30, 705–708.

Martinez-Corral, I., Makinen, T., 2013. Regulation of lymphatic vascular morphogenesis: Implications for pathological (tumor) lymphangiogenesis. Exp. Cell Res. 319, 1618–1625. https://doi.org/10.1016/j.yexcr.2013.01.016

Masada, T., Takagi, T., Minami, K., Kataoka, M., Takeyama, S., Fujii, Y., Takahashi, M., Yamashita, S., 2021. New biphasic system in side-by-side chambers for testing drug dissolution and permeation in vitro (BiDP system). J Drug Deliv Sci Technol 65. https://doi.org/10.1016/j.jddst.2021.102747

May, R.C., Stone, N.R.H., Wiesner, D.L., Bicanic, T., Nielsen, K., 2016. Cryptococcus: From environmental saprophyte to global pathogen. Nat Rev Microbiol 14, 106–117. https://doi.org/10.1038/nrmicro.2015.6

McCarroll, J.A., Gan, P.P., Liu, M., Kavallaris, M., 2010. βIII-tubulin is a multifunctional protein involved in drug sensitivity and tumorigenesis in non-small cell lung cancer. Cancer Res 70, 4995–5003. https://doi.org/10.1158/0008-5472.CAN-09-4487

McDaniel, J.R., Pero, S.C., Voss, W.N., Shukla, G.S., Sun, Y., Schaetzle, S., Lee, C.H., Horton, A.P., Harlow, S., Gollihar, J., Ellefson, J.W., Krag, C.C., Tanno, Y., Sidiropoulos, N., Georgiou, G., Ippolito, G.C., Krag, D.N., 2018. Identification of tumor-reactive B cells and systemic IgG in breast cancer based on clonal frequency in the sentinel lymph node. Cancer Immunol. Immunother. 67, 729–738. https://doi.org/10.1007/s00262-018-2123-2

McLennan, D.N., Porter, C.J.H., Charman, S.A., 2005. Subcutaneous drug delivery and the role of the lymphatics. Drug Discov. Today Technol. 2, 89–96. https://doi.org/10.1016/j.ddtec.2005.05.006

Men, L., Zhang, Y., Li, K., Li, Z., Li, C., Zhang, X., Gong, X., Fang, L., 2022. Metabolism and pharmacokinetics of mebendazole in Japanese pufferfish (Takifugu rubripes). Food Additives and Contaminants - Part A 39, 912–924. https://doi.org/10.1080/19440049.2022.2052974

Michaelis, M., Agha, B., Rothweiler, F., Löschmann, N., Voges, Y., Mittelbronn, M., Starzetz, T., Harter, P.N., Abhari, B.A., Fulda, S., Westermann, F., Riecken, K., Spek, S., Langer, K., Wiese, M., Dirks, W.G., Zehner, R., Cinatl, Jaroslav, Wass, M.N., Cinatl, Jindrich, 2015. Identification of flubendazole as potential anti-neuroblastoma compound in a large cell line screen. Sci Rep 5. https://doi.org/10.1038/srep08202

Milo, R., Phillips, R., 2015. How quickly do different cells in the body replace themselves.

Minda, D., Mioc, A., Banciu, C., Soica, C., Racoviceanu, R., Mioc, M., Macasoi, I., Avram, S., Voicu, A., Motoc, A., Trandafirescu, C., 2021. Cyclodextrin dispersion of mebendazole and flubendazole improves in vitro antiproliferative activity. Processes 9. https://doi.org/10.3390/pr9122185

Molloy, S.F., Chiller, T., Greene, G.S., Burry, J., Govender, N.P., Kanyama, C., Mfinanga, S., Lesikari, S., Mapoure, Y.N., Kouanfack, C., Sini, V., Temfack, E., Boulware, D.R., Dromer, F., Denning, D.W., Day, J., Stone, N.R.H., Bicanic, T., Jarvis, J.N., Lortholary, O., Harrison, T.S., Jaffar, S., Loyse, A., 2017. Cryptococcal meningitis: A neglected NTD? PLoS Negl Trop Dis 11. https://doi.org/10.1371/journal.pntd.0005575

Morgan, S., Grootendorst, P., Lexchin, J., Cunningham, C., Greyson, D., 2011. The cost of drug development: A systematic review. Health Policy (New York). https://doi.org/10.1016/j.healthpol.2010.12.002

237

Mousa, S.A., Bharali, D.J., 2011. Nanotechnology-based detection and targeted therapy in cancer: Nano-bio paradigms and applications. Cancers (Basel). 3, 2888–2903. https://doi.org/10.3390/cancers3032888

Moussion, C., Girard, J.P., 2011. Dendritic cells control lymphocyte entry to lymph nodes through high endothelial venules. Nature 479, 542–546. https://doi.org/10.1038/nature10540

Mudie, D.M., Murray, K., Hoad, C.L., Pritchard, S.E., Garnett, M.C., Amidon, G.L., Gowland, P.A., Spiller, R.C., Amidon, G.E., Marciani, L., 2014. Quantification of gastrointestinal liquid volumes and distribution following a 240 mL dose of water in the fasted state. Mol Pharm 11, 3039–3047. https://doi.org/10.1021/mp500210c

Muraoka, D., Harada, N., Hayashi, T., Tahara, Y., Momose, F., Sawada, S.I., Mukai, S.A., Akiyoshi, K., Shiku, H., 2014. Nanogel-based immunologically stealth vaccine targets macrophages in the medulla of lymph node and induces potent antitumor immunity. ACS Nano 8, 9209–9218. https://doi.org/10.1021/nn502975r

Nasedkin, A., Ermilova, I., Swenson, J., 2021. Atomistic molecular dynamics simulations of tubulin heterodimers explain the motion of a microtubule. European Biophysics Journal 50, 927–940. https://doi.org/10.1007/s00249-021-01553-1

Negi, J.S., Chattopadhyay, P., Sharma, A.K., Ram, V., 2013. Development of solid lipid nanoparticles (SLNs) of lopinavir using hot self nano-emulsification (SNE) technique. Eur. J. Pharm. Sci. 48, 231–239. https://doi.org/10.1016/j.ejps.2012.10.022

Ngamskulrungroj, P., Chang, Y., Sionov, E., Kwon-Chunga, K.J., 2012. The primary target organ of cryptococcus gattii is different from that of cryptococcus neoformans in a murine model. mBio 3. https://doi.org/10.1128/mBio.00103-12

Ngan, C.L. oong, Basri, M., Lye, F.F. ang, Fard Masoumi, H.R. eza, Tripathy, M., Karjiban, R.A. bedi, Abdul-Malek, E., 2014. Comparison of process parameter optimization using different designs in nanoemulsion-based formulation for transdermal delivery of fullerene. Int J Nanomedicine 9, 4375–4386. https://doi.org/10.2147/IJN.S65689

Nguyen, T.T., Nguyen, T.T.D., Tran, N.M.A., van Vo, G., 2022. Lipid-Based Nanocarriers via Nose-to-Brain Pathway for Central Nervous System Disorders. Neurochem Res. https://doi.org/10.1007/s11064-021-03488-7

Ni, S., Qiu, L., Zhang, G., Zhou, H., Han, Y., 2017. Lymph cancer chemotherapy: Delivery of doxorubicin-gemcitabine prodrug and vincristine by nanostructured lipid carriers. Int. J. Nanomedicine 12, 1565–1576. https://doi.org/10.2147/IJN.S120685

Nixon, G.L., McEntee, L., Johnson, A., Farrington, N., Whalley, S., Livermore, J., Natal, C., Washbourn, G., Bibby, J., Berry, N., Lestner, J., Truong, M., Owen, A., Lalloo, D., Charles, I., Hope, W., 2018. Repurposing and reformulation of the antiparasitic agent flubendazole for treatment of cryptococcal meningoencephalitis, a neglected fungal disease. Antimicrob Agents Chemother 62. https://doi.org/10.1128/AAC.01909-17

Niu, C., Wang, Z., Lu, G., Krupka, T.M., Sun, Y., You, Y., Song, W., Ran, H., Li, P., Zheng, Y., 2013. Doxorubicin loaded superparamagnetic PLGA-iron oxide multifunctional microbubbles for dual-mode US/MR imaging and therapy of metastasis in lymph nodes. Biomaterials 34, 2307–2317. https://doi.org/10.1016/j.biomaterials.2012.12.003

Nixon, G.L., McEntee, L., Johnson, A., Farrington, N., Whalley, S., Livermore, J., Natal, C., Washbourn, G., Bibby, J., Berry, N., Lestner, J., Truong, M., Owen, A., Lalloo, D., Charles, I., Hope, W., 2018. Repurposing and reformulation of the antiparasitic agent flubendazole for treatment of cryptococcal meningoencephalitis, a neglected fungal disease. Antimicrob Agents Chemother 62. https://doi.org/10.1128/AAC.01909-17

Nobilis, M., Jira, T., Lísa, M., Holčapek, M., Szotáková, B., Lamka, J., Skálová, L., 2007. Achiral and chiral high-performance liquid chromatographic determination of flubendazole and its metabolites in biomatrices using UV photodiode-array and mass spectrometric detection. J Chromatogr A 1149, 112–120. https://doi.org/10.1016/j.chroma.2007.01.013

Nobilis, M., Vybíralová, Z., Křížová, V., Kubíček, V., Soukupová, M., Lamka, J., Szotáková, B., Skálová, L., 2008. Sensitive chiral high-performance liquid chromatographic determination of anthelmintic flubendazole and its phase I metabolites in blood plasma using UV photodiode-array and fluorescence detection. Application to pharmacokinetic studies in sheep. J Chromatogr B Analyt Technol Biomed Life Sci 876, 89–96. https://doi.org/10.1016/j.jchromb.2008.10.032

Nuhn, L., Vanparijs, N., De Beuckelaer, A., Lybaert, L., Verstraete, G., Deswarte, K., Lienenklaus, S., Shukla, N.M., Salyer, A.C.D., Lambrecht, B.N., Grooten, J., David, S.A., De Koker, S., De Geest, B.G., 2016. PH-degradable imidazoquinoline-ligated nanogels for lymph node-focused immune activation. Proc. Natl. Acad. Sci. U. S. A. 113, 8098–8103. https://doi.org/10.1073/pnas.1600816113

Nygren, P., Fryknäs, M., Ågerup, B., Larsson, R., 2013. Repositioning of the anthelmintic drug mebendazole for the treatment for colon cancer. J Cancer Res Clin Oncol 139, 2133–2140. https://doi.org/10.1007/s00432-013-1539-5

O'Dwyer, P.J., Box, K.J., Koehl, N.J., Bennett-Lenane, H., Reppas, C., Holm, R., Kuentz, M., Griffin, B.T., 2020. Novel Biphasic Lipolysis Method to Predict in Vivo Performance of Lipid-Based Formulations. Mol Pharm 17, 3342–3352. https://doi.org/10.1021/acs.molpharmaceut.0c00427

Oh, E., Kim, Y.J., An, H., Sung, D., Cho, T.M., Farrand, L., Jang, S., Seo, J.H., Kim, J.Y., 2018. Flubendazole elicits anti-metastatic effects in triple-negative breast cancer via STAT3 inhibition. Int J Cancer 143, 1978–1993. https://doi.org/10.1002/ijc.31585

Okumu, A., DiMaso, M., Löbenberg, R., 2008. Dynamic dissolution testing to establish in vitro/in vivo correlations for montelukast sodium, a poorly soluble drug, in: Pharmaceutical Research. pp. 2778–2785. https://doi.org/10.1007/s11095-008-9642-z

Oladipo, A.O., Oluwafemi, O.S., Songca, S.P., Sukhbaatar, A., Mori, S., Okajima, J., Komiya, A., Maruyama, S., Kodama, T., 2017. A novel treatment for metastatic lymph nodes using lymphatic delivery and photothermal therapy. Sci. Rep. 7, 1–10. https://doi.org/10.1038/srep45459O'Neill, M., Geary, J.F., Agnew, D.W., Mackenzie, C.D., Geary, T.G., 2015. Invitro flubendazole-induced damage to vital tissues in adult females of the filarial nematode Brugia malayi. Int J Parasitol Drugs Drug Resist 5, 135–140. https://doi.org/10.1016/j.ijpddr.2015.06.002

Ong, M.S., Deng, S., Halim, C.E., Cai, W., Tan, T.Z., Huang, R.Y.J., Sethi, G., Hooi, S.C., Kumar, A.P., Yap, C.T., 2020. Cytoskeletal proteins in cancer and intracellular stress: A therapeutic perspective. Cancers (Basel). https://doi.org/10.3390/cancers12010238

Oyewumi, M.O., Kumar, A., Cui, Z., 2010. Nano-microparticles as immune adjuvants: Correlating particle sizes and the resultant immune responses. Expert Rev. Vaccines 9, 1095–1107. https://doi.org/10.1586/erv.10.89

Pardridge, W.M., 2003. Blood-brain barrier drug targeting: the future of brain drug development. Mol Interv 3, 90–105. https://doi.org/10.1124/mi.3.2.90

Park, M., Hwang, J.W., Cho, Y., Kim, S., Han, S.H., Yu, J., Ha, S., Kim, W.Y., Kim, S.N., Kim, I.S., Kim, Y.K., 2021. A novel synthetic microtubule inhibitor exerts antiproliferative effects in multidrug resistant cancer cells and cancer stem cells. Sci Rep 11. https://doi.org/10.1038/s41598-021-90337-w

Parker, A.L., Teo, W.S., McCarroll, J.A., Kavallaris, M., 2017. An emerging role for tubulin isotypes in modulating cancer biology and chemotherapy resistance. Int J Mol Sci. https://doi.org/10.3390/ijms18071434

Parker, A.L., Turner, N., McCarroll, J.A., Kavallaris, M., 2016. βIII-Tubulin alters glucose metabolism and stress response signaling to promote cell survival and proliferation in glucose-starved non-small cell lung cancer cells. Carcinogenesis 37, 787–798. https://doi.org/10.1093/carcin/bgw058

Parveen, R., Baboota, S., Ali, J., Ahuja, A., Vasudev, S.S., Ahmad, S., 2011. Oil based nanocarrier for improved oral delivery of silymarin: In vitro and in vivo studies. Int J Pharm 413, 245–253. https://doi.org/10.1016/j.ijpharm.2011.04.041

Pasquier, E., Honoré, S., Braguer, D., 2006. Microtubule-targeting agents in angiogenesis: Where do we stand? Drug Resistance Updates 9, 74–86. https://doi.org/10.1016/j.drup.2006.04.003

Pathak, D., Sepp, K.J., Hollenbeck, P.J., 2010. Evidence that myosin activity opposes microtubule-based axonal transport of mitochondria. Journal of Neuroscience 30, 8984–8992. https://doi.org/10.1523/JNEUROSCI.1621-10.2010

Peckham, M., 2016. How myosin organization of the actin cytoskeleton contributes to the cancer phenotype. Biochem Soc Trans 44, 1026–1034. https://doi.org/10.1042/BST20160034

Pecqueur, L., Duellberg, C., Dreier, B., Jiang, Q., Wang, C., Plückthun, A., Surrey, T., Gigant, B., Knossow, M., 2012. A designed ankyrin repeat protein selected to bind to tubulin caps the microtubule plus end. Proc Natl Acad Sci U S A 109, 12011–12016. https://doi.org/10.1073/pnas.1204129109

Peng, L., Dai, Y., 2019. Effect of metronidazole combined with autolytic debridement for the management of malignant wound malodor. Journal of International Medical Research 48. https://doi.org/10.1177/0300060519889746

Pereira, E.R., Jones, D., Jung, K., Padera, T.P., 2015. The lymph node microenvironment and its role in the progression of metastatic cancer. Semin Cell Dev Biol. https://doi.org/10.1016/j.semcdb.2015.01.008

Pestieau, A., Evrard, B., 2017. In vitro biphasic dissolution tests and their suitability for establishing in vitro-in vivo correlations: A historical review. European Journal of Pharmaceutical Sciences. https://doi.org/10.1016/j.ejps.2017.03.019

Phillips, D.J., Pygall, S.R., Cooper, V.B., Mann, J.C., 2012. Overcoming sink limitations in dissolution testing: A review of traditional methods and the potential utility of biphasic systems. Journal of Pharmacy and Pharmacology. https://doi.org/10.1111/j.2042-7158.2012.01523.x

Poljšak, N., Kreft, S., Kočevar Glavač, N., 2020. Vegetable butters and oils in skin wound healing: Scientific evidence for new opportunities in dermatology. Phytotherapy Research. https://doi.org/10.1002/ptr.6524

Poustforoosh, A., Nematollahi, M.H., Hashemipour, H., Pardakhty, A., 2022. Recent advances in Bio-conjugated nanocarriers for crossing the Blood-Brain Barrier in (pre-)clinical studies with an emphasis on vesicles. Journal of Controlled Release. https://doi.org/10.1016/j.jconrel.2022.02.015

Pozuelos, G.L., Kagda, M., Rubin, M.A., Goniewicz, M.L., Girke, T., Talbot, P., 2022. Transcriptomic Evidence That Switching from Tobacco to Electronic Cigarettes Does Not Reverse Damage to the Respiratory Epithelium. Toxics 10. https://doi.org/10.3390/toxics10070370

Prassanawar, S.S., Panda, D., 2019. Tubulin heterogeneity regulates functions and dynamics of microtubules and plays a role in the development of drug resistance in cancer. Biochemical Journal. https://doi.org/10.1042/BCJ20190123

Qiao, R., Liu, Changhao, Liu, M., Hu, H., Liu, Chunyan, Hou, Y., Wu, K., Lin, Y., Liang, J., Gao, M., 2015. Ultrasensitive in vivo detection of primary gastric tumor and lymphatic metastasis using upconversion nanoparticles. ACS Nano 9, 2120–2129. https://doi.org/10.1021/nn507433p

Rao, J., Li, N., 2004. Microfilament Actin Remodeling as a Potential Target for Cancer Drug Development, Current Cancer Drug Targets.

Rehman, J., Zhang, H.J., Toth, P.T., Zhang, Y., Marsboom, G., Hong, Z., Salgia, R., Husain, A.N., Wietholt, C., Archer, S.L., 2012. Inhibition of mitochondrial fission prevents cell cycle progression in lung cancer. The FASEB Journal 26, 2175–2186. https://doi.org/10.1096/fj.11-196543

Ren, T., Xu, N., Cao, C., Yuan, W., Yu, X., Chen, J., Ren, J., 2009. Preparation and therapeutic efficacy of polysorbate-80-coated amphotericin B/PLA-b-PEG nanoparticles. J Biomater Sci Polym Ed 20, 1369–1380. https://doi.org/10.1163/092050609X12457418779185

Renda, F., Miles, C., Tikhonenko, I., Fisher, R., Carlini, L., Kapoor, T.M., Mogilner, A., Khodjakov, A., 2022. Non-centrosomal microtubules at kinetochores promote rapid chromosome biorientation during mitosis in human cells. Current Biology 32, 1049-1063.e4. https://doi.org/10.1016/j.cub.2022.01.013

Riihimäki, M., Hemminki, A., Fallah, M., Thomsen, H., Sundquist, K., Sundquist, J., Hemminki, K., 2014. Metastatic sites and survival in lung cancer. Lung Cancer 86, 78–84. https://doi.org/10.1016/j.lungcan.2014.07.020

Roa, W.H., Azarmi, S., Al-Hallak, M.H.D.K., Finlay, W.H., Magliocco, A.M., Löbenberg, R., 2011. Inhalable nanoparticles, a non-invasive approach to treat lung cancer in a mouse model. J. Control. Release 150, 49–55. https://doi.org/10.1016/j.jconrel.2010.10.035

Roberts, E.R., Thomas, K.J., 2013. The role of mitochondria in the development and progression of lung cancer, in: Computational and Structural Biotechnology Journal. Research Network of Computational and Structural Biotechnology, p. e201303019. https://doi.org/10.5936/csbj.201303019

Rodrigues, H.G., Vinolo, M.A.R., Magdalon, J., Vitzel, K., Nachbar, R.T., Pessoa, A.F.M., dos Santos, M.F., Hatanaka, E., Calder, P.C., Curi, R., 2012. Oral administration of oleic or linoleic acid accelerates the inflammatory phase of wound healing. Journal of Investigative Dermatology 132, 208–215. https://doi.org/10.1038/jid.2011.265

Rodrigues, H.G., Vinolo, M.A.R., Sato, F.T., Magdalon, J., Kuhl, C.M.C., Yamagata, A.S., Pessoa, A.F.M., Malheiros, G., dos Santos, M.F., Lima, C., Farsky, S.H., Camara, N.O.S., Williner, M.R., Bernal, C.A., Calder, P.C., Curi, R., 2016. Oral administration of Linoleic acid induces new vessel formation and improves skin wound healing in diabetic rats. PLoS One 11. https://doi.org/10.1371/journal.pone.0165115

Rohner, N.A., Thomas, S.N., 2017. Flexible Macromolecule versus Rigid Particle Retention in the Injected Skin and Accumulation in Draining Lymph Nodes Are Differentially Influenced by Hydrodynamic Size. ACS Biomater. Sci. Eng. 3, 153–159. https://doi.org/10.1021/acsbiomaterials.6b00438

Rosas-Salvans, M., Sutanto, R., Suresh, P., Dumont, S., 2022. The Astrin-SKAP complex reduces friction at the kinetochore-microtubule interface. Current Biology 32, 2621-2631.e3. https://doi.org/10.1016/j.cub.2022.04.061

Rovini, A., 2019. Tubulin-VDAC interaction: Molecular basis for mitochondrial dysfunction in chemotherapy-induced peripheral neuropathy. Front Physiol 10. https://doi.org/10.3389/fphys.2019.00671

Roy S, Dhaneshwar S, Bhasin B. Drug Repurposing: An Emerging Tool for Drug Reuse, Recycling and Discovery. Curr Drug Res Rev. 2021;13(2):101-119. doi: 10.2174/2589977513666210211163711. PMID: 33573567.

Ryan, G.M., Kaminskas, L.M., Porter, C.J.H., 2014. Nano-chemotherapeutics: Maximising lymphatic drug exposure to improve the treatment of lymph-metastatic cancers. Journal of Controlled Release 193, 241–256. https://doi.org/10.1016/j.jconrel.2014.04.051

Sagitani, H., 1988. Formation of o/w emulsions by surfactant phase emulsification and the solution behavior of nonionic surfactant system in the emulsification process. J Dispers Sci Technol 9, 115–129. https://doi.org/10.1080/01932698808943980

Sagitani, H., 1986. Formation of Fine Emuisions by Surface Chemical Methods Focusing on the Mechanism of the Inversion Emulsification Method and the Surfactant (D) Phase Emulsification Method. Journal of Japan Oil Chemists' Society 35, 198–202. https://doi.org/10.5650/jos1956.35.198

Sarfraz, M., Roa, W., Bou-Chacra, N., Löbenberg, R., 2016. Inflammation caused by nanosized delivery systems: Is there a benefit? Mol. Pharm. 13, 3270–3278. https://doi.org/10.1021/acs.molpharmaceut.6b00530

Sastri, K.T., Gupta, N.V., M, S., Chakraborty, S., Kumar, H., Chand, P., Balamuralidhara, V., Gowda, D. v., 2022. Nanocarrier facilitated drug delivery to the brain through intranasal route: A promising approach to transcend bio-obstacles and alleviate neurodegenerative conditions. J Drug Deliv Sci Technol. https://doi.org/10.1016/j.jddst.2022.103656

Sato, T., Mori, S., Arai, Y., Kodama, T., 2014. The combination of intralymphatic chemotherapy with ultrasound and nano-/microbubbles is efficient in the treatment of experimental tumors in mouse lymph nodes. Ultrasound Med. Biol. 40, 1237–1249. https://doi.org/10.1016/j.ultrasmedbio.2013.12.012

Sato, T., Mori, S., Sakamoto, M., Arai, Y., Kodama, T., 2015. Direct delivery of a cytotoxic anticancer agent into the metastatic lymph node using nano/microbubbles and ultrasound. PLoS One 10, 1–16. https://doi.org/10.1371/journal.pone.0123619

Savjani, K.T., Gajjar, A.K., Savjani, J.K., 2012. Drug Solubility: Importance and Enhancement Techniques. ISRN Pharm 2012, 1–10. https://doi.org/10.5402/2012/195727

Saxton, W.M., Hollenbeck, P.J., 2012. The axonal transport of mitochondria. J Cell Sci 125, 2095–2104. https://doi.org/10.1242/jcs.053850

Serpico, A.F., Visconti, R., Grieco, D., 2020. Exploiting immune-dependent effects of microtubule-targeting agents to improve efficacy and tolerability of cancer treatment. Cell Death Dis. https://doi.org/10.1038/s41419-020-2567-0

Sève, P., Dumontet, C., 2008. Is class III β-tubulin a predictive factor in patients receiving tubulin-binding agents?

Shah, D., Joshi, M., Patel, B.M., 2022. Role of NIMA-related kinase 2 in lung cancer: Mechanisms and therapeutic prospects. Fundam Clin Pharmacol. https://doi.org/10.1111/fcp.12777

Sharifi-Rad, J., Quispe, C., Patra, J.K., Singh, Y.D., Panda, M.K., Das, G., Adetunji, C.O., Michael, O.S., Sytar, O., Polito, L., Živković, J., Cruz-Martins, N., Klimek-Szczykutowicz, M., Ekiert, H., Choudhary, M.I., Ayatollahi, S.A., Tynybekov, B., Kobarfard, F., Muntean, A.C., Grozea, I., Daştan, S.D., Butnariu, M., Szopa, A., Calina, D., 2021. Paclitaxel: Application in Modern Oncology and Nanomedicine-Based Cancer Therapy. Oxid Med Cell Longev. https://doi.org/10.1155/2021/3687700

Sharma, M., Salisbury, R.L., Maurer, E.I., Hussain, S.M., Sulentic, C.E.W., 2013. Gold nanoparticles induce transcriptional activity of NF-κB in a B-lymphocyte cell line. Nanoscale 5, 3747–3756. https://doi.org/10.1039/c3nr30071d

Shi, H., Yan, R., Wu, L., Sun, Y., Liu, S., Zhou, Z., He, J., Ye, D., 2018. Tumor-targeting CuS nanoparticles for multimodal imaging and guided photothermal therapy of lymph node metastasis. Acta Biomater. 72, 256–265. https://doi.org/10.1016/j.actbio.2018.03.035

Shih, V.F.S., Tsui, R., Caldwell, A., Hoffmann, A., 2011. A single NFκB system for both canonical and non-canonical signaling. Cell Res. 21, 86–102. https://doi.org/10.1038/cr.2010.161

Schmidt, F.M.Q., Firmino, F., Lenza, N. de F.B., Santos, V.L.C. de G., 2020. Nursing team knowledge on care for patients with fungating wounds. Rev Bras Enferm 73, e20170738. https://doi.org/10.1590/0034-7167-2017-0738

Shim, J.S., Liu, J.O., 2014. Recent advances in drug repositioning for the discovery of new anticancer drugs. Int J Biol Sci. https://doi.org/10.7150/ijbs.9224

Shoshan-Barmatz, V., Ben-Hail, D., 2012. VDAC, a multi-functional mitochondrial protein as a pharmacological target. Mitochondrion. https://doi.org/10.1016/j.mito.2011.04.001

Shrivas, Meera, Khunt, D., Shrivas, Meenakshee, Choudhari, M., Rathod, R., Misra, M., 2020. Advances in In Vivo Predictive Dissolution Testing of Solid Oral Formulations: How Closer to In Vivo Performance? J Pharm Innov. https://doi.org/10.1007/s12247-019-09392-6

Silva, D.A., Al-Gousous, J., Davies, N.M., Chacra, N.B., Webster, G.K., Lipka, E., Amidon, G.L., Löbenberg, R., 2020. Biphasic dissolution as an exploratory method during early drug product development. Pharmaceutics 12. https://doi.org/10.3390/pharmaceutics12050420

Singh, R., Pantarotto, D., Lacerda, L., Pastorin, G., dric Klumpp, C., Prato, M., Bianco, A., Kostarelos, K., 2006. Tissue biodistribution and blood clearance rates of intravenously administered carbon nanotube radiotracers.

Soares-de-Oliveira, J., Maiato, H., 2022. Mitosis: Kinetochores determined against random search-and-capture. Current Biology. https://doi.org/10.1016/j.cub.2022.02.003

Sobierajska, K., Wieczorek, K., Ciszewski, W.M., Sacewicz-Hofman, I., Wawro, M.E., Wiktorska, M., Boncela, J., Papiewska-Pajak, I., Kwasniak, P., Wyroba, E., Cierniewski, C.S., Niewiarowska, J., 2016. β-III tubulin modulates the behavior of Snail overexpressed during the epithelial-to-mesenchymal transition in colon cancer cells. Biochim Biophys Acta Mol Cell Res 1863, 2221–2233. https://doi.org/10.1016/j.bbamcr.2016.05.008

Solans, C., Izquierdo, P., Nolla, J., Azemar, N., Garcia-Celma, M.J., 2005. Nano-emulsions. Curr Opin Colloid Interface Sci. https://doi.org/10.1016/j.cocis.2005.06.004

Solans, C., Solé, I., 2012. Nano-emulsions: Formation by low-energy methods. Curr Opin Colloid Interface Sci. https://doi.org/10.1016/j.cocis.2012.07.003

Song, X., Chen, Q., Liu, Z., 2015. Recent advances in the development of organic photothermal nano-agents. Nano Res. 8, 340–354. https://doi.org/10.1007/s12274-014-0620-y

Song, Y., Cai, H., Yin, T., Huo, M., Ma, P., Zhou, J., Lai, W., 2018. Paclitaxel-loaded redox-sensitive nanoparticles based on hyaluronic acid-vitamin E succinate conjugates for improved lung cancer treatment. Int J Nanomedicine 13, 1585–1600. https://doi.org/10.2147/IJN.S155383

Song, Z., Shi, Y., Han, Q., Dai, G., 2018. Endothelial growth factor receptor-targeted and reactive oxygen species-responsive lung cancer therapy by docetaxel and resveratrol encapsulated lipid-polymer hybrid nanoparticles. Biomedicine and Pharmacotherapy 105, 18–26. https://doi.org/10.1016/j.biopha.2018.05.095

Souquet, P.J., Geriniere, L., 2001. Docetaxel and non small-cell lung cancer. Prescrire Int 10, 43–45. https://doi.org/10.2217/14750708.3.5.579

Spadari, C. de C., Wirth, F., Lopes, L.B., Ishida, K., 2020. New approaches for cryptococcosis treatment. Microorganisms. https://doi.org/10.3390/microorganisms8040613

Spagnuolo, P.A., Hu, J., Hurren, R., Wang, X., Gronda, M., Sukhai, M.A., di Meo, A., Boss, J., Ashali, I., Zavareh, R.B., Fine, N., Simpson, C.D., Sharmeen, S., Rottapel, R., Schimmer, A.D., 2010. The antihelmintic flubendazole inhibits microtubule function through a mechanism distinct from Vinca alkaloids and displays preclinical activity in leukemia and myeloma. Blood 115, 4824–4833. https://doi.org/10.1182/blood-2009-09-243055

Speed, B., Dunt, D., 1995. Clinical and Host Differences Between Infections with the Two Varieties of Cryptococcus neoformans.

Steinmetz, M.O., Prota, A.E., 2018. Microtubule-Targeting Agents: Strategies To Hijack the Cytoskeleton. Trends Cell Biol. https://doi.org/10.1016/j.tcb.2018.05.001

Stuchlíková, L., Králová, V., Lněničková, K., Zárybnický, T., Matoušková, P., Hanušová, V., Ambrož, M., Šubrt, Z., Skálová, L., 2018. The metabolism of flubendazole in human liver and cancer cell lines. Drug Test Anal 10, 1139–1146. https://doi.org/10.1002/dta.2369

Sugiura, T., Matsuki, D., Okajima, J., Komiya, A., Mori, S., Maruyama, S., Kodama, T., 2015. Photothermal therapy of tumors in lymph nodes using gold nanorods and near-infrared laser light with controlled surface cooling. Nano Res. 8, 3842–3852. https://doi.org/10.1007/s12274-015-0884-x

Sun, B.L., Wang, L. hua, Yang, T., Sun, J. yi, Mao, L. lei, Yang, M. feng, Yuan, H., Colvin, R.A., Yang, X. yi, 2018. Lymphatic drainage system of the brain: A novel target for intervention of neurological diseases. Prog Neurobiol. https://doi.org/10.1016/j.pneurobio.2017.08.007

Sun, D., Wei, X., Xue, X., Fang, Z., Ren, M., Lou, H., Zhang, X., 2014. Enhanced oral absorption and therapeutic effect of acetylpuerarin based on D-α-tocopheryl polyethylene glycol 1000 succinate nanoemulsions. Int J Nanomedicine 9, 3413–3423. https://doi.org/10.2147/IJN.S63777

Sun, L., Wan, K., Hu, X., Zhang, Y., Yan, Z., Feng, J., Zhang, J., 2016. Functional nanoemulsion-hybrid lipid nanocarriers enhance the bioavailability and anti-cancer activity of lipophilic diferuloylmethane. Nanotechnology 27. https://doi.org/10.1088/0957-4484/27/8/085102

Sun, Y., Xia, Z., Zheng, J., Qiu, P., Zhang, L., McClements, D.J., Xiao, H., 2015. Nanoemulsion-based delivery systems for nutraceuticals: Influence of carrier oil type on bioavailability of pterostilbene. J Funct Foods 13, 61–70. https://doi.org/10.1016/j.jff.2014.12.030

Suresh, R., Diaz, R.J., 2021. The remodelling of actin composition as a hallmark of cancer. Transl Oncol. https://doi.org/10.1016/j.tranon.2021.101051

Surov, A.O., Volkova, T. v., 2022. Solubility/distribution thermodynamics and permeability of two anthelmintics in biologically relevant solvents. J Mol Liq 354. https://doi.org/10.1016/j.molliq.2022.118835

Swartz, M.A., 2001. The physiology of the lymphatic system. Adv. Drug Deliv. Rev. 50, 3–20. https://doi.org/10.1016/S0169-409X(01)00150-8

Świtalska, M., Filip-Psurska, B., Milczarek, M., Psurski, M., Moszyńska, A., Dąbrowska, A.M., Gawrońska, M., Krzymiński, K., Bagiński, M., Bartoszewski, R., Wietrzyk, J., 2022. Combined anticancer therapy with imidazoacridinone analogue C-1305 and paclitaxel in human lung and colon cancer xenografts—Modulation of tumour angiogenesis. J Cell Mol Med 26, 3950–3964. https://doi.org/10.1111/jcmm.17430

Tangutur, A.D., Kumar, D., Krishna, K.V., Kantevari, S., 2017. Microtubule Targeting Agents as Cancer Chemotherapeutics: An Overview of Molecular Hybrids as Stabilizing and Destabilizing Agents. Curr Top Med Chem 17, 2523–2537. https://doi.org/10.2174/1568026617666170104

Tanideh, N., Abdordideh, E., Yousefabad, S.L.A., Daneshi, S., Hosseinabadi, O.K., Samani, S.M., 2016. A comparison of the effects of honey, fish oil and their combination on wound healing in rat. Journal of Coastal Life Medicine 4, 683–688. https://doi.org/10.12980/jclm.4.2016j6-93

Tao, J., Zhao, H., Xie, X., Luo, M., Gao, Z., Sun, H., Huang, Z., 2019. The anthelmintic drug flubendazole induces cell apoptosis and inhibits NF-κb signaling in esophageal squamous cell carcinoma. Onco Targets Ther 12, 471–478. https://doi.org/10.2147/OTT.S193206

Thakur, C., 2019. An Overview, Current Challenges of Drug Resistance, and Targeting Metastasis Associated With Lung Cancer, in: Nanotechnology-Based Targeted Drug Delivery Systems for Lung Cancer. Elsevier, pp. 21–38. https://doi.org/10.1016/b978-0-12-815720-6.00002-2

Thiry, J., Broze, G., Pestieau, A., Tatton, A.S., Baumans, F., Damblon, C., Krier, F., Evrard, B., 2016. Investigation of a suitable in vitro dissolution test for itraconazole-based solid dispersions. European Journal of Pharmaceutical Sciences 85, 94–105. https://doi.org/10.1016/j.ejps.2016.02.002

Thiry, J., Kok, M.G.M., Collard, L., Frère, A., Krier, F., Fillet, M., Evrard, B., 2017. Bioavailability enhancement of itraconazole-based solid dispersions produced by hot melt extrusion in the framework of the Three Rs rule. European Journal of Pharmaceutical Sciences 99, 1–8. https://doi.org/10.1016/j.ejps.2016.12.001

Thomas, S.N., Schudel, A., 2015. Overcoming transport barriers for interstitial-, lymphatic-, and lymph node-targeted drug delivery. Curr. Opin. Chem. Eng. 7, 65–74. https://doi.org/10.1016/j.coche.2014.11.003

Thomas, S.N., Vokali, E., Lund, A.W., Hubbell, J.A., Swartz, M.A., 2014. Targeting the tumor-draining lymph node with adjuvanted nanoparticles reshapes the anti-tumor immune response. Biomaterials 35, 814–824. https://doi.org/10.1016/j.biomaterials.2013.10.003

Thompson, S.L., Compton, D.A., 2011. Chromosome missegregation in human cells arises through specific types of kinetochore-microtubule attachment errors. Proc Natl Acad Sci U S A 108, 17974–17978. https://doi.org/10.1073/pnas.1109720108

Tilley, A.E., Walters, M.S., Shaykhiev, R., Crystal, R.G., 2015. Cilia dysfunction in lung disease. Annu Rev Physiol 77, 379–406. https://doi.org/10.1146/annurev-physiol-021014-071931

Tilley, C., Lipson, J., Ramos, M., 2016. Palliative Wound Care for Malignant Fungating Wounds: Holistic Considerations at End-of-Life. Nursing Clinics of North America. https://doi.org/10.1016/j.cnur.2016.05.006

Tilley, C.P., Fu, M.R., van Cleeve, J., Crocilla, B.L., Comfort, C.P., 2020. Symptoms of Malignant Fungating Wounds and Functional Performance among Patients with Advanced Cancer: An Integrative Review from 2000 to 2019. J Palliat Med. https://doi.org/10.1089/jpm.2019.0617

Tiwari, S., Amiji, M., 2006. A Review of Nanocarrier-Based CNS Delivery Systems. Curr Drug Deliv 3, 219–232. https://doi.org/10.2174/156720106776359230

Tiwari, S.B., Amiji, M.M., 2006. Improved oral delivery of paclitaxel following administration in nanoemulsion formulations. J Nanosci Nanotechnol 6, 3215–3221. https://doi.org/10.1166/jnn.2006.440

Tonello, S., Rizzi, M., Migliario, M., Rocchetti, V., Renò, F., 2017. Low concentrations of neutrophil extracellular traps induce proliferation in human keratinocytes via NF-kB activation. J Dermatol Sci 88, 110–116. https://doi.org/10.1016/j.jdermsci.2017.05.010

Trujillo-Cayado, L.A., Santos, J., Ramírez, P., Alfaro, M.C., Muñoz, J., 2018. Strategy for the development and characterization of environmental friendly emulsions by microfluidization technique. J Clean Prod 178, 723–730. https://doi.org/10.1016/j.jclepro.2018.01.028

Truong, M., Monahan, L.G., Carter, D.A., Charles, I.G., 2018. Repurposing drugs to fast-track therapeutic agents for the treatment of cryptococcosis. PeerJ 2018, 1–18. https://doi.org/10.7717/peerj.4761

Tsujimoto, H., Morimoto, Y., Takahata, R., Nomura, S., Yoshida, K., Hiraki, S., Horiguchi, H., Miyazaki, H., Ono, S., Saito, D., Hara, I., Ozeki, E., Yamamoto, J., Hase, K., 2015. Theranostic Photosensitive Nanoparticles for Lymph Node Metastasis of Gastric Cancer. Ann. Surg. Oncol. 22, 923–928. https://doi.org/10.1245/s10434-015-4594-0

Vandenberge, V., Delezie, E., Delahaut, P., Pierret, G., de Backer, P., Daeseleire, E., Croubels, S., 2012. Transfer of flubendazole and tylosin at cross contamination levels in the feed to egg matrices and distribution between egg yolk and egg white. Poult Sci 91, 1248–1255. https://doi.org/10.3382/ps.2011-02071

Vialpando, M., Smulders, S., Bone, S., Jager, C., Vodak, D., van Speybroeck, M., Verheyen, L., Backx, K., Boeykens, P., Brewster, M.E., Ceulemans, J., Novoa de Armas, H., van Geel, K., Kesselaers, E., Hillewaert, V., Lachau-Durand, S., Meurs, G., Psathas, P., van Hove, B., Verreck, G., Voets, M., Weuts, I., Mackie, C., 2016. Evaluation of Three Amorphous Drug Delivery Technologies to Improve the Oral Absorption of Flubendazole. J Pharm Sci 105, 2782–2793. https://doi.org/10.1016/j.xphs.2016.03.003

Vigh, T., Démuth, B., Balogh, A., Galata, D.L., Van Assche, I., Mackie, C., Vialpando, M., Van Hove, B., Psathas, P., Borbás, E., Pataki, H., Boeykens, P., Marosi, G., Verreck, G., Nagy, Z.K., 2017. Oral bioavailability enhancement of flubendazole by developing nanofibrous solid dosage forms. Drug Dev Ind Pharm 43, 1126–1133. https://doi.org/10.1080/03639045.2017.1298121

Vona, R., Mileo, A.M., Matarrese, P., 2021. Microtubule-based mitochondrial dynamics as a valuable therapeutic target in cancer. Cancers (Basel). https://doi.org/10.3390/cancers13225812

Vyas, T.K., Shahiwala, A., Amiji, M.M., 2008. Improved oral bioavailability and brain transport of Saquinavir upon administration in novel nanoemulsion formulations. Int J Pharm 347, 93–101. https://doi.org/10.1016/j.ijpharm.2007.06.016

Wallmeier, J., Nielsen, K.G., Kuehni, C.E., Lucas, J.S., Leigh, M.W., Zariwala, M.A., Omran, H., 2020. Motile ciliopathies. Nat Rev Dis Primers 6. https://doi.org/10.1038/s41572-020-0209-6

Wang, H., Zeng, X., Zhang, X., Liu, H., Xing, H., 2021. Ammonia exposure induces oxidative stress and inflammation by destroying the microtubule structures and the balance of solute carriers in the trachea of pigs. Ecotoxicol Environ Saf 212. https://doi.org/10.1016/j.ecoenv.2021.111974

Wang, X., Chen, W., Lin, Y., 2007. Sensitization of TNF-induced cytotoxicity in lung cancer cells by concurrent suppression of the NF-κB and Akt pathways. Biochem Biophys Res Commun 355, 807–812. https://doi.org/10.1016/j.bbrc.2007.02.030

Wang, X., Ju, W., Renouard, J., Aden, J., Belinsky, S.A., Lin, Y., 2006. 17-Allylamino-17-demethoxygeldanamycin synergistically potentiates tumor necrosis factor-induced lung cancer cell death by blocking the nuclear factor-κB pathway. Cancer Res 66, 1089–1095. https://doi.org/10.1158/0008-5472.CAN-05-2698

Wang, Y., Xie, Y., Li, J., Peng, Z.H., Sheinin, Y., Zhou, J., Oupický, D., 2017. Tumor-Penetrating Nanoparticles for Enhanced Anticancer Activity of Combined Photodynamic and Hypoxia-Activated Therapy. ACS Nano 11, 2227–2238. https://doi.org/10.1021/acsnano.6b08731

Wang, X.S., Zhang, L., Li, X., Kong, D.J., Hu, X.C., DIng, X.Z., Yang, J.Q., Zhao, M.Q., He, Y., Lam, K.S., Gao, S.G., Lin, T.Y., Li, Y., 2018. Nanoformulated paclitaxel and AZD9291 synergistically eradicate non-small-cell lung cancers in vivo. Nanomedicine 13, 1107–1120. https://doi.org/10.2217/nnm-2017-0355

Watanabe, K., Shimo, A., Tsugawa, K., Tokuda, Y., Yamauchi, H., Miyai, E., Takemura, K., Ikoma, A., Nakamura, S., 2016. Safe and effective deodorization of malodorous fungating tumors using topical metronidazole 0.75 % gel (GK567): a multicenter, open-label, phase III study (RDT.07.SRE.27013). Supportive Care in Cancer 24, 2583–2590. https://doi.org/10.1007/s00520-015-3067-0

Weinstein, M.P., Lewis, J.S., Bobenchik, A.M., Campeau, S., Cullen, S.K., Galas, M.F., Gold, H., Humphries, R.M., Kirn, T.J., Limbago, B., Mathers, A.J., Mazzulli, T., Richter, S.S., Satlin, M., Schuetz, A.N., Simner, P.J., 2021. M100 Performance Standards for Antimicrobial Susceptibility Testing, 31st Edition, 31st ed, CLSI.

Wijdeven, R.H., Pang, B., Assaraf, Y.G., Neefjes, J., 2016. Old drugs, novel ways out: Drug resistance toward cytotoxic chemotherapeutics. Drug Resistance Updates 28, 65–81. https://doi.org/10.1016/j.drup.2016.07.001

Wijesekara, P., Yadav, P., Perkins, L.A., Stolz, D.B., Franks, J.M., Watkins, S.C., Reinoso Jacome, E., Brody, S.L., Horani, A., Xu, J., Barati Farimani, A., Ren, X., 2022. Engineering rotating apical-out airway organoid for assessing respiratory cilia motility. iScience 25. https://doi.org/10.1016/j.isci.2022.104730

Williamson, P.R., Jarvis, J.N., Panackal, A.A., Fisher, M.C., Molloy, S.F., Loyse, A., Harrison, T.S., 2016. Cryptococcal meningitis: Epidemiology, immunology, diagnosis and therapy. Nat Rev Neurol. https://doi.org/10.1038/nrneurol.2016.167

Wohlfart, S., Gelperina, S., Kreuter, J., 2012. Transport of drugs across the blood-brain barrier by nanoparticles. Journal of Controlled Release. https://doi.org/10.1016/j.jconrel.2011.08.017

Wong, T.W., 2020. Choice of nanocarrier for pulmonary delivery of cancer therapeutics. Expert Opin Drug Deliv. https://doi.org/10.1080/17425247.2020.1702021

Woodward, L., Haisfield-Wolfe, M.E., 2003. Management_of_a_Patient_With_a_Malignant_Cutaneous_2003. Journal of Wound Ostomy & Continence Nursing 30, 231–236. https://doi.org/10.1067/mjw.2003. 138

World Health Organization, n.d. Cancer. URL https://www.who.int/health-topics/cancer#tab=tab_1 (accessed 11.27.22).

World Health Organization, 2023. HIV/AIDS. URL https://www.who.int/health-topics/hiv-aids/#tab=tab_1 (accessed 1.4.23).

World Health Organization, 2022. Lymphatic filariasis.

Xia, A., Zhang, Y., Xu, J., Yin, T., Lu, X.J., 2019. T Cell Dysfunction in Cancer Immunity and Immunotherapy. Front. Immunol. 10, 1719. https://doi.org/10.3389/fimmu.2019.01719

Xie, Y., Bagby, T.R., Cohen, M.S., Forrest, M.L., 2009. Drug delivery to the lymphatic system: importance in future cancer diagnosis and therapies. Expert Opin. Drug Deliv. 6, 785–792.

Xiong, R., Wu, Y., Wu, Q., Muskhelishvili, L., Davis, K., Tripathi, P., Chen, Y., Chen, T., Bryant, M., Rosenfeldt, H., Healy, S.M., Cao, X., 2021. Integration of transcriptome analysis with pathophysiological endpoints to evaluate cigarette smoke toxicity in an in vitro human airway tissue model. Arch Toxicol 95, 1739–1761. https://doi.org/10.1007/s00204-021-03008-0

Xu, H., Vela, S., Shi, Y., Marroum, P., Gao, P., 2017. In Vitro Characterization of Ritonavir Drug Products and Correlation to Human in Vivo Performance. Mol Pharm 14, 3801–3814. https://doi.org/10.1021/acs.molpharmaceut.7b00552

Xu, H.Y., Liu, C.S., Huang, C.L., Chen, L., Zheng, Y.R., Huang, S.H., Long, X.Y., 2019. Nanoemulsion improves hypoglycemic efficacy of berberine by overcoming its gastrointestinal challenge. Colloids Surf B Biointerfaces 181, 927–934. https://doi.org/10.1016/j.colsurfb.2019.06.006

Xua, S., Dai, W.G., 2013. Drug precipitation inhibitors in supersaturable formulations. Int J Pharm. https://doi.org/10.1016/j.ijpharm.2013.05.013

Yáñez, J.A., Wang, S.W.J., Knemeyer, I.W., Wirth, M.A., Alton, K.B., 2011. Intestinal lymphatic transport for drug delivery. Adv Drug Deliv Rev. https://doi.org/10.1016/j.addr.2011.05.019

Yi, M., Weaver, D., Hajnóczky, G., 2004. Control of mitochondrial motility and distribution by the calcium signal: A homeostatic circuit. Journal of Cell Biology 167, 661–672. https://doi.org/10.1083/jcb.200406038

Yoshida, G.J., 2017. Therapeutic strategies of drug repositioning targeting autophagy to induce cancer cell death: From pathophysiology to treatment. J Hematol Oncol. https://doi.org/10.1186/s13045-017-0436-9

Yoshimatsu, Y., Miyazaki, H., Watabe, T., 2016. Roles of signaling and transcriptional networks in pathological lymphangiogenesis. Adv Drug Deliv Rev. https://doi.org/10.1016/j.addr.2016.01.020

Yoshimura, K., Shibata, M., Koike, M., Gotoh, K., Fukaya, M., Watanabe, M., Uchiyama, Y., 2006. Effects of RNA interference of Atg4B on the limited proteolysis of LC3 in PC12 cells and expression of Atg4B in various rat tissues. Autophagy 2, 200–208. https://doi.org/10.4161/auto.2744

Yukuyama, M.N., Araújo, G.L.B. de, Bou-Chacra, N.A., 2020. Nanomaterials for hair care applications, in: Nanocosmetics. Elsevier, pp. 205–225. https://doi.org/10.1016/b978-0-12-822286-7.00010-3

Yukuyama, M.N., Ferreira Guimaraes, L.M., Segovia, R.S., Lameu, C., de Araujo, G.L.B., Löbenberg, R., de Souza, A., Bazán Henostroza, M.A., Folchini, B.R., Peroni, C.M., Saito Miyagi, M.Y., Oliveira, I.F., Rinaldi Alvarenga, J.F., Fiamoncini, J., Bou-Chacra, N.A., 2022. Malignant wound – The influence of oil components in flubendazole-loaded nanoemulsions in A549 lung cancer xenograft-bearing mice. J Drug Deliv Sci Technol 103963. https://doi.org/10.1016/j.jddst.2022.103963

Yukuyama, M.N., Ghisleni, D.D.M., Pinto, T.J.A., Bou-Chacra, N.A., 2016. Nanoemulsion: Process selection and application in cosmetics - A review. Int J Cosmet Sci. https://doi.org/10.1111/ics.12260

Yukuyama, M.N., Ishida, K., de Araujo, G.L.B., Spadari, C. de C., de Souza, A., Löbenberg, R., Henostroza, M.A.B., Folchini, B.R., Peroni, C.M., Peters, M.C.C., de Oliveira, I.F., Miyagi, M.Y.S., Bou-Chacra, N.A., 2021. Rational design of oral flubendazole-loaded nanoemulsion for brain delivery in cryptococcosis. Colloids Surf A Physicochem Eng Asp 630. https://doi.org/10.1016/j.colsurfa.2021.127631

Yukuyama, M.N., Kato, E.T.M., de Araujo, G.L.B., Löbenberg, R., Monteiro, L.M., Lourenço, F.R., Bou-Chacra, N.A., 2019. Olive oil nanoemulsion preparation using high-pressure homogenization

and D-phase emulsification – A design space approach. J Drug Deliv Sci Technol 49, 622–631. https://doi.org/10.1016/j.jddst.2018.12.029

Yukuyama, M.N., Oseliero, P.L.F., Kato, E.T.M., Lobënberg, R., de Oliveira, C.L.P., de Araujo, G.L.B., Bou-Chacra, N.A., 2018. High internal vegetable oil nanoemulsion: D-phase emulsification as a unique low energy process. Colloids Surf A Physicochem Eng Asp 554, 296–305. https://doi.org/10.1016/j.colsurfa.2018.06.023

Zaragoza, O., Rodrigues, M.L., de Jesus, M., Frases, S., Dadachova, E., Casadevall, A., 2009. Chapter 4 The Capsule of the Fungal Pathogen Cryptococcus neoformans. Adv Appl Microbiol. https://doi.org/10.1016/S0065-2164(09)01204-0

Zeng, Q., Li, H., Jiang, H., Yu, J., Wang, Y., Ke, H., Gong, T., Zhang, Z., Sun, X., 2017. Tailoring polymeric hybrid micelles with lymph node targeting ability to improve the potency of cancer vaccines. Biomaterials 122, 105–113. https://doi.org/10.1016/j.biomaterials.2017.01.010

Zhang, L., Guo, M., Li, J., Zheng, Y., Zhang, S., Xie, T., Liu, B., 2015. Systems biology-based discovery of a potential Atg4B agonist (Flubendazole) that induces autophagy in breast cancer. Mol Biosyst 11, 2860–2866. https://doi.org/10.1039/c5mb00466g

Zhang, W., An, M., Xi, J., Liu, H., 2017. Targeting CpG Adjuvant to Lymph Node via Dextran Conjugate Enhances Antitumor Immunotherapy. Bioconjug. Chem. 28, 1993–2000. https://doi.org/10.1021/acs.bioconjchem.7b00313

Zirakzadeh, A.A., Marits, P., Sherif, A., Winqvist, O., 2013. Multiplex B Cell Characterization in Blood, Lymph Nodes, and Tumors from Patients with Malignancies. J. Immunol. 190, 5847–5855. https://doi.org/10.4049/jimmunol.1203279

APPENDIX 1 – NANOMATERIALS FOR HAIRCARE APPLICATIONS

I am the first author and was responsible for Conceptualization, Investigation, Resources, Data Curation, Project administration, Writing - Original Draft and Visualization

A1.1. INTRODUCTION

Apparently, hair seems to be a basic structure comprised of simple filaments that offer thermal protection, and that reflect social status and relations of individuals, including such aspects as healthy appearance, age, and lifestyle trends. But in fact, hair is made up of complex structures that implicated in cell differentiation, proliferation, the lifecycle, and disorders. The daily application of topical components may highly affect the final appearance of hair, considering that different compounds can penetrate and act on different segments of the hair structure.

Hair care products, including shampoo, conditioner, and leave-on products, focus on improving the appearance along hair length, while the dermo-cosmetic products such as anti-hair loss, anti-dandruff products focus on treatment based on absorption of active compounds into the hair scalp.

The efficacy of applied active compounds on hair or scalp depends on their penetration via three different pathways: intercellular, hair follicle, and transcellular. The first pathway is established by diffusion of substances in the stratum corneum of the scalp through the corneocyte surfaces, which are surrounded by lipid layers. The second occurs by the diffusion of compounds through the opening of follicular orifices and can reach the deep region of the scalp. Therein, a dense network of blood capillaries surrounds the hair follicles. This second pathway has gained increasing attention in recent years, and is one of the main focuses of this chapter. The third one is the penetration of substances directly through the corneocytes and lipid layers, overcoming the stratum corneum barrier to reach the living cells (Mihranyan et al., 2012) (**Figure A1.1**).

Hair products are extensively marketed, and several types of nanostructured systems have been developed in recent years. Therefore, this chapter aims to present the different disorders and needs related to hair structure, and new tendencies based on the prospective nano systems.
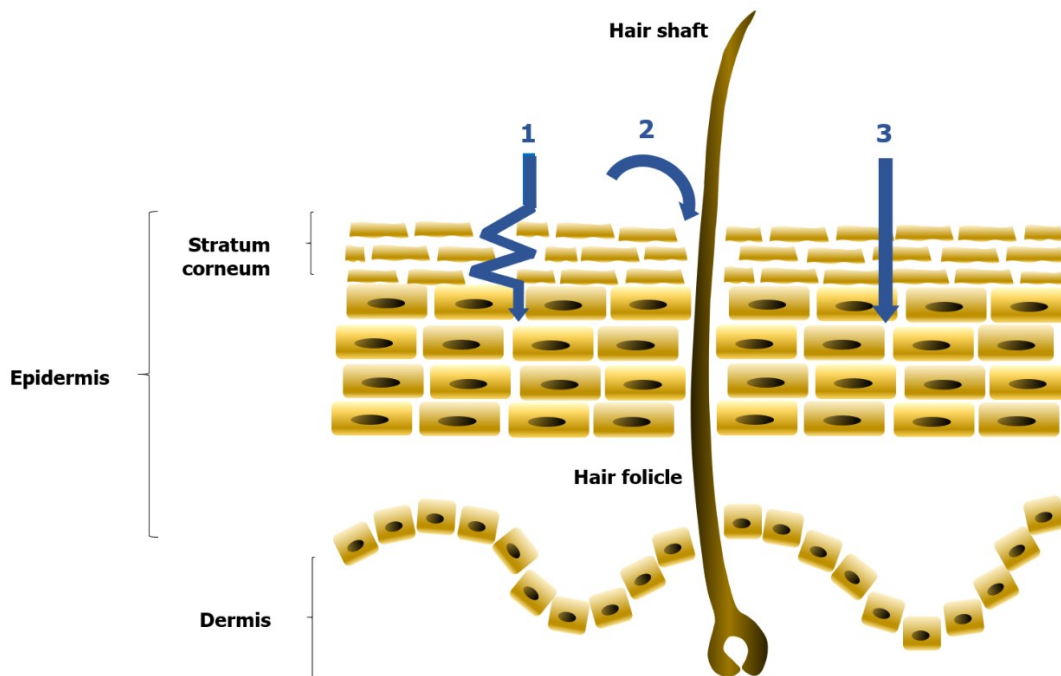
Figure A1.1: Penetration of active compounds on hair or scalp

Source: Own authorship

A1.2. HAIR STRUCTURE

To better understand the mechanisms involved in hair application, we focused on the hair structure in two major segments: the hair shaft and hair follicles, which are the main targets of the nanostructures for the current and prospective hair treatments.

The schematic structure of the hair shaft and hair follicle are shown in **Figure A1.2**.
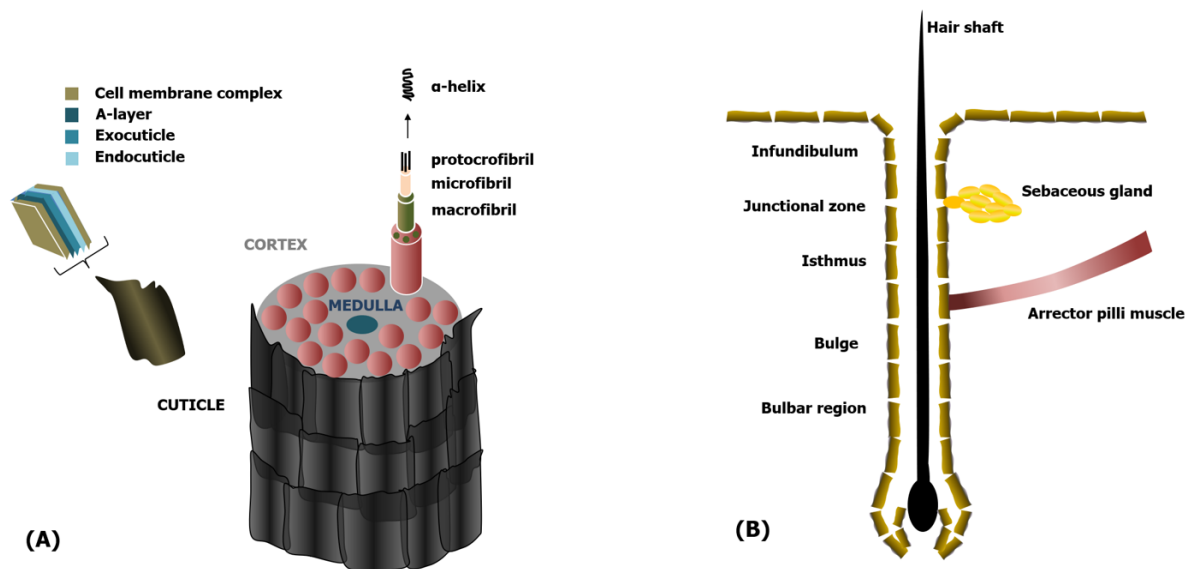
Figure A1.2: Schematic structure of the hair shaft and hair follicle

Source: Own authorship

A1.2.1. Hair Shaft

The hair shaft is the upper part of the hair structure, which emerges through the skin surface, and is composed of dead cells. The hair shaft is made up of three concentric regions, named from the external to the internal part: cuticle, cortex, and medulla (Robins, 1988).

The cuticle is the outermost region of the hair, which forms a resistant film that surrounds the cortex. The cuticle is organized as flat overlapping cells in a scale-like structure, and each cuticle cell contains an epicuticle, a thin outer membrane. Under the epicuticle, there are three membranes: the A layer, the exocuticle, and the endocuticle. Therein, the content of cystine decreases from the highest ~30% to the lowest ~3% (Robins, 1988). The cuticle is responsible for protecting the hair from external damage, such as daily brushing, excess heat, or the use of chemicals products (e.g., dying, relaxing or straightening processes). The damage of the cuticle leads to loss of natural glow, which reflects the loss of healthy hair structure, caused by these injuries (Robins, 1988; Rosen et al., 2015).

The cortex comprises the majority of fiber mass of hair, giving mechanical strength to the hair. The cortex, located in the middle of the cuticle and medulla, is composed of cells and the cell membrane complex (CMC), also called intercellular binding material, a cement located between cell membranes (Robins, 1988). Inside the cortex, there are pigment granules (melanin) responsible for the color of hair, that undergo influences of the type, distribution, and number of melanin granules (Su et al., 2017). There are also twisted-bundle fibrous cells called macrofibrils or macrofilaments, corresponding to the major portion of the cortex. Each macrofibril contains several microfibrils distributed within a matrix. Microfibrils are highly organized subfilamentous structures, ordered in a spiral formation. Each microfibril is composed of helicoidal subfilamentous units called protofibrils, which are made up of several polypeptide chains of proteins, called an alpha-helix (Robins, 1988). The innermost part of the hair shaft is called the medulla. This porous region, which has a variable diameter, supports the hair structure, but its function remains unclear (Rosen et al., 2015; Su et al., 2017).

A1.2.2. Hair Follicle

Structured as an extended cavity of the epidermis that reaches the depth of the skin, follicles can act as an efficient reservoir of active compounds, compared to the stratum corneum (Fang et al., 2014). The density and size of follicles depend on the sites. Impressively, about 10.0% of the total surface area of the skin constitutes follicular orifices of the face and scalp, while only 0.1% is found in other sites of the body (Patel et al., 2018). This fact demonstrates the influence of the follicle on the absorption of active compounds when applied topically on those desired sites. The hair follicle is composed of infundibulum, a junctional zone / isthmus, and bulb, which consists of the upper, middle, and lower segments of the hair follicle, respectively (Rosen et al., 2015).

Infundibulum is the most extensive interface between epithelium and the environment. It starts from the follicular orifice of the hair follicle extending to the sebaceous gland. It provides additional absorption of topically applied compounds, promoting their high accumulation (Fang et al., 2014; Patel et al., 2018; Rosen et al., 2015). The infundibulum also influences the hair follicle

biology and pathology, harboring a rich residential microflora, and is implicated in the pathogenesis of several skin disorders (Schneider and Paus, 2014).

One or more sebaceous glands are attached in the hair follicle. The junctional zone is located near the sebaceous gland duct, while the isthmus is located near the bottom of the sebaceous gland duct to the arrector pilli muscle. The sebaceous glands are responsible for the production of sebum, a complex lipid mixture, found in the follicular duct. (Fang et al., 2014; Rosen et al., 2015; Schneider and Paus, 2014).

Below the isthmus, there is a bulging region, where epithelial and melanocyte stem cells are found. (Rosen et al., 2015; Schneider and Paus, 2014). At the base of the hair follicles, there is a tulip bulb-like structure, which actively produces the hair shaft. This keratinization site determines the morphology of the hair. According to Thibaut et al. (2005), the bulb is responsible for programming the hair shape. The asymmetry or symmetry in differentiation programs is responsible for determining the curliness or the straightness of the hair (Thibaut et al., 2005). The bulge and bulb site also have critical roles in melanogenesis, which determines the pigmentation of the hair. The melanocytes are located in the bulb region and the melanocyte stem cells in the bulge-sub-bulge region. These regions function as a reservoir of melanocytes for hair pigmentation and maintenance, in each hair cycle. (Nishimura, 2011).

A more detailed description of each mechanism of hair pigmentation, hair growth, and the disorder related to the sebum secretion is provided in the following sections.

A1.3. NANOSTRUCTURED SYSTEMS FOR HAIR TREATMENT

In recent years, nanostructured systems have attracted attention in the dermo and cosmetic fields. They may offer treatment or protection of the hair shaft from external damage, in addition to facilitating specific penetration of active compounds through the follicular pathway. It is worth noting that nanoparticles of 100nm are around 1,000 times smaller in size than the average diameter of a human hair. (Niska et al., 2018). In principle, nanostructured systems have several advantages over those of larger particle sizes, as a result of the improved stability of the active

compounds, efficient delivery of these compounds to the desired site, safety, and controlled release (Lohan et al., 2016). A considerable number of nanostructured systems have been developed in recent years, focusing on treating hair shaft and treatment through the hair follicles.

Starting with the hair shaft, the function of the hair does not only refer to the primary function, such as the regulation of body temperature. Healthy, shiny, and silky hair offers daily aesthetic features that significantly affect the social and individual quality of life. The flexibility provided by the ability to modify hair, such as hair dyeing, straightening, or curling, may improve the well-being of an individual. However, they lead to increased damage to hair. Also, increased life expectancy and the aging of society may raise concerns: thinning hair, hair loss, dryness due to sebum production reduction, and gray hair. Consequently, efficient improvement of the hair shaft using nanostructured systems for immediate or long-term effect is desirable.

Regarding the second point, targeting hair follicles with active compounds has delivered increasing insights and gained interest of researchers. The use of nanostructured systems offers better guidance in the desired site, increasing their retention and, avoiding the side effects and irritations caused by the excessive introduction of these compounds (Matamá et al., 2015). Evaluation of porcine skin by *in vitro* testing using nanoparticles with different mean particle sizes indicated that particles between 400 and 700 nm reached deeper sites in the hair follicle. They were compared to those with a mean size higher or lower than this range (Patzelt et al., 2011). Although the correct mean size for the best transfollicular permeation or penetration is still under discussion (Patel et al., 2018), nanostructured systems are very promising, since they are generally smaller than the size of the follicular openings (Corrias et al., 2017).

The results of *in vitro* penetration or deposition evaluation of the nanostructured systems might be carefully compared with *in vivo* performance through the transfollicular pathway. Reduced impact on the penetration and follicular reservoir capacity was observed in *in vitro* testing, due to the contraction of the elastic fibers of the excised skin. (Poljšak et al., 2012). Another element to consider is hair movement. The hair follicle and this surface structure perform as a pumping system that conducts particles into the hair follicle, under the movement of hair. This movement, which improves the penetration of the particles, can be simulated by a massage appliance in the *in vitro* penetration test (Lademann et al., 2007).

The hair follicle is responsible for sebum formation due to its attached sebaceous gland, producing a lipid-enriched environment from the follicular duct to the stratum corneum (Fang et al., 2014; Rosen et al., 2015; Schneider and Paus, 2014). Different types of nanostructured systems, which are mentioned in the next sections, interact differently with sebum for subsequent transport into hair follicles (Rancan et al., 2013). The hair follicle acts as a reservoir of active compounds, showing the longest accumulation time compared to the stratum corneum. The shorter accumulation of active compounds at stratum corneum is due to the intense turnover of the uppermost cellular layer of the horny layer, where the stratum corneum is located. Moreover, the hair follicle has a deeper extension that reaches the dermal tissue, further enhancing its carrier role (Lademann et al., 2007). Landermann et al. (2006) demonstrated that the reservoir of hair follicles could store particles ten times longer than in the reservoir of the stratum corneum (Lademann et al., 2006).

A1.3.1. Types of nanostructured systems

Different performances are expected in the hair shaft or hair follicle, according to the vehicle, type, surface, or the mean particle size of the applied nanostructure. Several nanostructured types have been developed in the past and recent years, showing specific interactions according to their specificities. Examples of nanostructured systems for hair treatments are liposomes, cyclodextrins, dendrimers, polymeric nanoparticles, metallic nanoparticles, nanocrystals, solid lipid nanoparticles (SLNs) and nanostructured lipid carriers (NLCs), and nanoemulsions.

A1.3.1.1. Liposomes

Liposomes are vesicular structures composed of phospholipid bilayers. These nanostructures improve the interaction with sebum and the penetration of the active compounds into the hair follicles. The active compounds can be located in the membrane or the inner part of the liposomes, according to their lipophilicity or hydrophilicity, respectively (Betz et al., 2001). The high selectivity and safety of liposomes were successfully demonstrated in 1995 by entrapment of DNA in liposomes for penetration into the hair follicles. This gene therapy was performed by topical application in mice. (Li and Hoffman, 1995).

A1.3.1.2. Cyclodextrins

Cyclodextrins are cyclic sugar compounds with a lipidic internal cavity and hydrophilic external surface. Lipophilic drugs are enabled to form nanoscale aggregates by their internalization in the central cavity of cyclodextrins. Using a fluorescence image microscopy, a study with the curcumin-cyclodextrin nano complex showed selective and efficient penetration of curcumin into deep sites of hair follicles (Konrádsdóttir et al., 2009).

A1.3.1.3. Dendrimers

Dendrimers, also called dendritic polymers, are synthetic, tree-like macromolecules with flexibility to modify the architecture according to the desired functionality. They consist of a central core surrounded by repeated branches in the outer part. The unique property of dendrimers is not only their ability to encapsulate a drug in its core but also to conjugate with their surface groups. Different types of dendrimers have been designed since the 1970s, including hyperbranched polymers, perfect dendrimers, dendronized polymers, functional dendrons, dendrimer core-shells, and core-multi-shell particles (Sun et al., 2012; Zoschke et al., 2015).

An example of a dendrimer for hair application is the dendritic core-multi shell particles (CMS), developed to load spin-labeled 5-doxyl stearic acid (5DSA). CMS is a dendritic polar polyglycerol polymer core hyperbranched with C18 diacide building blocks, at the inner shell, and hydrophilic polyethylene glycol, at the outer shell. 5DSA is a spin-labeled stearic acid, functioning as a hydrophobic spin probe, which enables evaluating the loading and transport capacity of particles into the skin under the use of electron paramagnetic resonance (EPR) spectroscopy. Results showed the effective penetration of this CMS into hair follicles to a depth of 340 μm ± 82 μm (Lohan et al., 2016).

Another interesting example is the pH-responsive-dendritic-polyglycerol-nanogel (dPG-NG), developed to evaluate the pH of the hair follicle at different depths, applying an *ex vivo* porcine-ear model. An inverse nanoprecipitation method was used to prepare this pH-labeled dPG-NG, with a mild and surfactant-free Thiol-Michael reaction. Determination of pH within the hair follicle, through analysis of confocal laser scanning microscopy images, showed a pH increase from 6.5 to 7.4, from the skin surface to the deepest part of the hair follicle, respectively. It also

showed that there is a sudden increase in pH in the first half of the penetration depth. This potential non-toxic dPG-NG may open new possibilities for future pH-triggered nano-drug delivery systems, aiming at the intrafollicular delivery of drugs (Dimde et al., 2017).

A1.3.1.4. Polymeric nanoparticles

Another nanoparticle that has gained attention, especially for follicular delivery is polymeric nanoparticles. These solid-spherical nanosized colloidal systems can be classified as nanospheres, nanocapsules, or nanogels. The first is formed by a polymeric matrix that entraps a drug. The second consists of a polymeric membrane surrounding an encapsulating drug cavity (Krishnaswamy and Orsat, 2017). And the latter are hydrophilic or organic gelling agents, which form three-dimensional networks through physical or chemical crosslinks (Rancan et al., 2014).

Two different technologies are mainly used for preparing polymeric nanoparticles: the top-down method and the bottom-up method. The top-down process applies preformed polymers dispersed in nano-scaled structures under several approaches, such as nanoprecipitation, solvent evaporation, emulsion diffusion, or interfacial deposition. The bottom-up method consists of polymerization of monomers, using different approaches, such as emulsion, microemulsion, interfacial polymerization, or molecular inclusion (Krishnaswamy and Orsat, 2017; Rancan et al., 2009).

Different polymer materials are used to develop these polymeric nanoparticles: the natural ones, and the synthetic ones, which are preferentially biodegradable or biocompatible. The natural polymers are of plant or animal origin, such as hyaluronic acids, collagen, alginate, chitosan or dextran. The biodegradable materials are those eliminated or metabolized by the body, after being broken down into nontoxic substances. The biocompatible materials are nondegradable ones, but their final elements, after excretion by renal clearance, are considered safe in *in vivo* studies. Examples of biodegradable polymers are poly(ε-caprolactone) (PCL), for preparation of polymeric matrixes. Example of biocompatible materials are the poly(lactic-co-glycolic acid) (PLGA), poly(ethylene glycol) (PEG), or methyl methacrylate (MMA), for preparation of hydrogels (Rancan et al., 2014).

Many researchers have extensively studied the penetration and prolonged-release effect of polymer nanoparticles in hair follicles. Lademann et al. (2007) compared a 320-nm fluorescent polymeric nanoparticle with a non-particulate form, under *in vitro* and *in vivo* topical applications. This polymeric nanoparticle, composed of polyvinyl alcohol and poly(D, L-lactide-co-glycolide), presented deeper penetration than the non-particulate form in *in vitro* test, after simultaneous application of massage on porcine skin. It also showed a more extended storage period in the *in vivo* evaluation, by differential stripping test on human skin (ten days and four days, for nanoparticle and non-particulate form, respectively) (Lademann et al., 2007). Another author tested poly (D, L-lactide) nanoparticles of approximately 150 nm and demonstrated their presences along the entire follicular duct (Fernandes et al., 2015).

Size influence studies on the penetration and long-term release of polymer nanoparticles in hair follicles were also performed. Rancan et al. (2009) compared fluorescent dye-loaded poly-lactic acid (PLA) nanoparticles with different particle sizes (228 and 365 nm) in human skin explants. Equal penetration and release profiles were observed for both particle sizes in the hair follicles, indicating that there is no size influence in this range (Rancan et al., 2009). Another study compared poly(D, L-lactide-co-glycolide) (PLGA) nanoparticles with same particle sizes (163–170 nm), however, with different surface modifications: the plain PLGA, chitosan-coated PLGA, and chitosan-coated PLGA with different phospholipids. The *in vitro* test indicated that negatively-charged nanoparticles and lipophilic-surface properties were more favorable for follicular uptake. This study showed the relevance of the surface property over the size in nanoparticle follicular distribution (Raber et al., 2014).

A comparison study between the dexamethasone nanocrystal (221 ± 4 nm) and a polymeric nanoparticle, the dexamethasone-loaded ethyl cellulose nanocarriers (147 ± 2 nm), indicated the influence of nanoparticle composition on follicle uptake. The former improved the dissolution rate of the drug, showing to be a good candidate for poor solubility drugs, with limited penetration. On the other hand, the latter allowed for prolonged-release, and the particles remained for many days in the hair follicle, which is interesting for a drug with a high penetration profile such as dexamethasone (Döge et al., 2016).

A fluorescein isothiocyanate (FITC)-labeled BSA hydrogel nanocarrier was used to evaluate the gradient dependent release of the drug tetramethylrhodamine-dextran (TRITC-dextran), by *in vitro* test on porcine ear skin. Nanoparticles of approximately 663 nm were evaluated by confocal laser scanning microscope, and TRITC-dextran was found in the infundibular region of porcine hair follicles (Tran et al., 2017).

A1.3.1.5. Metallic nanoparticles

Metallic nanoparticles (NPs) are rigid particles that present several benefits, such as increased effectiveness of nano-organic drugs. They can be made of different metallic materials (e.g., gold nanoparticles, silver nanoparticles) and metal oxide (e.g., iron oxide nanoparticles, zinc oxide nanoparticles). The complexation of the active compounds with the metal particles within this core, or by adsorption on this surface, increases the potential to increase binding to the specific target and reduces toxicity (Fang et al., 2014; Lademann et al., 2006). TiO2NPs and AgNPs are used in shampoo formulations for various purposes, such as preventing hair loss, shine or antifungal properties (Niska et al., 2018).

Mahmouda et al. (2017) investigated the behavior of gold nanoparticles, with different surface composition and charge, with the follicular compartments of the skin. Hydrophobic gold nanoparticles exhibited higher affinity with hair follicles, providing preferential accumulation within the hair compartments. On the other hand, charged gold nanoparticles presented a physical and chemical skin barrier, in which the penetration percentage was insignificant (Mahmoud et al., 2017).

AuNP-doped bovine serum albumin nanoparticles were developed to deliver fluorescein isothiocyanate by a heat-activated release mechanism. These metallic nanoparticles were applied on porcine ear skin, and water-filtered infrared A radiation was used for induction and subsequent release of fluorescent dye. This inducing method for metallic nanoparticle enabled deeper penetration of the dye into the follicular duct, with a tolerable radiation level to the skin. The preparation method, without the addition of chemical crosslinkers, provided a more biocompatible nanocarrier with approximately 545 nm in diameter. *In vitro* testing detected an increased fluorescent signal in the hair follicles and the sebaceous glands for the treatment group, compared

to the weak signal in the control group. The strong fluorescent signal is evidence of successful dye release at the targeted site. These findings encourage future development of heat-induced drug-loaded metallic nanocapsules for potential delivery in hair follicles (Lademann et al., 2016).

A1.3.1.6. Nanocrystal

Nanocrystals are nanoscale-sized pure drug particles without any matrix material. They are stabilized with adsorption of low quantity of surfactants (e.g., ionic, nonionic surfactants) or polymers (e.g., polyvinyl alcohol, hydroxypropyl methylcellulose, polyvinyl pyrrolidone/povidone) at their interface, which prevents particle aggregation and allows their suspension in an external liquid phase. Their high drug loading capacity, high dissolution rate, and high saturation solubility make it possible to produce nanoparticles with good stability, delivery, and safety. Nanocrystals can be prepared by two different processes: bottom-up and top-down processes (Patel et al., 2018; Vidlárová et al., 2016). The first is the classic precipitation method, where a solvent-dissolved drug is added to another non-solvent phase, and the drug precipitation occurs to yield a nanocrystal. The limitation of this process is the need to remove of this solvent, which may have stability, safety, or cost issues. The second approach is the reduction of a micrometer drug crystal to a nanometric drug crystal by the use of mechanical processes. These processes include high-pressure homogenization, microfluidization or media milling, in which high-shear, cavitation, or pressure are applied to convert the drug to a nanometer size (Patel et al., 2018).

Several experiments have evaluated the affinity of nanocrystals with hair follicles. Corrias et al. (2017) prepared a nanocrystal of water-insoluble dye, Nile Red, in combination with Polysorbate 80 or Poloxamer 188 as a stabilizer. The 230-nm nanocrystal was made using the media milling technique. The *in vitro* skin permeation studies have demonstrated the accumulation of Nile Red nanocrystal in the follicular duct (Corrias et al., 2017). Another hair follicle location study was performed with curcumin nanocrystal prepared by the smartCrystals® process. This process involves a combination of the bead milling technique followed by high-pressure homogenization, yielding a nanocrystal of 200 nm. The alkyl polyglycoside surfactant was used as a stabilizer. An *in vitro* porcine skin test using fluorescent microscopy was performed comparing curcumin nanosuspensions of different concentrations, and either the curcumin

nanosuspension mixed with high viscosity hydroxypropyl cellulose gel. The results identified curcumin deposition in hair follicles when the concentration of nanosuspension was up to 0.02% by weight. There was no significant influence of the viscosity on the hair follicle deposition, indicating the use of nanocrystals as a promising carrier for water-insoluble compounds for hair follicles (Vidlárová et al., 2016).

A1.3.1.7. Solid lipid nanoparticles and nanostructured lipid carriers

Solid lipid nanoparticles (SLNs) were introduced in the 1990s as a lipidic nanoparticle consisting of solid lipids in its core. Later, Muller et al. introduced nanostructured lipid carriers (NLCs) to provide better stability to the encapsulated drug compared to SLNs. This is due to the NLCs core composition, which is comprised of a mixture of solid and liquid lipids with a less organized structure, preventing expulsion of the encapsulated drug from the rigid matrix of SLNs (Müller et al., 2002). Both lipid nanostructures are present in a solid-state at room temperature. Examples of the solid lipids are fatty acids (e.g., palmitic acid), mono, di and triglycerides (e.g., glyceryl monostearate, glyceryl behenate, tristearin), cholesterol and waxes (Noor et al., 2017). Although new components have been emerging for SLN and NLC preparations in recent years, the advantage of these carriers is usually the nature of their lipids, which are mainly biodegradable or biocompatible. A systematic review of SLNs and NLCs was done by Doktorovová et al (2016), with providing data on the safety of these lipid nanoparticles. The authors reported that the *in vitro* test indicated acceptable SLN/NLC total lipids concentrations up to 1 mg/mL; lower tolerance of mean particle size up to 500nm in cell culture; greater biocompatibility of lipid nanoparticles stabilized by a single surfactant rather than combinations; and good SLN/NLC skin tolerability by both *in vitro* and *in vivo* dermal tests (Doktorovová et al., 2016).

The efficacy of SLN along the hair follicle was demonstrated by the development of Flutamide-loaded SLNs, for treating androgenic alopecia. Under topical application, this 198 nm SLN showed higher drug deposition in the skin compared to Flutamide hydroalcoholic solution, and higher growth of new hair follicle in the *in vitro* evaluation. This study indicated more significant accumulation of SLN in the hair follicles and the slow and controlled release of Flutamide along the hair follicles (Hamishehkar et al., 2016).

Podophyllotoxin (POD) - loaded solid lipid nanoparticles were prepared by high-pressure homogenization method. Poloxamer 188 and soybean lecithin were used as stabilizers, yielding SLN with a particle size of 73.4 nm, and 48.36 mV zeta potential value. After application of POD-loaded SLN to porcine skin, fluorescence microscopy image indicated POD penetration by two pathways, the stratum corneum, and the hair follicle route (Chen et al., 2006).

Several lipid nanocarriers have been developed for treating alopecia, aiming at safe and effective delivery of drugs to hair follicles. This issue will be discussed in great detail in the next alopecia treatment section.

A1.3.1.8. Nanoemulsions

Nanoemulsions are composed of a mixture of the liquid oil phase, surfactants, and water phase. They are classified as oil-in-water (O/W) or water-in-oil (W/O) nanoemulsions, depending on the type and quantity of their components, mainly influenced by the surfactant type. The former consists of the internal oil core surrounded by a hydrophilic surfactant, which is dispersed in the outer water phase. The latter consists of the inner water core surrounded by a hydrophobic surfactant, where this micelle is dispersed in the external oil phase. Most dermal products on the market are O/W emulsions, which provide a lighter touch than W/O emulsions (Yukuyama et al., 2019).

Nanoemulsions differ from microemulsion since the latter is a thermodynamically stable isotropic phase (Sonneville-Aubrun et al., 2018). Nanoemulsions, being thermodynamically unstable, are not formed spontaneously; therefore, some external energy input is required for their formation. There are two different processes for preparing nanoemulsions: high-energy and low-energy ones. The former, the mechanical process, is based on high shear, pressure, or cavitation phenomena, yielding emulsion on the nanosized scale. As a high-energy process, we highlight the high-pressure homogenization, ultrasonication, microfluidizers, and membrane emulsification. The latter, the physicochemical process, is based on lowering the surface interfacial tension during preparation, by the correct balance of the phases. Examples of low-energy processes are, spontaneous emulsification, phase inversion temperature (PIT), phase inversion composition

(PIC), self-nano emulsifying method (Yukuyama et al., 2017), and D-phase emulsification methods (Sagitani et al., 1986; Yukuyama et al., 2018).

Some advantages of nanoemulsion over other nanostructures have been reported. A comparative study of nanosized formulation composed of liquid-lipid state core (such as nanoemulsions) and solid-lipid state core (such as SLNs) was done using testosterone (TP) as a hydrophobic drug. The results showed higher solubility of TP in the liquid-lipid state nanosized formulation than the solid-lipid state, illustrating nanoemulsions as a promising delivery system for poorly soluble components (Wasutrasawat et al., 2013). Nanoemulsions were also cited as more efficient transdermal carriers compared to rigid nanoparticles, due to their flexible and fluid microstructure (Su et al., 2017).

In another study, improvement of transfollicular delivery of various caffeine-loaded nanoemulsions was investigated by *in vitro* permeation test. Skin permeation enhancers such as oleic acid and eucalyptol were part of the composition of these nanoemulsions. Blocked and open follicle models were used: the former model was designed to evaluate transepidermal or transfollicular caffeine permeation; the latter model aimed to evaluate the permeation by transfollicular permeation pathway. The cyanoacrylate skin surface biopsy method was further used to analyze the follicular contents directly. These combined methods demonstrated that nanoemulsions were able to deliver the hydrophilic drug caffeine into and through hair follicles (Abd et al., 2018).

There is also a study showing the influence of nanoemulsion particle size on different routes and locations in hair follicles. P4-dye-loaded nanoemulsions were used for this proposal and indicated that nanoemulsion particle size of around 80nm might diffuse along with the viable epidermis and fill the entire hair follicles, while nanoemulsions of around 500-nm particle size have limited penetration into the stratum corneum and easily migrate along the hair follicle (Su et al., 2017).

As described, an increasing number of nanostructured systems were developed to address hair treatment. Different advantages or disadvantages were presented for each structure, and the growing number of discoveries shows their potential, targeting hair shafts and hair follicle treatments. It is essential to consider that the regular or daily application of cosmetic products by

users can facilitate the retention of the active-compounds loaded in the nanostructured systems, in the desired location. Some of the specific uses of nanostructured systems are presented in the next sections.

A1.3.2. Hair treatment

A1.3.2.1. Hair damage

Hair damage can be caused by different factors: intrinsic, such as genetic origin, and extrinsic, from various external sources. The visible damage of hair shafts may be the first concern of general hair care users, as this is the direct and immediate result of various harmful experiences caused by routine life. Such damage may be induced by physical stress (e.g., daily washing, hair brushing), or chemical stress (e.g., hair dyeing, straightening), heat stress (curling iron), or photoaging (ultraviolet light and visible light) (Bolduc and Shapiro, 2001; Poljšak et al., 2012).

The growth of new technologies to easily change hair shape or color has resulted in a number of modern hairstyles that express personality and style. It has also improved understanding of the complexity of distinct hair damage types, as a result of combinations of different technologies to alter hair morphologies. Kim et al. (2010) classified the degree of extrinsically damaged hair. The authors used a morphological evaluation based on the use of electron microscopy. They proposed a standard three-stage evaluation grading system to categorize the status of the distinct parts of the hair shaft: the surface, inner layers of the cuticle, and the cortex. The different cuticle damage levels were graded on a scale of 1 to 4; observation by scanning electron microscope (SEM) and transmission electron microscope (TEM) were graded as 'S' and 'T', respectively, and the cuticle and cortex by 'cu' and 'co', respectively. Accordingly, hair damaged by dyeing and permanent wave, for example, indicated irregular cuticle overlap, presence of bubbles in the cortex, and this damage was classified as Scu1/Tcu2/Tco2. Although this classification grade is not enough to evaluate the entire degree of damage hair, it is a starting point to simplify and schematize assessment and repair degree of extrinsically damaged hair (Kim et al., 2010).

Developments of nanotechnology-based haircare products have gained attention in recent years, with an increasing number of perspectives and varieties of nanostructured types.

The low solubility of plant extracts can be a challenge to developing rinse-off hair care products. A cationic nanoemulsion of natural quercetin extract of 20 nm was developed by the sub-PIT method. This nanoemulsion indicated, by Atomic Force Microscopy evaluation, high adhesion to the external surface of the hair. The incorporation of this low-solubility extract into a nanoemulsion may offer a treatment product with high antioxidant and conditioning properties for hair application (Dario et al., 2016).

Another challenge is silicone oil, widely used in cosmetic preparations for lubrication and preservation of hair moisture. This oil has high affinity and deposition on the hair scalp rather than the hair shaft, which can generate build-up and greasy touch after routine application to the hair. The Phase Inversion Composition method and nonionic surfactants (Span 80 and Tween 80) were used to prepare silicone oil nanoemulsions with 100 to 705 nm particle sizes. An X-ray analysis system using a scanning electron microscope indicated an increased deposition of silicone of nanoemulsion on the surface of the hair shaft compared to the control (Hu et al., 2012).

Patented products aiming at treating damaged hair have focused on nanostructured systems in recent years. A concentrated nanoemulsion of particle size from 1 to 100 nm using a mechanical dispenser was designed, for easy application as a rinse-off haircare foam (Glenn et al., 2017b). These concentrated nanoemulsions were further prepared using silicone and anionic or cationic surfactant, with the same mechanical dispenser concept. These applications in foam format offered an improved conditioning effect for the hair (Glenn et al., 2017a, 2016, 2015, Torres Rivera et al., 2016a, 2016b; Zhao et al., 2016).

Epoxy silicone nanoemulsions have been developed to treat damaged hair, mainly caused by chemical processes including straightening, relaxation, dyeing, and lightening. These nanoemulsions, prepared by a microfluidization method, resulted in nanoemulsions with an average particle size of 100 to 250 nm. The treatment processes, applying these epoxy silicone nanoemulsions, provides greater strength, elasticity, and fatigue resistance upon repeated brushing compared to the control (Syed and Lenick, O', 2019). Another preparation of nanoemulsion for

hair conditioning was the use of amino silicone, providing mean particle sizes from 20 nm to 350 nm, and a transparent to the slightly milky visual appearance (Oh et al., 2015).

Different active compounds, such as sericin, were included in a cationic nanoparticle. This nanoparticle was prepared by the sericin protein reticulation with quaternized guar gum, followed by cationic surfactant coating. This sericin cationic nanoparticle provided gloss, softness, aiming at treating and protecting damaged hair, such as dyed hair (Pereda et al., 2014).

A1.3.2.2. Hair graying

Hair graying may be a personal concern that can affect one's social life and self-esteem. Although gray hair has been increasingly accepted in modern society, there has been growing interest in better understanding hair graying factors, and alternative solutions for the current dyeing process.

The natural pigmentation process of hair starts in the hair bulb, where melanocyte cells synthesize melanosomes, organelles responsible for synthesis, storage, and transport of melanin. This process of melanin synthesis, induced by several enzymatic or chemical reactions, is called melanogenesis (Nishimura, 2011).

Managing the hair pigmentation process is quite complex, since melanogenesis takes place only during the active growth phase of the hair cycle, which is called the anagen phase. The duration of hair cycles and the number of cycles throughout life differ from hair to hair in the same individual, and from individual to individual. There are also various enzymes involved in melanogenesis, which are activated only after their entry into the melanosome, where they initiate the reaction cascade for melanin formation (D'Ischia et al., 2015).

Hair color is determined by the amount of melanin type in individuals. Black and brown hair color is due to the high presence of eumelanin, a highly polymerized melanin. Yellow to reddish-brown hair color is the result of the pheomelanin, a less polymerized melanin (Matamá et al., 2015).

Gray hair occurs due to melanogenesis deficiency, from several causes that are not yet completely understood. Possibilities include apoptosis of differentiated follicular melanocytes;

discontinuation of melanin production (Matamá et al., 2015); and progressive reduction of melanocyte stem cells in hair follicles (Nishimura, 2011).

The excessive presence of reactive oxygen species in hair follicles, as a consequence of age-related oxidative stress, is considered to be one of the main triggers of hair graying. The natural defense mechanism of oxidative damage, which is accomplished by the expression of antioxidant proteins (e.g., BCL-2, TRP-2) is weakened, reducing melanocyte stem cells and repopulation of newly formed anagen follicles. This process results in a gradual depletion of melanocyte in the bulb, and, consequently, the reduced number of melanin content up to the hair shaft (Seiberg, 2013).

Aiming at protecting melanogenesis, an extract of *Pueraria lobata*, an Asian native plant with antioxidant effects, was used to prevent hair graying. A randomized, double-blind clinical trial in 44 women was performed for 24 weeks. As a result, a slight reduction in new gray hair growth was observed in the test sample compared to placebo. This trial was based on the idea that proper removal of reactive oxygen species may protect the expression of a master transcriptional regulator of melanocytes - the microphthalmia transcription factor (MITF) - by use of an effective antioxidant, preventing hair graying (Jo et al., 2013).

Different antioxidants may be able to influence melanin synthesis, such as vitamin C and E, flavonoids, phenolic compounds. However, due to several factors (e.g., alternative substrate pathways for tyrosinase inhibition, reducers of melanin synthesis intermediates), they have been limited in achieving satisfactory results (D'Ischia et al., 2015).

The need for new alternative dye products is due to consumer dissatisfaction (e.g., color fading) with conventional synthetic dyes (e.g., oxidative hair dyes), which are most commonly used, or natural dyes such as dioxyindole (DHI) and derivatives. Furthermore, synthetic dyes can have a risk of hair damage and the possibility of skin sensitivity (D'Ischia et al., 2015).

In the last decade, melanin nanoparticles have been highlighted as an attractive material for clinical fields. They have been indicated for radiation therapies aimed at protecting bone marrow for higher dose application (Schweitzer et al., 2010). Other research considered them as a pH-responsive nanocarrier, being biocompatible and lacking cytotoxicity in delivery to the colon

and intestine (Araújo et al., 2014). Besides, melanin nanoparticles doped with self-assembled hydrogel networks have been developed as a new potential light-responsive polymeric biomaterial for clinical use (Ninh et al., 2014).

Since active melanocytes for melanin synthesis still remain in gray hair (even in small numbers), unlike white hair (Commo et al., 2004), boosting this natural coloring of hair through an inside-out approach seems promising. Therefore, it has drawn attention to the possibility of a new class of hair dyes with melanin precursors or the use of already identified genes for melanin synthesis (D'Ischia et al., 2015; Matamá et al., 2015).

In vivo and *in vitro* human hair follicle assays have identified increased melanin content by silencing the core clock genes, BMAL1 or PER1. The small molecule modulator of these genes, the small interfering RNA, has stimulated human melanogenesis and melanocyte activity, opening new perspectives for future therapeutic strategies for human pigmentary disorders (Hardman et al., 2015).

In addition to the activation of natural hair color, hair color change was also highlighted by the possible use of small interfering RNA capable of interfering with KITLG gene transcription, and hair color as a consequence. Also, targeted inhibition of tyrosinase-related protein 1 (Tyrp1) in hair follicles may support cosmetic products capable of inducing pheomelanin production, a non-Tyrp1 dependent pathway, alternatively to the Tyrp1 dependent eumelanin pathway, offering a lighter hair shade (Matamá et al., 2015).

Nevertheless, concerns remain since a deeper understanding of the multiple interferences of biological networks between different genes is required to ensure the safety of future innovative products for cosmetic use.

A1.3.2.3. Alopecia

The hair shaft is made up of dead cells, although it originates from a constant supply of materials that continually maintain the hair cycle during their lifetime. This cycle occurs in the hair follicle, which is divided into three main phases: anagen, catagen, and telogen. The anagen phase is the most active stage: matrix cell proliferation and differentiation occur at the follicle

base, and constant production of hair cells move cells from root to tip. Cell differentiation generates cysteine-rich hair keratins, responsible for the high strength and flexibility of the hair shaft. The duration of the anagen phase determines the hair length. The transition from anagen to catagen phase is promoted by some molecular regulators, such as growth factors (e.g., FGF5 and EGF), neurotrophins (e.g., BDNF), p53, but interactions between them at this transition point is not yet known. During the catagen phase, apoptosis of epithelial cells occurs in the bulb and outermost epithelial layer, discontinuing hair shaft differentiation. The lower part of the hair shaft converts to a rounded structure called the hair club, and the lower follicle retracts, forming a temporary structure called the epithelial strand. Then, in the telogen phase, the hair follicles enter the dormant period. The transition from telogen to anagen phase occurs under the activation of stem cells, located in the bulge, initiating a new cycle of hair differentiation and proliferation (Alonso and Fuchs, 2006).

In a normal healthy scalp, anagen is the predominant phase (approximately 80 to 85% of hairs). But in alopecia, there is a transition of the dominant period, from anagen to the telogen phase (Robins, 1988).

Alopecia, or scalp hair loss, is a significant concern of people affected by this disorder. Its origin differs among the different types of alopecia: androgenic alopecia, alopecia areata, and chemotherapy-induced alopecia. Androgenic alopecia (AGA), the predominant alopecia in Caucasian males, presents balding at the vertex and hairline recession at the templates of the affected population (Santos et al., 2015). In AGA, the anagen phase is shortened, leading to hair follicle miniaturization, and then to hair loss (Fang et al., 2014). The main cause of this anomaly is a decrease in total scalp testosterone and an increase in androgen hormone dihydrotestosterone (DHT). Testosterone is converted to DHT by the enzymes 5-α reductase (5 α-R). Among them, specifically, isoenzyme 5 α-R1, which is presented at a high level in the scalp of men with AGA, seems to be the leading cause of hair loss (Herman and Herman, 2017). In contrast, alopecia areata (AA) affects approximately 2% of the general population, which includes children and female adults (Mathes et al., 2016). AA is considered an autoimmune disease, which may be induced by inflammation caused by certain host proteins acting as autoantigens. Chemotherapy-induced alopecia (CIA) is caused by dividing cells apoptosis associated with a side effect of antineoplastic chemotherapy (Santos et al., 2015).

For treating hair loss by AGA, minoxidil, an antihypertensive vasodilator drug, and finasteride, an antiandrogen with inhibition activity of 5-α reductase, are the only two drugs approved by the US Food and Drug Administration (FDA). The concern about efficiency and safety, due to unpredictable side effects, is the main limitation and barrier for the approval of new drugs for hair loss therapies (Madaan et al., 2018). However, the use of currently approved antiandrogen can lead to side effects (e.g., sexual dysfunction and feminization), which may result in a deadlock between treating hair loss or avoiding these side effects (Santos et al., 2015). Topically applied corticosteroids for AA treatment also have several side effects, such as skin atrophy or irritation, and return to the same stage of hair loss before treatment, when the drug application is discontinued (Herman and Herman, 2017; Mathes et al., 2016).

Considering the hair follicle as the primary target in alopecia treatment, the interaction of the active ingredient as well as its vehicle with the hair follicle is the key element for the successful transport of the active ingredient into the follicle. Nano systems have been favored for topical applications due to their potential to easily penetrate and promote accumulation in hair follicles. Therefore, the development of a more effective and safe therapy using them as a carrier may be a squarticles, lipid nanocarriers composed of fatty esters and squalene as their matrix. Squalene is a sebum-derived lipid and, due to the high concentration of sebum in the hair follicle, can improve the affinity and accumulation of squarticles in the hair follicle. Squarticles loaded with minoxidil and diphencyprone, or conjugated with anti-platelet-derived growth factor (PDGF)-receptor β antibody presented higher follicular accumulation compared to the free control solution. Designed to target dermal papilla cells (DPCs), which are located in the deeper part of the hair follicle and responsible for hair growth and regeneration, squarticles also improved vascular endothelial growth factor (VEGF) expression and proliferation of DPCs (Aljuffali et al., 2015, 2014).

Other minoxidil-loaded nanocarriers were developed. Nanostructured lipid carriers (NLCs) consisting of stearic acid and oleic acid as lipids showed a faster drug release profile compared to minoxidil loaded in the solid-lipid nanostructure, and no erythema was observed in this NLC (Wang et al., 2017). Another preparation was the minoxidil encapsulated in 2-hydroxypropyl-β-cyclodextrin (HP-β-CD) which promoted aqueous solubility of the drug to prevent the use of organic solvent, and showed an effect on the hair cycle of mice by *in vivo* evaluation (Chen et al., 2017).

Alternative active compounds such as dutasteride were loaded in the nanostructured lipid carrier (NLC) coated with chitosan oligomer-stearic acid (CSO-SA). This drug is known for treating benign prostate hyperplasia, acting as an inhibitor of type I and type II 5α-reductase. As a result, this nanocarrier showed good stability, slow-release over 12 h and low cytotoxicity, appearing as a potential promoter of hair growth (Noor et al., 2017). Natural origin active compounds with 5α-reductase inhibitory effects were either loaded onto nano systems: hinokitiol and glycyrrhetinic acid were delivered to the hair follicles by incorporation into the poly(lactic-co-glycolic acid (PLGA) nanosphere carriers (Tsujimoto et al., 2007), poly(ε-caprolactone) nanocapsules were used as a carrier of hinokitiol (H6), and extract of *Platycladus orientalis* leaves was encapsulated in liposomes (Asili et al., 2012). These are promising candidates for hair growth therapies (Herman and Herman, 2017).

A1.3.2.4. Anti dandruff

Dandruff is a scalp disorder induced by several factors that can lead to social discomfort for the patient. Scaling and redness of the scalp are symptoms, associated with age (usually from puberty), season-related (generally in winter), occur in the same range between men and women, and are caused by different factors. The imbalance between sebum production, lipophilic yeast flora on the scalp and individual susceptibility are listed as the source of this disorder (Rai et al., 2013). Among them, Malassezia yeast (formerly *Pityrosporum ovale*) is highlighted as an essential element, although some studies point to the presence of other microorganisms (e.g., *Propionibacterium* spp. and *Staphylococcus* spp) as an active contributor to dandruff (Meray et al., 2018).

The dandruff scalp has a thinner stratum corneum, and the epidermal turnover rate is higher than the healthy scalp (Robins, 1988). Increased sebum production produces free fatty acids, wax esters, and fatty glycerides, which are the primary lipid substrate for the scalp microorganism. Malassezia secretes lipase, an enzyme that catalyzes lipids, releasing free fatty acids, which increase inflammation. Sebum production in the scalp is increased as microorganisms consume sebum, more free fatty acids are produced, inducing more inflammation in the scalp (Meray et al., 2018). Imbalance of sebum production, microorganism growth, and scalp irritation seems to be correlated; therefore, dandruff is not correlated with poor hygiene. Commonly used ingredients for

anti-dandruff therapy include antifungal agents (such as zinc pyrithione, coal tar preparations) and anti-inflammatory agents (e.g. salicylic acid) (Meray et al., 2018; Robins, 1988).

The development of nanosystems is proving to be a promising new approach to dandruff treatment. Pant et al. (2013) developed silver nanoparticles using different preparation conditions (sunlight, microwave, and room temperature). The 15-20 nm silver nanoparticle obtained by sunlight provided high efficacy against various bacterial strains tested (Gram-negative and Gram-negative), fungal strains (*Candida albicans* and *Candida parapsilosis*), and the shampoo containing nanoparticles increased anti-dandruff effectiveness against *Pityrosporum ovale* and *Pityrosporum folliculitis (Pant et al., 2013).*

Solid lipid nanoparticles (SLN) containing garlic as an antifungal agent were prepared by the hot homogenization method and mixed with shampoo. Tween 80 and soy lecithin were used as surfactants, and the obtained garlic loaded SLN showed up to 90% *in vitro* drug release profile. The shampoo containing this SLN resulted in excellent appearance, foamability, viscosity and spreadability (Rai et al., 2013), showing to be a good alternative to zinc pyrithione, for which it is often difficult to improve the opaque and unattractive appearance when incorporated in shampoo.

Following a homeopathic approach, Kalpana et al. (2017) biosynthesized ZnO nanoparticles using *Lagenaria siceraria* pulp extract. ZnO is widely known as an antifungal, antibacterial, and UV filtering agent. L. siceraria (Cucurbitaceae) is a well-known plant in India for treating anasarca, ascites, beriberi, and other diseases. This plant extract was identified to participate in the bio-reduction process for the conversion of metal ions into metal and metal oxide nanoparticles. The method of biosynthesis of ZnO nanoparticles from L. siceraria extract was very simple, and *in vitro* test provided potent anti-dandruff and antimicrobial activities (Kalpana et al., 2017).

A1.4. FUTURE PERSPECTIVES

Hair structure involves complex and dynamic mechanisms influenced by several internal and external factors. Interference in the normal dynamic flow of hair growth and maintenance can lead

to disorders of the hair shaft or hair follicles. Therefore, understanding the specific needs of each disorder is essential to directing consumers to the right treatment.

Studies have shown the efficacy of nanostructured systems in improving active compound penetration and accumulation, and their modified release profile. Several factors can influence their final efficacy, such as the particle size, composition, and type of nanostructured systems.

A wide range of nanostructured systems has been developed in recent years, aiming at treating these specific needs. Nevertheless, considering the cosmetics field, careful monitoring of the active compounds to avoid systemic absorption, as well as the right selection of the nano systems to deliver active compounds to the desired site remains standard practice. Overcoming these challenges will open possibilities for innovative nanostructured systems, designed for a new level of treatment in the hair field.

A1.5. REFERENCES

Abd, E., Benson, H.A.E., Roberts, M.S., Grice, J.E., 2018. Follicular Penetration of Caffeine from Topically Applied Nanoemulsion Formulations Containing Penetration Enhancers : In vitro Human Skin Studies. Skin Pharmacol. Physiol. 31, 252–260. https://doi.org/10.1159/000489857

Aljuffali, I.A., Pan, T.L., Sung, C.T., Chang, S.H., Fang, J.Y., 2015. Anti-PDGF receptor β antibody-conjugated squarticles loaded with minoxidil for alopecia treatment by targeting hair follicles and dermal papilla cells. Nanomedicine Nanotechnology, Biol. Med. 11, 1321–1330. https://doi.org/10.1016/j.nano.2015.04.009

Aljuffali, I.A., Sung, C.T., Shen, F., Huang, C., Fang, J., 2014. Squarticles as a Lipid Nanocarrier for Delivering Diphencyprone and Minoxidil to Hair Follicles and Human Dermal Papilla Cells. AAPS J. 16, 140–150. https://doi.org/10.1208/s12248-013-9550-y

Alonso, L., Fuchs, E., 2006. The hair cycle. J. Cell Sci. 2006, 391–393. https://doi.org/10.1242/jcs02793

Araújo, M., Viveiros, R., Correia, T.R., Correia, I.J., Bonifácio, V.D.B., Casimiro, T., Aguiar-ricardo, A., 2014. Natural melanin : A potential pH-responsive drug release device. Int. J.

Pharm. 469, 140–145. https://doi.org/10.1016/j.ijpharm.2014.04.051

Asili, J., Mosallaei, N., Shaterzadeh, A., Malaekeh-Nikouei, B., 2012. Preparation and characterization of liposomes containing methanol extract of aerial parts of Platycladus orientalis (L .) Franco. Avicenna J. Phytomedicine 2, 17–23. https://doi.org/10.22038/ajp.2011.24

Betz, G., Imboden, R., Imanidis, G., 2001. Interaction of liposome formulations with human skin in vitro. Int. J. Pharm. 229, 117–129. https://doi.org/10.1016/S0378-5173(01)00824-9

Bolduc, C., Shapiro, J., 2001. Hair Care Products: Waving, Straightening, Conditioning, and Coloring. Clin. Dermatol. 19, 431–436. https://doi.org/10.1016/S0738-081X(01)00201-2

Chen, H., Chang, X., Du, D., Liu, W., Liu, J., Weng, T., 2006. Podophyllotoxin-loaded solid lipid nanoparticles for epidermal targeting. J. Control. Release 110, 296–306. https://doi.org/10.1016/j.jconrel.2005.09.052

Chen, T.C., Yu, S.C., Hsu, C.M., Tsai, F.J., Tsai, Y., 2017. Minoxidil – 2-hydroxypropyl-β-cyclodextrin inclusion complexes : characterization and in vivo evaluation of an aqueous solution for hair growth in rats. J. Incl. Phenom. Macrocycl. Chem. 88, 27–34. https://doi.org/10.1007/s10847-017-0705-9

Commo, P., Gaillard, O., Thibaut, S., Bernard, B.A., 2004. Absence of TRP-2 in Melanogenic Melanocytes of Human Hair. Pigment Cell Res. 17, 488–497. https://doi.org/0.1111/j.1600-0749.2004.00170.x

Corrias, F., Schlich, M., Sinico, C., Pireddu, R., Valenti, D., Maria, A., Marceddu, S., Lai, F., 2017. Nile red nanosuspensions as investigative model to study the follicular targeting of drug nanocrystals. Int. J. Pharm. 524, 1–8. https://doi.org/10.1016/j.ijpharm.2017.03.042

D'Ischia, M., Wakamatsu, K., Cicoira, F., Mauro, E. Di, Garcia-borron, J.C., Ghanem, G., Kenzo, K., Meredith, P., Pezzella, A., Santato, C., Sarna, T., Simon, J.D., Zecca, L., Zucca, F.A., Napolitano, A., Ito, S., 2015. Melanins and melanogenesis: from pigment cells to human health and technological applications. Pigment Cell Melanoma Res. 28, 520–544. https://doi.org/10.1111/pcmr.12393

Dario, M.F., Santos, M.S.C.S., Viana, A.S., Arêas, E.P.G., Bou-chacra, N.A., Conceic, M., Minas, M.E., Baby, A.R., Valéria, M., Velasco, R., 2016. A high loaded cationic nanoemulsion for quercetin delivery obtained by sub-PIT method. Colloids Surfaces A Physicochem. Eng. Asp. 489, 256–264. https://doi.org/10.1016/j.colsurfa.2015.10.031

Dimde, M., Sahle, F.F., Wycisk, V., Steinhilber, D., Camacho, L.C., Licha, K., Lademann, J., Haag, R., 2017. Synthesis and Validation of Functional Nanogels as pH-Sensors in the Hair Follicle. Macromol. Biosci. 17, 1–8. https://doi.org/10.1002/mabi.201600505

Döge, N., Hönzke, S., Schumacher, F., Balzus, B., Colombo, M., Hadam, S., Rancan, F., Blume-peytavi, U., Schäfer-korting, M., Schindler, A., Rühl, E., Stahl, P., Church, M.K., Hedtrich, S., Kleuser, B., Bodmeier, R., Vogt, A., 2016. Ethyl cellulose nanocarriers and nanocrystals differentially deliver dexamethasone into intact , tape-stripped or sodium lauryl sulfate-exposed ex vivo human skin - assessment by intradermal microdialysis and extraction from the different skin layers. J. Control. Release 242, 25–34. https://doi.org/10.1016/j.jconrel.2016.07.009

Doktorovová, S., Kovacevic, A.B., Garcia, M.L., Souto, E.B., 2016. Preclinical safety of solid lipid nanoparticles and nanostructured lipid carriers : Current evidence from in vitro and in vivo evaluation. Eur. J. Pharm. Biopharm. 108, 235–252. https://doi.org/10.1016/j.ejpb.2016.08.001

Fang, C., Aljuffali, I.A., Li, Y., Fang, J., 2014. Delivery and targeting of nanoparticles into hair follicles. Ther. Deliv. 5, 991–1006. https://doi.org/10.4155/tde.14.61

Fernandes, B., Silva, R., Ribeiro, A., Matam, T., 2015. Improved Poly (D , L-lactide) nanoparticles-based formulation for hair follicle targeting. Int. J. Cosmet. Sci. 37, 282–290. https://doi.org/10.1111/ics.12197

Glenn, R.W.J., Hosseinpour, D., Doyle, K.L., 2017a. METHOD OF TREATING HAIR. US 2017/0165157 A1.

Glenn, R.W.J., Hosseinpour, D., Doyle, K.L., Kaufman, K.M., 2017b. METHOD OF TREATING HAIR. US 2017/0165162 A1.

Glenn, R.W.J., Kaufman, K.M., Hosseinpour, D., 2015. Method of treatinghair with a concentrated conditioner. US 2015/0359727 A1.

Glenn, R.W.J., Kaufman, K.M., Iwata, T., 2016. Method of treating hair with a concentrated conditioner. US 2016/0310372 A1.

Hamishehkar, H., Ghanbarzadeh, S., Sepehran, S., Adib, Z.M., Kouhsoltani, M., Hamishehkar, H., Ghanbarzadeh, S., Sepehran, S., Javadzadeh, Y., Adib, Z.M., 2016. Histological assessment of follicular delivery of flutamide by solid lipid nanoparticles : potential tool for the treatment of androgenic alopecia Histological assessment of follicular delivery of flutamide by solid

lipid nanoparticles : potential tool fo. Drug Dev. Ind. Pharm. 42, 846–853. https://doi.org/10.3109/03639045.2015.1062896

Hardman, J.A., Tobin, D.J., Haslam, I.S., Farjo, N., Farjo, B., Al-nuaimi, Y., Grimaldi, B., Paus, R., 2015. The Peripheral Clock Regulates Human Pigmentation. J. Invest. Dermatol. 135, 1053–1064. https://doi.org/10.1038/jid.2014.442

Herman, A., Herman, A.P., 2017. Topically used herbal products for the treatment of hair loss : preclinical and clinical studies. Arch. Dermatol. Res. 309, 595–610. https://doi.org/10.1007/s00403-017-1759-7

Hu, Z., Liao, M., Chen, Y., Cai, Y., Meng, L., Liu, Y., Lv, N., Liu, Z., Yuan, W., 2012. A novel preparation method for silicone oil nanoemulsions and its application for coating hair with silicone. Int. J. Nanomedicine 7, 5719–5724. https://doi.org/10.2147/IJN.S37277

Jo, S.J., Shin, H., Paik, S.H., Na, S.J., Jin, Y., Park, W.S., Kim, S.N., Kwon, O.S., 2013. Efficacy and Safety of Pueraria lobata Extract in Gray Hair Prevention : A Randomized , Double-Blind , Placebo-Controlled Study. Ann. Dermatol. 25, 218–222. https://doi.org/10.5021/ad.2013.25.2.218

Kalpana, V.N., Payel, C., Rajeswari, D. V, 2017. Lagenaria siceraria aided green synthesis of ZnO NPs : Res. J. Chem. Environ. 21, 14–19.

Kim, Y., Jeon, S., Ji, J.H., Lee, W., 2010. Development of a Classification System for Extrinsic Hair Damage : Standard Grading of Electron Microscopic Findings of Damaged Hairs. Am. J. Dermatopathol. 32, 432–438. https://doi.org/10.1097/DAD.0b013e3181c38549

Konrádsdóttir, F., Ogmundsdóttir, H., Sigurdsson, V., Loftsson, T., 2009. Drug Targeting to the Hair Follicles : A Cyclodextrin-Based Drug Delivery. AAPS PharmSciTech 10, 266–269. https://doi.org/10.1208/s12249-009-9205-6

Krishnaswamy, K., Orsat, V., 2017. Sustainable Delivery Systems Through Green Nanotechnology, Nano- and Microscale Drug Delivery Systems. Elsevier Inc. https://doi.org/10.1016/B978-0-323-52727-9/00002-9

Lademann, J., Richter, H., Knorr, F., Patzelt, A., Darvin, M.E., Rühl, E., Cheung, K.Y., Lai, K.K., Renneberg, R., Mak, W.C., 2016. Triggered release of model drug from AuNP-doped BSA nanocarriers in hair follicles using IRA radiation. Acta Biomater. 30, 388–396. https://doi.org/10.1016/j.actbio.2015.11.052

Lademann, J., Richter, H., Schaefer, U.F., Blume-Peytavi, U., 2006. Hair Follicles – A Long-Term

Reservoir. Skin Pharmacol. Physiol. 19, 232–236. https://doi.org/10.1159/000093119

Lademann, J., Richter, H., Teichmann, A., Otberg, N., Blume-Peytavi, U., Luengo, J., Weiß, B., Schaefer, U.F., Lehr, C.M., Wepf, R., Sterry, W., 2007. Nanoparticles - An efficient carrier for drug delivery into the hair follicles. Eur. J. Pharm. Biopharm. 66, 159–164. https://doi.org/10.1016/j.ejpb.2006.10.019

Li, L., Hoffman, R.M., 1995. The feasibility of targeted selective gene therapy of the hair follicle. Nat. Med. 1, 705–706.

Lohan, S.B., Icken, N., Teutloff, C., Saeidpour, S., Bittl, R., Lademann, J., Fleige, E., Haag, R., Haag, S.F., Meinke, M.C., 2016. Investigation of cutaneous penetration properties of stearic acid loaded to dendritic core-multi-shell (CMS) nanocarriers. Int. J. Pharm. 501, 271–277. https://doi.org/10.1016/j.ijpharm.2016.02.004

Madaan, A., Verma, R., Singh, A.T., Jaggi, M., 2018. Review of Hair Follicle Dermal Papilla cells as in vitro screening model for hair growth. Int. J. Cosmet. Sci. 40, 429–450. https://doi.org/10.1111/ics.12489

Mahmoud, N.N., Alkilany, A.M., Dietrich, D., Karst, U., Al-bakri, A.G., Khalil, E.A., 2017. Preferential accumulation of gold nanorods into human skin hair follicles : Effect of nanoparticle surface chemistry. J. Colloid Interface Sci. 503, 95–102. https://doi.org/10.1016/j.jcis.2017.05.011

Matamá, T., Gomes, A.C., Cavaco-paulo, A., 2015. Hair Coloration by Gene Regulation : Fact or Fiction ? Trends Biotechnol. 33, 707–711. https://doi.org/10.1016/j.tibtech.2015.10.001

Mathes, C., Melero, A., Conrad, P., Vogt, T., Rigo, L., Selzer, D., Prado, W.A., Rossi, C. De, Garrigues, T.M., Hansen, S., Guterres, S.S., Pohlmann, A.R., Beck, R.C.R., Lehr, C., Schaefer, U.F., 2016. Nanocarriers for optimizing the balance between interfollicular permeation and follicular uptake of topically applied clobetasol to minimize adverse effects. J. Control. Release 223, 207–214. https://doi.org/10.1016/j.jconrel.2015.12.010

Meray, Y., Gençalp, D., Güran, M., 2018. Putting It All Together to Understand the Role of Malassezia spp . in Dandruff Etiology. Mycopathologia 4, 893–903. https://doi.org/10.1007/s11046-018-0283-4

Mihranyan, A., Ferraz, N., Strømme, M., 2012. Current status and future prospects of nanotechnology in cosmetics. Prog. Mater. Sci. 57, 875–910. https://doi.org/10.1016/j.pmatsci.2011.10.001

Müller, R.H., Radtke, M., Wissing, S.A., 2002. Solid lipid nanoparticles (SLN) and nanostructured lipid carriers (NLC) in cosmetic and dermatological preparations. Adv. Drug Deliv. Rev. 54, S131–S155. https://doi.org/10.1016/S0169-409X(02)00118-7

Ninh, C., Cramer, M., Bettinger, C.J., 2014. Photoresponsive hydrogel networks using melanin nanoparticle photothermal sensitizers. Biomater. Sci. 2, 766–774. https://doi.org/10.1039/c3bm60321k

Nishimura, E.K., 2011. Pigment Cell & melanoma pigmentation. Pigment Cell Melanoma Res. 24, 401–410. https://doi.org/10.1111/j.1755-148X.2011.00855.x

Niska, K., Zielinska, E., Witold, M., Inkielewicz-stepniak, I., 2018. Metal nanoparticles in dermatology and cosmetology: Interactions with human skin cells. Chem. Biol. Interact. 295, 38–51. https://doi.org/10.1016/j.cbi.2017.06.018

Noor, N.M., Sheikh, K., Somavarapu, S., Taylor, K.M.G., 2017. Preparation and characterization of dutasteride-loaded nanostructured lipid carriers coated with stearic acid-chitosan oligomer for topical delivery. Eur. J. Pharm. Biopharm. 117, 372–384. https://doi.org/10.1016/j.ejpb.2017.04.012

Oh, H., Gartstein, V., Bates, T., 2015. Amino silicone nanoemulsion. US 2015/0030644 A1.

Pant, G., Nayak, N., Prasuna, R.G., 2013. Enhancement of antidandruff activity of shampoo by biosynthesized silver nanoparticles from Solanum trilobatum plant leaf. Appl. Nanosci. 3, 431–439. https://doi.org/10.1007/s13204-012-0164-y

Patel, V., Sharma, O.P., Mehta, T., 2018. Nanocrystal : a novel approach to overcome skin barriers for improved topical drug delivery. Expert Opin. Drug Deliv. 15, 351–368. https://doi.org/10.1080/17425247.2018.1444025

Patzelt, A., Richter, H., Knorr, F., Schäfer, U., Lehr, C., Dähne, L., 2011. Selective follicular targeting by modi fi cation of the particle sizes. J. Control. Release 150, 45–48. https://doi.org/10.1016/j.jconrel.2010.11.015

Pereda, M.D.C.V., Polezel, M.A., Dieamant, G. de, Campos, Nogueira, C., Rossan, M.R., Santana, M.H.A., 2014. Sericin cationic nanoparticles for application in products for hair and dyed hair. US 8,709,455 B2.

Poljšak, B., Dahmane, R.G., Godic, A., 2012. Intrinsic skin aging : The role of oxidative stress. Acta Dermatovenerol APA 21, 1–4. https://doi.org/10.2478/v10162-012-0012-5

Raber, A.S., Mittal, A., Schäfer, J., Bakowsky, U., Reichrath, J., Vogt, T., Schaefer, U.F., Hansen,

S., Lehr, C., 2014. Quantification of nanoparticle uptake into hair follicles in pig ear and human forearm. J. Control. Release 179, 25–32. https://doi.org/10.1016/j.jconrel.2014.01.018

Rai, N., Jain, A.K., Abraham, J., 2013. Formulation and Evaluation of Herbal Antidandruff Shampoo Containing Garlic Loaded Solid Lipid Nanoparticles. Int. J. Pharma Res. Rev. 2, 12–24.

Rancan, F., Afraz, Z., Combadiere, B., Blume-peytavi, U., 2013. Hair Follicle Targeting with Nanoparticles, in: Nasir, A., Friedman, A., Wang, S. (Eds.), Nanotechnology in Dermatology. Springer. https://doi.org/10.1007/978-1-4614-5034-4

Rancan, F., Blume-Peytavi, U., Vogt, A., 2014. Utilization of biodegradable polymeric materials as delivery agents in dermatology. Clin. Cosmet. Investig. Dermatol. 7, 23–34. https://doi.org/10.2147/CCID.S39559

Rancan, F., Papakostas, D., Hadam, S., Hackbarth, S., Delair, T., Primard, C., Verrier, B., Sterry, W., Blume-peytavi, U., Vogt, A., 2009. Investigation of Polylactic Acid (PLA) Nanoparticles as Drug Delivery Systems for Local Dermatotherapy. Pharm. Res. 26. https://doi.org/10.1007/s11095-009-9919-x

Robins, C.R., 1988. Chemical and Physical Behavior of Human Hair, Second. ed. Springer, New Jersey. https://doi.org/10.1007/978-1-4757-2009-9

Rosen, J., Landriscina, A., Friedman, A.J., 2015. Nanotechnology-Based Cosmetics for Hair Care. Cosmetics 2, 211–224. https://doi.org/10.3390/cosmetics2030211

Sagitani, H., Hirai, Y., Nabeta, K., Nagai, M., 1986. Effect of Types of Polyols on Surfactant Phase Emulsification. J. Japan Oil Chem. Soc. 35, 102–107. https://doi.org/10.5650/jos1956.35.102

Santos, Z., Avci, P., Hamblin, M.R., 2015. Drug discovery for alopecia : gone today , hair tomorrow. Expert Opin. Drug Discov. 10, 269–292. https://doi.org/10.1517/17460441.2015.1009892

Schneider, M.R., Paus, R., 2014. Deciphering the functions of the hair follicle infundibulum in skin physiology and disease. Cell Tissue Res. 358, 697–704. https://doi.org/10.1007/s00441-014-1999-1

Schweitzer, A.D., Revskaya, E., Chu, P., Pazo, V., Friedman, M., Nosanchuk, J.D., Cahill, S., Frases, S., Casadevall, A., Dadachova, E., 2010. Melanin-covered nanoparticles for protection of bone marrow During radiation therapy of cancer. Int. J. Radiat. Oncol. Biol.

Phys. 78, 1494–1502. https://doi.org/10.1016/j.ijrobp.2010.02.020

Seiberg, M., 2013. Age-induced hair greying – the multiple effects of oxidative stress. Int. J. Cosmet. Sci. 35, 532–538. https://doi.org/10.1111/ics.12090

Sonneville-Aubrun, O., Yukuyama, N.M., Pizzino, A., 2018. Application of Nanoemulsions in Cosmetics, in: Nanoemulsion. pp. 435–475. https://doi.org/10.1016/B978-0-12-811838-2.00014-X

Su, R., Fan, W., Yu, Q., Dong, X., Qi, J., Zhu, Q., 2017. Size-dependent penetration of nanoemulsions into epidermis and hair follicles : implications for transdermal delivery and immunization. Oncotarget 8, 38214–38226.

Sun, M., Fan, A., Wang, Z., Zhao, Y., 2012. Dendrimer-mediated drug delivery to the skin †. Soft Matter 8, 4301–4305. https://doi.org/10.1039/c2sm07280g

Syed, A.N., Lenick, O', A.J., 2019. Methods and compositions for treating damaged hair. US 20190029945A1.

Thibaut, S., Gaillard, O., Bouhanna, P., Cannell, D.W., Bernard, B.A., 2005. Human hair shape is programmed from the bulb. Br. J. Dermatol. 152, 632–638. https://doi.org/10.1111/j.1365-2133.2005.06521.x

Torres Rivera, J.V., Kaufman, K.M., Glenn, R.W.J., 2016a. Hair care regimen using liquid concentrated conditioner. US 2016/0310377 A1.

Torres Rivera, J.V., Kaufman, K.M., Glenn, R.W.J., 2016b. Hair care regimen using a mechanical foam concentrated conditioner. US 2016/0310376 A1.

Tran, N.B.N.N., Knorr, F., Mak, W.C., Cheung, K.Y., Richter, H., Meinke, M., Lademann, J., Patzelt, A., 2017. Gradient-dependent release of the model drug TRITC-dextran from FITC-labeled BSA hydrogel nanocarriers in the hair follicles of porcine ear skin. Eur. J. Pharm. Biopharm. 116, 12–16. https://doi.org/10.1016/j.ejpb.2016.09.016

Tsujimoto, H., Hara, K., Tsukada, Y., Huang, C.C., Kawashima, Y., Arakaki, M., Okayasu, H., Mimura, H., Miwa, N., 2007. Evaluation of the permeability of hair growing ingredient encapsulated PLGA nanospheres to hair follicles and their hair growing effects. Bioorg. Med. Chem. Lett. 17, 4771–4777. https://doi.org/10.1016/j.bmcl.2007.06.057

Vidlárová, L., Romero, G.B., Hanuš, J., Štepánek, F., Müller, R.H., 2016. Nanocrystals for dermal penetration enhancement – Effect of concentration and underlying mechanisms using curcumin as model. Eur. J. Pharm. Biopharm. 104, 216–225.

https://doi.org/10.1016/j.ejpb.2016.05.004

Wang, W., Chen, L., Huang, X., Shao, A., 2017. Preparation and Characterization of Minoxidil Loaded Nanostructured Lipid Carriers. AAPS PharmSciTech 18, 509. https://doi.org/10.1208/s12249-016-0519-x

Wasutrasawat, P., Al-obaidi, H., Gaisford, S., Lawrence, M.J., Warisnoicharoen, W., 2013. Drug solubilisation in lipid nanoparticles containing high melting point triglycerides. Eur. J. Pharm. Biopharm. 85, 365–371. https://doi.org/10.1016/j.ejpb.2013.04.020

Yukuyama, M.N., Kato, E.T.M., de Araujo, G.L.B., Löbenberg, R., Monteiro, L.M., Lourenço, F.R., Bou-Chacra, N.A., 2019. Olive oil nanoemulsion preparation using high-pressure homogenization and D-phase emulsification – A design space approach. J. Drug Deliv. Sci. Technol. 49, 622–631. https://doi.org/10.1016/j.jddst.2018.12.029

Yukuyama, M.N., Kato, E.T.M., Löbenberg, R., Bou-Chacra, N.A., 2017. Challenges and future prospects of nanoemulsion as a drug delivery system. Curr. Pharm. Des. 23, 495–508. https://doi.org/10.2174/1381612822666161027111957

Yukuyama, M.N., Oseliero, P.L.F., Kato, E.T.M., Lobënberg, R., de Oliveira, C.L.P., de Araujo, G.L.B., Bou-Chacra, N.A., 2018. High internal vegetable oil nanoemulsion: D-phase emulsification as a unique low energy process. Colloids Surfaces A Physicochem. Eng. Asp. 554, 296–305. https://doi.org/10.1016/j.colsurfa.2018.06.023

Zhao, J.J., Glenn, R.W.J., Mullen, S.E., 2016. Hair care conditioning composition. US 2016/0310371 A1.

Zoschke, C., Schilrreff, P., Romero, E.L., Brandner, J.M., Schäfer-, M., 2015. Dendritic Nanoparticles for Cutaneous Drug Delivery - Testing in Human Skin and Reconstructed Human Skin. Curr. Pharm. Des. 21, 2784–2800.

APPENDIX 2 – NANOEMULSIONS CONTAINING PLANT OILS: HOW DO THEY INFLUENCE HAIR TREATMENT?

This research article was published in *International Journal of Cosmetic Science*, 2021, under DOI number 10.1111/ics.12667, by Fernanda Leika Tamashiro, Megumi Nishitani Yukuyama (equivalent author), Maria Valéria Robles Velasco, GLB De Araújo, and Nadia Araci Bou-Chacra.

I contributed equally as an author and was responsible for methodology, validation, writing - original draft, visualization and supervision.

A2.1. INTRODUCTION

Cosmetic, specifically haircare, is an expanding market , with an estimated USD 116.33 billion by 2024 (1). Thus, advances aiming at innovative products to meet the ever-increasing consumer demand are constantly required. In the last decade, emerging technologies have shown potential to influence the cosmetics by enhancing efficacy and safety. In this context, nanotechnologies are an intriguing area which show new perspectives for this market. Different types of nanotechnologies have been developed as potential vehicles to load active ingredients for their modified release, stability, safety or efficacy enhancement. They can be classified as liposomes (vesicular structures composed mainly of phospholipid bilayers), cyclodextrins (composed of cyclic sugar compound), polymeric nanoparticles (polymeric matrix), dendrimers (dendritic polymers with flexible tree-like structure), nanocrystals (no matrix core and composed mainly of active ingredient), metallic nanoparticles (complexation or adsorption of active ingredient with metallic materials), solid lipid nanoparticles (solid lipid core), nanostructured lipid carrier (amourphous lipid core) or nanoemulsions (liquid lipid core) (2).

Examples of its application in cosmetics are listed below: water-based nanoperfumes have been patented by the Agate perfume to provide nanoemulsion of 10-100 nm droplet size, aiming for a transparent, alcohol-free perfume. This approach may offer advantages such as fragrance stability (i.e. protection against oxidation), control release, non-flammable and cost-effective product, using water as a base (3). The application in suncare products includes cinnamate-functionalized cellulose nanocrystals (Cin-CNCs) that offer transparent UV-shielding polymer film and high UV protection (4); gelatin nanoparticle loaded with rutin, a natural antioxidant ingredient, in association with conventional chemical UV filters which showed increased antioxidant activity, upgraded sun protection factor and good compatibility with skin (5). Furthermore, Moraes and Vieira (2020) surveyed several patents and researches related to makeup nanotechnology in recent years (6): nail polishes with color changing properties were developed using spiropyran, a chromophore compound, resulting in emulsions with nanoparticles of 30 to 60 nm, enhanced photo-reversibility and -stability (7); a cosmetic film-forming nanocomposite for treatment or makeup, composed of graftable Polyhedral Oligo Silsequioxanes (POSS), presented a long-lasting, non-transferable and comfortable feeling over a long period of use (8–10). In the hair care application, silicone oil nanoemulsions with a particle size of 100 – 705 nm were prepared

to coat the hair, and an increase in the deposition of silicone on the hair shaft was determined when compared to the control (11); targeting hair follicle for safer treatment of alopecia, minoxidil and diphencyprone loaded in sebum-derived lipid nanocarriers (12), minoxidil loaded in stearic and oleic acid solid-lipid nanostructure (13), and 2-hydroxypropyl-β-cyclodextrin encapsulated with minoxidil (14) have also been described. Another interesting development is the application of a unique low-energy process, the D-Phase Emulsification, for the preparation of a 20-30 nm nanoemulsion containing 40% olive oil and 2% non-ionic surfactant, without the use of specific high-energy equipment, nor solvents (15). These results show the wide applicability of nanotechnology in several areas of cosmetics.

Also, increasingly used in product formulations, plants oils have gained wide acceptance over the years as interesting components that promote a safer, natural and sustainable approach. Coconut oil showed significant reduction of protein loss in both damaged and undamaged hair, treated with pre-wash and post-wash preparations containing this oil (16). The association of antioxidant shampoo and coconut oil as post-shampoo application provided protection against hair damage due to the effect of pollution, in several study participants (17). These interesting features of coconut oil are due to the high polarity of its C_{12} chain, which is the main component. Its affinity to keratin of hair promotes high penetrability of oil inside the shaft, limiting hair swelling and protecting from stress damage (18). Olive oil demonstrated anti-inflammatory activity (19), protection from UV-B damage (20), and showed to be an effective nanocarrier (21). These properties are mainly attributed to the association of monounsaturated oleic acid ($C_{18:1}$ chain) which is present in high amounts, and small presence of carotenoids and phenolics (22,23). Recent studies using shampoo and conditioner containing abyssinian oil, rich in erucic acid (C_{22} chain), showed improved conditioning and removal of sebum (24), treatment effect on scalp dryness and curly hair (25), and better detangling ability, shine, anti-frizz and combability when applied as hair oil (26).

However, literature related to the use of plant-loaded nanoemulsions on hair treatment, comparing their different physical-chemical properties and effects on hair, is still scarce. Thus, the aim of the present study was to develop and evaluate the use of three different plant oils for O/W nanoemulsions formulation and determine whether the mean particle size (MPS), zeta potential

(which is correlated with the external charge of the nanoemulsion) or the composition, have an impact on hair treatment effectiveness.

MATERIAL AND METHODS

A2.2. MATERIAL

The coconut oil was supplied by Aboissa Commodity Brokers® (Brazil), olive oil and abyssinian oil were supplied by Clariant® (Brazil), cetyltrimethylammonium chloride as cationic surfactant was supplied by Sigma-Aldrich (Brazil), and water was Ultrapure MiliQ.

A2.3. METHODS

A2.3.1. Preparation of nanoemulsions

Six cationic nanoemulsions were prepared with a fixed amount of total plant oils at 20.0% (w / w) (**Table A2.1**). Coconut oil was chosen as the platform in the mixed oil preparations due to its composition rich in short chain fatty acids. The concentration of surfactant was also varied, to evaluate the influence of surfactant and oils compositions of the final nanoemulsions on the particle size, polydispersity index, zeta potential and their performances on hair shaft.

The oil and water phases were separately heated to 70.0 ± 5.0 °C. Then the water phase was added to the oil phase with continuous stirring at 400 rpm keeping the same temperature. This mixture was immediately submitted to Ultra Turrax® mechanical stirrer (IKA, Wilmington, USA) for 2 min at 10,000 rpm/min. Then, the coarse emulsion obtained was subjected to high-pressure homogeneization (HPH) method (NanoDebee®) (BEE International, Massachusetts, USA) for 5 cycles at 60 MPas.

Tabela A2.1: Composition of cationic nanoemulsions

Ingredient	Concentration (w/w%)					
Oil Phase						
Olive oil	10.0	10.0	0.0	20.0	0.0	0.0

Coconut oil	10.0	10.0	10.0	0.0	20.0	0.0
Abyssinian oil	0.0	0.0	10.0	0.0	0.0	20.0
Water Phase						
Cetrimonium chloride	4.0	2.0	2.0	2.0	2.0	2.0
Water	76.0	78.0	78.0	78.0	78.0	78.0

A2.3.2. Nanoemulsions Characterization

A2.3.2.1. Determination of Mean Particle Size (MPS) and Polydispersity Index (PI)

The mean particle size (z-average diameter) was determined by the Dynamic Light Scattering (DLS) method in a Zetasizer ZS90 equipment (Malvern Instruments, Malvern, UK) and PI calculated from cumulant analysis (square of the standard deviation/ mean diameter). The scattered radiation was observed at an angle of 90º, using the diluted samples in water to avoid the effect of multiple scattering. The results were expressed as average of three measurements.

A2.3.2.2. Determination of Zeta Potential (ZP)

The particle surface charge was assessed by measuring the ZP using the electrophoretic mobility method. The particle's electrophoretic mobility is measured in the Zetasizer ZS90 equipment (Malvern Instruments, Malvern, UK) and converted into ZP in mV units using the Helmholtz-Smoluchowski equation. The nanoemulsion samples were previously diluted (20 µL in 4 mL of water) and adjusted to an appropriate conductivity with NaCl solution, in order to avoid fluctuations of values.

A2.3.2.3. Measurement of pH

The pH values of formulations were determined in a pH meter (Mettler Toledo, Sao Paulo, Brazil) using a direct immersion electrode, previously calibrated with buffer solutions (pH 4.0 and 7.0).

A2.3.3. Stability study

All nanoemulsions were stored at 4.0 ± 0.5 °C in 10 ml glass bottles. Physical stability over 5 months was checked by visual observations of oil or water separation, as well as MPS, PI and ZP to ensure that there were no significant changes over time.

A2.3.4. Efficacy study on hair tresses

The evaluation of the effectiveness of nanoemulsions containing different plant oils and surfactant concentration was evaluated by screening test and instrumental evaluation. Dark brown natural Caucasian hair tresses with 15 cm of length and 2.0 of width were used to perform both evaluations.

Seven hair tresses were used for each evaluation, one for the control (no sample application) and the other six for the application of the six nanoemulsions. The hair tresses were previously washed to remove any residual product according to the following standardization protocol: moistened for 30 s with warm water (40.0 ± 1.0 ºC) and 2.0 ml of a sodium lauryl sulfate dispersion (10% w/w) was uniformly applied over the entire length of the tresses. The hair was massaged for 1 min with gentle movements from root to tip, using the thumb and middle finger. Then, they were washed again under tap water for 1 min and the excess water was removed (27).

The application process of the nanoemulsions samples followed the same methodology before described. A total of 2.0 mL of sample was applied uniformly on the standardized hair tresses. Then it was massaged into the hair for 1 min from root to tip, washed out in tap water for 1 min, and the excess water was removed. Then it was dried naturally at room temperature (22.0 ± 2.0ºC).

The sensorial screening test of hair tresses treated with the nanoemulsions were performed according to the following criteria: uniformity, softness and shine compared to the control.

The instrumental test was performed using a Dia-Stron® device (London, United Kingdom) with UvWin® PC Software to control the measurements and edition of the results. The treated hair tresses were positioned in the upper support of the device (5.0 kg load cell). The results of the analysis were determined by average combing values (5 measurements). The distance between the comb and the upper support is 20 mm and the length was 200 mm. The speed of the comb for the measurements was 300 mm/min.

A2.4. RESULTS

A2.4.1. Determining mean particle size, polydispersity index, zeta potential and pH of nanoemulsions

The results of mean particle size (MPS), polydispersity index (PI), zeta potential (ZP) and pH of the nanoemulsions are shown in **Table A2.2**. The MPS ranged from 126.9 to 231.9 nm, confirming the nanoscaled size of the emulsions prepared by the method employed (**Fig. A2.S1 to A2.S6**). Coconut oil-loaded nanoemulsion presented the smallest MPS, and abyssinian oil-loaded nanoemulsion presented the largest one. The olive oil-loaded and mixed oil-loaded nanoemulsions presented intermediate particle sizes. The increase of surfactant concentration from 2.0 % to 4.0 % (w/w) decreased the MPS from 198.0 nm to 162.0 nm. This indicates little interference of surfactant concentration on the final nanoemulsion size, even at a two-fold increase. The PI values were of approximately 0.1, corresponding to monodispersed emulsions in all preparations. ZP ranged from +62.9 to +79.2 mV, confirming that the preparations presented positive charge, which is the aim of our study to promote affinity of these nanoemulsions to the negative charged hair surface. The pH values ranged from 5.3 to 6.3, which is a typical range of values when cationic surfactant is employed, and suitable values for cosmetic application.

Table A2.2: Mean particle size (MPS), polydispersity Index (PI), zeta potential (ZP) and pH of the plant oil loaded nanoemulsions

Oil phase	Surfactant (w/w%)	MPS (nm)	PI	ZP (mV)	pH
Coconut + olive	4.0	162.4 ± 1.6	0.126 ± 0.007	+79.2 ± 3.7	6.3
Coconut + olive	2.0	198.2 ± 5.9	0.092 ± 0.006	+68.7 ± 1.9	5.7
Coconut +abyssinian	2.0	199.5 ± 2.1	0.124 ± 0.033	+67.3 ± 0.2	5.3
Olive	2.0	216.4 ± 1.3	0.144 ± 0.017	+65.7 ± 1.0	5.6
Coconut	2.0	126.9 ± 0.5	0.128 ± 0.014	+72.9 ± 1.2	5.4
Abyssinian	2.0	231.9 ± 3.7	0.103 ± 0.005	+62.9 ± 1.0	5.1

A2.4.2. Stability study

The MPS of the six preparations were measured over five months at 4.0 ± 0.5 °C, and the results are shown in **Table A2.3**. We did not observe significant variation of MPS during this period. The PI ranged from 0.09 to 0.19 with monomodal distribuiton. By visual evaluation, the preparations presented uniformity and were stable for five months, except for the coconut + olive oils-loaded nanoemulsion, which presented a very slight separation at the fifth month (**Figure A2.1**). This indicates that, besides the nanoemulsion size, the cationic surfactant acted as an essential electrostatic agent to maintain long-term stability of these nanoemulsions.

Table A2.3: Mean particle size (MPS) of the plant oil loaded nanoemulsions during five-month (M) stability test at 4.0 °C

Oil phase	Surfactant (w/w%)	MPS (nm)				
		1 M	2 M	3 M	4 M	5 M
Coconut+olive	4.0	197.5±2.4	192.1±2.6	190.6±4.4	190.1±2.2	193.4±5.5
Coconut+olive	2.0	190.2±2.0	194.1±0.9	193.0±0.7	191.4±0.6	192.6±1.8
Coconut+abyssinian	2.0	192.7±1.0	191.7±1.6	193.0±0.4	194.7±3.2	193.5±2.7
Olive	2.0	211.4±1.7	211.9±1.7	224.8±1.3	222.3±1.9	211.3±2.0
Coconut	2.0	129.8±0.1	132.2±1.2	139.0±2.8	131.0±3.0	128.2±1.9
Abyssinian	2.0	229.6±1.2	225.1±2.1	231.4±2.8	227.2±1.6	219.4±1.6

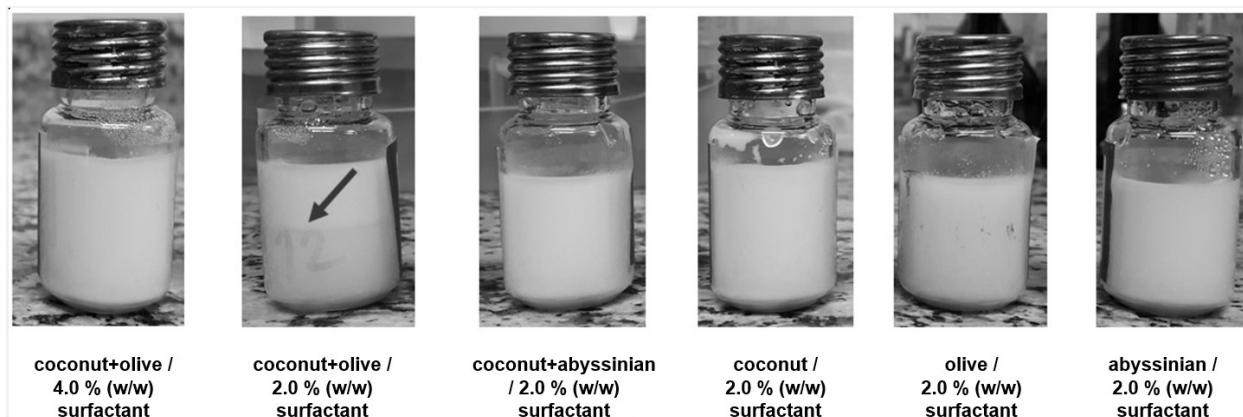| coconut+olive / 4.0 % (w/w) surfactant | coconut+olive / 2.0 % (w/w) surfactant | coconut+abyssinian / 2.0 % (w/w) surfactant | coconut / 2.0 % (w/w) surfactant | olive / 2.0 % (w/w) surfactant | abyssinian / 2.0 % (w/w) surfactant |

Figure A2.1: Five-month stability test of plant oil-loaded nanoemulsions at 4°C. The arrow indicates the slight separation of phases.

Source: Own authorship

A2.4.3. Efficacy study of hair tresses treated with plant oil-loaded nanoemulsions

The screening evaluation after application of plant-oil loaded nanoemulsions indicated that they showed better uniformity, softness and shine compared to the control. In comparing between them, the olive + coconut oil-loaded nanoemulsion containing 4.0% (w/w) surfactant presented better performance, in addition to the lower frizz and resistance to comb and detangling with the hands. The Abyssinian + coconut oil- and Abyssinian oil-loaded nanoemulsions showed lighter touch among all.

The results obtained with the instrumental test are shown in **Figure A2.2**. All hair tresses treated with nanoemulsions acted with a conditioning effect, reducing the combing work when compared to the control. The olive + coconut oil-loaded nanoemulsion containing 4.0% (w/w) surfactant resulted in a greater decrease in combing work (around 50%) compared to control, and better than the other preparations. Regarding the other oil-loaded nanoemulsions, despite reducing the combing work than in the control, no considerable differences were observed among them.
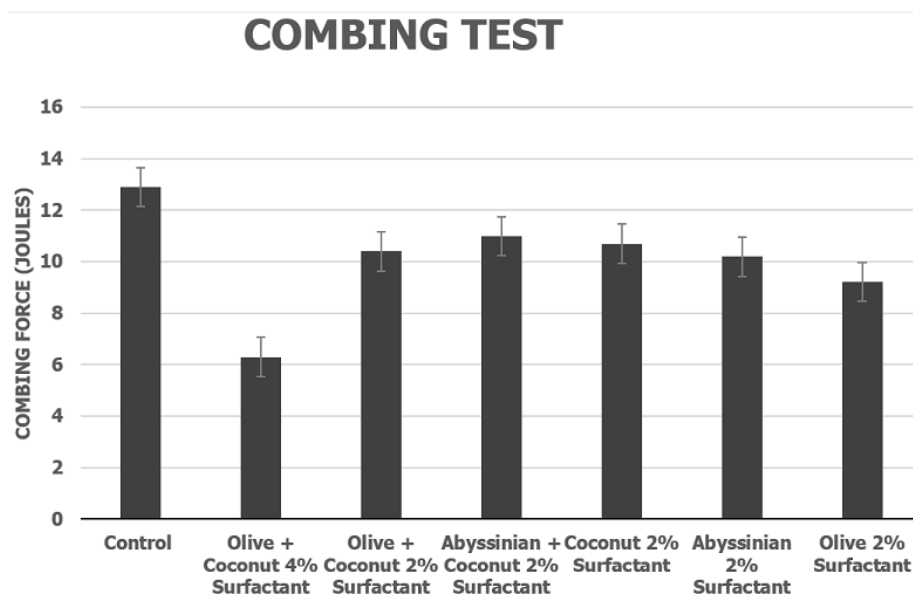
Figure A2.2: Combing test on hair tresses treated with plant oil-loaded nanoemulsions.

Source: Own authorship

Thus, it was not possible to identify a significant difference of efficacy due to the presence of distinctive plant oils, incorporated in these nanoemulsions. Under this condition, both screening and instrumental test showed similar results, indicating a correlation between these tests.

A2.5. DISCUSSION

Cosmetic products based on natural ingredients such as plant oils increasingly appeal to consumers as an alternative to synthetic oils. Nanoemulsions, that contain plant oils in their core, are a desired substitute for synthetic oil preparations acting efficiently as carriers. Additionally, they offer higher stability and safety. In this study, we intended to evaluate the influence of the use of three different plant oils and the cationic surfactant concentration on the final MPS, PI and ZP of the nanoemulsions prepared by HPH process. Additionally, we aimed to determine whether the different sizes or oil components impact the stability of nanoemulsions and their combing efficacy on the hair tresses.

A2.5.1. Influence of particle size

Initially, we point out the appropriate process condition to prepare nanoemulsions by HPH. The pressure, number of passage and surfactant concentration are important parameters to guarantee efficient nanoemulsification by this process.

Several studies indicate that pressures between 40 and 200 MPas in HPH process are more relevant to prepare nanoemulsions of approximately < 200 nm. Regardign passage, a single passage of HPH is not indicate for formation of uniform and small MPS nanoemulsions, since it is not enough to allow for the large drops to undergo a primary breakup event to a second breakup. Three to five passages seem to be the most commonly used numbers in several experiments. The increase in pressure and number of passages in HPH are generally linked to reducing MPS. However, too high pressure might result in conformational changes or breaking covalent bonds of surfactants and decrease their efficiency. Also, the excess number of passages might start to increase MPS, possibly due to the emulsifier's denaturation and limited adsorption time. Thus, respecting the suitable range of pressure and passage is important to avoid over processing during nanoemulsion preparation by HPH (28). In our present study, the applied pressure and number of passages were 60 MPa and five, respectively. This resulted in nanoemulsions with MPS between 126.9 to 231.9 nm, in accordance with the indicated conditions for HPH process.

With respect to the surfactant, several studies illustrated that its concentration have impact on the emulsions and nanoemulsions performance. The increase in nonionic surfactant in silicone emulsions reduced deposition of silicone oil onto the hair fibers, possibly due to the excess surfactant not bound at the oil-water interface, which prevents deposition (29). Differently, reducing surfactant concentration also in silicone oil emulsion showed higher MPS and low stability performance (30). According to Sonneville-Aubrun et al. (2018), the oil/ surfactant weight ratio is one of the key factors that influences the nanoemulsion formation. As is well known, by lowering the interfacial tension between oil/ water phases, surfactants facilitate the droplet breakup in the emulsification process. In addition, a suitable amount of surfactant enables its adsorption to oil/ water interfaces to prevent droplets coalescence during the HPH process. The authors suggest two regimes of the oil/surfactant weight ratio: the 'surfactant-rich' and 'surfactant-poor' regime. The former, in which the ratio is < 4, surfactants are expected to be in excess in the water phase. Under this regime, the MPS is lower than 50 nm and almost constant in size. The latter, in which the ratio is between 4 to 10, the MPS is estimated to increase linearly with the oil/ surfactant

weight ratio (31). Our emulsion system corresponds to the 'surfactant-poor' regime, with the ratio of 5 and 10 corresponding to 4.0 and 2.0% surfactant concentration (both w/w), respectively, in 20.0% (w/w) oil phase. However, results demonstrated no direct correlation between surfactant concentration and the MPS. The increase in surfactant concentration from 2.0 to 4.0 % (both w/w) did not linearly impacted the MPS. Thus, other factors should be taken into consideration in our systems.

Several studies indicate the influence of MPS on the emulsion's performance. Fengyan et al. (2011) describes this reduction in MPS of emulsions improves stability, owing to the increased adsorption amount in the emulsion system, combined with the reduced critical surface tension. They also point out that it increases permeability and film-forming efficacies (30). Other authors demonstrated that microemulsions with different MPS presented different behaviors: 40.0 μm uniform-sized microemulsion was more stable compared to non-uniform-sized ones. Additionally, the decreasing MPS of a uniform-sized microemulsion, in shampoos and conditioners, resulted in increasing deposition of silicone oil, and lower values of coefficient of friction on hair tresses. Thus, some authors suggest the MPS and uniformity are important factors for improving emulsions stability and their deposition on hair (32). Also, one study of silicon-oil-containing nanoemulsion in shampoo showed silicone deposition was significantly enhanced with nanoemulsion, compared to the non-nanosized control (11). This is explained by the fact that the small particles provide a large surface-to-volume ratio, enhancing the internal oil phase deposition on the hair and improving their penetration. Additionally, they provide a thin and uniform lipid film, enabling greater adsorption onto the hair (31).

Here, the coconut oil-loaded nanoemulsion resulted in the lower MPS (126.9 nm) and the abyssinian oil-loaded nanoemulsion, the highest (231.9 nm), both with the same oil/ surfactant weight ratio. Coconut oil has high content of lauric acid (C_{12} chain), and the abyssinian oil the erucic acid (C_{22} chain). This provides differences in oil polarity and lipophilicity, changing their interaction with surfactant. Thus, in the present condition, we observed that the final MPS value is mostly driven by oil composition, rather than the surfactant concentration. However, among nanoemulsions with different MPS, we did not identify significant differences in the efficacy on treated hair tresses, in contrast to previous papers.

A2.5.2. Influence of zeta potential (ZP)

Regarding the difference of combing performance on nanoemulsion- treated hair in our work, ZP must be considered. It increased from +68.7 to +79.2 mV by surfactant increase from 2.0 to 4.0 % (w/w).

Nazir et al. (2012) investigated the effect of surface charge on narrow-size distribution silicone oil on hair deposition. The deposition of positively charged silicone oil droplets was higher compared to the negatively charged droplets, the latter showing similar deposition to uncoated droplets (33). Ionic surfactants are able to modify electrostatic characteristics of oil droplets, subsequently of the emulsions, affecting the deposition process. Emulsions containing cationic surfactants or coated with positive surface charge polymers favor their precipitation by electrostatic interaction on the negative surface of hair, enhancing the deposition (29,34).

Therefore, it was expected that the increase of ZP would increase the hair deposition process, resulting in the positive performance of treated hair. But if the efficacy is related to the ZP value, the coconut oil-loaded nanoemulsion (ZP +72.9 mV) should provide better combability results than abyssinian oil-loaded nanoemulsion (ZP +62.9 mV). As noted in **Figure A2.2**, they showed similar results, indicating no significant influence of ZP increase on treated hair, under this condition.

A2.5.3. Influence of composition

Montenegro et al. (2015) compared several emulsions composed of mixture of three different oils and of emulsifier system (12.0% and 5.0% w/w, respectively). The oils (decyl oleate, caprylic/capric triglyceride and isopropyl myristate), presenting different lipophilicity (LogP) and surfactants (polysorbate 60, Steareth-21, Steareth-2, sorbitan monostearate and cetearyl glucoside/ cetearyl alcohol) with different hydrophilic lipophilic balance (HLB) values were added in these systems. Although no clear relationship was identified between emulsion physicochemical properties and sensory properties, the *in vitro* spreadability measurement and *in vivo* panel test demonstrated that both oil type and surfactant system affected the sensory properties of emulsions on skin (35). Other studies including different esters and silicon as emollient oil phase point to the significant effect of oil phase on the spreading of emulsions in skin sensory analysis. This may be

due to the different polarities and the molecular size of the oil components, where the higher these values are, the longer the time to penetrate into the stratum corneum (36,37).

Taking into consideration these results, the particular influence of each oil on treated hair was also expected in our study. A slight unique difference by screening test was observed in abyssinian oil-loaded nanoemulsions. However, when considering the general aspects, no significant differences between oil components at same surfactant concentration were detected. Interestingly, a considerable improvement of performance was observed, both by screening and instrumental test, when surfactant concentration was increased from 2.0 % to 4.0 % (w/w), even with no significant changes in the MPS.

Therefore, under this experimental test condition, we suppose that the concentration of surfactant with regard to the oil phase may be the most relevant factor when addressing hair treatment efficacy by nanoemulsions. This indicates that the treatment efficacy can be driven mainly by the electrostatic interaction between cationic surfactant and treated hair, rather than the plant oil components, MPS or ZP in the case of nanoemulsions. Complementary studies still need to be performed, such as, evaluating the interactions between other oils and surfactant at 4.0% (w/w) to analyze synergistic effects, or several-treatment number (increasing number of application and washing out), using damaged hair tresses, or even reducing the total concentration of surfactant and oils, but keeping this ratio for different hair needs. Although 4.0 % (w/w) may be an acceptable concentration, it is important to consider that high presence of cationic surfactant may lead to the risk of skin irritation, since there are few studies applying cationic nanoemulsions in hair treatment. Thus, safety tests may be necessary to guarantee the protection of our consumers.

A2.6. CONCLUSIONS

Plant oils have increased attention in the cosmetic field for haircare. In this present study, we aimed at comparing the effect of mean particle size (MPS), zeta potential (ZP), plant oil components and cationic surfactant concentration in the conditioning (combing) of the hair treated with plant oil-loaded nanoemulsions.

The oil components influenced the nanoemulsion MPS, and less influence was observed by surfactant concentration. Although, no differences in hair combing efficacy were observed for the different oil compositions, MPS or ZP. Surprisingly, the increase in cationic surfactant concentration indicated a reduction in the combing force by instrumental analysis, when compared

to the control tresses and other nanoemulsions. Although further studies are needed for a deeper understanding, this suggests that the electrostatic interaction between the cationic surfactant and the hair surface may be the most influential effect on this system.

Thus, the possible influence of the balance between the cationic surfactant and vegetable oil ratio, on the effectiveness of hair treatment, was raised by this experimental study. The nature of these influences has not been established and their importance remains a matter of speculation. Nevertheless, these results may open opportunities to further evaluate and develop interesting plant-based nanoemulsions, suited to consumer needs.

A2.7. REFERENCES

1.   Mordor. Hair Care Market - Growth, Trends, and Forecast (2020 - 2025) [Internet]. 2019. p. 1–7. Available from: https://www.mordorintelligence.com/industry-reports/hair-care-market-industry

2.   Yukuyama MN, Araújo GLB De, Bou-Chacra NA. Nanomaterials for hair care applications. Nanocosmetics. 2020;205–25.

3.   Miastkowska M, Lasoń E. Water-based nanoperfumes. Nanocosmetics. 2020;173–83.

4.   Zhang Z, Zhang B, Grishkewich N, Berry R, Tam KC. Cinnamate-Functionalized Cellulose Nanocrystals as UV-Shielding Nanofillers in Sunscreen and Transparent Polymer Films. Adv Sustain Syst. 2019;3(4):1800156.

5.   Oliveira CA De, Peres DDA, Graziola F, Chacra NAB, Araújo GLB De, Flórido AC, et al. Cutaneous biocompatible rutin-loaded gelatin-based nanoparticles increase the SPF of the association of UVA and UVB filters. Eur J Pharm Sci. 2016;81:1–9.

6.   Moraes CAP, Vieira AR. Nanomaterials for lip and nail cares applications [Internet]. Nanocosmetics. INC; 2020. 375–389 p. Available from: http://dx.doi.org/10.1016/B978-0-12-822286-7.00029-2

7.   Su J, Chen J, Zeng F, Chen Q, Wu S, Tong Z. Synthesis and photochromic property of

nanoparticles with spiropyran moieties via one-step miniemulsion polymerization. Polym Bull. 2008;61(4):425–34.

8. Maitra P, Zheng T. Cosmetic nanocomposites bases on in-situ crosslinked POSS materials [Internet]. USA; US 8,133,478 B2, 2012. Available from: https://patents.google.com/patent/US8133478B2/en

9. Valia D, Ellis J. Nail coatings having enhanced adhesion [Internet]. US; US9713585B2, 2017. Available from: https://patents.google.com/patent/US9713585B2/en

10. Welton J, Dixon K, Lichtenhan J, Hait S, Schwab J. Silsesquioxanes and use in nail coatings thereof [Internet]. Patent Application Publication. US; US2019/0192411A1, 2019. Available from: https://patents.google.com/patent/US10603264B2/en

11. Hu Z, Liao M, Chen Y, Cai Y, Meng L, Liu Y, et al. A novel preparation method for silicone oil nanoemulsions and its application for coating hair with silicone. Int J Nanomedicine. 2012;7:5719–24.

12. Aljuffali IA, Sung CT, Shen F, Huang C, Fang J. Squarticles as a Lipid Nanocarrier for Delivering Diphencyprone and Minoxidil to Hair Follicles and Human Dermal Papilla Cells. AAPS J. 2014;16(1):140–50.

13. Wang W, Chen L, Huang X, Shao A. Preparation and Characterization of Minoxidil Loaded Nanostructured Lipid Carriers. AAPS PharmSciTech [Internet]. 2017;18:509. Available from: http://dx.doi.org/10.1208/s12249-016-0519-x

14. Chen TC, Yu SC, Hsu CM, Tsai FJ, Tsai Y. Minoxidil – 2-hydroxypropyl-β-cyclodextrin inclusion complexes : characterization and in vivo evaluation of an aqueous solution for hair growth in rats. J Incl Phenom Macrocycl Chem. 2017;88(1):27–34.

15. Yukuyama MN, Oseliero PLF, Kato ETM, Lobënberg R, de Oliveira CLP, de Araujo GLB, et al. High internal vegetable oil nanoemulsion: D-phase emulsification as a unique low energy process. Colloids Surfaces A Physicochem Eng Asp. 2018;554(May):296–305.

16. Rele AS, Mohile RB. Effect of mineral, sunflower and coconut oil on prevention of hair damage. J Cosmet Sci. 2003;54(2):175–92.

17. Rajput R. Understanding Hair Loss due to Air Pollution and the Approach to Management. Hair Ther Transplant. 2015;05(01):1–5.

18. Wallace TC. Health Effects of Coconut Oil—A Narrative Review of Current Evidence. J Am Coll Nutr [Internet]. 2019;38(2):97–107. Available from: https://doi.org/10.1080/07315724.2018.1497562

19. Carluccio MA, Siculella L, Ancora MA, Massaro M, Scoditti E, Storelli C, et al. Olive oil and red wine antioxidant polyphenols inhibit endothelial activation: Antiatherogenic properties of Mediterranean diet phytochemicals. Arterioscler Thromb Vasc Biol. 2003;23(4):622–9.

20. Budiyanto A. Protective effect of topically applied olive oil against photocarcinogenesis following UVB exposure of mice. Carcinogenesis [Internet]. 2000;21(11):2085–90. Available from: https://academic.oup.com/carcin/article-lookup/doi/10.1093/carcin/21.11.2085

21. Sun Y, Xia Z, Zheng J, Qiu P, Zhang L, McClements DJ, et al. Nanoemulsion-based delivery systems for nutraceuticals: Influence of carrier oil type on bioavailability of pterostilbene. J Funct Foods [Internet]. 2015;13:61–70. Available from: http://dx.doi.org/10.1016/j.jff.2014.12.030

22. Owen RW, Giacosa A, Hull WE, Haubner R, Würtele G, Spiegelhalder B, et al. Olive-oil consumption and health: the possible role of antioxidants. Lancet Oncol [Internet]. 2000;1:107–12. Available from: http://www.ncbi.nlm.nih.gov/pubmed/11905662

23. Yukuyama MN, Kato ETM, de Araujo GLB, Löbenberg R, Monteiro LM, Lourenço FR, et al. Olive oil nanoemulsion preparation using high-pressure homogenization and D-phase emulsification – A design space approach. J Drug Deliv Sci Technol [Internet]. 2019;49(October 2018):622–31. Available from: https://doi.org/10.1016/j.jddst.2018.12.029

24. Schrott A. Cleaning / conditioning shampoo. United States of America; US 2018 / 0110708 A1, 2018.

25. Hicks - Graham S. Treatment for scalp dryness and curly hair. Patent Application

Publication. United States of America; US 2018 / 0303746 A1, 2018.

26. Von Aspern E, Delowsky J, Schroeder T. Hair oils for conditioning keratin fibres. United States of America; US 2019 / 0192397 A1, 2019.

27. Dario MF, Santos MSCS, Viana AS, Arêas EPG, Bou-chacra NA, Conceic M, et al. A high loaded cationic nanoemulsion for quercetin delivery obtained by sub-PIT method. Colloids Surfaces A Physicochem Eng Asp. 2016;489:256–64.

28. Håkansson A. Fabrication of Nanoemulsions by High-Pressure Valve Homogenization. Nanoemulsions: Formulation, Applications, and Characterization. 2018. p. 175–206.

29. Berthiaume MD, Jachowicz J. The effect of emulsifiers and oil viscosity on deposition of nonionic silicone oils from oil-in-water emulsions onto keratin fibers. J Colloid Interface Sci. 1991;141(2):299–315.

30. Fengyan L, Wenli Z, Tianbo Z, Danghui D, Fang Y. Factors influencing droplet size of silicone oil emulsion with high solid content. China Pet Process Petrochemical Technol. 2011;13(3):21–6.

31. Sonneville-Aubrun O, Yukuyama MN, Pizzino A. Application of Nanoemulsions in Cosmetics. In: Nanoemulsion. 2018. p. 435–75.

32. Nazir H, Lv P, Wang L, Lian G, Zhu S, Ma G. Uniform-sized silicone oil microemulsions: Preparation, investigation of stability and deposition on hair surface. J Colloid Interface Sci [Internet]. 2011;364(1):56–64. Available from: http://dx.doi.org/10.1016/j.jcis.2011.07.096

33. Nazir H, Wang L, Lian G, Zhu S, Zhang Y, Liu Y, et al. Multilayered silicone oil droplets of narrow size distribution: Preparation and improved deposition on hair. Colloids Surfaces B Biointerfaces [Internet]. 2012;100:42–9. Available from: http://dx.doi.org/10.1016/j.colsurfb.2012.05.018

34. Nazir H, Zhang W, Liu Y, Chen X, Wang L, Naseer MM, et al. Silicone oil emulsions: Strategies to improve their stability and applications in hair care products. Int J Cosmet Sci. 2014;36(2):124–33.

35. Montenegro L, Rapisarda L, Ministeri C, Puglisi G. Effects of lipids and emulsifiers on the

physicochemical and sensory properties of cosmetic emulsions containing vitamin E. Cosmetics. 2015;2(1):35–47.

36.   Savary G, Grisel M, Picard C. Impact of emollients on the spreading properties of cosmetic products: A combined sensory and instrumental characterization. Colloids Surfaces B Biointerfaces [Internet]. 2013;102:371–8. Available from: http://dx.doi.org/10.1016/j.colsurfb.2012.07.028

37.   Parente ME, Gámbaro A, Ares G. Sensory characterization of emollients. J Sens Stud. 2008;223:149–161.

A2.8. SUPPLEMENTARY MATERIAL
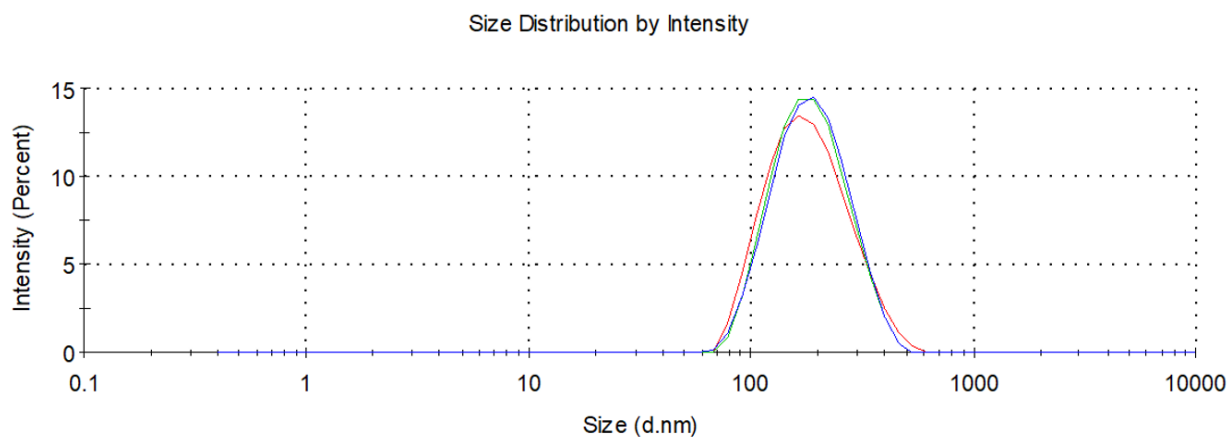
Figure A2.S1: mean particle size of coconut+olive oils-loaded nanoemulsion with 4.0 % (w/w) surfactant (n=3)

Source: Own authorship

Size Distribution by Intensity
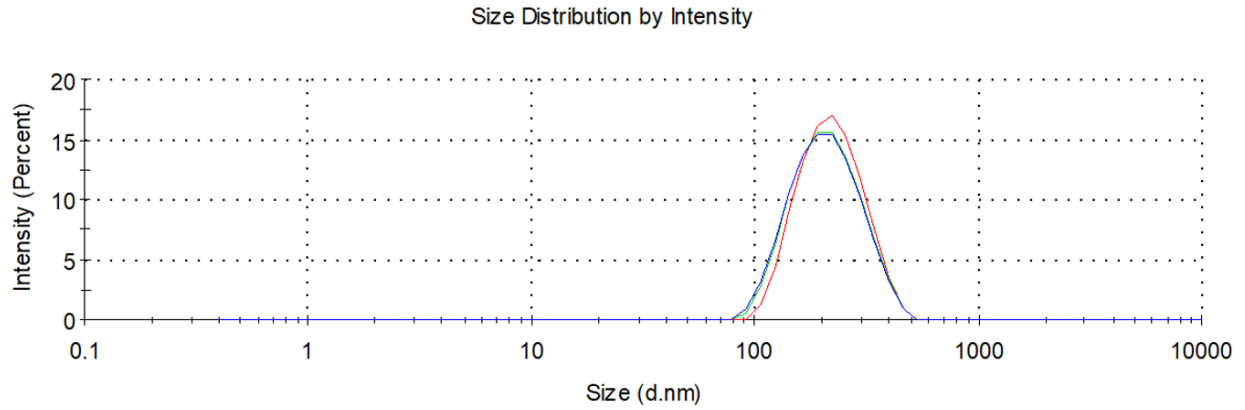
Figure A2.S2: mean particle size of coconut+olive oils-loaded nanoemulsion with 2.0 % (w/w) surfactant (n=3)

Source: Own authorship

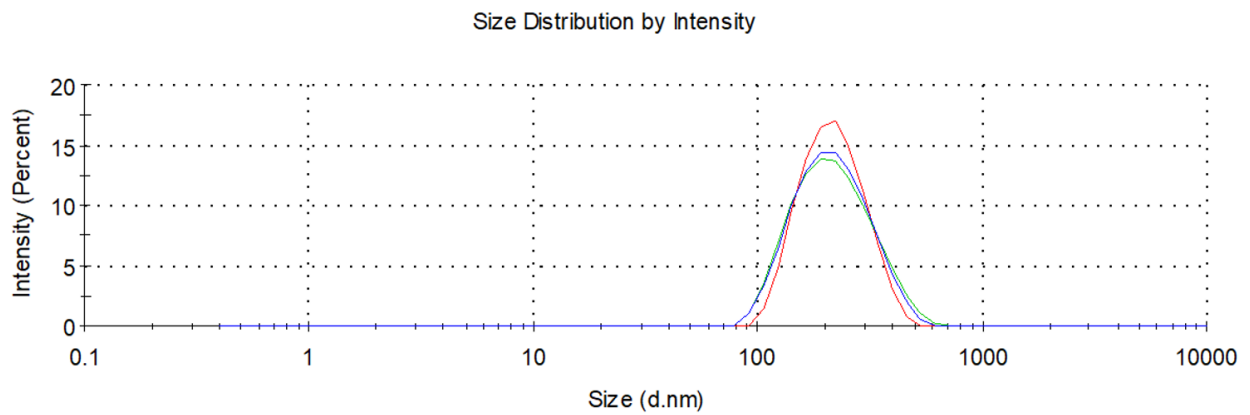Size Distribution by Intensity

Figure A2.S3: mean particle size of coconut+abyssinian oils-loaded nanoemulsion with 2.0 % (w/w) surfactant (n=3)
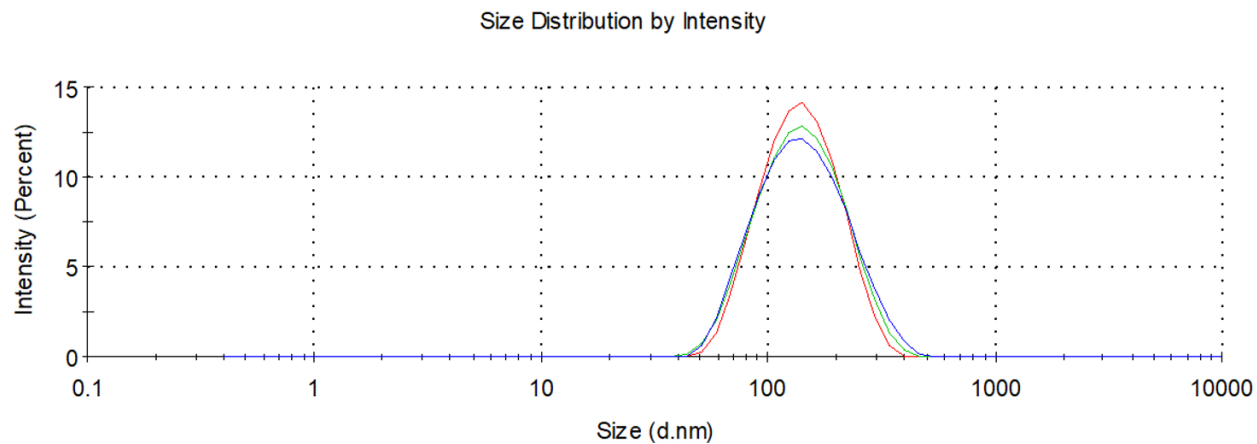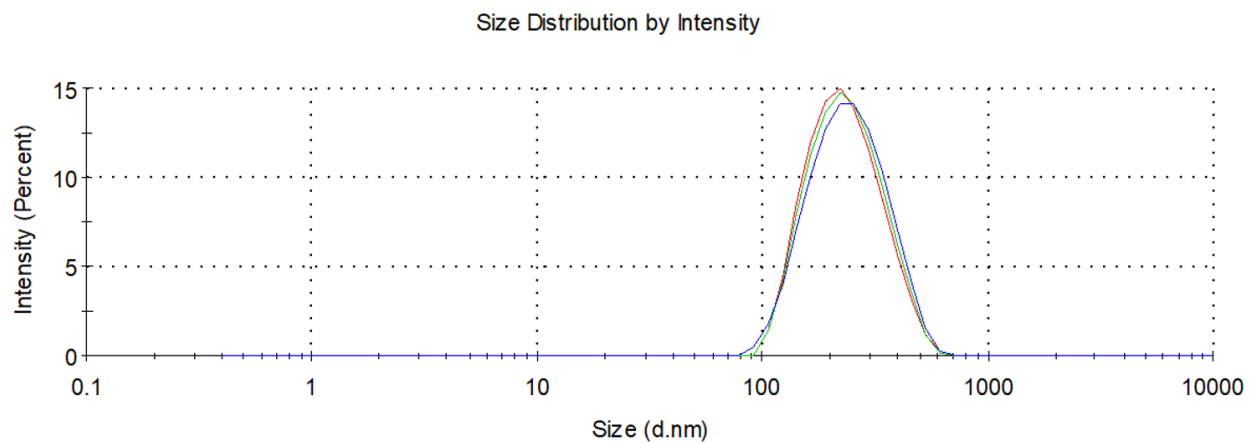
Source: Own authorship

Figure A2.S4: mean particle size of coconut oil-loaded nanoemulsion with 2.0 % (w/w) surfactant (n=3)

Source: Own authorship

Figure A2.S5: mean particle size of olive oil-loaded nanoemulsion with 2.0 % (w/w) surfactant (n=3)
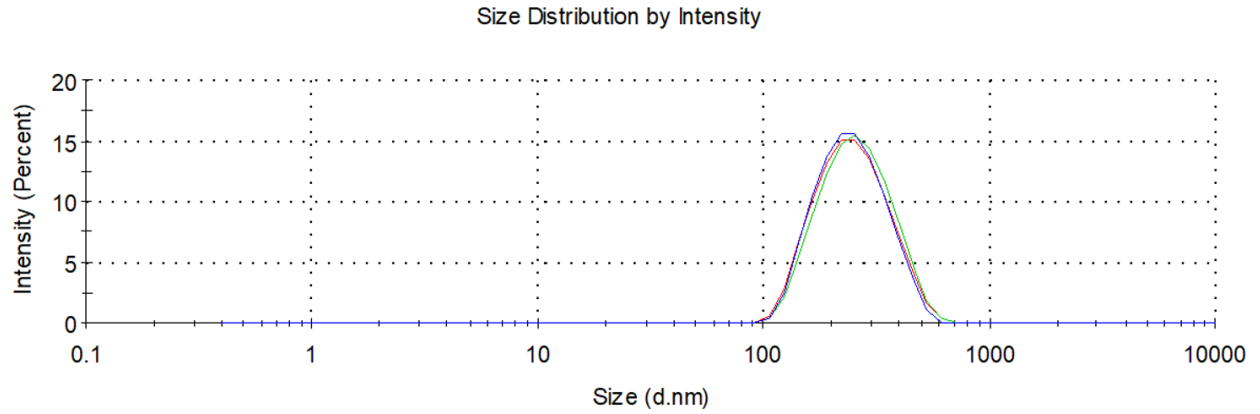
Source: Own authorship

Figure A2.S6: mean particle size of abyssinian oil-loaded nanoemulsion with 2.0 % (w/w) surfactant (n=3)

Source: Own authorship

APPENDIX 3 – ABSTRACTS OF PATENTS

The patent numbers BR1020210138050 and BR1020210138017 were approved for deposit in Brazilian registration institution - National Institute of Industrial Property (INPI), based on the results of studies conducted in Brazil.

A.3.1. PATENT NUMBER BR1020210138050

Title: Process for obtaining nanoemulsions comprising flubendazole and glyceryl monolinoleate, the referred nanoemulsions and their use in the treatment of cryptococcal meningitis

Authors: Yukuyama, Megumi Nishitani.; Bou-Chacra, Nádia Araci; De Araújo, Gabriel Lima Barros; Folchini, Beatriz Rabelo.; Peroni, Camilla Midori.

Date of deposit: 13th, July, 2021

Field of the invention

The present invention is inserted in the field of medicinal chemistry and, more specifically, in the field of nanobiotechnology, since it refers to the process of obtaining and the composition of a nanoemulsion comprising flubendazole, glyceryl monolinoleate oil and using the technique of D-Phase emulsification (DPE). The application of the DPE technique associated with flubendazole and glyceryl monolinoleate oil allows the development of an effective nanoemulsion in treating cryptococcal meningitis, with low toxicity, high efficacy and stability.

A.3.2. PATENT NUMBER BR1020210138017

Title: Process of obtaining a nanoemulsion, obtained nanoemulsion and use of this in the preparation of a medicine for the treatment of fungal disease

Authors: Yukuyama, Megumi Nishitani; Bou-Chacra, Nádia Araci; De Araújo, Gabriel Lima Barros; Lopes, Luciana Biagini; Folchini, Beatriz Rabelo.; Peroni, Camilla Midori.

Date of deposit: 13th, July, 2021

Field of invention:

[001] The present invention refers to the field of chemistry and nanotechnology and describes a process for obtaining and the optimized composition of a nanoemulsion comprising a high polarity oil, stabilized with an oil derived from vegetable origin, using the technique of D-Phase emulsification (DPE).

[002] More particularly, the present invention refers to the use of oil derived from vegetable origin in a nanoemulsion with high oil content and high polarity in an optimized proportion, offering a surprising solution for increasing the stability of this nanoemulsion prepared by the DPE technique. Additionally, said nanoemulsion showed effective in vitro antifungal activity.

APPENDIX 4 – REVISITING FLUBENDAZOLE THROUGH NANOCRYSTAL TECHNOLOGY: STATISTICAL DESIGN, CHARACTERIZATION AND ITS POTENTIAL INHIBITORY EFFECT ON XENOGRAFTED LUNG TUMOR PROGRESSION IN MICE

I contributed equally as an author and was responsible for Writing - Original Draft, Writing - Review & Editing and Visualization

The content of these experiments are in first author's thesis in Portuguese language, in the digital library of University of Sao Paulo, link https://www.teses.usp.br/teses/disponiveis/9/9139/tde-29032019-142701/pt-br.php, and the English article in the Journal of Cluster Science, as described above.